EARTHQUAKE HAZARD AND RISK ASSESSMENT FOR TURKEY

by

Mine Betül Demircioğlu

B.S., Civil Engineering, Istanbul Technical University, 1997

M.S., Earthquake Engineering, Boğaziçi University, 2003

Submitted to the Kandilli Observatory and Earthquake Research Institute
in partial fulfillment of
the requirements for the degree of
Doctor of Philosophy

Graduate Program in Earthquake Engineering

Boğaziçi University

2010

To my family and especially to my mother, F. Enise Günebakan with all my love

ACKNOWLEDGEMENTS

I would like to express my deepest gratitude to my supervisor Professor Mustafa Erdik for his guidance through this research. In particular, Prof. Dr. Nuray Aydinoğlu's recommendations and suggestions have been invaluable for their suggestions.

The contributions of my dissertation defense committee members, Prof. Dr. Atilla Ansal, Prof. Dr. Oğuz Özel, Prof. Dr. Erdal Şafak and Prof. Dr. Kutay Özaydın are gratefully appreciated, for reviewing this dissertation and valuable comments.

I also wish to thank to Yaver Kamer, who developed a Matlab based routine. Special thanks should be given to my colleagues. My colleagues from the Department of Earthquake Engineering supported me in my research work. I want to thank them for all their help, support, interest and valuable hints. Especially I am obliged to Dr. Gökçe Tönük, Dr. Cüneyt Tüzün, Dr. Karin Şeşetyan and Dr. Ufuk Hancılar.

I would like to thank to Dr. Mario Ordaz and Dr. Laurentiu Danciu from ETHZ for their constructive comments and professional help related with the usage of Crisis 2007 software. I also wish to thank to Prof. Dr. Celal Şengör for their guidance to model the source zonation for Turkey.

Finally, I would like to give my special thank to my family, to my mother F. Enise Günebakan, to my sister Banu Safran,to my nephew Aylin Safran and to my uncle Levent Safran, whose patient love enabled me to complete this work.

ABSTRACT

EARTHQUAKE HAZARD AND RISK ASSESSMENT FOR TURKEY

Using a GIS-environment to present the results, seismic risk analysis is considered as a helpful tool to support the decision making for planning and prioritizing seismic retrofit intervention programs at large scale. The main ingredients of seismic risk analysis consist of seismic hazard, regional inventory of buildings and vulnerability analysis.

There are two main objectives of this thesis. The first objective is the assessment of the national earthquake hazard based on the next generation attenuation (NGA) ground motion prediction models and comparisons of the results with the previous models. The second objective is an evaluation of seismic risk based on a probabilistic intensity ground motion prediction for Turkey. According to the macroseismic approach of Giovinazzi and Lagomarsino (2005), two alternative vulnerability models have been used to estimate building damage. The vulnerability and ductility indices for Turkey have been taken from the study of Giovinazzi (2005). These two vulnerability models have been compared with the observed earthquake damage database. A good agreement between curves has been clearly observed. In additional to the building damage, casualty estimations based on three different methods for each return period and for each vulnerability model have been presented to evaluate the earthquake loss.

Using three different models of building replacement costs, an average annual loss (AAL) and probable maximum loss ratio (PMLR) due to regional earthquake hazard have been provided to form a basis for the improvement of the parametric insurance model and determination of premium rates for compulsory earthquake insurance in Turkey.

ÖZET

TÜRKİYE'NİN DEPREM TEHLİKE VE RİSKİNİN BELİRLENMESİ

Sismik risk analizi, Coğrafi Bilgi Sistemi (CBS) yardımı ile depreme bağlı şehir planlama ve sismik güçlendirme uygulamalarında öncelikli bölgelerin belirlenmesinde yararlı bir yöntem olarak ortaya çıkmaktadır. Sismik risk analizinin temel girdileri, bölgesel bina envanteri, sismik tehlike, ve hasargörebilirlik analizidir.

Bu çalışmanın iki amacı bulunmaktadır. Birinci amaç, ulusal deprem tehlike çalışmasının yeni üretilen NGA yer hareketi tahmin modellerini kullanılarak güncellenmesi ve eski modeller kullanılarak elde edilen sonuçlarla karşılatırılmasını içermektedir. İkinci amaç ise şiddet bazlı olasılıksal yer hareketine dayalı olarak sismik riskin belirlenmesidir. Giovinazzi ve Lagomarsino (2005)'nun Makrosismik yaklaşımı kullanılarak iki farklı hasargörebilirlik modeli ile her bir hasar seviyesi için tahmini bina hasar dağılımları elde edilmiştir. Kullanılan hasargörebilirlik eğrileri aynı zamanda gözlemlerden elde edilen deprem hasar bilgileri ile karşılaştırılmış ve uyumlu ilişki gözlemlenmiştir.Tahmini bina hasar dağılımının belirlenmesinin yanı sıra yaralanma dağılımları da literatürde yer alan üç farklı yöntem ile tahmin edilmiştir. Elde edilen sonuçlar, deprem kayıplarının değerlendirilmesinde kullanılmıştır.

Deprem sigortası amaçlı sigorta modellerinin geliştirilmesinde ve zorunlu deprem sigorta primlerinin belirlenmesinde kullanılmak üzere, üç farklı bina yenileme maliyet oranı kullanılarak, deprem kaynaklı yıllık ortalama kayıp (AAL) ve olası en büyük kayıp oranları (PMLR) belirlenmiştir.

TABLE OF CONTENTS

LIST OF FIGURES

LIST OF TABLES

LIST OF SYMBOLS / ABBREVIATIONS

a, *b*, *t* and *r*	Parameters of beta distribution
a,b	Seismic constants for any given region
c1,c2,c3	Empirical constants
D	Ductility index
E	Logarithm
Fa	Short period amplification factors
$f_M(m)$	Probability density functions for M
$f_R(r)$	Probability density functions for R
Fv	Medium period amplification factors
$\lfloor H_j \rfloor$	Hazard
I	Earthquake intensity
$\lfloor R_{i,j} \rfloor$	Risk
M	Earthquake magnitute
M1	Factor taking into account regional variation of population per building
M2	Factor taking into account variation of occupancy depending on the time
M3	Factor taking into account percentage of trapped occupants under collapsed buildings
M4	Factor taking into account different injury levels of trapped people
M5	Factor taking into account change of injury levels of trapped people with time
N	Number of shocks with magnitude greater or equal to M per unit time and unit area
Pn	Population at n date
Pn+t	Population at n+t date (t years later)
R	Distance between the source and the site
R	Annual growth rate of population

RP(ΔT)	Return period (yrs)
S1	Spectral accelerations at T=1.0 sec
Ss	Spectral accelerations at T=0.2 sec
T	The time period between two dates (in years)
TCb	Total number of collapsed buildings of type b
V	Vulnerability index
Vr	Regional vulnerability factor
$\lfloor V_{i,j} \rfloor$	Vulnerability
X	Continues variable
λ	Constant
λ[Y>y]	Mean annual rate of exceedance
μ_x	Mean of the discrete beta distribution
Γ	Gamma function
σ_x^2	Variance
AAL	Average annual loss
AALR	Average annual loss ratio
AEDR	Average earthquake damage ratio
AFZ	Amanos Fault Zone
AF	Akhourian Fault
ATC	Applied technology council
CAFZ	Central Anatolian Fault Zone
CBS	Coğrafi bilgi sistemi
CC1	Reinforced concrete frame non engineered type of buildings
DEE	Department of Earthquake Engineering
DF	Doğubeyazıt Fault
DLH	Demiryolu, liman ve havaalanı
DS	Dökmetaş Segment
DPM	Damage probability matrix

DS	Dead Sea Fault
DY	Ditizyayla
DSFZ	Dead Sea Fault Zone
EAFZ	East Anatolian Fault Zone
EMS	European macro-seismic scale
ERD	Disaster and Emergency Management Presidency Earthquake Department
ESF	Zheltorechensk- Sarighamish Fault
FEMA	Federal Emergency Management Agency
FF	Nakhicheva Fault
IBC	International building code
IDNDR	International decade of natural disaster reduction
IMM	Istanbul Metropolitan Municipality
GMPE	Ground motion prediction equation
GPS	Global positioning system
GSHAP	Global seismic hazard assessment program
GSKF	Gailatu Siah Cheskmeh Khay Fault
GSS	Gemerek-Şarkışla Segment
GYFZ	Göksu-Yazyurdu Fault Zone
KDS	Kavlaktepe-Dikilitas Segment
KOERI	Kandilli Observatory and Earthquake Research Institute
KS	Kızılırmak Segment
HAZUS-MH	Hazards U.S. multi hazard
HAZUS	Hazards United State
MaF	Maku Fault
MDR	Mean damage ratio
MMI	Modified Mercalli intensity scale
MOFZ	Malatya Ovacık Fault Zone
MTA	Maden Teknik Arama
NAZ	North Anatolian Fault
NAFZ	North Anatolian Fault Zone
NE	North east

NGA	Next generation attenuation
NNE	North northeast
PGA	Peak ground acceleration
PGR	Population growth rate
PGV	Peak ground velocity
PEER	Pasific Earthquake Engineering Research
PHOENIX	Preeminent Hyogo's emergency management network for disaster information exchange
PML	Probably maximum loss
PMLR	Probably maximum loss ratio
PSHA	Probabilistic seismic hazard analysis
PSRA	Probabilistic seismic risk assessments
PSSF	Pambak Sevan Sunik Fault
RC	Reinforced Concrete
RP	Return period
SA	Spectral acceleration
SAF	Sultandağ Fault Zone
SESAME	Seismic hazard assessment of the mediterranean basin
SW	South west
SF	Sardarapat Fault
SHA	Seismic hazard analysis
SS	Sivas Segment
SSW	South southwest
TCIP	Turkish catastrophe insurance pools
TEFER	Turkey emergency flood and earthquake recovery
TurkStat	Turkish statistical institute
TS	Tecer Segment
QTM	Quaternary, mesozoic and tertiary
UDIM	Ulusal deprem izleme merkezi
USGS	The United States Geological Survey
U.S	United State

1. INTRODUCTION

Spatial earthquake hazard and risk assessment studies play an important role in identifying the potential consequences of an earthquake and taking actions towards their mitigation. The seismic hazard assessment represents a basic tool for the management of activities devoted to the reduction of the effects of future damaging seismic events. Early approaches to the seismic design of critical facilities were characterized by deterministic based seismic hazards. Deterministic based ground motions are typically defined for a single scenario earthquake whose magnitude and closest distance are specified. However, if the uncertainty in the timing, location, and magnitude of the future earthquakes, and the objectives of performance-based engineering are taken into consideration, it is often more meaningful to utilize a probabilistic approach in characterizing the ground motion that a given site will experience in the future. A probabilistic seismic hazard analysis (PSHA) takes into account the ground motions from the full range of earthquake magnitudes that can occur on each fault or zone that can affect the site. The PSHA integrates this information using probability theory to produce the annual frequency of exceedance of each different ground-motion level for each ground-motion parameter of interest.

The input into a seismic hazard analysis should be carefully evaluated. In addition to seismic data and the tectonic information of the region, the most basic information to be compiled is the faults and the earthquake sources within the area, as well as their structural properties. Well-delineated faults may be regarded as linear earthquake sources, and their characteristics may be obtained from geologic and neo-tectonic studies. However, if there is not enough information about these features, a sequence of small faults which are related to considerable amount of seismicity, the region is considered as an areal seismic source zone.

Additionally, the probabilistic hazard assessment approach requires an appropriate strong motion prediction equation (GMPE), which depicts the propagation and modification of strong ground motion as a function of earthquake size (magnitude) and the distance between the source and the site of interest. Earthquake ground motion parameters

as Peak Ground Acceleration (PGA), Peak Ground Velocity (PGV), Spectral Acceleration (SA) and macroseismic intensity (I) may be used to depict the ground motion.

Due to the high increases of occurrences of natural disasters all over the world, new approaches have been developed for disaster assessment. After recent earthquakes caused destructive damages, hazard assessment and management have become a crucial research issue to develop new methodologies to direct appropriate post-disaster renovations. In the United States and Japan, new disaster assessment and management methodologies have been improved recently. An important and widely used earthquake disaster assessment strategy tool is the HAZUS methodology developed by Federal Emergency Management Agency (FEMA) in U.S. HAZUS-MH (HAZUS Multi Hazard) is a GIS based earthquake loss estimation methodology provided in a software package or by application of the theory documented. The methodology provides regional officials with the tools necessary to plan and stimulate efforts to reduce risk from earthquakes and to prepare for emergency response and recovery from an earthquake. The methodology has been developed to perform similar loss evaluation for calculation of potential exposure to flood (*e.g.*, dam break) or fire (following earthquake) flood and hurricanes. Other effective tools are ATC13-20-21 and 156 prepared by Applied Technology Council (ATC 1985, 1989, 2001).

Japan is one of the hazard prone countries. Natural disasters such as earthquake, typhoons, torrential rains and flooding, heavy snowfall, landslide and volcanic eruption occur frequently. However, the earthquake is the most destructive natural disaster among them. In 1961, the central government has improved the disaster prevention system by upgrading the knowledge based on the lesson learned from the great disasters both in Japan and abroad. Such effort was further intensified in the International Decade of Natural Disaster Reduction (IDNDR). After the Great Hanshin Awaji Earthquake of 1995, Hyogo Prefecture Government drastically revised its previous disaster management strategy and introduced PHOENIX (Preeminent HyogO's Emergency management Network for disaster Information eXchange) disaster management system. Its aim is to consolidate disaster related facilities in one place and to upgrade telecommunication system for information collection, procession and damage calculation and dissemination among related agencies for disaster preparedness as well as for emergency crisis management. Moreover, this system can also be effectively used for early warning purpose.

The earthquake hazard assessment methodologies have become important in Turkey just as the other earthquake- prone countries. Especially, after the Kocaeli and Duzce Earthquakes in 1999, assessment studies are increasing and seismic risk will continue to increase without application of fundamental changes in policy, design and construction. For that reason, the Government of Turkey has decided to enforce the earthquake insurance on the nationwide basis with the sole purpose of privatizing the potential risk by offering insurance by the Turkish Catastrophic Insurance Pools (TCIP) and then exporting the major part of this risk to the international reinsurance and capital markets (Bommer *et al.*, 2002).

Yucemen (2005) has studied about a probabilistic model for the calculation of the earthquake insurance rates. The earthquake insurance rates are based on the Seismic Hazard Assessment (SHA) carried out and Damage Probability Matrices (DPM) assessed within the scope of his study. Seismic source model of Gulkan *et al.* (1993) to assess seismic hazard in Turkey and the DPM model of the modified Yucemen (2002); and Yucemen and Askan (2003) to determine the building damage have been used, respectively. The earthquake insurance premium rates obtained in his study under different assumptions have been compared with the current practice of the insurance companies in Turkey (TCIP). The difference between rates is about 2.7 times more than the insurance companies currently are charging against earthquake risk, making the purchase of earthquake insurance quite feasible.

Musson (2000) has studied the intensity based seismic risk assessment. Using a generated synthetic earthquake catalogues, a Monte Carlo simulation approach has been utilized to determine the seismicity parameters. As a ground motion parameter, the earthquake magnitude (M) has been converted to the EMS98 intensity scale (note that MSK and EMS98 values are equivalent) by using the Ambraseys (1988). As a result, Musson has said more research on regional intensity attenuation is needed with the replacement of absolute intensity scale with modern ones such as the EMS98.

In a similar point of view, the main purpose of this thesis is that the probabilistic intensity based earthquake risk assessment is taken into consideration by using the regional intensity ground motion prediction equation. The second purpose is that the probabilistic

earthquake hazard for Turkey is quantified in terms of peak ground acceleration (PGA) and spectral acceleration (SA) at various periods for 72, 475, and 2475 return periods.

1.1. Objectives of the Thesis

This thesis encompasses a state–of-the art assessment of seismic hazard for Turkey, and develops earthquake hazard maps in term of PGA, SA at various periods and intensity in a probabilistic context to be used for design and evaluation of facilities at the site. Additionally, the second objective of the thesis is to assess the seismic risk for Turkey by the combination of seismic hazard, regional inventory of buildings and vulnerability analysis. The results provided by a seismic risk analysis can provide guidelines for risk management activities.

There are four main ingredients in an earthquake risk assessment: (1) assessment of seismic hazard which includes the collection of data on the seismo-tectonics and geology of the region, development of probabilistic seismic hazard maps for Turkey; (2) estimation of building damage for different damage states, which involves the collection of data on structures, classification of structural inventory, development of intensity based fragility curves (3) estimation of the casualty using the distribution of the population and the estimated building damage and (4) estimation of the economic losses. The framework of the thesis is shown in Figure 1.1.

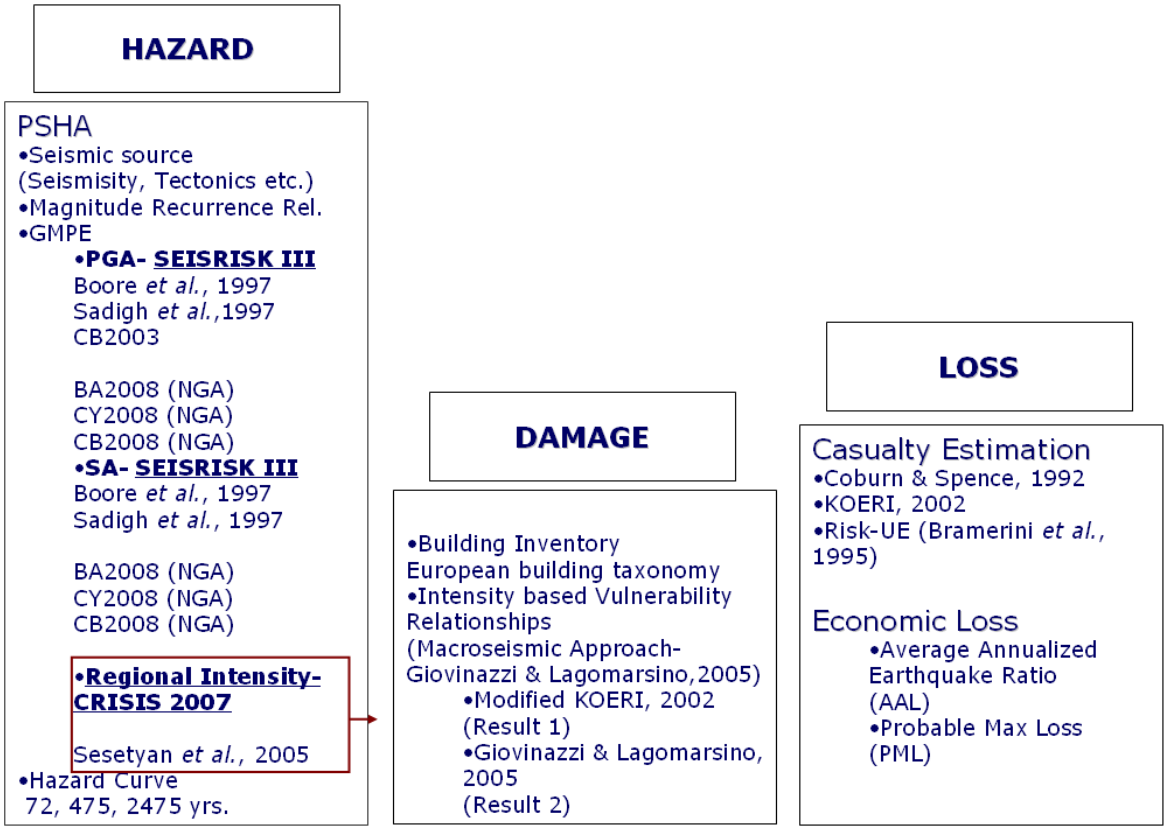

Figure 1.1. The framework of the thesis

1.2. Outline of the Thesis

The thesis is organized into seven chapters. Section 1 describes the presentation of some preliminary and fundamental concepts and provides a general overview of the objectives of the thesis. In Section 2., the procedures for probabilistic hazard are presented. The methodology and concerned parameters as active tectonics, seismic evaluations, source zonation, and earthquake recurrence relationships are covered in Section 2.1 through Section 2.6. There are two different programs used in this study. Section 2.7 briefly describes the necessarily input files and makes a calibration analysis to see the similarity. The site independent and dependent seismic hazard results are shown in Section 2.8 to Section 2.10.

Section 3 involves the necessary steps for the seismic risk analysis implementation. Section 3.3.1 includes the derivation of an observed vulnerability method from EMS98

Macroseismic scale employing probability and fuzzy set theory and the definition of synthetic Vulnerability and Ductility indices for both building taxonomies and for vulnerability classes. The macroseismic method (Giovinazzi and Lagomarsino, 2005) convolution with hazard and exposure analysis to evaluate damage is presented. The characteristic of the proposed macroseismic vulnerability methods are presented. With regard to vulnerability analysis, the result of estimated building damage for return period 72, 475 and 2475 years and validation analysis between the estimated building damage for return period of 72 years with the observed damages are encompassed in Section 3.3.4 and Section 3.3.5. In Section 3.4, the intensity based casualty estimation approaches of Coburn and Spence (1992), Risk UE (Bramerini *et al.*, 1995) and KOERI (2002) are utilized for the estimation of casualties. The validation of the estimated casualty results with respect to the reported earthquake life-loss data is presented in Section 3.4.5.

Section 4 describes the presentation of the main concepts to determine the average annualized earthquake. The conclusion along with some recommendations for future studies and the uncertainty of this study are presented in Section 5 to Section 6.

2. ANALYSING THE EARTHQUAKE HAZARD

Turkey is one of the most seismically active countries in the European – Mediterranean region and, earthquakes frequently cause extensive damage and life loss as evidenced by the recent earthquakes of Varto (1966); Erzincan (1992); Kocaeli (1999), and Duzce (1999).

National seismic hazard zonation should be based on seismic hazard estimates computed with the most recent and realistic seismotectonic information available (McGuire, 1993). Seismic hazard analysis plays an important role in seismic design decisions concerning the civil engineering structures. Due to the uncertainty of location, the time of occurrence, magnitude, and the other characteristics of a future earthquake; the probabilistic forecasting and decision making are the appropriate tools for the evaluation of seismic hazard. Seismic hazard can be defined as the probability of occurrence at a given site and within a given time period of ground motion due to an earthquake event capable of causing loss of value through damage. Seismic hazard convolved with vulnerability analysis constitutes one of the factors of seismic risk which is defined as the probability of loss of property or loss of function of engineering structure and human life due to the occurrence of seismic events.

The main physical ingredients of the probabilistic seismic hazard assessment are the tectonic setting and the seismicity of the region, applicable ground motion prediction equation and an appropriate stochastic model for the probabilistic hazard analysis. The information about geological, seismotectonic characteristics of Turkey region, as well about historical seismic activity, ground characteristics and seismic micro zoning of its territory has been collected. In the following chapters, these features are elaborated.

There exists a number of probabilistic seismic hazard mapping for Turkey (*e.g.*, Yarar *et al.*, 1980; Erdik and Oner, 1982; Erdik *et al.*, 1985; Gülkan *et al.*, 1993; Onur, 1997; GSHAP, 1999, TEFER, 2000; Baku-Ceyhan Crude Oil Pipeline Projects 2001 (Barka *et al.*,1999); SESAME, 2003; Kayabali and Akin, 2003, Tsapanos *et al.*, 2005). These previous studies are summarized in Section 2.4.

2.1. Probabilistic Seismic Hazard Analysis (PSHA) Methodology

McGuire (1993) classified the main procedures of PSHA into deductive and historic categories. Both the deductive and historic methods allow all available information on tectonics, seismicity and earthquake related ground motions to be incorporated into the PSHA computations.

Historic methods utilize only information from earthquake catalogues, for instance, the nonparametric historic method by Veneziano *et al.* (1984). On the other hand, deductive methods focus also on the determination and estimation of the cause and origin of earthquakes. The most popular deductive method follows the Cornell (1968) approach and is based on the determination of seismogenic source zones with homogeneous seismic activity rate. The method involves two separate models: a seismicity model describing a geographical distribution of event sources and the distribution of magnitudes, and an attenuation model describing the effect at any site given as a function of magnitude and source-to-site-distance. The seismicity model may comprise a number of source regions, the seismicity of which should be expressed in terms of a recurrence relationship of events with magnitudes greater or equal to a certain value. The attenuation model relates the earthquake intensity (*i.e.* the effect of it, as a general term) at a site to magnitude, distance, source parameters and site conditions.

For forecasting seismic occurrences numerous models have been developed. The simplest stochastic model for earthquake occurrences is the homogeneous poisson model, which is used in this study.

Poisson model is the most commonly employed stochastic model for modeling the distribution of times between successive earthquakes. Poisson model does not have a memory, or, in other words, the rate of occurrence is independent of the time of the past earthquake and is determined only by the average frequency (rate) of past earthquakes. As such, it fails to incorporate the basic elements of earthquake physics, such as the rebound theory. Poisson model is known to be generally applicable for large areal seismic sources or background source zones and may not accurately represent the earthquake occurrences associated with individual faults or fault source zones. For these faults, with sufficient

information on paleo-seismicity and strain rates, the earthquake occurrence models that account for the past activity of large magnitude (characteristic) earthquakes should be considered.

Generally, the Poisson model is taken into the consideration to be the standard model for PSHA and it is utilized for the preparation of a multitude of national, regional and international seismic hazard maps (*i.e.* Frankel, 1997; GSHAP, 1997; SESAME, 2000).

The probability density function associated with the Poisson model is given by:

$$f_P(t) = \lambda[Y > y] \times e^{\lambda[Y>y]\times t} \tag{2.1}$$

Where $\lambda[Y>y]$ is the mean annual rate of exceedance as provided by Equation 2.1 Note that in the Poisson model λ is constant and does not change with waiting period since the past earthquake.

Return period $RP(\Delta T)$ is defined by:

$$RP(\Delta T) = 1/\lambda[Y_{\Delta T} \geq y] = -\Delta T/[\ln(1 - P(Y_{\Delta T} \geq y))] \tag{2.2}$$

Obviously for the above assumptions to be applicable to a data set, it should be free of fore- and aftershocks. This has been achieved in our study by removing all the dependent events from the earthquake catalogue.

The recurrence relationship of the events is expressed with the help of the empirical relationship first defined by Gutenberg - Richter: $\log N = a - bM$ where N is the number of shocks with magnitude greater or equal to M per unit time and unit area, and a and b are seismic constants for any given region. The source regions may be described as lines representing the known faults or areas of diffuse seismicity, so that M may be related to unit length or unit area. The value of N will also generally be found assuming that M has upper and lower bounds M_1 and M_o.

Using an application of the total probability theorem, the probability per unit time that the estimation of frequency of exceeding a specified ground motion level, a*, at a site due to an earthquake that occurs on a given fault/source (McGuire, 1993). The total seismic hazard (or frequency of exceedance of level a^* for the ground motion parameter, (A) at a site for source *i* is obtained by summing the contribution from all the active seismic sources:

$$\lambda[A > a^*]_i = \sum_i v_i \int_m \int_r P\left(A > a^* \middle| (m,r)\right) f_M(m) f_R(r|m) dm dr \tag{2.3}$$

Where M refers to earthquake magnitude, R refers to the distance between the source and the site, and where $f_M(m)$ and $f_R(r)$ represent probability density functions for M and R, respectively. The term $P\left(A > a^* \middle| m,r\right)$ may be computed by using the ground motion attenuation model selected.

2.2. Active Tectonics in Turkey

Turkey is a tectonically active region that experiences frequent destructive earthquakes. In a tectonic map, Turkey is located in the Mediterranean sector of the Alpine- Himalayan orogenic system, which runs west-east from the Mediterranean to Asia. The seismic activity of the Mediterranean region can be explained with the plate tectonics theory, with the relative motions of the three main plates of the region, that are Africa, Eurasia, and Arabia, and two generally acknowledged minor plates: Aegean and Anatolian. The general view of the plate tectonics theory may be defined briefly as follows:

The lithosphere, which is the earth's crust and upper mantle, are broken into sections called plates. Plates move around on top of the mantle like rafts. There are two types of plates: Ocean Plates below the oceans and continental Plates below the continents.

Figure 2.2 presents the double lines pointing out the zones spreading from the plates which are moving apart. The lines with barbs show zones under thrusting (subduction),

where one plate is sliding beneath another. The barbs on the lines indicate the overriding plate. The single line defines a strike-slip fault along which plates are sliding horizontally past one another. The stippled areas indicate a part of a continent, exclusive of that along a plate boundary. There are three primary types of tectonic plate boundaries: divergent boundaries; convergent boundaries; and transform boundaries (http://csmres.jmu.edu/geollab/fichter/PlateTect/plateboundry.html).

At divergent boundaries, the plates separate from each other, and magma goes up from the mantle into the crack (a fissure volcano) making the ocean basin wider. This is known as sea floor spreading. As an example, Iceland is splitting along the Mid-Atlantic Ridge - a divergent boundary between the North American and Eurasian Plates. As North America moves westward and Eurasia eastward, new crust is created on both sides of the diverging boundary. While the creation of new crust adds mass to Iceland on both sides of the boundary, it also creates a rift along the boundary.

At transform boundaries, two plates are sliding horizontally past each other. Most transform boundaries are found below the sea level. They commonly offset active spreading ridges, producing zig-zag plate margins, and are generally defined by shallow earthquakes. The San Andreas Fault in California is a transform boundary that connects the East Pacific Rise, a divergent boundary to the south, with the South Gorda and Juan de Fuca Explorer Ridge, another divergent boundary to the north.

At convergent boundaries, plates come together, but to do so one of the plates must dive below the surface into the mantle along a subduction zone. Convergent boundaries produce mountain chains of very large, explosive volcanos (composite type). There are three types of convergent boundaries: Oceanic-Continental Convergence; Oceanic-Oceanic Convergence; and Continental-Continental Convergence.

When an oceanic plate pushes into and subducts under a continental plate, the overriding continental plate is lifted up and a mountain range is created. These types of convergent boundaries are called Oceanic-Continental Convergence. On the other hand, when two oceanic plates converge one is usually subducted under the other and in the process a deep oceanic trench is formed. The Marianas Trench, for example, is a deep

trench created as the result of the Phillipine Plate subducting under the Pacific Plate. Oceanic-oceanic Plate convergence also results in the formation of undersea volcanoes. Over millions of years, however, the erupted lava and volcanic debris pile up on the ocean floor until a submarine volcano rises above sea level to form an island volcano. Such volcanoes are typically strung out in chains called island arcs.

When two continents meet head-on, neither are subducted because the continental rock are relatively light and, like two colliding icebergs, resist downward motion. Instead, the crust tends to buckle and be pushed upward or sideways. The collision of India into Asia 50 million years ago caused the Eurasian Plate to crumple up and override the Indian Plate. After the collision, the slow continuous convergence of the two plates over millions of years pushed up the Himalayas and the Tibetan Plateau to their present heights. Most of this growth occurred during the past 10 million years.

Turkey geologically is part of the great Alpine belt that extends from the Atlantic Ocean to the Himalaya Mountains. This belt was formed during the Tertiary Period (about 65 million to 1.6 million B.C.), as the Arabian, African, and Indian continental Plates began to collide with the Eurasian Plate. This process is still at work today as the African Plate converges with the Eurasian Plate and the Anatolian Plate escapes towards the west and southwest along strike-slip faults. These are the North Anatolian Fault Zone, which forms the present day plate boundary of Eurasia near the Black Sea coast and, the East Anatolian Fault Zone, which forms part of the boundary of the North Arabian Plate in the southeast. As a result, Turkey is one of the world's most active earthquake and volcano regions.

Turkey is surrounded by three major plates: African, Eurasian, and Arabian, and is located on two generally acknowledged minor plates: Aegean and Anatolian, as shown in Figure 2.3 (McKenzie, 1970). The relative motion between Eurasian, Arabian Plates and the westward motion of the Anatolian-Aegean Block is also illustrated in Figure 2.6 and Figure 2.7 (Armijo *et al*., 1999 and Armijo *et al*., 2005).

Various plate tectonic models such as McKenzie (1972 and 1970), Dewey *et al.* (1972), Alptekin (1973), and Papazachos (1974) for the Eastern Mediterranean region have been proposed.

According to McKenzie (1972), in his widely accepted model, the region is divided into three additional small plates (Iranian, South Caspian and Black Sea) and two minor plates. His preliminary study of plate boundaries and motions are shown in Figure 2.3. The arrows indicate the directions of motion relative to Eurasia and their lengths are approximately proportional to the magnitude of relative velocity. The Africa Plate is moving northwards towards Eurasian Plate, pushing the Turkish Plate in a westward motion. The Anatolian Plate contains most of Turkey and Cyprus. The northern boundary of the Anatolian Plate is the North Anatolian Fault (NAF), which is an active east-west trending right-lateral strike slip fault. The southern part of the Anatolian Plate appears to join the southern boundary of the Aegean Plate extending to the southwest of Turkey and continue to the south of Cyprus into the Gulf of Iskenderun and to meet the East Anatolian Fault which is an active left strike - slip fault (Figure 2.3). McKenzie (1972) defines that the boundary between the Aegean and the Anatolian Plates in the west is a boundary slightly east of east – west trending graben complexes of Western Anatolia. On the contrary, Alptekin (1973) indicates the shortcomings of this boundary by reflecting the mechanism with which such a boundary causes the graben system in Western Anatolia and thus they come together as two plates and describe it as the "Aegean –Turkish Plate".

The Aegean Plate is moving towards the southwest relative to the European Plate, producing extension and strike-slip motion along the boundary between the two plates and the southern boundary of the Aegean Plate passes through the Helenic Trench and the Pliny /Strabo Trench complex, south of Crete and Rhodos, respectively (McKenzie, 1970 and Dewey and Sengor, 1979) and is characterized by thrust faults indicating the overriding of this plate onto the Africa Plate (Morelli, 1978 and Woodside, 1976).

The seismotectonic model proposed by Papazachos (1974) defined several other smaller blocks (plates) within the Aegean region due to the geographic distribution of the earthquakes occurred between 1901 and 1971 in addition to the fault solution of the earthquakes occurred between 1948 and 1969. From north to south, these blocks consist of

the Rhodopean, Olympus, Saros, Northern Anatolian, Western Turkey, Taurus and Aegean.

An alternative solution for the Aegean tectonics is proposed by Dewey and Sengor (1979). Quite the opposite of the McKenzie model, the west of the Anatolian Plate is defined as the Peloponnisian Plate whose boundary is ripped off from the Black Sea Plate as a result of the obstructive locking geometry caused by the bending of the Anatolian Fault in the Northern Aegean. This boundary is also defined as the Macedonian Plate.

The Arabian Plate, although thrusting under the Van Plate along the Zagros and the Bitlis Zones, is pushing the Van Plate north and wedging the Turkish Plate westward along the Anatolian Fault (Dewey *et al*., 1973). The northward motion of the Arabian Plate is also taken up by the thrust faults associated with the Caucasus. The result of the geometry is the thickening of the continent throughout the region and the continuous elevation of the Caucasus.

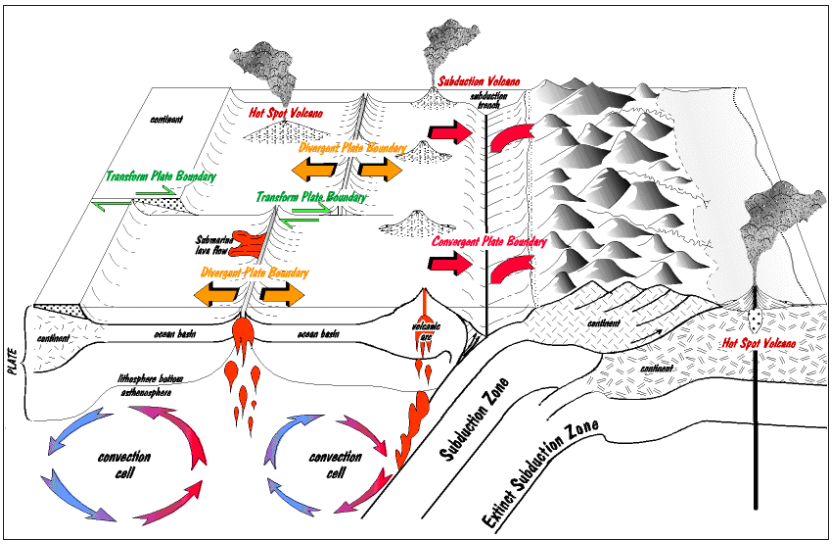

Figure 2.1. Structure of the earth and tectonic plates

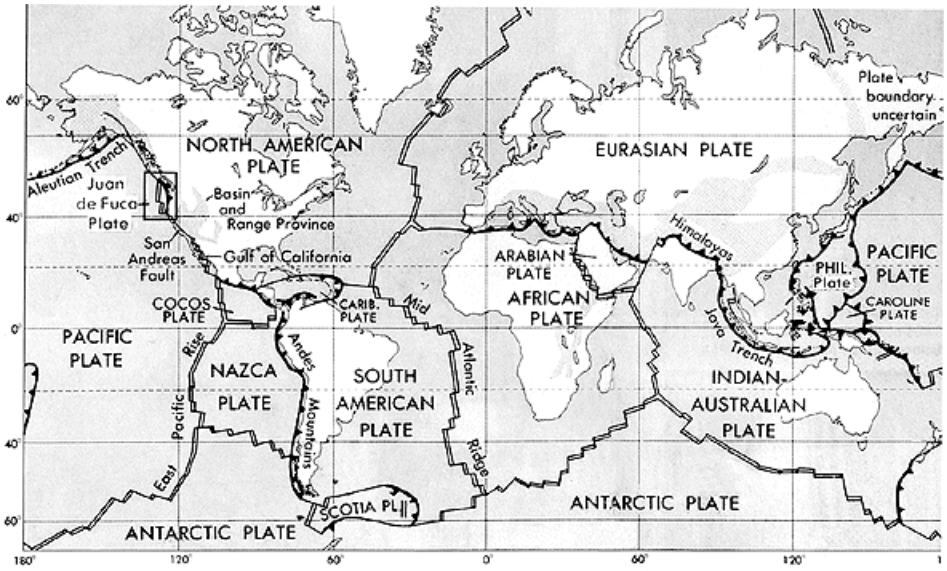

Figure 2.2. The boundaries of lithosphere plates that are active at present (U.S. Geological Survey)

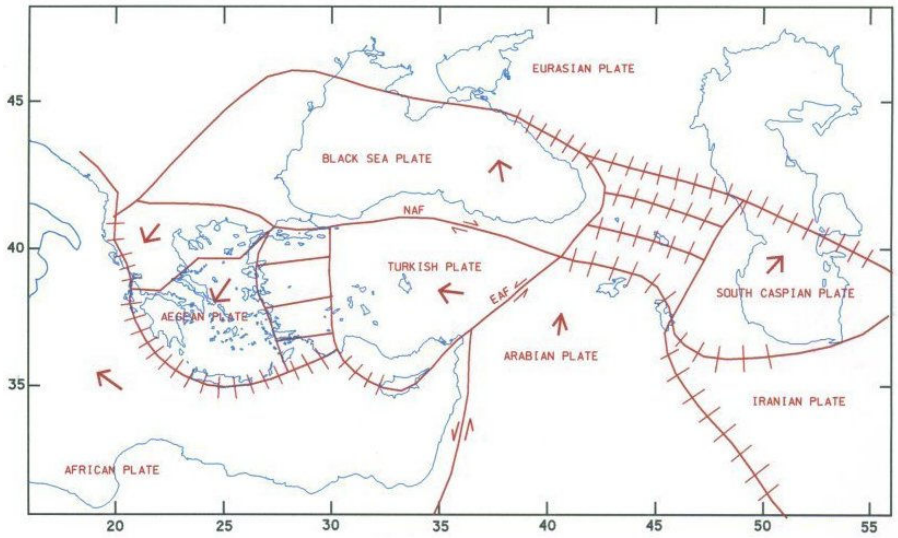

Figure 2.3. Plate tectonics of the Eastern Mediterranean and Caucasus regions (after McKenzie, 1970)

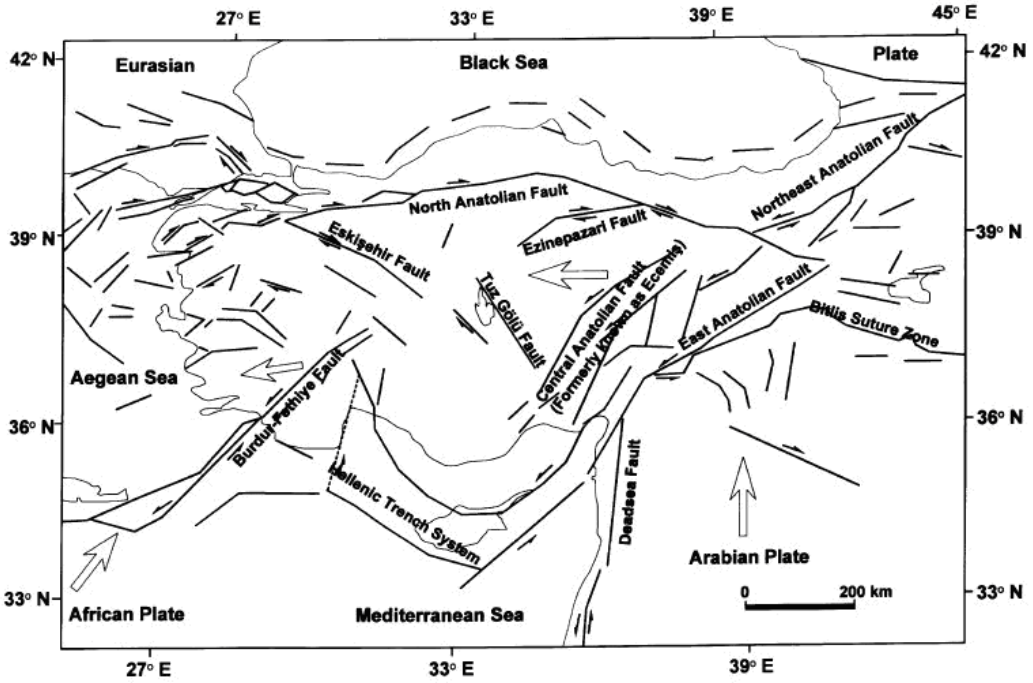

Figure 2.4. Map of tectonics of Turkey compiled by Yaltirak *et al*. (1998)

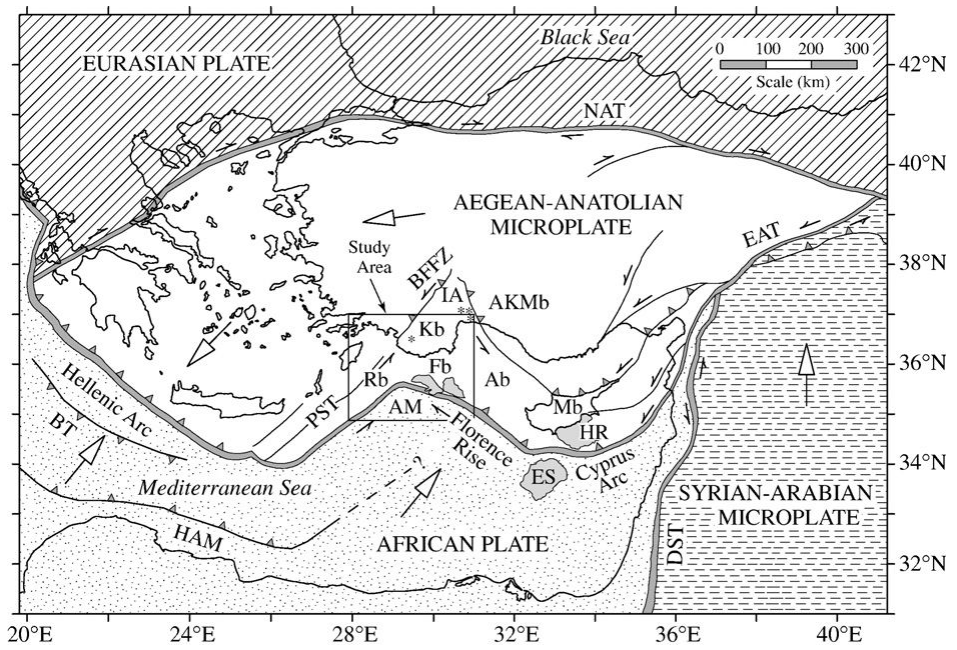

Figure 2.5. Simplified tectonic map of the eastern Mediterranean Sea and surrounding regions, compiled from Şengör and Yılmaz (1981), Dewey *et al*. (1986) and Ten Veen *et al*. (2009)

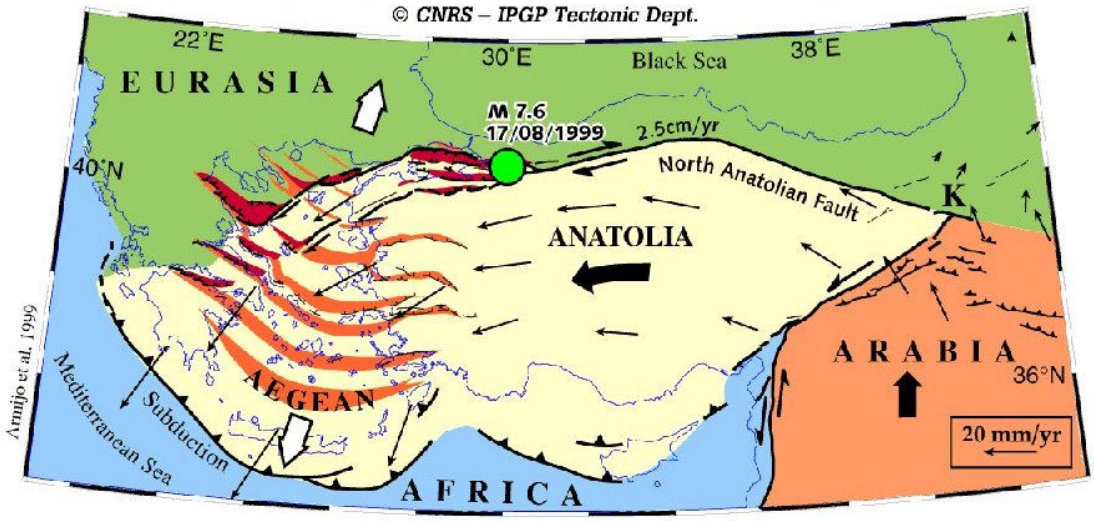

Figure 2.6. The relative motion between Eurasian and Arabian Plates and the westward motion of the Anatolian and Aegean Blocks (Armijo *et al*., 1999)

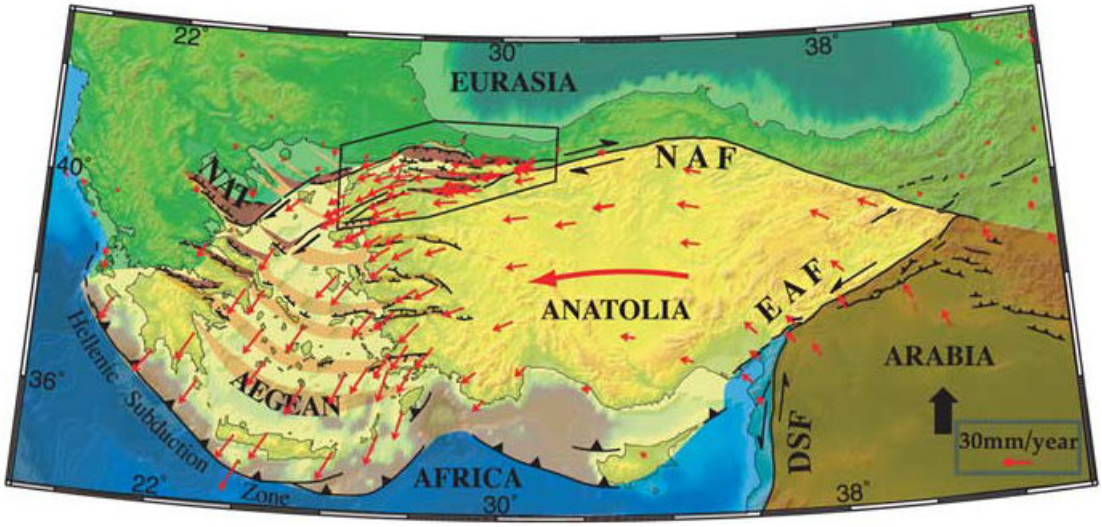

Figure 2.7. The relative motion between Eurasian and Arabian Plates and the westward motion of the Anatolian and Aegean Blocks (Armijo *et al*., 2005)

The Global Positioning System (GPS) has become a very useful tool in the area of earth sciences because of its capability that provides high precision assessment of continental and regional deformation (Segall and Davis, 1997; Herring, 1999; Tari, 1999). GPS measurements carried out in Turkey during the period of 1988-1994 expose valuable knowledge about the rate of motion of the plates relative to one another in the region along

major faults (Barka *et al*., 1997; Barka & Reilinger, 1997, McClusky *et al*., 2000). The results can be summarized as follows:

The Arabian Plate is moving in a north-northwest direction relative to Eurasia at a rate of about 25 mm/yr, 10 mm/yr of this rate is taken up by shortening in the Caucasus. Resulting in a continental collision along the Bitlis –Zagros fold and thrust belt, this motion is thought to cause intense seismic activity (Figure 2.8, Barka and Reilinger, 1997).

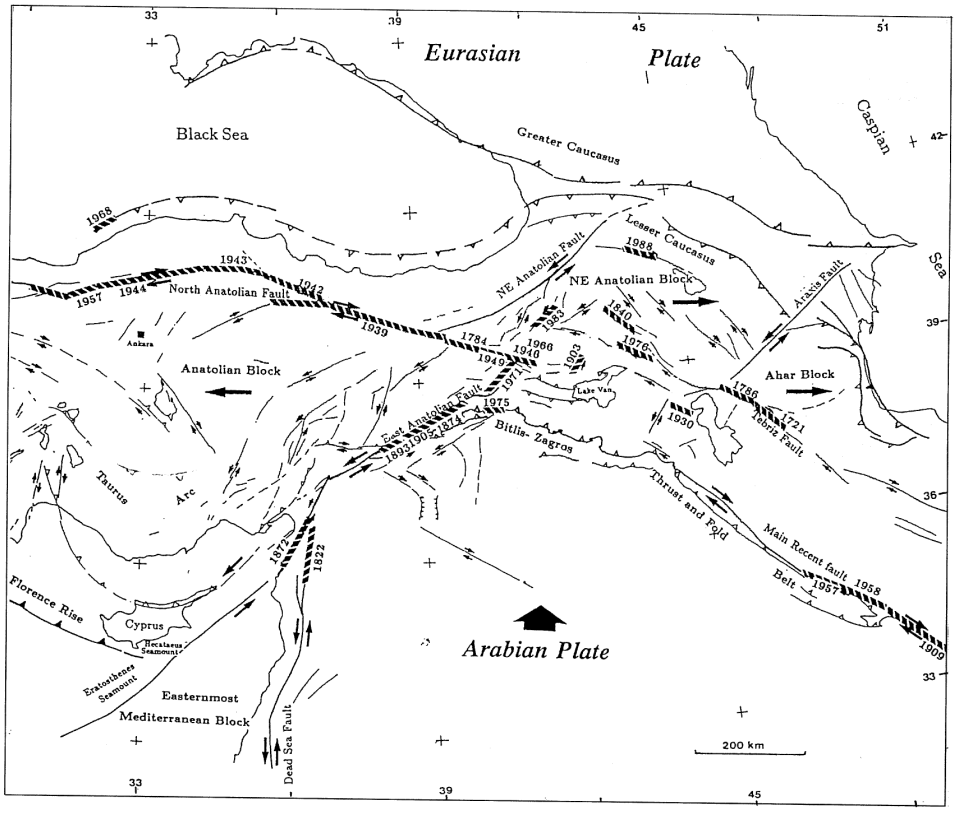

Figure 2.8. The Active tectonic features of the Eastern Mediterranean region (Barka and Reilinger, 1997)

The African Plate is moving in a northerly direction relative to Eurasia, at a rate of about 10 mm/yr. The differential motion between Africa and Arabia (~15 mm/yr) is thought to be taken up predominantly by left-lateral motion along the Dead Sea transform fault (*e.g*. Freud *et al*., 1970). GPS velocities for the two sites situated south of the Bitlis suture both indicate NW oriented motion relative to Eurasia (18±5 mm/yr), (Reilinger *et*

al., 1995, Reilinger *et al*., 1997, McClusky *et al*., 2000) fairly slower, but not statistically different from NUVEL 1 A estimates (24±6 mm/yr, Figure 2.9)

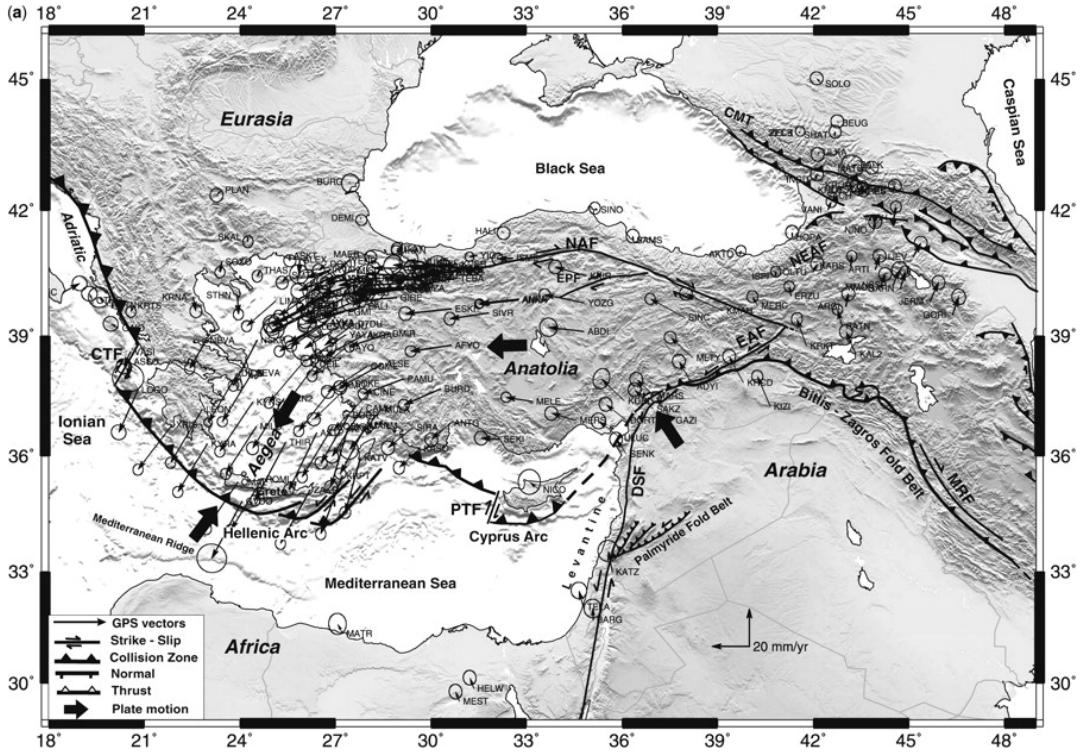

Figure 2.9. GPS measurements results with fault and bathymetry in the Eastern Mediterranean region (Taymaz *et al*., 2007)

The North-South motions mostly in the eastern Black Sea are in a few mm/yr, while the velocities in the Anatolian region are approximately 10–20 mm/yr (Tari *et al*., 2000). The GPS derived slip rate on the North Anatolian Fault is found to be 24 ± 1 mm/yr (McClusky *et al*., 2000) while the geologically derived slip rate amounts to 16/24 ±5 mm/yr (Reilinger *et al*., 2006). The Northeast Anatolian Fault, which extends from the Erzincan Basin to Caucasus, accommodates about 8 ± 5 mm/yr of left-lateral motion. Central Anatolia behaves as a rigid block and moves westward relative to Eurasia at about 15 mm/yr (Oral *et al*., 1995). Western Anatolia moves in a southwest direction at about 30 mm/yr. The Western Anatolian Grabens take up a total of 15 mm/yr of the NE-SW extension. Eastern Anatolian Fault accommodates an 11± 1 mm/yr relative motion.

2.2.1. Major Regional Tectonic Entities

The tectonic structure of Turkey can be investigated as separate regions. The division made herein consists of North Anatolian Fault Zone, East Anatolian Fault Zone, Eastern Mediterranean region, Central Anatolian region, Black Sea, Marmara Sea region, Aegean region, Dead Sea, Cyprus Arc and Northeast Anatolian region (Figure 2.10).

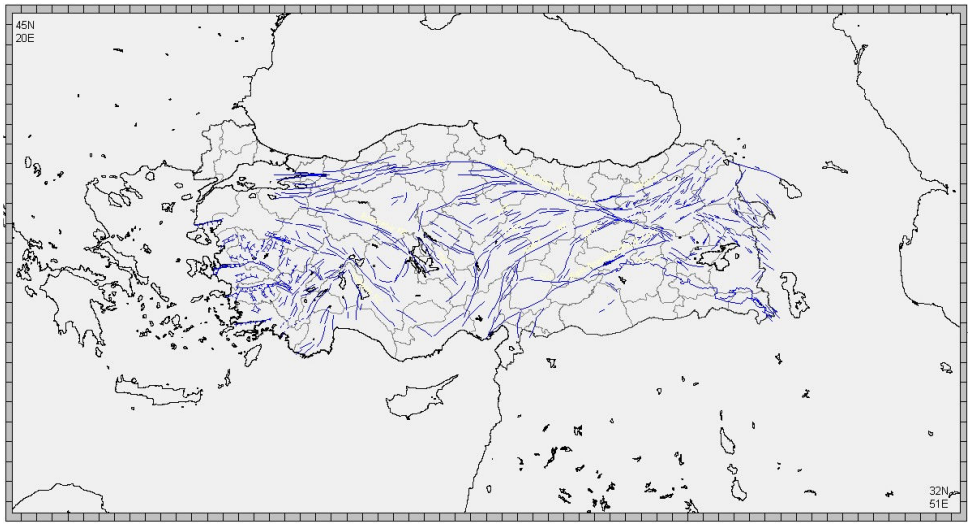

Figure 2.10. The fault map of Turkey (E. Bozkurt (2002) model)

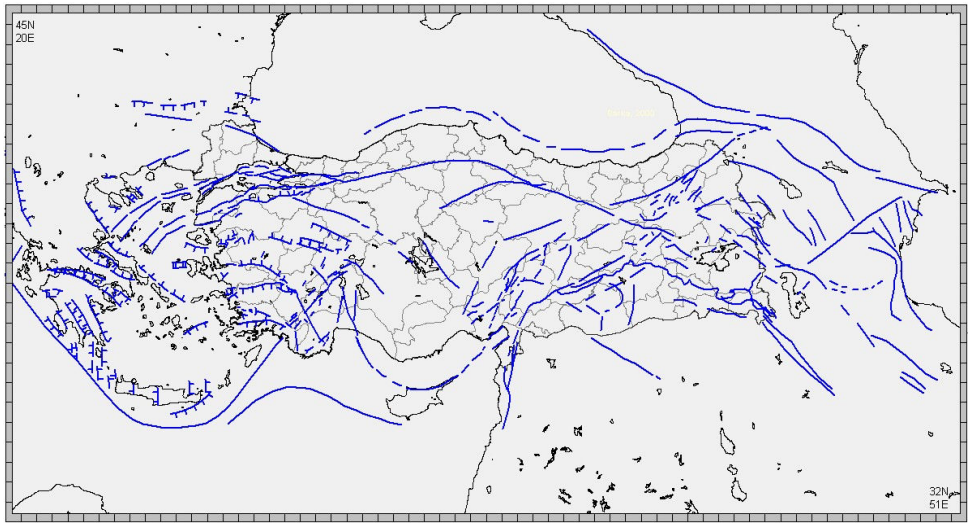

Figure 2.11. The fault map of Turkey (A. Barka (2002) model)

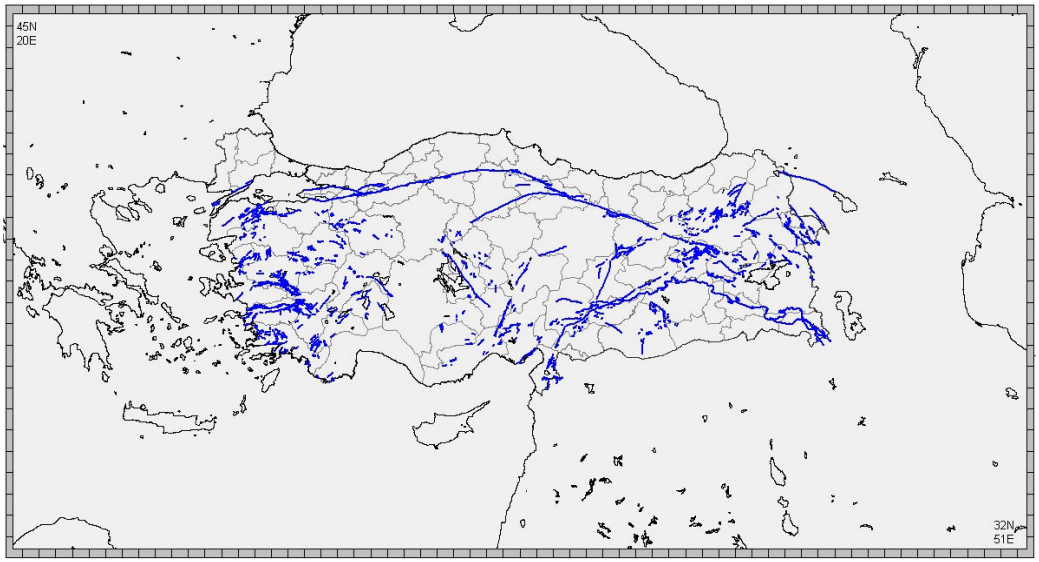

Figure 2.12. The fault map of Turkey (Saroglu *et al.,* (1992) model)

2.2.2. Tectonic Elements of the North Anatolian Region

The North Anatolian Fault Zone (NAFZ) is an intra-continental and seismically active right-lateral strike slip transform fault, extending 1500 km from Karliova in Eastern Turkey (Hubert-Ferrati *et al.*, 2002; Sengor *et al.*, 200) through northern Anatolia to mainland Greece as a broad shear zone (termed the Grecian Shear Zone by Şengör 1979a). It takes up the relative motion between the Anatolian and Eurasian Plates (Ketin, 1948, Şengör *et al.*, 1985; Barka, 1992; Şaroğlu, 1988). The NAFZ does not stop at the Karliova triple junction but, goes on towards south- east way (Tchalenk, 1977). The triple junction has migrated westward and so strike slip faulting occurred east of Karliova before the triple junction migrated to its present position (Westaway and Arger, 1996). During two successive earthquakes in 12 and 20 August 1966 with magnitude M6.8 and M6.2, respectively, this section has ruptured (Ambraseys *et al.*, 1968, Ambraseys, 1988; Figure 2.13). The subject of the Karliova triple junction, which is the eastern termination of NAF, is discussed in the tectonics of the East Anatolian region.

The NAF has an extremely well developed surface expression along most of its length. A sequence of earthquakes starting with the 1939 Erzincan Earthquake in the east and propagating westward for over 800 km activated the North Anatolian Fault between

1939 and 1999 (Figure 2.13). The fault break associated with the 1939 Erzincan Earthquake of magnitude about eight, was 350 km long displaying a maximum right-lateral movement larger than six meters and then the NAFZ ruptured by nine moderate to large earthquakes (M>6.7), and formed more than 1000 km surface rupture along the fault. These earthquakes occurred sequentially in a westward progression, consist of 26 December 1939 Erzincan (M7.9), 20 December 1942 Erbaa-Niksar (M7.1), 26 November 1943 Tosya (M7.6), 1 February 1944 Bolu-Gerede (M7.3), 26 May 1957 Abant (M7.0), 22 July 1967 Mudurnu valley (M7.1), 13 March 1992 Erzincan (M6.8), 17 August 1999 Kocaeli (M7.4), and 12 November 1999 Düzce Earthquakes (McKenzie, 1970; Ketin, 1963, Ambraseys, 1970; Dewey, 1976; Barka *et al*., 2000; Kocyigit, 1986, 1988, 1989; Pamir, 1941; Wrigth *et al.*, 2000; Parsons *et al*., 2000).

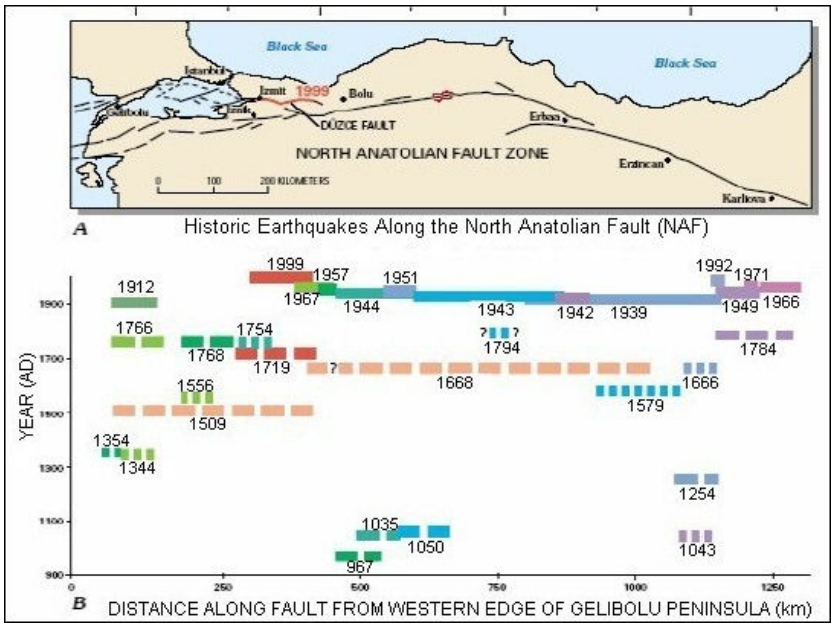

Figure 2.13. Historical Earthquakes along the North Anatolian Fault (NAF), (Barka and Kadinsky-Cade, 1988)

The NAF splits into two major strands, the northern and the southern (Wong *et al.*, 1995), and extends in a broad zone in the Marmara region (Figure 2.13). The analysis and distribution of historical earthquakes show that among the two westernmost branches of the NAFZ, it is the northern strand that is the most active one that has accommodated more large earthquakes. The Northern boundary fault enters the Sea of Marmara through the axis

of Izmit fault in the east and appears in Thrace in the west, forming the Ganos Fault. On the other hand, the southern boundary fault runs in an east- west direction and bounds the southern margin of Izmit Bay (known as Gölcük and Yalova segments). Moreover, Stein *et al*. (1997) envisaged that the city of Izmit was the most vulnerable location to a large earthquake on the Sapanca fault segment. Their study gave a 30-year probability (between 1996-2026) for a M>6.7 earthquake of 12 per cents. This probability was higher by a factor of 1.07 since the 1967 earthquake occurred which transferred its stress to the Izmit area. Stein also stated that the Yedisu segment on the eastern portion of the NAFZ had a 30-year probability (between 1996-2026) of a M>6.7 earthquake of 15 per cent. This probability was higher by a factor of 1.35 since the 1992 earthquake occurred. In addition, Stein *et al*. (1997) considered the historic earthquakes and detected a general pattern of progressive failure along the fault zone. This is thought to occur as each earthquake transfers its stress to another region along the fault zone. Figure 2.14 shows the relationship between the earthquakes and their stress accumulation laterally through the years.

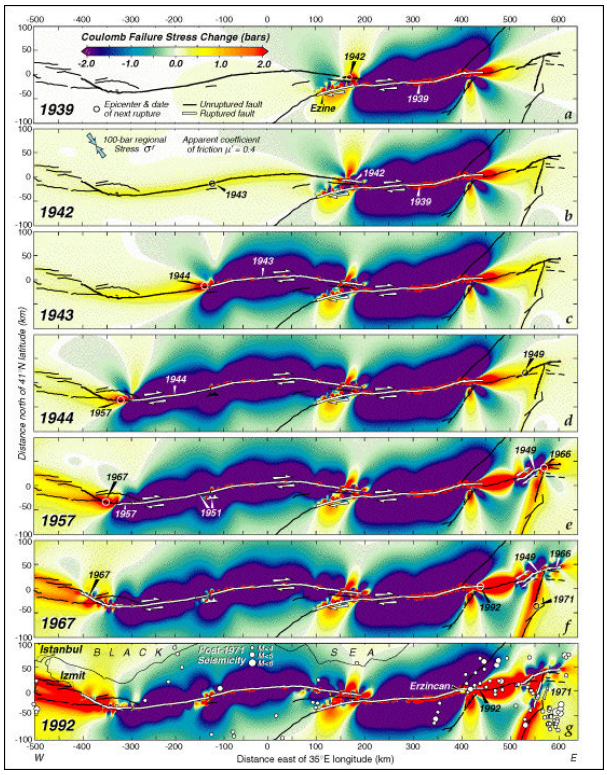

Figure 2.14. Cumulative stress changes stress changes caused by earthquakes on the NAFZ since 1939

2.2.3. Tectonic Elements of the Marmara Region

NAFZ extending in the Sea of Marmara have a more complex structure. Several researches have developed different tectonic models for NAF Marmara Sea region.

Le Pichon *et al.* (2001, 2003), Aksu *et al.* (2000), Imren *et al.* (2001), Gokasan *et al.* (2001), Kuscu *et al*. (2002), Alpar and Yaltirak (2002), and Demirbag *et al.* (2003) proposed that the NAF was composed of a pure right-lateral fault system along the trough of the Northern Marmara Sea. However, Armijo *et al.* (1999, 2002), Barka and Kadinsky-Cade (1988), Barka (1992), Stein *et al.* (1997), Okay *et al.* (2004), Parke *et al.* (2002), Flerit *et al.* (2003) and Polonia *et al*. (2004) proposed that the Sea of Marmara was a pull-apart basin formed by the right step-over between the strike-slip faults of Ganos and Izmit, further the normal faults in the Cinarcik Basin and the Central Marmara Sea were also active. Another alternative structural model is defined that NAF was composed of a pull a part system produced by fault segmentation, oversteps and slip partitioning (Armijo *et al.,* 1999; Armijo *et al.,* 2002; Barka and Kadisky-Cade, 1988; Barka, 1992; Stein e*t al.,* 1997; Okay *et al.,* 2000; Parke *et al*., 2002; Flerit *et al.,* 2003; Polonia *et al.,* 2004).

The North Marmara Basin is located by the conspicuous 70-km-wide step-over between two strike-slip faults, well-known on land, which have ruptured with purely right-lateral motion during recent earthquakes, both with similar magnitude (M 7.4) and clear surface rupture. One is the 1912 Ganos Earthquake that ruptured the Dardanelles region to the west of the Marmara Sea; the second is the Izmit Earthquake that ruptured in 1999 east of the Marmara Sea. Pinar (1943) had previously drawn a single fault, bisecting the Gulf of Izmit and the three Marmara deeps. Thus, this fault was named “the Main Marmara Fault”, which is located as an arc of great radius, going from Ganos to the entry of the Gulf of Izmit”. Based on the recent high resolution bathymetric and deep-tower seismic reflection data set acquired by the MARMARASCARPS CRUISE in 2000, Armijo *et al*. (2005) found out that the surface ruptures formed by the 1912 Ganos (Sarkoy-Murefte) Earthquake reached the eastern end of Central Basin, and also the fault scarps associated with the 1894 earthquake could be estimated in the southern edge of the Cinarcik Basin (Figure 2.15).

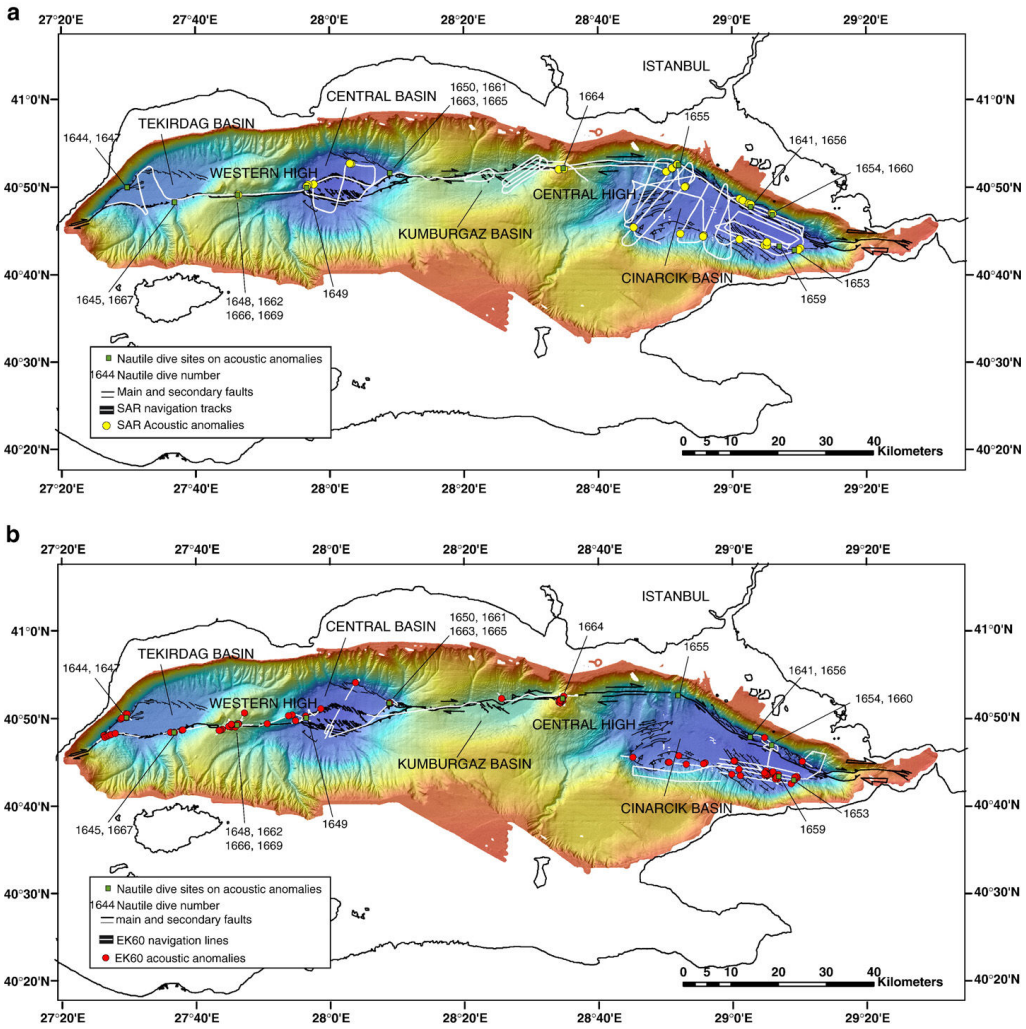

Figure 2.15. Distribution of acoustic anomalies, superimposed on the bathymetric map (Rangin *et al*., 2001, Armijo *et al.*, 2002; 2005; Imren *et al*., 2001, Le Pichon *et al*., 2001) of the deeper parts of the Marmara Sea

2.2.4. Tectonic Elements of Western Anatolian Region

Western Turkey, together with its western prolongation in the Aegean region, is situated in a remarkably deforming part of the Alpine- Himalayan orogenic belt, where diffuse extension is now occurring in a wide area along a number of sub-parallel normal faults bounding graben complexes.

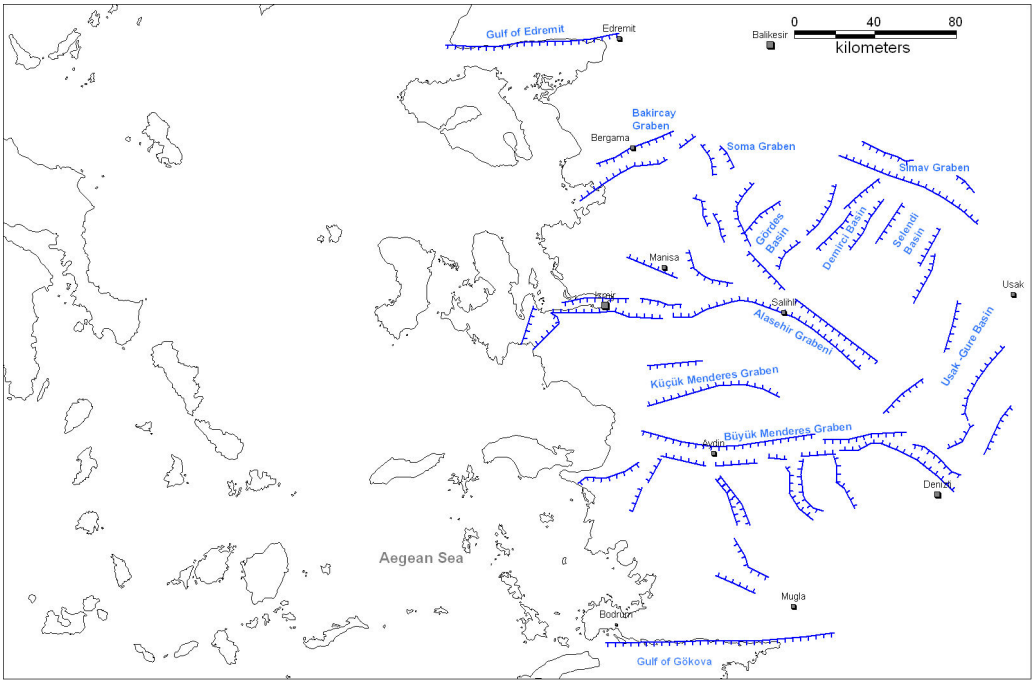

Figure 2.16. The fault system in the Aegean region

Figure 2.16 shows the E-W trending grabens such as Edremit, Bakırçay, Kütahya, Simav, Gediz, Küçük Menderes, Büyük Menderes, and Gökova Grabens. These and their basin- bounding active normal faults are the most prominent neotectonic features of Western Turkey. On the other hand, less prominent, structural elements of Western Turkey are the NNE-trending basins and their intervening horsts such as Gördes, Demirci, Selendi, and Uşak-Güre Basins (Figure 2.16; Bozkurt, 2001).

The Menderes Massif is comprised of large, coherent blocks that respond as rigid bodies during tectonic deformation; thus it plays a significant role in the regional tectonics affecting in the vicinity of the Aegean region. The massif is subdivided into four submassifs by the Büyük Menderes, Küçük Menderes, and Gediz Grabens and the smaller Simav Graben to the northeast of İzmir. These grabens control the major west-flowing consequent surface drainage of the Western Anatolia.

Even though there is no evidence on the active faults that could create a high earthquake activity except Gediz Graben, both historical and instrumental seismicity is rather dense between Karaburun–Chios (Sakiz), İzmir Bay-Lesbos (Midilli) and

Doğanbey-Samos (Sisam). The principal faults that were observed from both satellite images and site investigation can be summarized as; Dumanlıdağ, Bornova, İzmir, Cumaovası, Karaburun, Gümüldür, Tuzla Faults and western part of the Gediz Graben. (Figure 2.16).

Karaburun Fault is the major structure separating İzmir Bay from Karaburun Peninsula. The northern margin of Karaburun is near the macroseismic epicenter of the Chios Earthquake of 1949 and comprises a north-dipping topographic and bathimetric escarpment. Northwest-southeast trending Dumanlıdağ Fault Zone takes place in the northern part of the Menemen and can be accepted as the western continuation of the Manisa fault segments. Fault traces are clear from the aerial photographs. Due to the young morphological structure of the region the fault is assumed to be active.

There are no information on activity and characteristics of the Bornova Fault. It extends from northwest to southeast and takes place in the northwestern part of the Izmir Bay.

Cumaovası Fault takes place between Gediz Graben System and Tuzla Fault. It connects to the southern branch of Gediz Fault in the east and shows strike-slip mechanism. Even though there is no sufficient information, the microseismic epicenter shows that the March 21, 1928 Earthquake could have taken place on this fault.

East west trending normal Izmir Fault extends from Izmir Bay to Kemalpaşa and forms the southern boundary of the Izmir Bay. It is composed of two parts and assumed to be the western continuation of the Kemalpaşa Fault. According to the Ergin *e. al.* (1967), and Ambraseys and Finkel (1995) July 10, 1668 Earthquake was associated with this fault.

2.2.5. Tectonic Elements of the East Anatolian Region

The EAFZ was first described by Allen (1969) and mapped by Arpat and Saroglu (1972), Seymen and Aydin (1972), Arpat and Saroglu (1975), Saroglu *et al.* (1992), and Imamoglu (1993). The EAFZ runs in a northeasterly direction, starting from the Maraş triple junction at the northern end of the Dead Sea Transform, and terminating at the

Karlıova triple junction where it meets the North Anatolian Fault. It also extends to the Amik Basin near Antakya (Arpat and Şaroğlu, 1972; Perinçek and Cemen, 1990; Şaroğlu *et al.*, 1992; Over *et al.*, 2004a) or the Gulf of Iskenderun through Osmaniye, Yumurtalık (McKenzie, 1972; Jackson and McKenzie, 1988). The NAFZ runs approximately 1400 km from its interaction with the EAFZ in the east to the northern Aegean in the west. The NAFZ and EAFZ are two of the most active continental transform fault zones in the world and constitute high-risk zones in Turkey (McKenzie, 1972; Sengor, 1979; Dewey and Sengor, 1979; Bellier *et al.*, 1997). However, other studies maintain that these faults are not part of EAFZ.

The boundary between the Arabian and the African Plates is formed by the 1000 km (*e.g.*, Erdik *et al.*, 1980; Garfunkel *et al.*, 1981; Gursoy *et al.*, 2003) long north-south trending left-lateral transform referred to as the Dead Sea Transform (DSFZ)). It extends from the Gulf of Aqaba to the Maraş triple junction (Figure 2.17) where it intersects with the East Anatolian Fault (Figure 2.18). Westaway (1994) said that the DSFZ can be divided into three parts: the Zone's north-trending northern and southern parts north of ~34.5N and south of ~33.5N, and the ~N30E trending central part. In addition, the DSFZ becomes braided north of 36.5 latitude into three main fault segments comprising the (1) Amanos Fault Zone (AFZ) in the west, which is believed to have formed the main strands of the Africa-Arabian boundary (Erdik *et al.*, 1980; Yurtmen *et al.*, 2002) (2) East Hatay Fault, and (3) Afrin Fault (Tatar *et al.*, 2004). According to Yurtmen *et al.* (2002), the most subsequent strike slip has occurred to the east of the Karasu Rift and Amanos Rang, and sidesteps onto faults at the western margin of the Gaziantep Basin.

The northern section of the DSF is observed along the Yammouneh and Misyaf fault which extend between a region near Syrian- Lebanon boundary in the south and Ghap Basin in the north. Ghap Basin (Figure 2.17) is a pull-apart basin consisted of two master faults (Ponikarov *et al.*, 1967; Muehlberger and Gordon, 1987; Matar and Mascle, 1993) and its eastern and the western margins is bounded by the Apamea fault (Meghraoui *et al.*, 2003) and by Nusayriyah Fault (Westaway, 2004), respectively. The Apamea fault is extended along the northern of Misyaf fault. The two faults that bound the Rouj Basin in the west of Ghap Basin are Armanez and Salkin (Westeway, 2004). The Armanez fault

passes from Harim, and evaporates in Karasu depressional area 3.5 km west of Reyhanlı. In the north, the fault is joined the Eastern Hatay Fault (Westaway, 2004).

The slip-rate along the DSF is known as 6-10 mm/yr in seismic moment calculations (Gali, 1999; Khair *et al.*, 2000), 10 mm/yr in plate tectonic modeling (Demets *et al.*, 1990) and 6.9 ± 0.1 mm/yr in the paleoseismological trench study on the Misyaf Fault in the northern section of the fault (Megraoui *et al*., 2003). However, according to the study conducted by Juteau *et al*. (1983), the velocity changes for the whole Red Sea are observed. These change were in 20mm/yr between 1.71 – 0.9 my interval and 30mm/yr for 0.89 – 0.69 my interval and 10.4 mm/yr for 0.69-present day interval.

The slip rate in the İskenderun – Antakya region is given as 6.8 ±.3 mm/yr in right lateral strike slip motion and 6.4 ± .3 mm/yr in extension (Reilinger *et al.*, 2006). The region is known to be seismically active, but because of the short length of the faults in the area, large earthquakes (with magnitudes greater than seven) are not historically known or expected. The historical database refers to several damaging earthquakes with magnitudes less than seven.

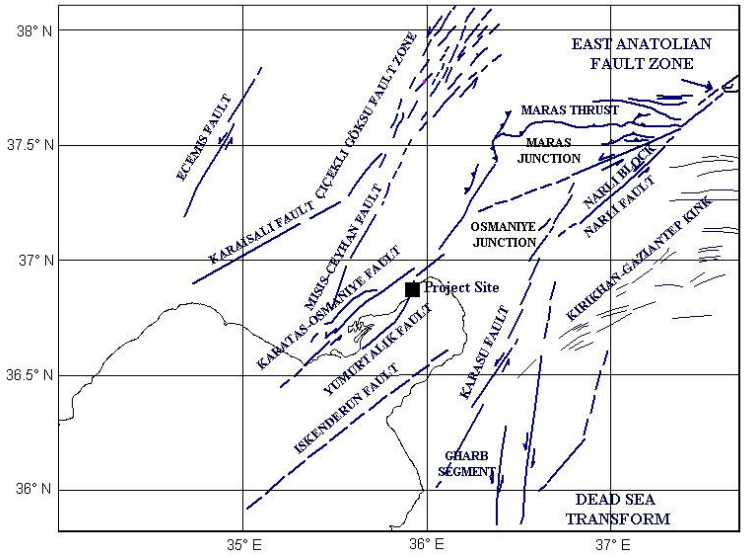

Figure 2.17. Active faults in Maraş triple junction area and distribution of earthquakes within the period 1901-1983 with M > 4.0 (Barka *et al.*, 1999, modified from Gülen *et al.*, 1988)

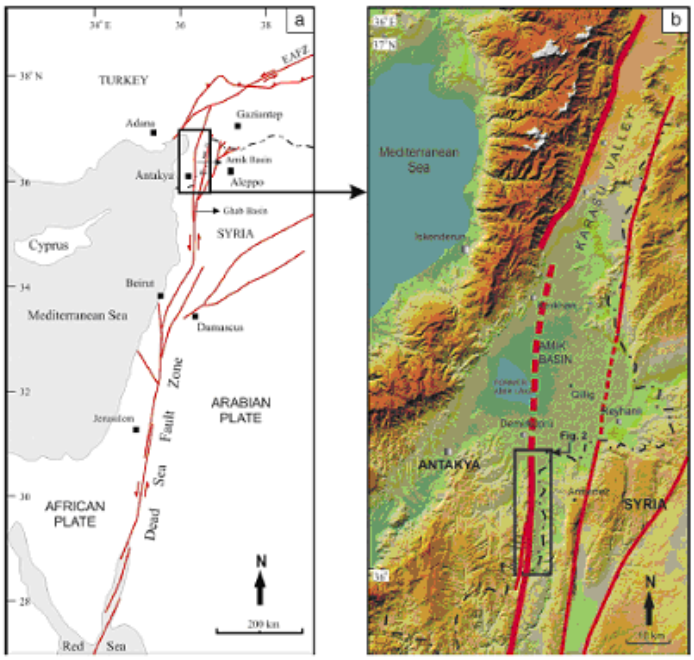

Figure 2.18. Main major fault system in the vicinity of Antakya region (Akyuz *et al*., 2006)

The probable age of the fault is Late Pliocene, while the total offset is assumed to be 20-25 km (Saroglu *et al.*, 1992). The slip rate along EAF is estimated based on geologic data as 11 ± 2 mm/yr which is in good agreement with the recent GPS derived slip rate of 10 ± 2 mm/yr (Reilinger *et al.*, 2006). Although the EAF is similar in many ways to the NAF, unlike the latter, the EAF has been relatively quiet in the 20th century when compared to historical records. Nalbant *et al.* (2002), used a sequence of 10 earthquakes from 1822 to 1971 (Table 2.1) in Coulomb stress modeling and identified the section of EAF between Kahramanmaraş and Malatya as a potential location for a future destructive earthquake (Figure 2.19). This segment is also associated with the historical earthquakes of 1114 and 1513.

Table 2.1. Seismicity along the East Anatolian Fault

Date	Mag.	Longitude	Latitude	Segment broken (reference)
1513	7.4+	37.5	36.5	Gölbaşı? (Ambraseys, 1989)
1544	6.7+	38.0	37.0	Elbistan? (Ambraseys, 1989)
1789, May.29	7.0+	39.0	40.0	Palu (Ambraseys, 1989)
1822, Aug. 13	7.5	36.7	36.9	Afrin (Ambraseys, 1989)
1866, May 12	7.2	39.2	41.0	Göynük (Ambraseys & Merville, 1995)
1872, Apr. 3	7.2	36.4	36.5	Doğu Hatay (Ambraseys, 1989)
1874, May 3	7.1	38.5	39.5	Palu (Ambraseys, 1989)
1875, Mar. 27	6.7	38.5	39.5	Şilo (Ambraseys, 1989)
1893, Mar. 2	7.1	38.0	38.3	Erkenek (Ambraseys, 1989)
1905, Dec. 4	6.8	38.1	38.6	Şiro (Ambraseys, 1989)
1949, Aug. 17	6.9	39.6	40.5	-
1964, June. 14	5.8			
1964, May. 5	5.8			
1966, Aug. 19	6.8	39.2	41.5	-
1971, May 22	6.8	38.9	40.5	Göynük Arpat, 1971
1986, June. 6	5.6			
1971, May. 22	7.0			Palu
2003, May. 1	6.4	39.00	40.44	
2005, Mar. 12	5.7	39.32	40.89	-
2005, Mar. 14	5.7	39.35	40.90	-
2005, June. 6	5.6	39.22	41.08	-
2007, Feb. 9	5.1	38.40	39.04	Şiro (DAF atlası, 2008)
2007, Feb. 21	5.7	38.36	39.29	-

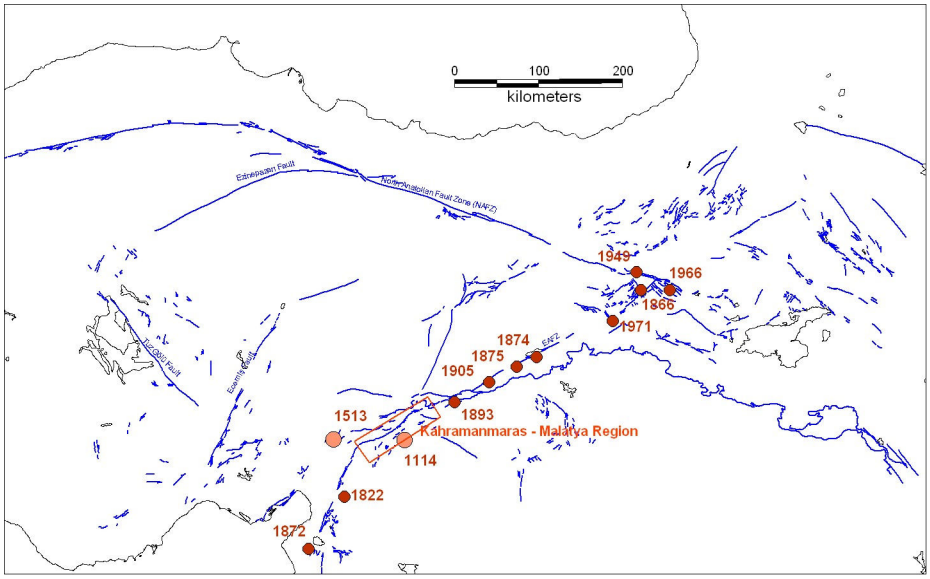

Figure 2.19. Earthquakes used by Nalbant *et al.,* (2002) in coulomb stress analysis overlain with the active fault map of Turkey (Saroglu *et al.*, 1987) Kahramanmaras – Malatya region is identified as a potential location for a future destructive earthquake

2.2.6. Tectonic Elements of Eastern Mediterranean Region

The Eastern Mediterranean region offers ideal examples of continental collision (*e.g.*, in Eastern Anatolia), ocean subduction (*e.g.*, along Helenic Arc) and transition between partly collision and partly subduction (*e.g.*, along the Cyprus Arc), moderate and extensive internal deformations within the overriding continental block (*e.g.* Anatolia).

The southwest boundary of the region is dominated by the Hellenic Arc—a zone of subduction where the African Plate moves under the Aegean Sea (Papazachos 1999). The Hellenic Arc contains the Hellenic Trench, the Hellenides mountain chain and an inner volcanic arc (Giunchi 1996). The Hellenic subduction zone ends at the Florence Rise, a submarine ridge (Scott 1981) that marks the starting of the Cyprus Arc, an area of apparent subduction in the past but which has since finished (Zitter *et al.*, 2000). This area between the Hellenic Arc and the Cyprus Arc has been characterized as "enigmatic" by Zitter *et al.* (2000). It shows transpressional deformation and strike-slip faulting. As the Cyprus Arc continues on inland leading into the East Anatolian Fault, an area of sinistral strike-slip motion that eventually terminates at the NAF.

The active tectonics of the eastern Mediterranean region is mainly dominated by the north-south post-collisional convergence between the African-Arabian Plates and the Eurasian Plate. The triple junction shaped by the Arabian, African and Anatolian Plates forms a large deformational region in the vicinity of Adana, Maraş and Antakya. The Dead Sea Transform, the East Anatolian Fault and the eastern section of the Cyprus Arc (which actually appears to continue into the Misis Mountains along the northwestern side of the Iskenderun Basin) form the boundaries of the Maraş triple junction. (Barka, 1999; Figure 2.17).

The boundary between the Arabian and the African Plates is formed by the 1000 km long north-south trending left-lateral transform referred to as the Dead Sea Transform. It extends from the Gulf of Aqaba to the Maraş triple junction where it intersects with the East Anatolian Fault. The Dead Sea Transform has been subject to numerous studies (*e.g*. Quennel 1958; 1959; Freund *et al.*, 1970; Garfunkel *et al.*, 1984). From these studies the current slip rate in the northern part of the Dead Sea Transform was found to be 0.5 cm/year, which is considerably low when compared to the slip rate in the southern part of it (1.1 cm/yr). The decrease is due to the Palmyra Kink where part of the strike-slip motion is taken up by folding and reverse faulting, and possibly by the northern part of Kırıkhan-Gaziantep Kink, although the effect of the latter is not documented yet (Figure 2.17).

The active faults in the Adana Basin are the Karataş-Osmaniye, Yumurtalık, Misis-Ceyhan and Kozan faults. The Karataş and Yumurtalık faults (Figure 2.17) are considered to be a continuation of the East Anatolian Fault. They form an angle of 25° with the Maraş-Osmaniye segment. The annual deformation is calculated to be around 8-9 mm. The slip rate in the İskenderun – Antakya region is given as 6.8 ± 0.3 mm/yr in right lateral strike slip motion and 6.4 ± 0.3 mm/yr in extension (Reilinger *et al*., 2006).

2.2.7. Tectonic Elements of Central Anatolian Region

The Central Anatolian Fault Zone (CAFZ) is an approximately 30-km-long, 2.0-80-km-wide megashear zone. It is a sinistral intra-continental transform fault zone, and is located between Ditizyayla Town to the northeast (DY) and the Eastern Mediterranean Sea floor near western Cyprus to the southwest. The CAFZ cuts across the Anatolian Plate and

divides it into two major blocks, the Central to West Anatolian block to the west and the Adana to Sivas, Munzur and Keban blocks to the east. It may have originated from the north-northeastward propagation of a paleotectonic structure, the so-called 'Ecemiş Corridor' on the Inner Tauride Suture Zone during the neotectonic period (Plio-Quaternary times).

The CAFZ is seismically active and total displacements along its paleotectonic and neotectonic segments are 75 km and 24 km, respectively. Rate of motion on the CAFZ is about 0.3 cm/yr.

The CAFZ consists of numerous segments based on geometric discontinuities including stepovers (offsets in the fault traces), bends and bifurcations. The major segments of the CAFZ are from northeast to southwest: (1) the Sivas segment (SS); (2) the Kızılırmak segment (KS): (3) the Gemerek-Şarkışla segment (GSS); (4) the Erkilet segment (ES); (5) the Yeşilhisar segment (YS); (6) the Kavlaktepe-Dikilita~ segment (KDS); (7) the Tecer segment (TS); (8) the Dökmetaş segment (DS); (9) the Dandar-Erciyes segment (Kocyigit and Beyhan, 1998).

The easternmost part of the Anatolian Plate is being deformed internally by several dextral to sinistral intraplate strike-slip faults. These are the Tuz Gölü Fault Zone (LSFZ), the Salanda Fault (SF), the CAFZ, the Göksu-Yazyurdu Fault Zone (GYFZ) and the Malatya-Ovacik Fault Zone (MOFZ). They take up lesser motion and are younger than boundary faults of the Anatolian Plate.

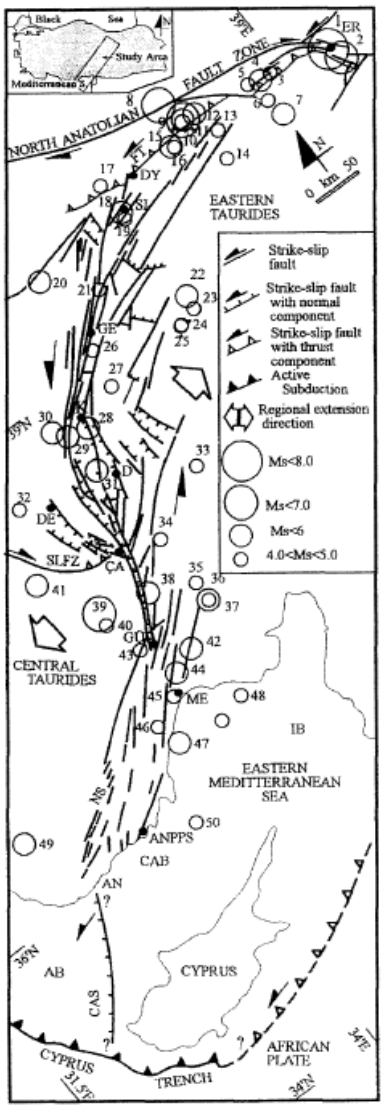

Figure 2.20. Simplified seismotectonic map of the CAFZ (Kocyigit and Beyhan, 1998)

Mainly there are three most prominent tectonic structures of the CAFZ: Alaca-Ezine Pazari Fault System, The Tuz Gölü Basin and Ecemis Fault Zone.

The right lateral Alaca-Ezinepazarı Fault consists of two segments. The 90 km long eastern segment is separated from the North Anatolian Fault by a 15° restraining bent southwest of Niksar Basin. This segment is the westernmost of the segments that have been ruptured during the December 26, 1939 Erzincan Earthquake (Ms = 8). The second segment of the Alaca-Ezinepazarı Fault is 150 km long. It is separated from the previous segment by a 24° bent and seismically it is less active (Barka and Kandinsky-Cade, 1988).

One of the well-known and more prominent active features in Central Anatolia is the Tuz Gölü Fault (TFZ, Beekman, 1966) being in NW-SE direction at the eastern shore of the basin and extending from north of Tuzgölü to south of Nigde. Different local names have been assigned to this fracture zone and its segments in earlier studies - *e.g*. Koçhisar – Aksaray Fault (Uygun, 1981; Görür *et al.*, 1984; Atabey *et al.*, 1987; Şengör *et al.*, 1985), the Hasandağ Fault set (Göncüoğlu *et al.*, 1991), the Koçhisar Fault set (Cemen and Dirik, 1992; 1999) , and the Tuz Gölü Fault set (Kocyigit and Beyhan, 1998; Koçyiğit, 1991. It is surrounded by large intraplate faults and approximately 125 km. long. The northern segment of the TFZ has s steeply westward-dipping normal-fault characteristic; however, the clockwise bending of streams, right-lateral offset of volcanic rocks and features, and striated surfaces indicating right-lateral (dextral) strike slip fault character of the southern segment of the TFZ.

The NNE-SSW trending Ecemiş Fault extending from the Erciyes Mountain to the Mediterranean Sea is a major left-lateral fault in Central Anatolia (Yetiş and Demirkol, 1984). It is about 100 km long. Although the fault initiated in the Eaocene time, its activity within the present-day escape system (Yetiş and Demirkol, 1984) is evidenced by the existence of many macroseismic correlations. Different names have been assigned to this fracture zone such as the Ecemiş Corridor by Blumenthal (1941, 1952), The Tekir Dislocation by Metz (1956), the Ecemiş Fault by Pavoni (1961), the Ecemiş Fault Zone by Yetiş (1978), and the Pozanti-Kayseri Fault by Scott (1981). Along the fault, morphological features between Kayseri and Tuzgölü such as offset streams and ridges and fault line scarps are very clear.

Historical and instrumental earthquake records present that seismic activity in Central Anatolia has been low relative to Western Anatolia (Ambraseys, 1970, 1975, 1988; Ambraseys and Finkel, 1987). The 1938 Kırşehir Earthquake with M6.8 and the 1717 and 1835 Ecemiş Earthquakes occurred near Kayseri (Öztin and Bayülke, 1990) can be listed as major important events in Central Anatolia.

2.2.8. Tectonic Elements of Black Sea Region

The Black Sea is located between Ukraine, Russia, Georgia, Turkey, Bulgaria and Romania. It is a semi-isolated extensional basin surrounded by thrust belts. The structure of the basin is known mainly through the acquisition and interpretation of seismic data (Tugolesov *et al.*, 1985; Finetti *et al.*, 1988; Beloussov and Volvovsky, 1989). In terms of crustal structure, The Black Sea is formed of two deep basins (Figure 2.21). The western Black Sea Basin is underlain by oceanic to sub-oceanic crust and contains a sedimentary cover of up to 19 km thick. On the other side, the eastern Black Sea Basin is underlained by thinned continental crust approximately 10 km in thickness and up to 12 km thickness of sediments (Nikishin *et al.*, 2003). These basins are seperated by the Mid Black Sea Ridge which consists of the Andrusov Ridge in the north and the Archangelsky Ridge in the south (Figure 2.23). The Andrusov Ridge is formed from continental crust and overlain by 5.–6. km thickness of sedimentary cover (Tugolesov *et al.*, 1985; Finetti *et al.*, 1988; Beloussov and Volvovsky, 1989; Robinson, 1997). The Archangelsky Ridge is bound to the south by the eastern Pontide belt, a complex terrane formed by a sequence of orogenic events during the Mesozoic and Cenozoic.

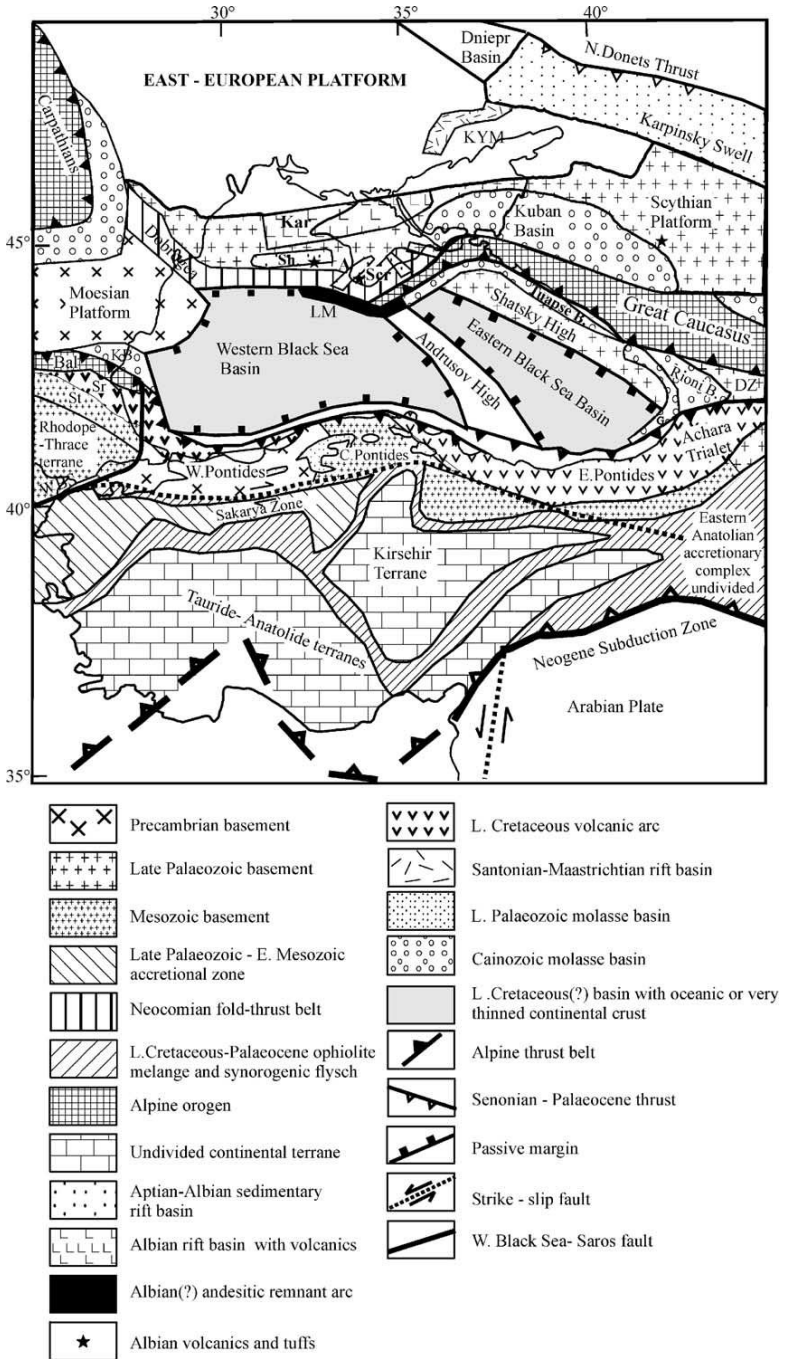

Figure 2.21. Tectonic setting of the Black Sea Basin (Nikishin *et al.*, 2003)

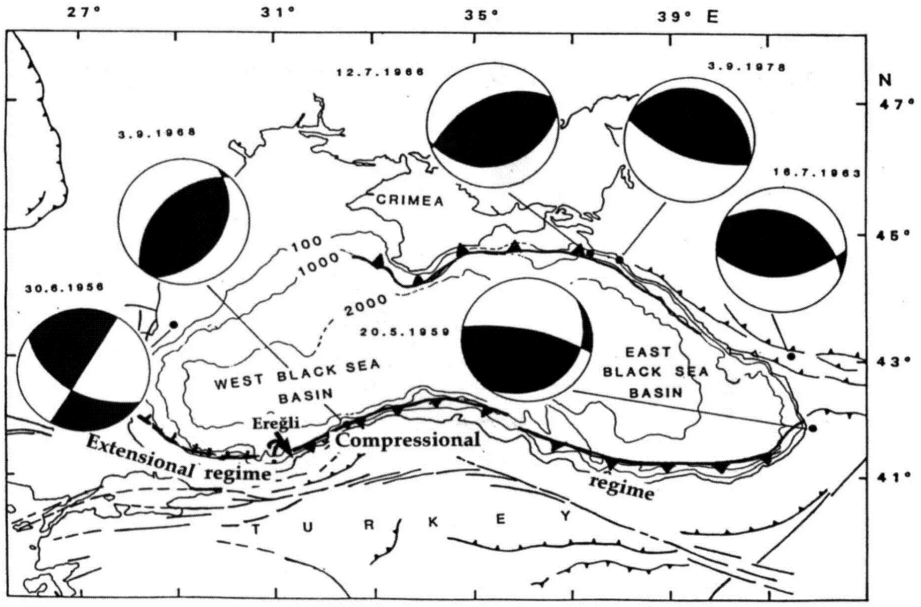

Figure 2.22. Tectonics of the Black Sea (from Barka and Reilinger, 1997)

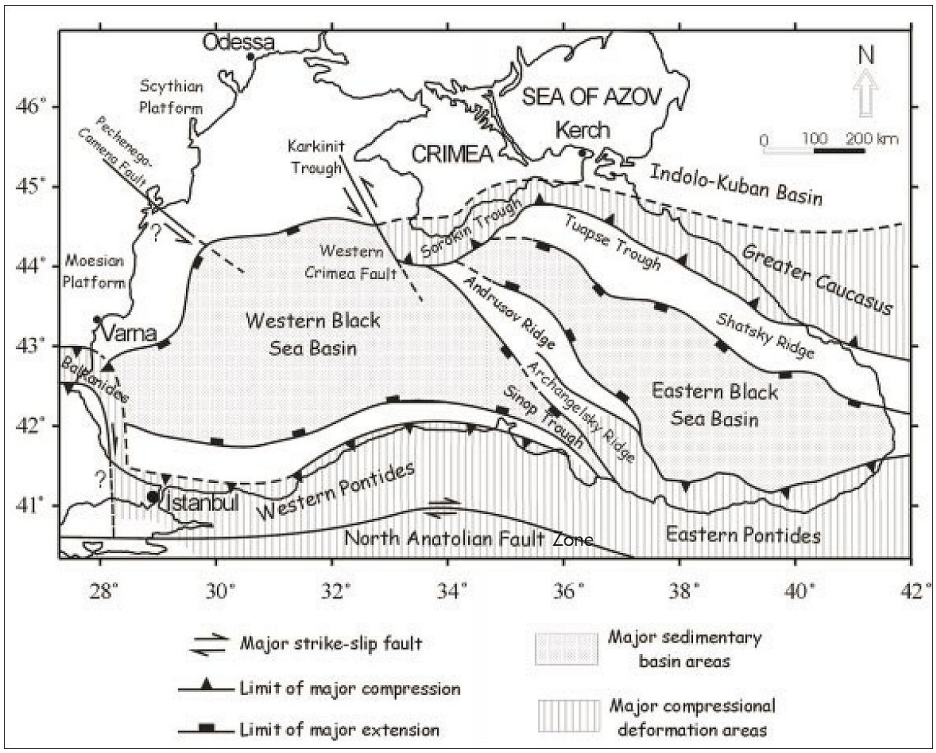

Figure 2.23. Tectonic framework of the Black Sea region (after Temel and Ciftci, 2002)

The Black Sea region is known to be an area of active tectonics and seismicity (Figure 2.24, after Chekunov *et al.*, 1994, Figure 2.22). The central, deepest part of the Black Sea depression is believed to be relatively aseismic. Thus, when estimating seismic hazard, only continental slope and on-shore tectonic structures are considered as zones of strong earthquake generation (Medvedev, 1968). The seismic activity within the circum Black Sea is assumed as low-moderate for this century. The seismic activity is influenced by the extensional tectonics in the Western Anatolia. There is also a speculation that the lithosphere of the Black Sea and Caspian Sea form a resistant "backstop" diverting the impinging Anatolian Plate to the west and "funneling" the continental lithosphere of Eastern Turkey and the Caucasus around the eastern side of the Black Sea (McClusky *et al.*, 2000).

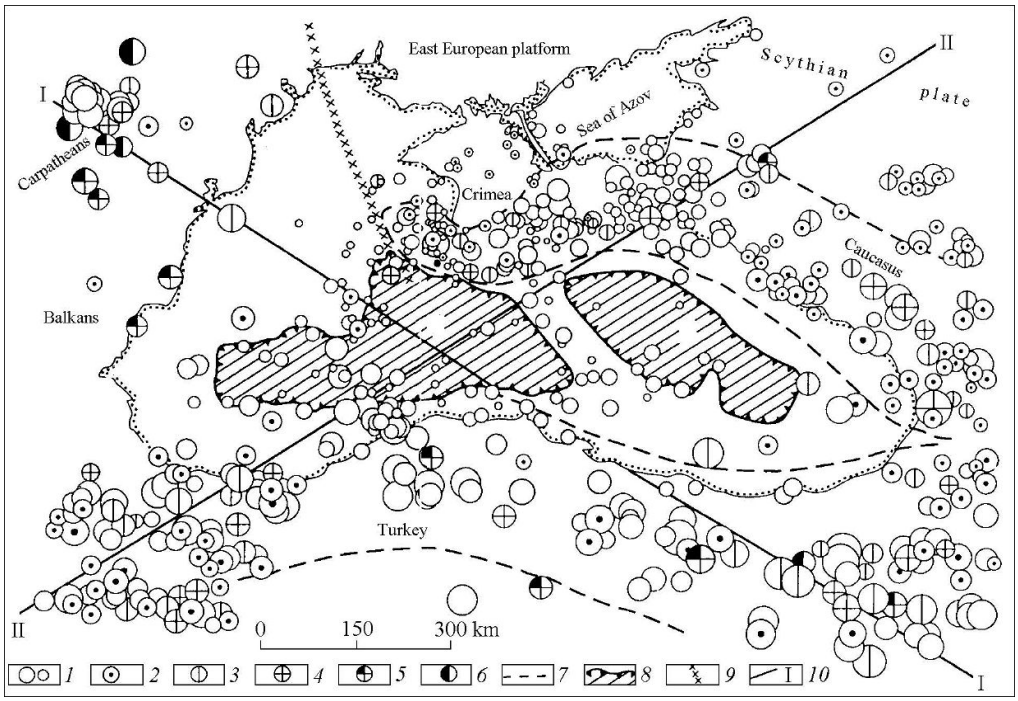

Figure 2.24. Map of the Black Sea region and seismic zones (after Chekunov, 1994)

Meredith and Egan (2002) showed that deeper parts of southern margin of the Black Sea are dominated by extensional faults (Figure 2.25). The Sinop Basin is located between the Archangelsky Ridge and the Turkish coastline and has been affected by normal faults along the Turkish margin and the Archangelsky Ridge (Rangin *et al.*, 2002).

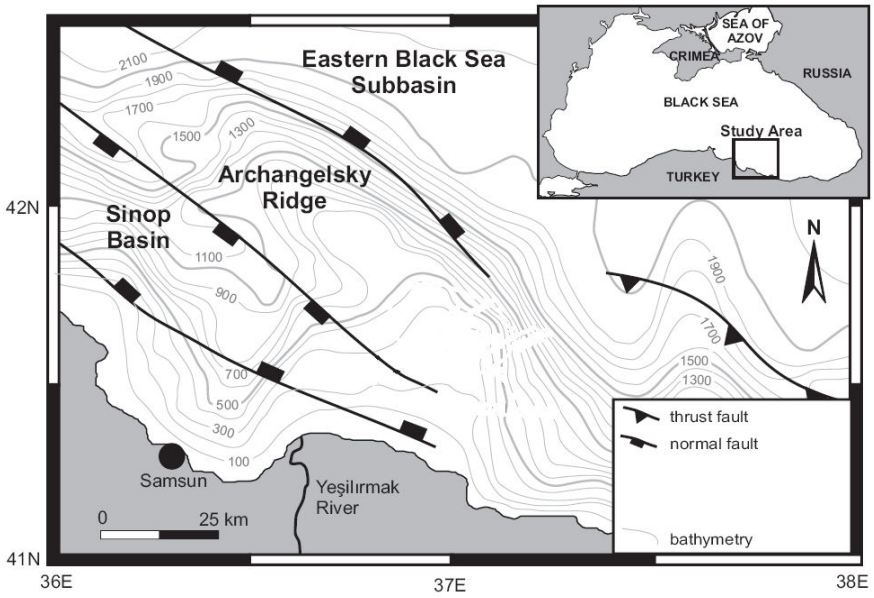

Figure 2.25. Offshore faulting associated with the Black Sea Escarpment (after Dondurur, 2009)

The tectonic features of the Eastern Black Sea are indicated on Figure 2.26. The geological cross section along the profile A-A' is indicated on Figure 2.27. These figures indicate the prominence of faulting in the Southern margin of the Black Sea.

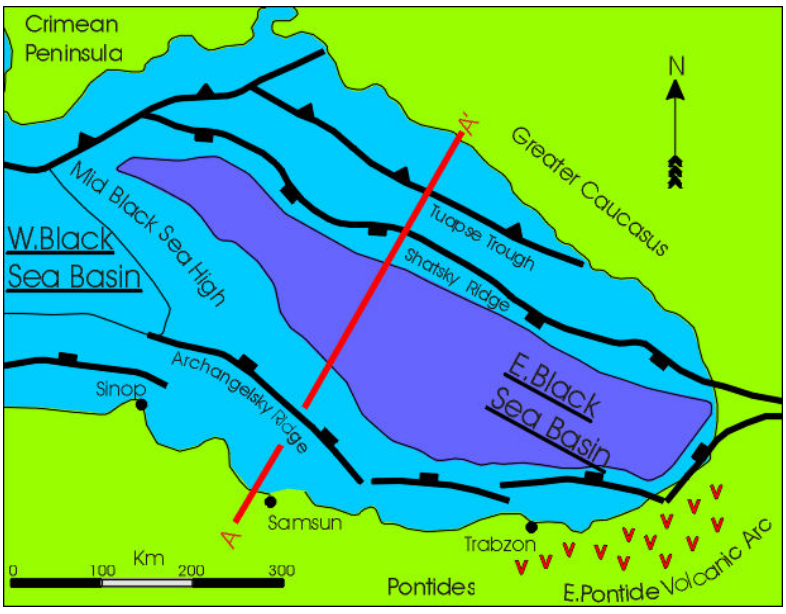

Figure 2.26. Tectonic features of the Eastern Black Sea (after Egan, 2006)

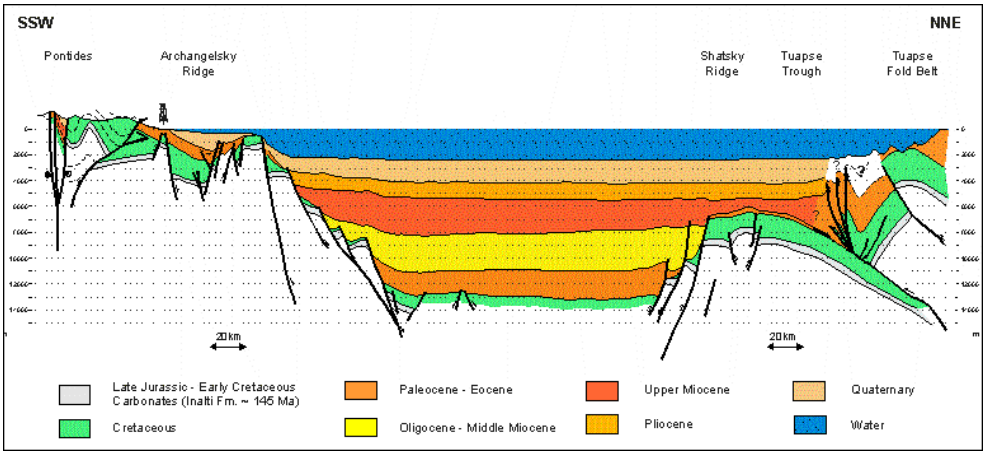

Figure 2.27. The geological cross section along the profile A-A (after Egan, 2006)

The faults associated with the escarpment along the southern margin of the Black Sea (Pontic Escarpment, Figure 2.22 through Figure 2.27) accounts for a rather low rate of intraplate seismic activity associated with the Tertiary and the Quaternary subsidence history of the Black Sea Basin as documented in Doyuran and Erdik (1983).

2.3. Seismicity of Turkey

Turkey and surrounding area has experienced the effects of several moderate sized earthquakes in the past that caused significant damages and destructions. Seismicity data can be considered in two categories: historical and instrumental.

In this study, the earthquake catalog compiled during the TEFER (Turkey Emergency Flood and Earthquake Recovery) project was utilized to calculate the earthquake recurrence parameters (a and b) for each seismic source. The historical earthquake databases available from many different catalogues present that substantial discrepancies exist between them. Therefore, numerous national and international catalogues were considered, correlated and homogenized. The historical data is incomplete and macroseismic ($M \geq 5.5$), whereas instrumental data is relatively complete for earthquakes of $M \geq 4.0$.

Ambraseys and Finkel (1995) states that although in general the Ottoman archives are very rich in documents providing evidence to macro-seismic events, there is an obvious lack of material concerning the eastern part of Anatolia. This phenomenon may be in part function of the Istanbul centricity of the Ottoman history-writers and also of the irregularity with which news traveled from remoter areas of the Empire. A great deal of material is available in the local languages. European sources, particularly contemporary travelers' accounts provide also valuable evidence of earthquake occurrence.

The data covered by Ambraseys and Jackson (1998, 2000), Ambraseys (1998, 2000); Nalbant *et al.* (2002, 2005) and UDIM (National Earthquake Monitoring Center) envelops the period from 5th Century B.C. to 1899. This section concentrates on the historical part (before 1900) of the catalog (Figure 2.28) whereas the 20th century seismicity is elaborated in the instrumental seismicity section.

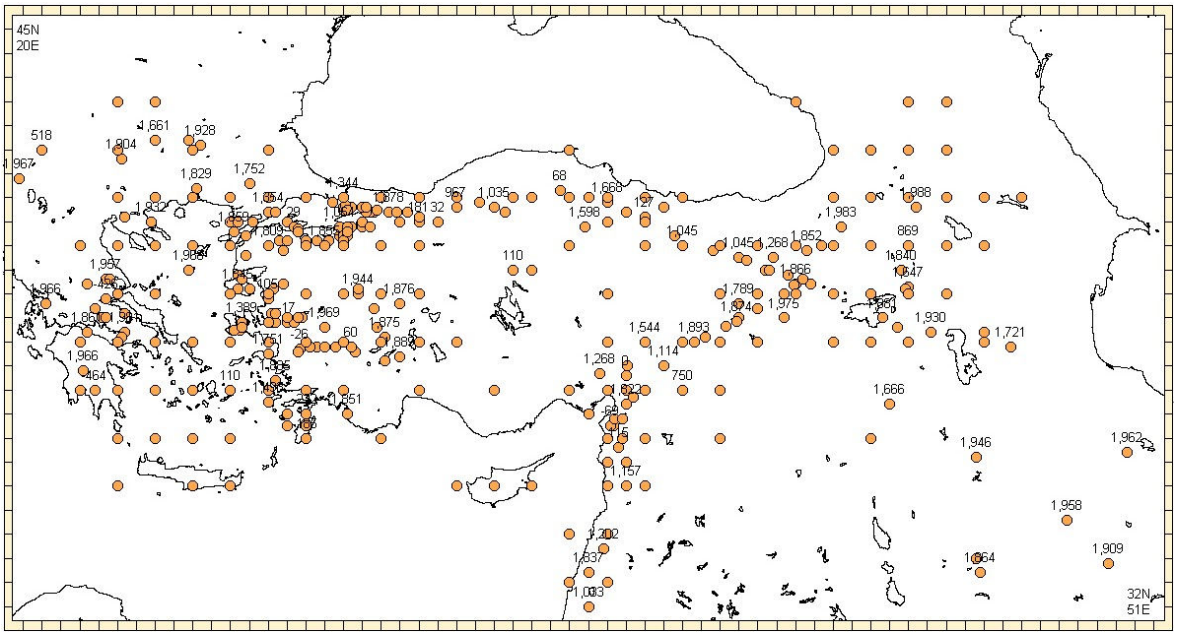

Figure 2.28. Distribution of historical seismicity for Turkey

The distributions of the instrumental seismicity from a various periods are presented in Figure 2.29 through Figure 2.31.

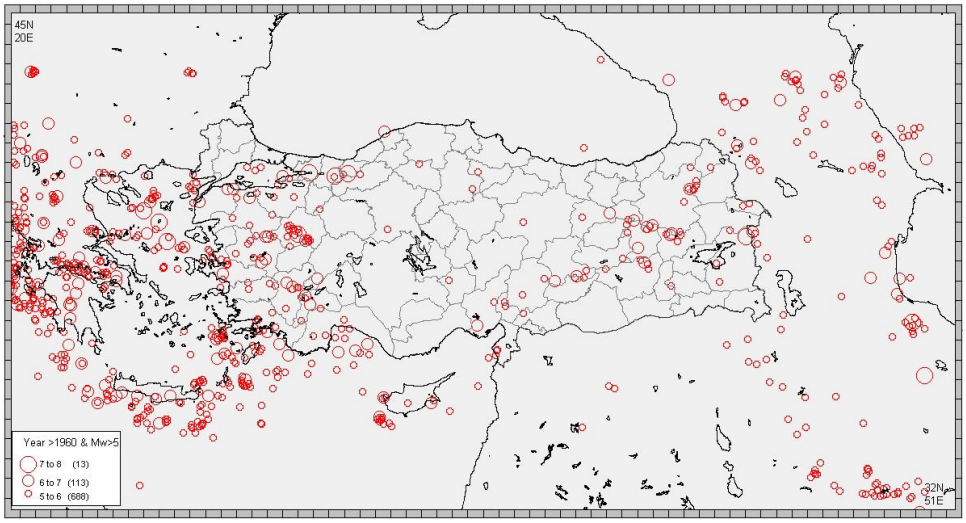

Figure 2.29. Distribution of the instrumental (year > 1960, Mw>5.) seismicity

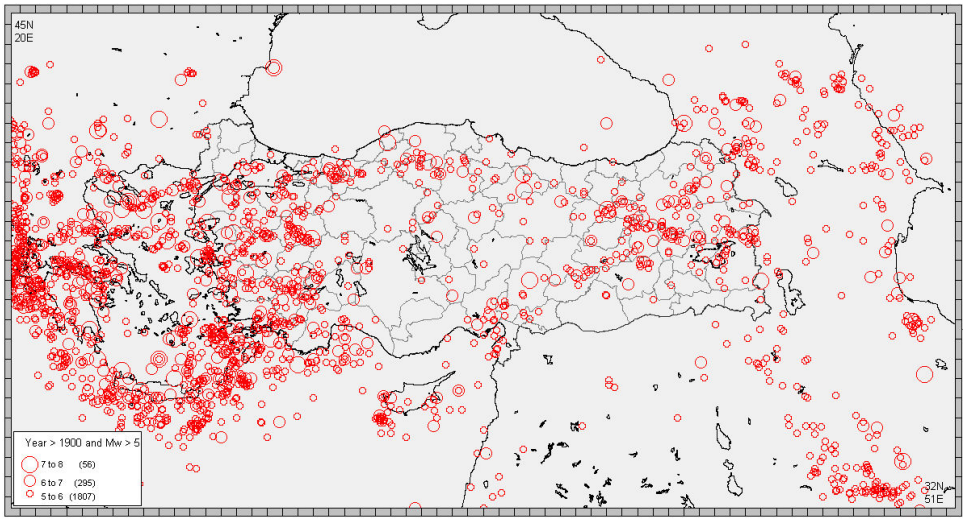

Figure 2.30. Distribution of the instrumental (year > 1900, Mw>5.) seismicity

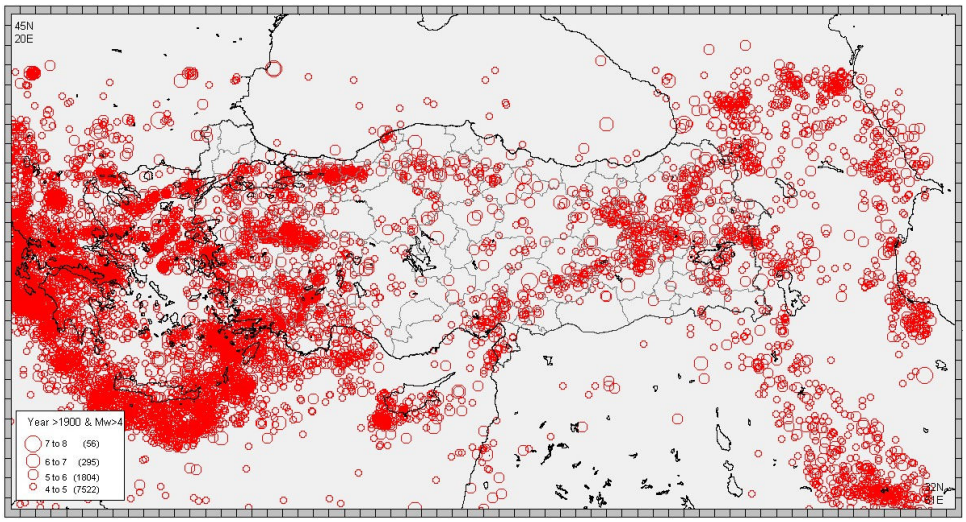

Figure 2.31. Distribution of the instrumental (year > 1900, Mw>4.) seismicity

2.4. Source Zonation

Literature survey indicated that due to the need for an earthquake resistant design code, the first earthquake macro-zonation map for Turkey appeared after the 1939 Erzincan Earthquake and the first official earthquake design code was prepared in 1945 and published, with some revisions, together with the second earthquake code in 1947. Considering an incomplete interpretation of historical seismicity, the zoning map has identified three zones which were included in possibly destructive earthquakes (Figure 2.32). In 1963, using new earthquake catalogues and seismotectonic maps, a second official earthquake zoning map was issued (Figure 2.33). This map classified Turkey into four hazard zones with maximum intensities (MSK) greater than VIII (first zone), (second zone), equal to VI (third zone) and less than V (no hazard zone). At the 1968 Strasbourg meeting of the European Seismological Commission, the preparation of the third (and current) issue of the zoning map in 1972 have been decided because of the several reasons such as: the presence of discontinuities in zones, occurrence of destructive earthquakes in "no hazard" zones and unconformities with the resolutions. This map (Figure 2.34) shows that the delineation in the five zones of earthquake hazard. In the 1st degree hazard zone the maximum intensity (MSK) is higher than or equal to IX, in the 2nd equal to VIII, in the 3rd equal to VII, in the 4th equal to VI, and in the 5th no hazard zone equal to V.

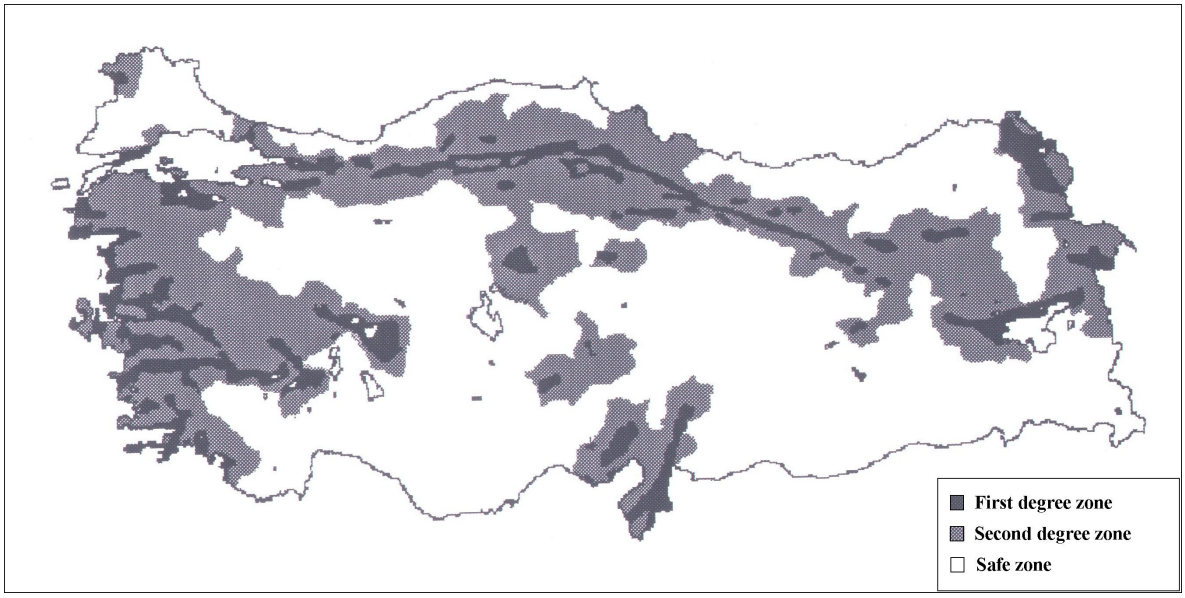

Figure 2.32. First seismic zoning map of Turkey (1945)

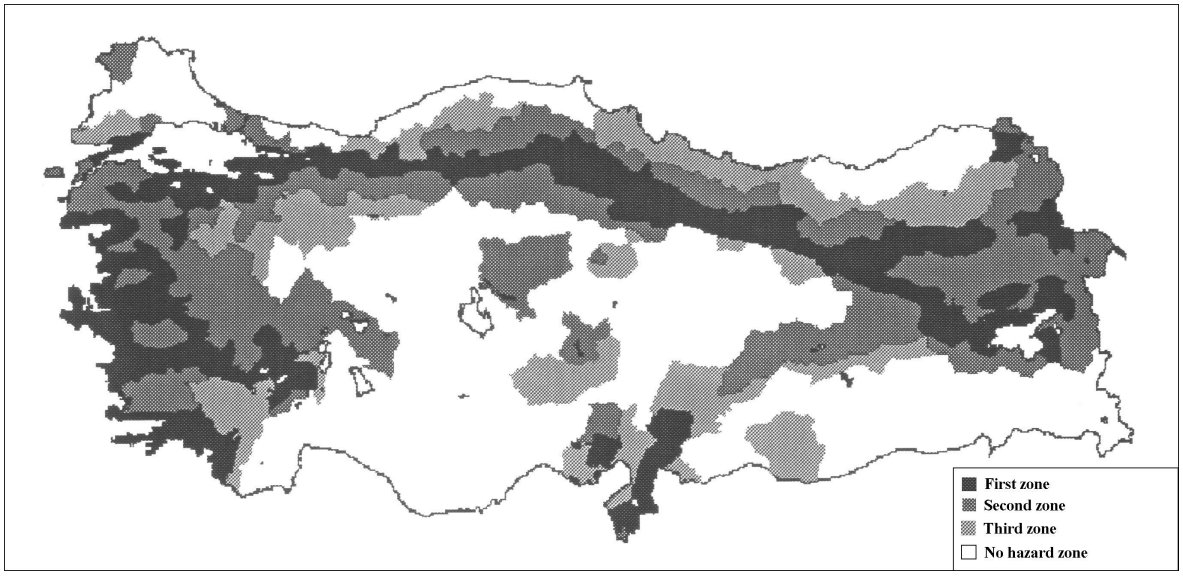

Figure 2.33. Seismic zonation map of Turkey as revised in 1963

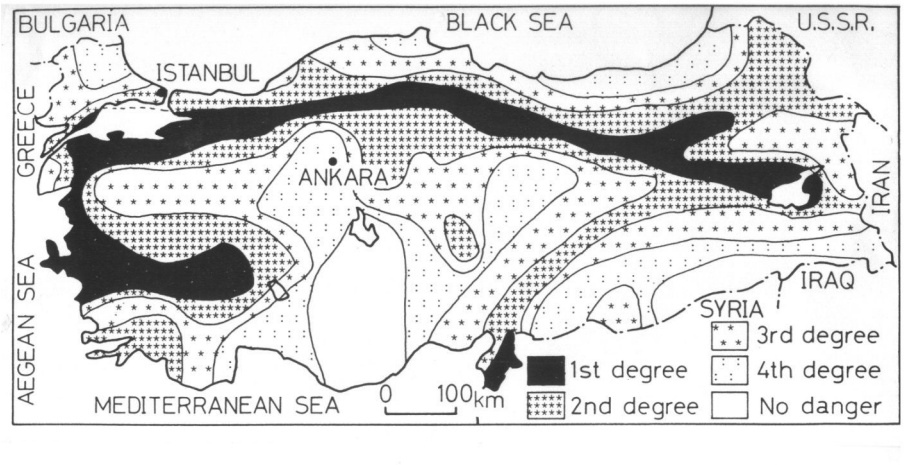

Figure 2.34. Seismic zonation map of Turkey, prepared in 1972

A seismic source zone is defined as a seismically homogenous area, in which every point within the source zone is assumed to have the same probability of being the epicenter of a future earthquake. An ideal delineation of seismic source zones requires a complete comprehension of the geology, tectonics, paleoseismology, historical and instrumental seismicity, and other neotectonic features of the region under study. However, it is not always possible to compile detailed information in all these fields for the majority of the world. Thus, frequently, seismic source zones are determined with two fundamental tools; a seismicity profile and the tectonic regime of the region under consideration. Although seismic source zonation is a widely used methodology to determine earthquake hazard, it is not the only approach. Since delineation of the seismic source zones still remains rather subjective, some researchers (*e.g.* Frankel, 1995) are suggesting other methods for evaluating seismic hazard, in order to eliminate the subjectivity of this procedure. This is particularly important in areas where the tectonic structure is very fragmented. Whereas in most regions of Turkey, the seismicity is relatively well documented, major faults are often well defined and the source zones are fairly obvious. Hence it is considered adequate to use the conventional method of seismic source zonation for Turkey in this study.

Seismic source zones used in this study are defined according to the principles that: Source boundaries should be defined with regard to the subsequently applied seismic hazard methodology; sources (or regions) should be defined as areas with seismic characteristic which are as homogeneous as possible; between sources (regions) of

different seismic potential, the boundary should be located close to the highest concentration around the hard core of the most active ones; In areas possessing statistically sufficient number of reliable events, boundaries should be mainly based on seismic data as an expression of tectonic activity and backed up by tectonic arguments; In case of an insufficient number of events or a large number of uncertainties attached to the events, existence of a boundary has been decided by arguments based on the most dominant tectonic or seismic features.

The main improvement of this model when compared to previous studies (*e.g*., Yarar *et al.*, 1980; Erdik and Oner, 1982; Erdik *et al.*, 1985; Gülkan *et al.*, 1993; Onur, 1997; GSHAP, 1999, TEFER, 2000; Baku-Ceyhan Crude Oil Pipeline Projects 2001 (Barka *et al.*,1999); SESAME, 2003; Kayabali and Akin, 2003, Tsapanos *et al*., 2005) is the representation of main fault traces (such as the North Anatolian and the East Anatolian Faults) with linear sources. Previous models used only areal zones to define seismic sources have been conducted by Yarar *et al.* (1980), Erdik and Öner (1982), Erdik *et al.* (1982, 1985), and Gülkan *et al.* (1993). These studies have culminated in probabilistic earthquake hazard assessment maps for Turkey in terms of peak ground acceleration and peak intensities corresponding to various return periods.

The comparison of source zonation models are presented in Figure 2.35 through Figure 2.41. A summary of the source zone information used in this study is presented in Table 2.2.

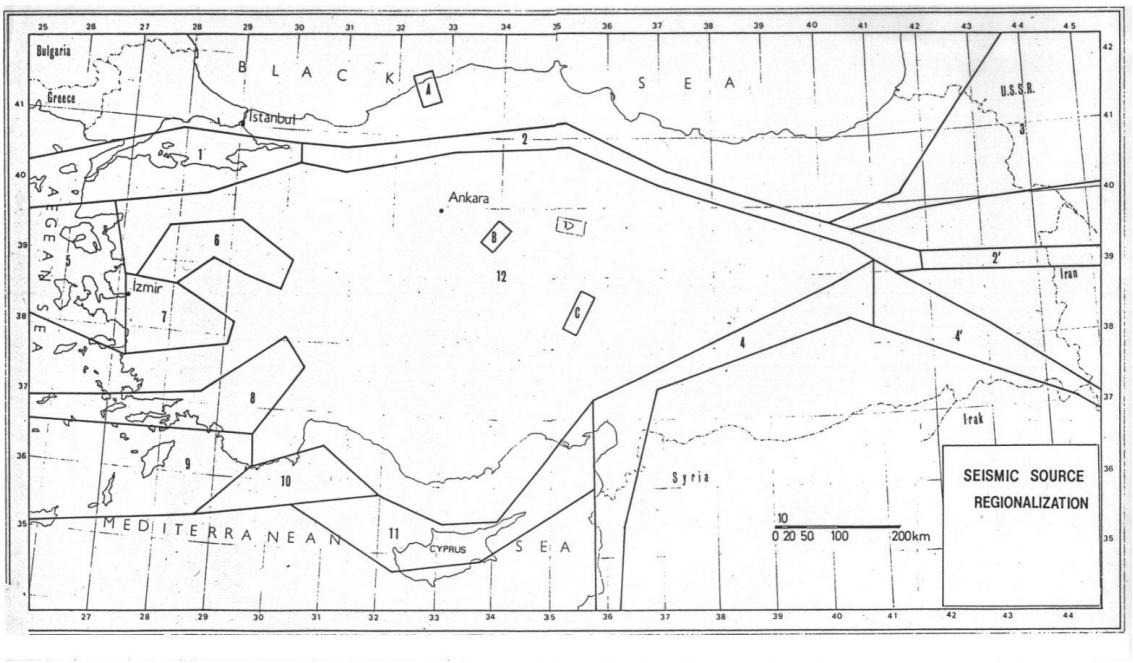

Figure 2.35. Seismic source zonation proposed by Erdik *et al.* (1985)

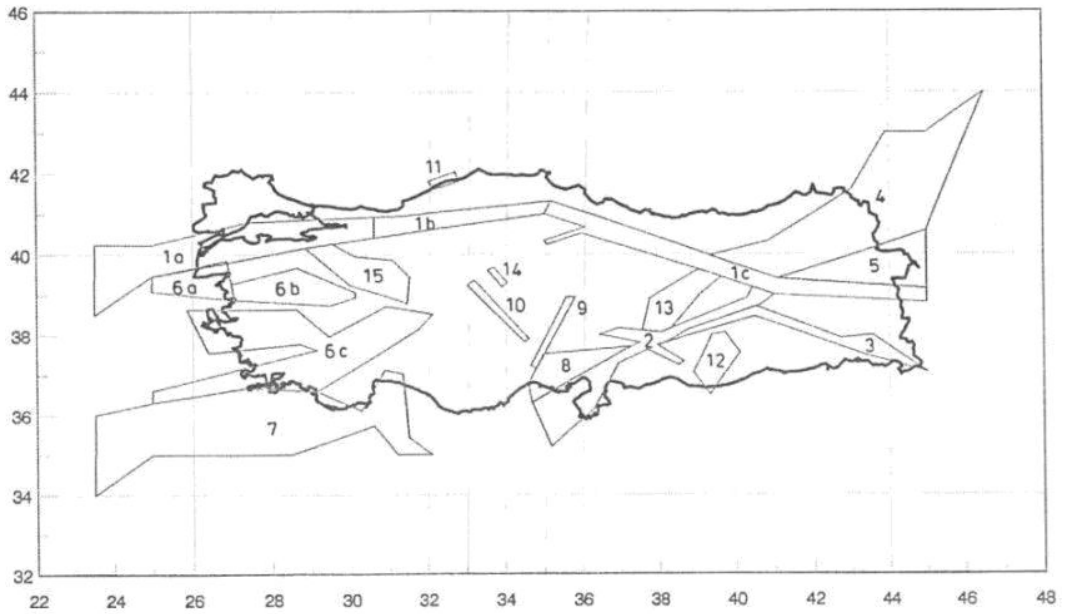

Figure 2.36. Seismic source zonation proposed by Gülkan *et al.* (1993)

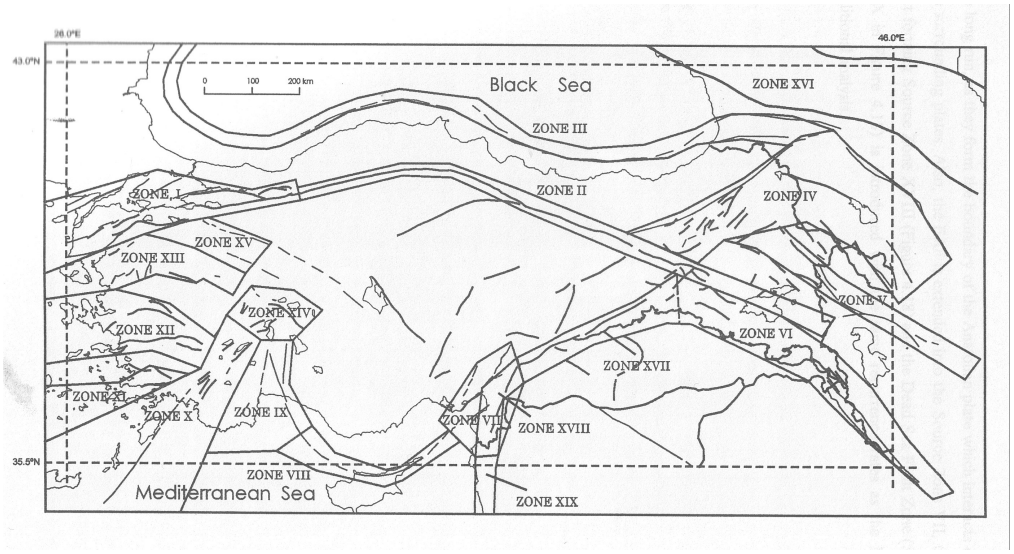

Figure 2.37. Seismic source zonation proposed by Onur, (1997)

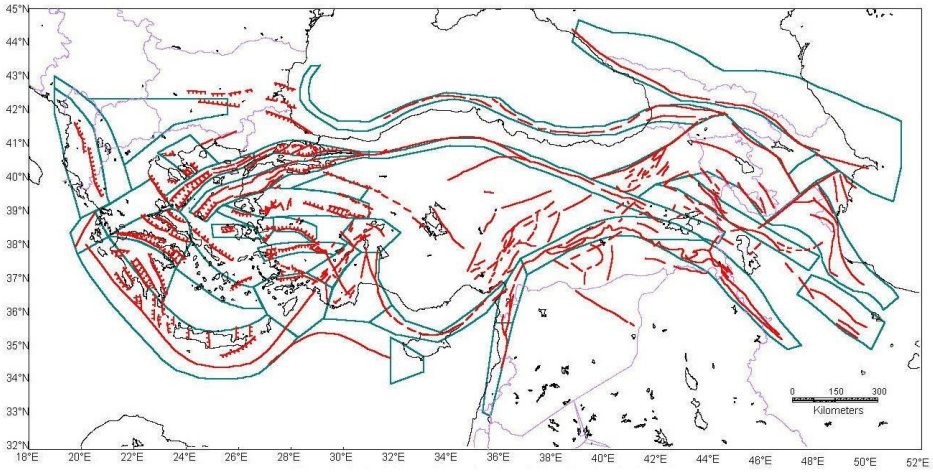

Figure 2.38. Seismic source zonation proposed by GSHAP (global seismic hazard assessment program contributed by KOERI) project, (1999a)

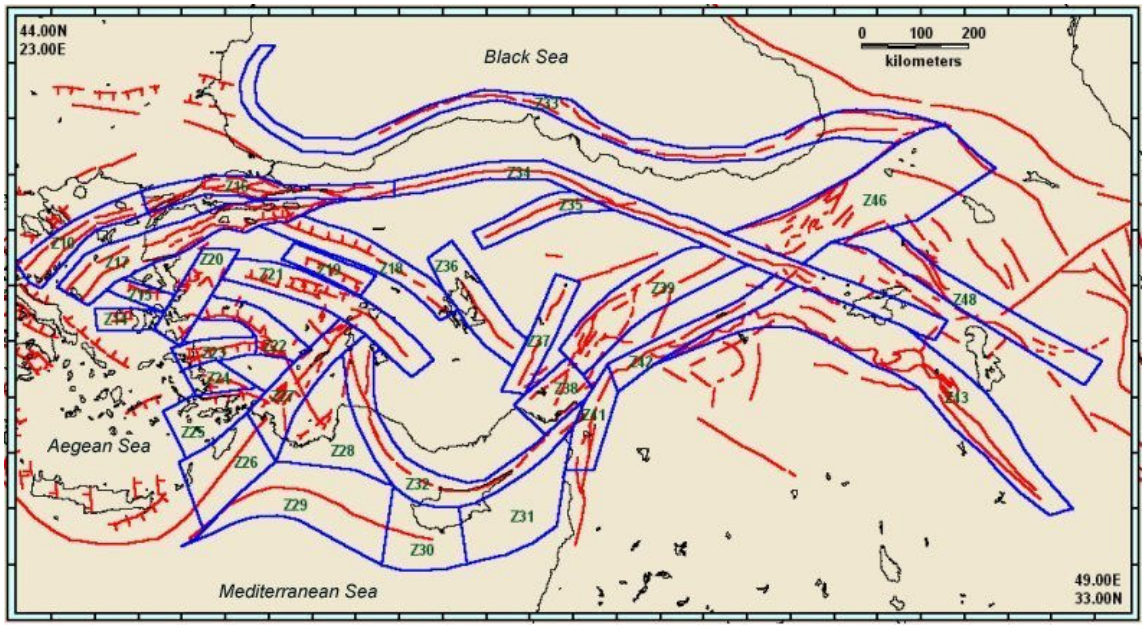

Figure 2.39. Seismic source zonation proposed by TEFER (a probabilistic seismic hazard assessment for Turkey and in connection with the improvement of natural hazard insurance and disaster funding strategy) project, (2000)

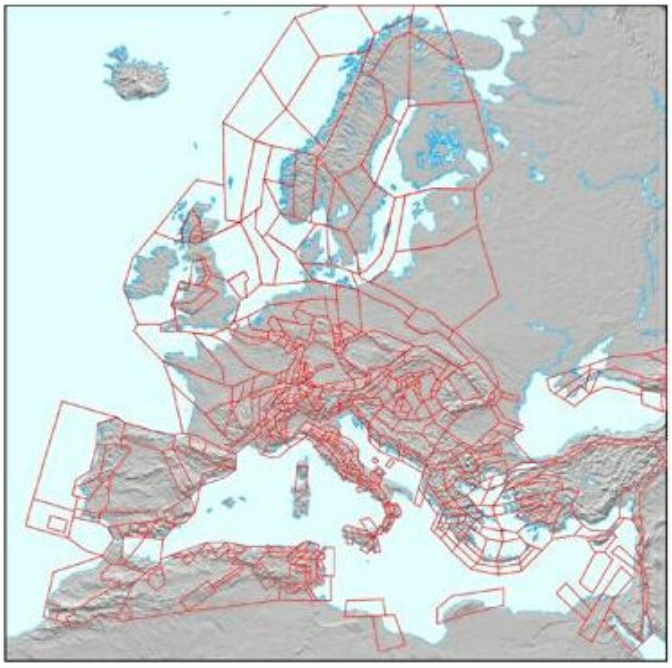

Figure 2.40. Seismic source zonation proposed by SESAME (seismotectonics and seismic hazard assessment of the Mediterranean Basin contributed by KOERI) project, (2003)

The seismic source zonation used in this study is essentially based on the seismic source zonation model of Turkey developed within the context of a project conducted for the Ministry of Transportion Turkey, aiming the preparation of an earthquake resistant design code for the construction of railways, seaports and airports (DLH, 2007). In order to account for the spatially more diffuse moderate size seismicity around these faults, widths of at least several kilometers were assigned to the zones even if the associated faults were well expressed on the surface. In the new model however, earthquakes with magnitude > 6.5 are assumed to take place on the linear zones, whereas the smaller magnitude events associated with the same fault are allowed to take place in the surrounding larger areal zone.

In addition to linear and areal source zones background seismicity zones are defined to model the floating earthquakes that are located outside these distinctly defined source zones and to delineate zones where no significant earthquake has taken place.

Considering the latest findings of tectonics, seismicity and topography of the region, the fault zones tabulated in Appendix A, have been delineated as areal and linear source models for Turkey and the neighboring regions in the study area.

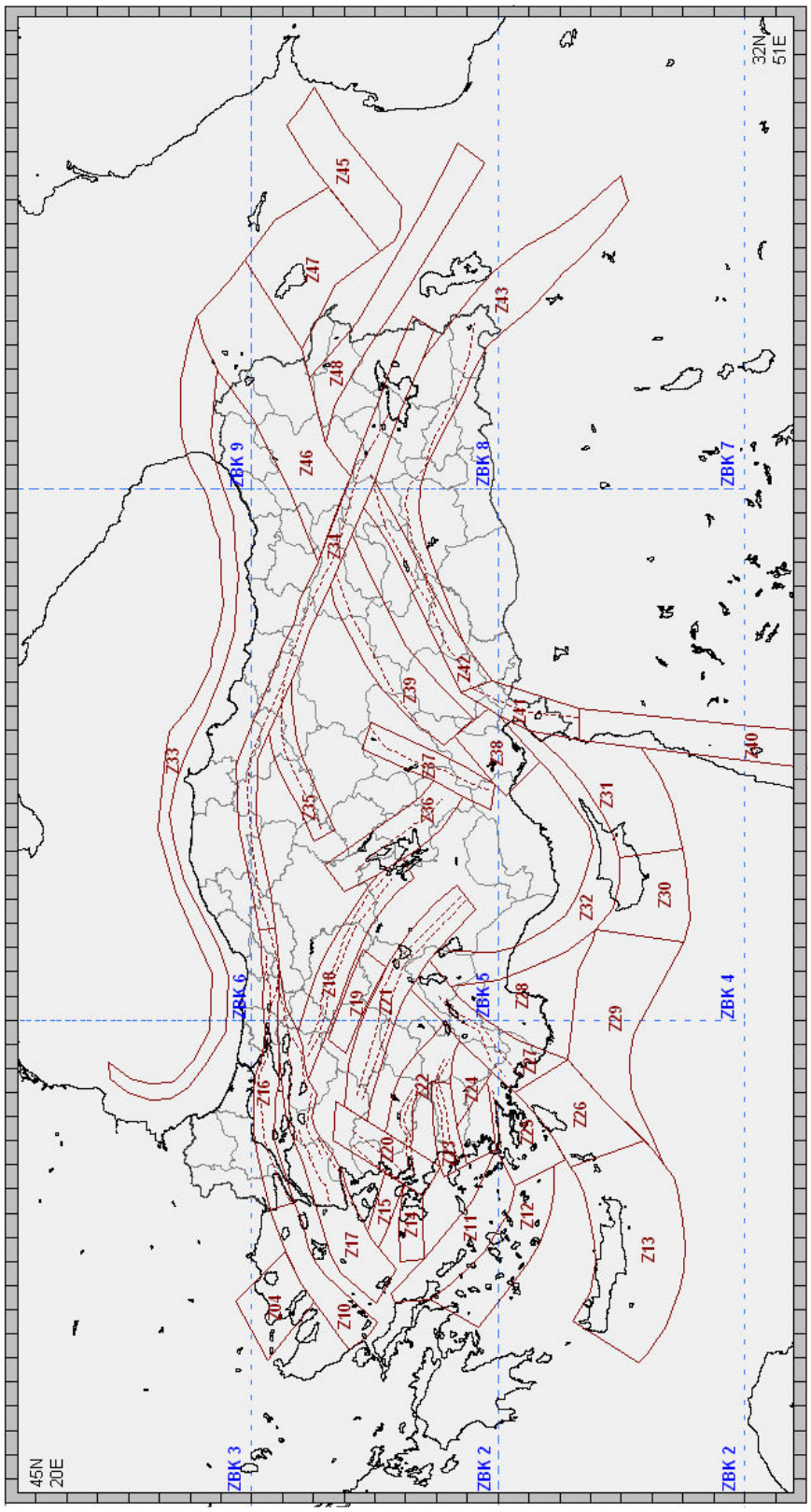

Figure 2.41. Source zonation model used in the study

2.5. Seismic Activity Rates (Earthquake Recurrence Relationships)

A crucial component of seismic hazard analysis is the magnitude – recurrence relation, which provides the cumulative rate of occurrence of earthquakes within a seismic source zone as function of magnitude.

Gutenberg and Richter Model (Richter, 1954) numerous subsequent studies presents that the number N(M) of earthquake with magnitude greater than or equal to a given value, M, follows a relation of the form

$$\log N = a - b M \tag{2.4}$$

where N is the number of the earthquakes above the magnitude M in a given region and within a given period and a and b are regression constants. The Gutenberg-Richter recurrence model has been extensively used in many seismicity studies and has also been confirmed to hold for micro-earthquakes. The coefficient *a* is a constant that is dependent on the location and time of the sample used and *b* represents a constant thought to be characteristic of the region.

The earthquake catalogues are often biased due to incomplete reporting for smaller magnitude earthquakes in earlier periods. Thus to fit the recurrence relationship to a region, one should choose among using

(1) a short sample that is complete in small events or
(2) a longer sample that is complete in larger events or
(3) a combination of the two data sets to complete the deficient data thereby obtaining a homogeneous data set.

A direct attempt to fit these data to a regression relationship may result in quadratic or higher order expressions to accommodate the inherent bias and in-homogeneity of the data. In the method used in this study, an artificially homogeneous data set is simulated through the determination of the period over which the data in a given magnitude group are completely reported (Stepp, 1973).

The computed recurrence parameters as well as the minimum and maximum magnitudes associated with the source zones are presented in Table 2.2.

Table 2.2. Source zone information

Source Zone No	Fault Name	Mechanism	a	b	M_{min} - M_{maks}
Z10	North Anatolian Fault Zone (North Strand)	Right Lateral Strike Slip	6.5	1.2	5.0 – 7.8
Z12			3.0	0.8	5.0 – 7.6
Z13			3.2	0.7	5.0 – 7.2
Z14	Sakız Fault	Normal	3.8	0.9	5.0 – 7.0
Z15	Midilli	Normal	4.5	1.0	5.0 – 6.8
Z16 Outside Zone	NAF (Marmara Sea)	Right Lateral Strike Slip + Normal	5.3	0.9	5.0 – 6.9
Z16 Inside Zone					7.0 – 7.9
Z17 Outside Zone	NAF South Strand	Right Lateral Strike Slip + Normal	4.7	0.9	5.0 – 6.6
Z17 Inside Zone					6.7 – 7.4
Z18 Outside Zone	Eskişehir Fault	Right Lateral-Strike Slip with Normal Component	4.3	1.0	5.0 – 6.6
Z18 Inside Zone					6.7 – 7.0
Z19	Kütahya Fault	Normal	3.8	1.0	5.0 – 5.8
Z20 Outside Zone	Bergama_Foça Fault	Left Lateral-Strike Slip	3.8	0.8	5.0 – 6.6
Z20 Inside Zone					6.7 – 7.0
Z21 Outside Zone	Simav-Sultandağ Fault Systems	Normal ve Ters Normal and Reverse	5.4	1.1	5.0 – 6.9
Z21 Inside Zone					7.0 – 7.3
Z22 Outside Zone	Gediz Fault	Normal	4.0	0.9	5.0 – 6.9

Z22 Inside Zone					7.0 – 7.3
Z23 Outside Zone	Menderes Fault	Normal	4.1	1.0	5.0 – 6.8
Z23 Inside Zone					6.9 – 7.6
Z24	Muğla-Yatağan Fault	Strike Slip + Normal	4.8	1.1	5.0 – 6.8
Z25 Outside Zone	Gökova Fault	Normal	5.3	1.0	5.0 – 6.8
Z25 Inside Zone					6.9 – 7.8
Z26	Hellenic Arc	Left Lateral Strike Slip with Normal Component	6.0	1.2	5.0 – 6.7
Z27 Outside Zone	Fethiye-Burdur Fault	Left Lateral Strike Slip with Normal Component	5.0	1.0	5.0 – 6.8
Z27 Inside Zone					6.9 – 7.4
Z28	Antalya Fault	Strike Slip	5.6	1.2	5.0 – 7.0
Z29	Cyprean Arc-Florence Rise	Strike Slip + Thrust	5.9	1.3	5.0 – 5.9
Z30	Cyprus Arc – Trodos	Strike Slip + Thrust	4.8	1.0	5.0 – 6.8
Z31	Hecataeus Ridge	Undefined	3.4	0.8	5.0 – 6.6
Z32	Cyprus Trough	Strike Slip + Thruste	2.7	0.7	5.0 – 6.8
Z33	Black Sea Fault	Thrust and Normal?-Geologically Known as active	3.8	0.9	5.0 – 7.3
Z34 Outside Zone	North Anatolian Fault Zone (NAF)	Right Lateral Strike Slip	5.0	0.8	5.0 – 6.7
Z34 Inside Zone					6.8 – 7.9
Z35 Outside Zone	Alaca Ezine Pazari Fault	Right Lateral Strike Slip ı	3.2	0.8	5.0 – 6.7
Z35 Inside Zone					6.8 – 7.9
Z36 Outside Zone	Tuz Gölü Fault	Right Lateral Strike Slip	2.9	0.8	5.0 – 6.7
Z36 Inside Zone					6.8 – 7.9
Z37 Outside Zone	Ecemiş Fault	Left Lateral Strike Slip	3.9	0.9	5.0 – 6.7

Z37 Inside Zone					6.8 – 7.9
Z38	Adana Bölgesi Fault Zone	Left Lateral Strike Slip	3.1	0.8	5.0 – 7.0
Z39 Outside Zone	Goksun Fault ı	Left Lateral Strike Slip	2.7	0.7	5.0 -6.9
Z39 Outside Zone					7.0 – 7 .5
Z40	Ölüdeniz Fault	Left Lateral Strike Slip	4.7	0.9	5.0 – 7.7
Z41 Outside Zone	Ölüdeniz-Hatay Fault	Left Lateral Strike Slip + Normal	3.6	1.0	5.0 – 6.7
Z41 Inside Zone					6.8 – 7.9
Z42 Outside Zone	East Anatolian Fault Zone(EAF)	Left Lateral Strike Slip	4.6	0.9	5.0 – 6.7
Z42 Inside Zone					6.8 – 7.9
Z43 Outside Zone	Bitlis_Zagros Fault Zone	Thrust	4.7	1.0	5.0 – 6.6
Z43 Inside Zone					6.7 – 7.0
Z45	Aras Fault	Left Lateral Strike Slip	4.2	1.0	5.0 - 7.8
Z46	North East Anatolian Fault Zone	Left and Right Lateral Strike Slip	5.6	1.1	5.0 - 7.7
Z47	PambaSevan Fault Zone	Right Lateral Strike Slip + Thrust	3.9	0.9	5.0 - 7.3
Z48	Tebriz Fault Zone	Right Lateral Strike Slip	4.4	1.0	5.0 - 7.3
ZBK1	Background		5.13	1.00	5.0-6.5
ZBK2	Background		5.13	1.00	5.0-6.5
ZBK3	Background		5.13	1.00	5.0-6.5
ZBK4	Background		5.13	1.00	5.0-6.5
ZBK5	Background		5.13	1.00	5.0-6.5
ZBK6	Background		5.13	1.00	5.0-6.5
ZBK7	Background		5.13	1.00	5.0-6.5
ZBK8	Background		5.13	1.00	5.0-6.5
ZBK9	Background		5.13	1.00	5.0-6.5

2.6. Ground Motion Prediction Equations

The prediction of the parameter associated with earthquake ground motion is performed by the use of empirical ground motion prediction equations obtained from statistical regression on ground motion database or statistical regression of macroseismic observations leading respectively to intensity or PGA/ spectral ordinates attenuation laws.

Geological and geo-tectonic similarity of Anatolia to the California (Strike slip faults similar to North and East Anatolian Faults) and favorable comparisons of the ground motions recorded from Turkish earthquakes with predictive models developed for Western US favor the use of western US data based empirical models for hazard assessment studies in Turkey. Boore *et al.* (1997), Sadigh *et al.* (1997) and Campbell (1997) ground motion prediction equations can be sited among them. These models however cover a period range of zero to four s. NGA models provide a good basis for the assessment of spectral amplitudes corresponding for larger periods. Most of these models are based on worldwide strong motion and provide favorable comparisons with European data and attenuation models.

In addition to that, in 2003, five developer teams were selected to participate in a PEER (Pasific Earthquake Engineering Research Center) project to empirically develop new empirical ground motion prediction models based on an expanded and improved database including an abundant number of recordings from recent earthquakes as well as supporting information on the causative earthquakes, the source-to-site travel path characteristics, and the site and structure conditions at ground motion recording stations. Each developer team was allowed to apply its own selection criteria concerning earthquakes, recordings, functional forms, and independent variables were to be used in the development of the model. The resulting empirical ground motion prediction models (The so-called NGA) are referred to as Campbell and Bozorgnia (2008), Boore and Atkinson (2008), Chiou and Youngs (2008), Abrahamson and Silva (2008) and Idriss (2008).

Review of the NGA models indicate that, in general, ground motions particularly at short-periods (*e.g.*, peak acceleration) are significantly reduced for very large magnitudes

(**M** ≥ 7.5) compared to traditional relationships such as Boore *et al*. (1997), Sadigh *et al*. (1997) and Campbell (2003) (Figure 2.42).

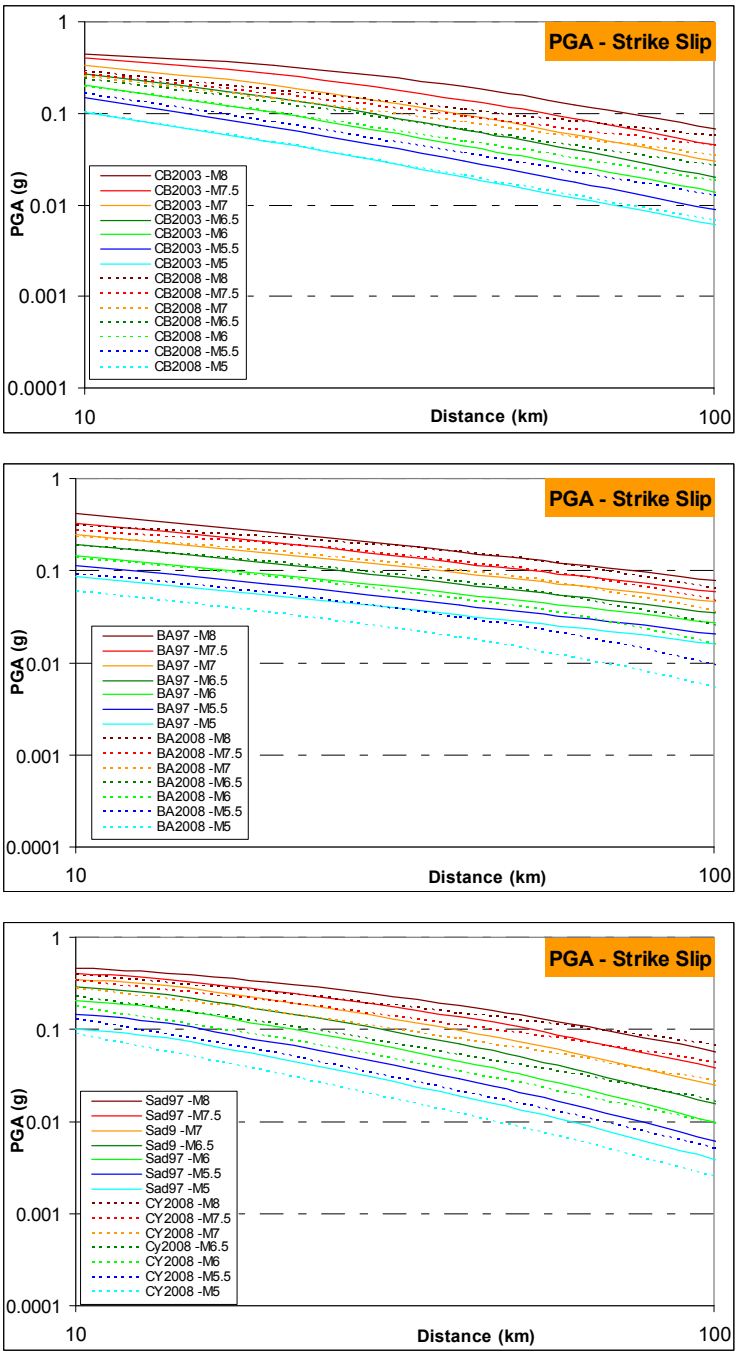

Figure 2.42. Comparison between NGA and current attenuation relationships for peak ground acceleriation

2.6.1. Intensity Attenuation Relationship

Ground motion predictions (attenuation relation) are traditionally given in terms of recorded ground motion parameters, *e.g*. PGA, based on strong ground motion data. However, because of its availability for both recent and historical earthquakes, the intensity hazard maps expressed in terms of macroseismic intensity have been widely used as a prediction of the damage potential of large earthquakes and loss assessment studies associated with such as insurance sector, industrial facilities and non-structural elements.

There are three intensity prediction equations developed for Turkey. Ohashi *et al.* (1983), proposed relationship for the assessment of seismic intensity at short to moderate epicentral distances. A refined model was constituted adding the effects of a "finite area source" to the usual intensity – magnitude relationships in order to estimate the intensity distribution. The acceleration "a", caused by displacement "D" at the unit area on the rupture surface was applied to the total fault area by a double integration procedure. Ohashi *et al.* (1983), relationship includes earthquakes (Ms>4.8) that took place between 1928 and 1976 along North and East Anatolian Faults and in the complex extensional system in Western Turkey.

The other study to asses the intensity prediction equation is Erdik and Eren (1983). They used strike-slip earthquakes (Ms>6.3) associated with the North Anatolian Fault in both parallel and transverse directions.

The recent intensity prediction equation is proposed by Sesetyan *et al.* (2005). The relationship consists of new data from recent earthquakes that took place 67 isoseismal maps of earthquakes with intensities greater or equal to V between 1909 and 2002. The preliminary results are presented for equations giving seismic intensities in terms of moment magnitude and distance for strike-slip and other (normal and complex) faulting mechanisms and for average site conditions. The equations and related coefficients for strike slip, normal fault and all type of fault mechanisms are given in the following.

$$\ln I = \ln(I_0) - c1 - c2\ln(R^2 - h^2)^{0.5} - c3(R^2 - h^2)^{0.5}$$
$$I_0 = 0.44M_w^2 - 4.19M + 17.05, \quad R^2 = 0.80 \tag{2.5}$$

Table 2.3. The coefficient of the Sesetyan *et al.* (2005) intensity based ground motion prediction equation

Focal Mechanism	C1	C2	C3	h	R^2	Standard Deviation
Strike Slip	0.3465	0.1979	0.001	4	0.95	0.2
Normal	0.366	0.1673	0.0009	4	0.86	0.14
All	0.569	0.2462	0.0005	8	0.90	0.16

2.7. Computation of Probabilistic Seismic Hazard

Probabilistic Seismic Hazard Analysis (PSHA) has become a fundamental tool in assessing seismic hazards and for estimating seismic design and seismic safety evaluation ground motions both on a site-specific basis for important and critical facilities and a national scale for building codes. In terms of definitions, given above, there have been many best-known computer programs for seismic hazard such as –RISK, EQRISK, FRISK, CRISIS 2007, USGS Hazard programs, and SEISRISK III. These programs have been used primarily to calculate hazard, not risk.

In this study, Earthquake Hazard Analysis except intensity based approach has been run with SEISRISK III program. On the other hand, intensity based seismic hazard assessment has been investigated by using the CRISIS 2007 software.

2.7.1. Computational Methodology of SEISRISK III

SEISRISK III, the computer program for seismic hazard estimation written by Bernice Bender and David M. Perkins (1987) was used in the analysis. SEISRISK III was designed to compute maximum ground motion levels that have a specified probability of

non-exceedence during fixed time periods at each set of sites uniformly spaced on a two-dimensional grid.

Earthquake occurrences are assumed to have a Poisson distribution, and rates that remain constant during the time periods of interest. Mean or median ground motion from an earthquake is an increasing function of magnitude and a decreasing function of site-to-source distance. Earthquakes in a zone or fault are restricted to occur within a specified magnitude range, the range may be different for different faults and zones. Seismicity is assumed to remain constant during the time periods being considered; that is the average rate of earthquakes per unit time for each magnitude interval does not change with time.

The program allows the modeling of the earthquake generating mechanisms as faults or source zones. Earthquakes can be modeled as finite ruptures along linear fault segments. The ground motion occurrences at a site resulting from fault rupture are added to those resulting from earthquakes within source zones.

The desired attenuation function may be entered as a table of values of the chosen ground motion parameter as a function of magnitude and distance. The software allows the modeling of acceleration variability. Rather than assuming a single value of acceleration resulting from earthquakes at each magnitude and distance, a range of accelerations log normally distributed with standard deviation σ_a in log_e acceleration is assumed to result. Calculated probabilistic ground motion levels at all sites tend to be higher if a lognormal distribution of accelerations is assumed, than when only median accelerations are used.

Assuming that seismicity is uniform within a source zone means that seismicity changes abruptly at each source zone boundary. An effect of those abrupt changes is that the ground motion calculated at sites a few kilometers apart may differ significantly if the sites are close to a source zone. To avoid sudden changes in seismicity at source zone boundaries, SEISRISK III permits an option of “earthquake location uncertainty”. Instead of assuming that source zones are homogeneous, that is each point within a source zone has the same probability of being the epicenter of a future earthquake, the earthquake location uncertainty allows the assumption of each point within a source zone being the mean or most likely location of a future earthquake. The locations of actual earthquakes

are normally distributed with standard deviation σ (an input parameter) about their mean locations. This permits earthquake rates to vary smoothly at a boundary, while the rates in the center of the zone are not affected significantly. As σ increases, a higher percentage of the earthquakes that would occur within the source zone if σ was zero, occurs beyond the boundaries.

2.7.2. Computational Methodology of CRISIS 2007

Using the regional Ground Motion Prediction (GMP) equation (Sesetyan *et al.*, 2005), intensity based hazard maps were generated for 2. per cent, 10 per cent and 50 per cent probability of exceedence in 50 years. The software used for this purpose was CRISIS 2007 (Ordaz *et al.,* 2003). CRISIS 2007 computes seismic hazard using a probabilistic model that considers the rates of occurrence, attenuation characteristics and geographical distribution of earthquakes. The main features of the program include the following: (a) earthquake occurrence can be defined either as a Poisson process or as a Characteristic Earthquake process; (b) sources can be defined as areas, lines or points; (c) Considering the fault type, GMP equations can be assigned for each seismic source zonation in a study area.

Two alternative models are implemented in CRISIS 2007 in order to describe the earthquake occurrence of a source: a truncated GR exponential model and the characteristic earthquake model (Youngs and Coppersmith 1985). The exponential model requires specification of: threshold magnitude, exceedence rate of threshold magnitude, "b-value" for the source, given in terms of the natural logarithm, maximum magnitude expected, and coefficiens of variation for all the parameters. The characteristic earthquake model requires specification of: (i) median value of the times between characteristic earthquakes; (ii) minimum possible magnitude of a characteristic earthquake; (iii) maximum magnitude of the characteristic earthquake; (iv) parameters that describe the expected magnitude as a function of time; and the (v) variability.

The user-defined GMPEs can be implemented in the table form, considering all the parameters: ground motion parameters, magnitude, distance, variability, truncation, and units. In CRISIS 2007, various ground motion parameters can be setup as long as the units are correct.

2.7.3. A Benchmark Study for PSHA

Macroseismic intensity has recently attracted attention as a tool for validating probabilistic seismic hazard assessment (PSHA) studies or as an alternative method for PSHA in countries. In Turkey, the new seismic hazard map was recently obtained using the Cornell–McGuire approach with new ground motion prediction equations in terms of the PGA, SA characterized by a 50 per cent, 10 per cent and 2. per cent exceedance probability for an exposure time of 50 years, respectively. By doing this, the hazard calculations are undertaken using a computer code based on the USGS program SEISRISK III. On the other hand, due to the software limitations, probabilistic intensity based hazard maps have been obtained as a result of another software namely CRISIS 2007. Before the intensity based hazard maps have been generated, it was necessary to check the results of the SEISRISK III and CRISIS 2007 softwares at the same input parameters.

The concept of probabilistic seismic hazard assessment was first established by A. Cornell in 1968. In this paper entitled “Engineering Seismic Risk Analysis”, a numerical example has been solved with using the mathematical formulations. As a benchmark study, the same example has been taken into consideration as an earthquake input file for SEISRISK III (Bender *et al.,* 1983) and CRISIS 2007 softwares, and the results have been compared with the results of the relevant paper.

Figure 2.43 illustrates the geometric cross-section of the earthquake source model. A 650 km long fault source for a site located at a minimum surface distance Δ, of 40 km from the area source of earthquakes at depth h = 20 km. has been used to produce a hazard map.

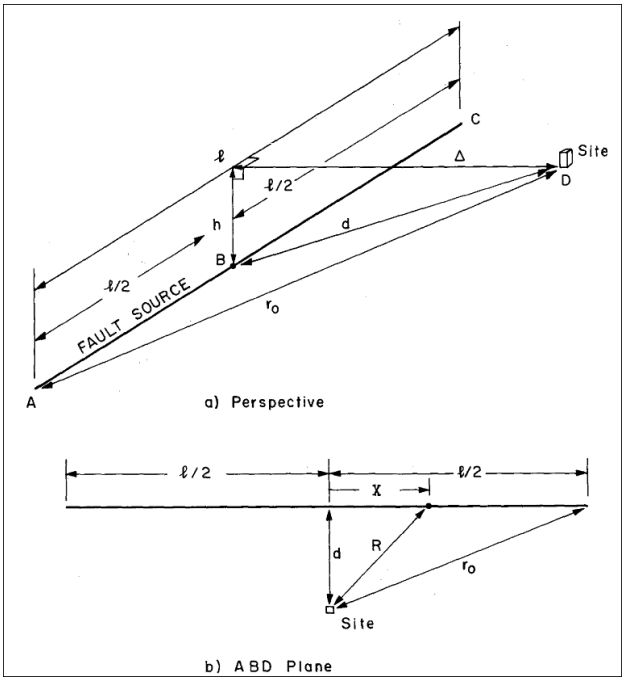

Figure 2.43. Explanation of the numerical example

The earthquake fault source with the following recurrence relationship for a time period of 1953 years is taken into consideration.

Magnitude recurrence relationship: log N = 5.51 – 0.644 M.

The intensity attenuation relationship has the following form:

$$I = c_1 + c_2 M - c_3 \ln R \tag{2.6}$$

where:

I:	Intensity
M:	Magnitude
R:	Distance
c_1, c_2, c_3:	Empirical constants

The empirical constants found by Esteva and Rosenblueth (1964) for California have been used, such that:

c_1: 8.16

c_2: 1.45

c_3: 2.46

The recurrence relationships for a time period of 1953 years has been converted to an annual recurrence relationships as shown in Figure 2.44.

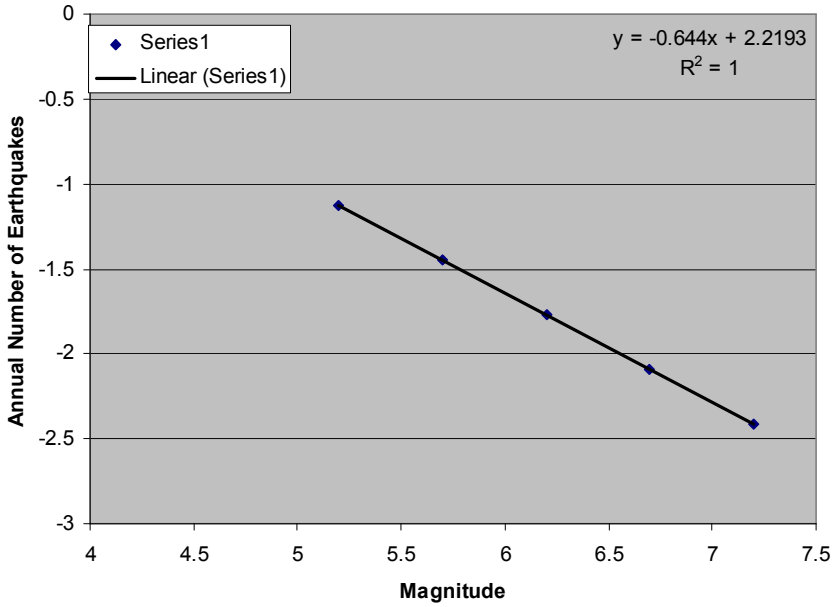

Figure 2.44. Annual number of earthquakes vs magnitude

Cornell study (Cornell, 1968) has calculated the intensity (i) at this site with return period T as

$$i \cong 0.98\, In(0.69T) \tag{2.7}$$

For return period 475 years, the intensity has been calculated as 7.9.

The same example has been solved by Seisrisk III and CRISIS 2007. As Seisrisk III and CRISIS 2007 stipulate the usage of a standard deviation for earthquake location uncertainty, σ = 20 km, compatible with the grid size used in the analysis (0.1°) has been taken into account. However no standard deviation has been used for attenuation variability, since the author does not mention it in his solution. In this example, the usage of earthquake recurrence parameters based on the software is tabulated in Table 2.4.

Table 2.4. Earthquake recurrence parameters used in the models

	SEISRISK III	CRISIS 2007
a	2.2193	-
b	0.644	-
Threshold magnitude (Mo)		5
Lamda(Mo)		0.1
Expected value of Beta - b* ln(10)		1.4829
Coefficient of variation of beta		0
Untruncated expected value		7.5
Untruncated standard devaation		0
Lower limit (M_1)		5
Upper limit (M_2)		7.5

The 18 points with a distance of 40 km from the area source have been determined to compare the results obtained using the two different software with the Cornell study (Cornell, 1968) at the same site. Figure 2.45 shows the location of the points and the area source.

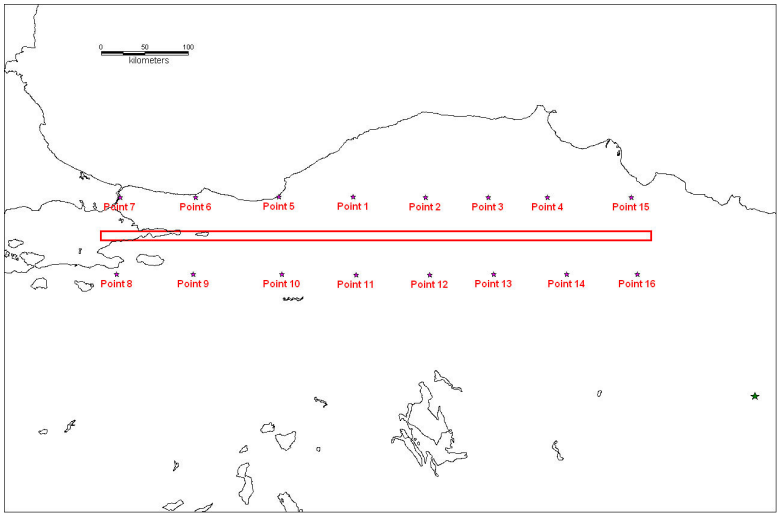

Figure 2.45. Area source model and 16 points with distance of 40km

Considering three different approaches, earthquake hazard results at the same points in terms of intensity with a return period of 475 years have been tabulated in Table 2.5.

Table 2.5. The result of a numerical example using three different approaches

475 Return Period (years)	Intensity (SEISRISK III)	Intensity (CRISIS 2007)	Intensity (A. Cornell)
Point 1	7.8080	7.26	7.7
Point 2	7.8300	7.27	
Point 3	7.8150	7.28	
Point 4	7.7800	7.28	
Point 5	7.8030	7.27	
Point 6	7.7690	7.37	
Point 7	7.4580	7.62	
Point 8	7.3860	7.6	
Point 9	7.5150	7.38	
Point 10	7.4100	7.27	
Point 11	7.3440	7.26	
Point 12	7.3070	7.26	
Point 13	7.4350	7.28	
Point 14	7.5250	7.29	
Point 15	7.4650	7.09	
Point 16	7.3800	7.05	

The result of the comparison (Table 2.5) shows that both of two programs can be used to perform an earthquake hazard map, although, the small differences are obtained due to the usage of a different algorithm in each software.

2.8. The Results of Site Independent Seismic Hazard

The present analysis has been conducted for return periods of 72, 475 and 2,475 years corresponding to 50 per cent, 90 per cent and 98 per cent probabilities of non-exceedence in 50 years respectively. The selected ground motion parameters of analysis were the PGA, the SA at periods of 0.2 sec and 1. sec and macro- seismic intensity. A grid size of 0.05° by 0.05° was used. The earthquake location uncertainty was taken as 10 km. The standard deviations in the attenuation functions were considered as given in the associated papers.

The earthquake hazard assessment is generally conducted for the free-field reference soil sites, generally chosen as the so-called “engineering bedrock” where the average shear wave propagation velocity in the upper 30m is less than about 750m/s (in US practice National Earthquake Hazard Reduction Program - NEHRP Site Class B/C boundary). The average of Boore *et al.* (1997), Sadigh *et al.* (1997), and Campbell (1997) for PGA and the average of Boore *et al.* (1997), Sadigh *et al.* (1997), for SA at short and long periods (S_s and S_1) have been utilized. Considering the older generation ground motion prediction models (previous to NGA models), the results for the engineering bedrock condition are presented in Figure 2.46 through Figure 2.54, respectively.

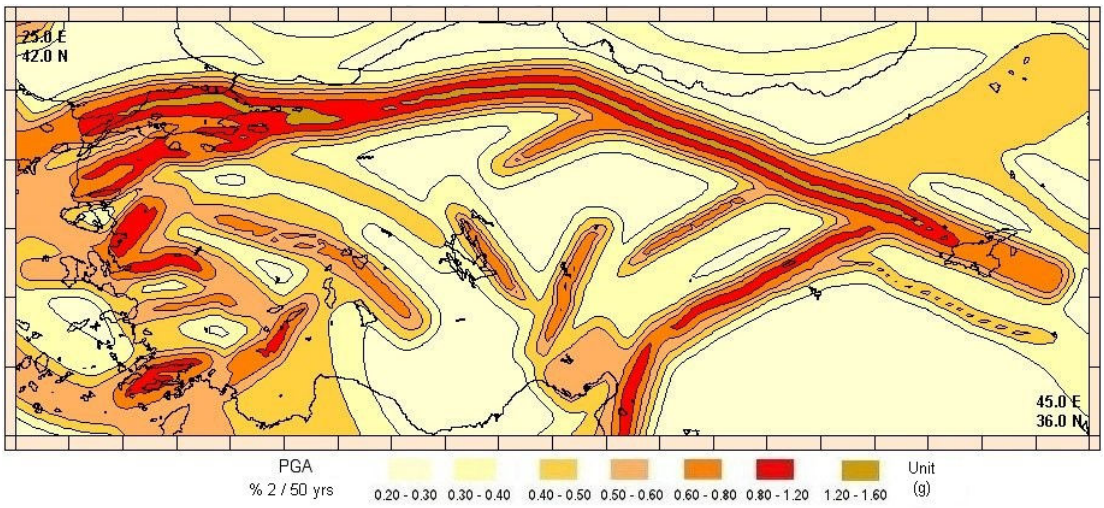

Figure 2.46. PGA for 2. per cent probability of exceedence in 50 years using previous GMPE

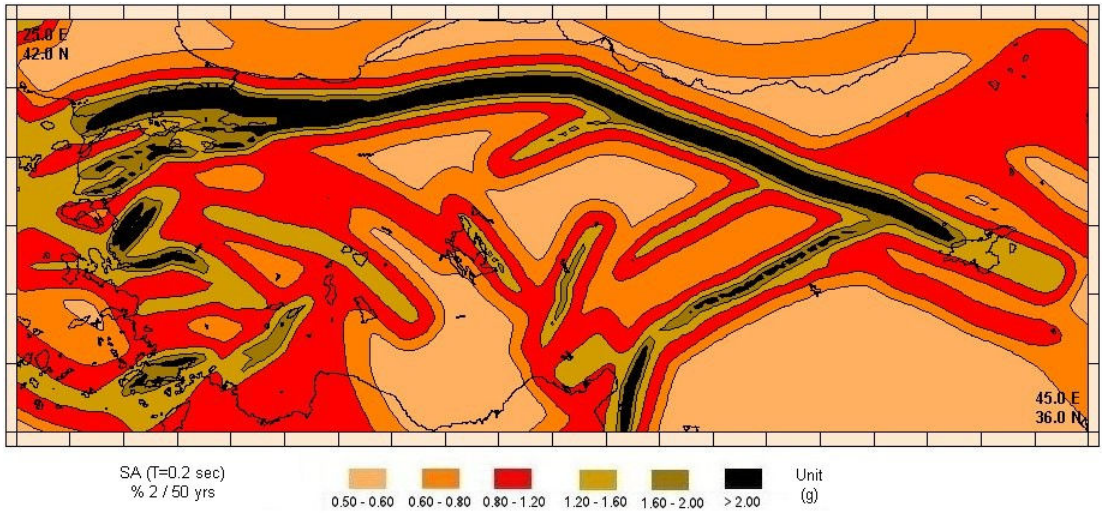

Figure 2.47. SA at T=0.2 sec for 2. per cent probability of exceedence in 50 years using previous GMPE

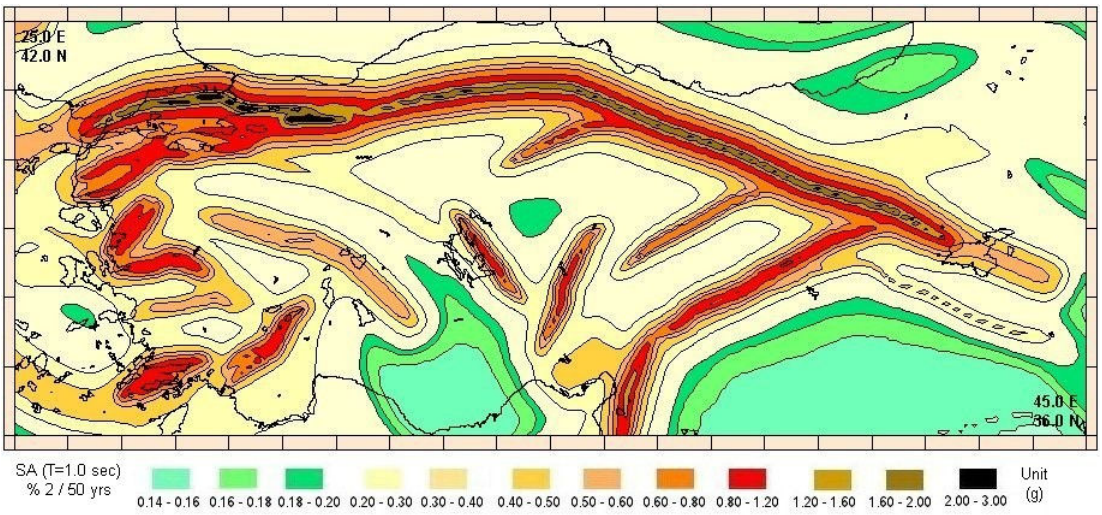

Figure 2.48. SA at T=1.0 sec for 2. per cent probability of exceedence in 50 years using previous GMPE

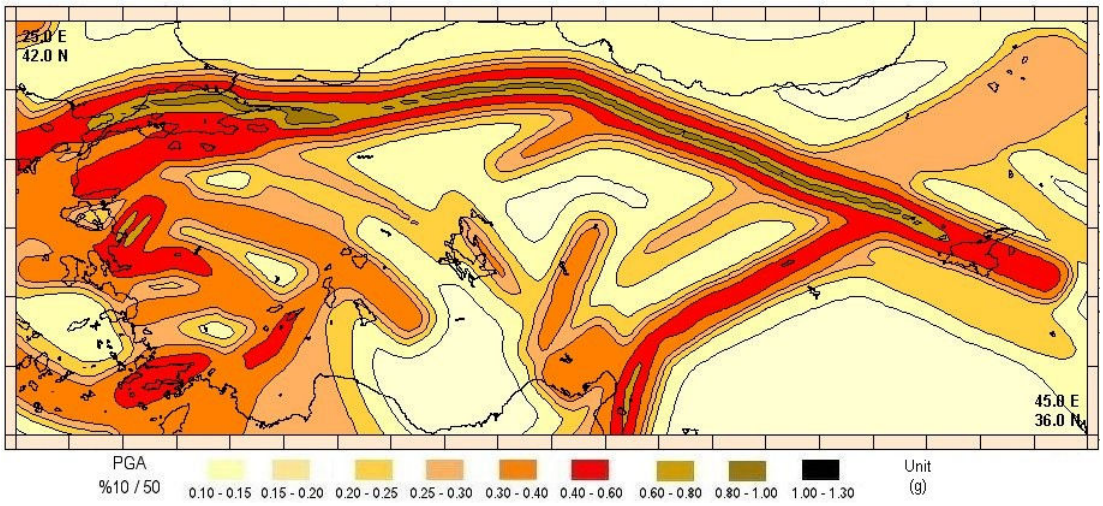

Figure 2.49. PGA for 10 per cent probability of exceedence in 50 years using previous GMPE

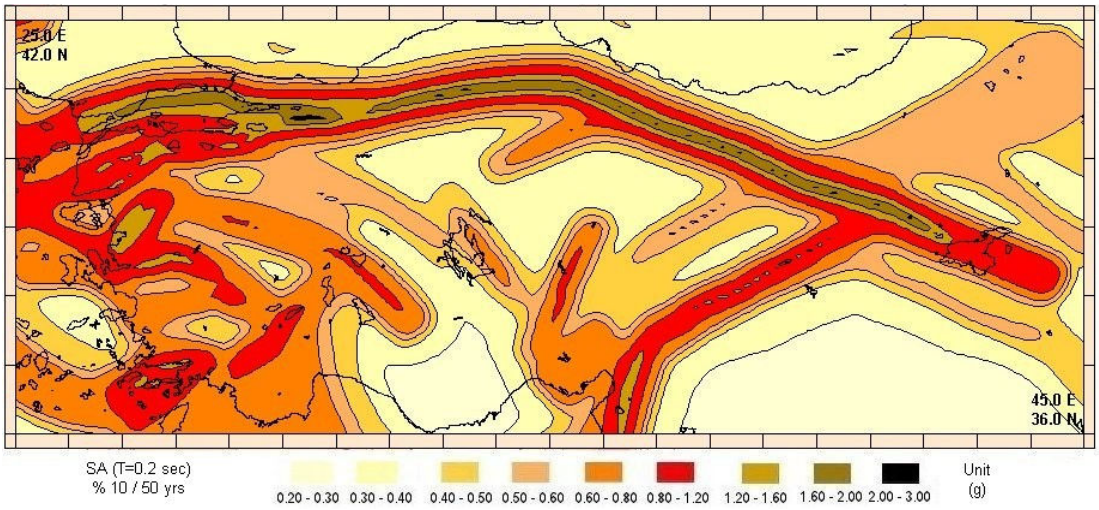

Figure 2.50. SA at T=0.2 sec for 10 per cent probability of exceedence in 50 years using previous GMPE

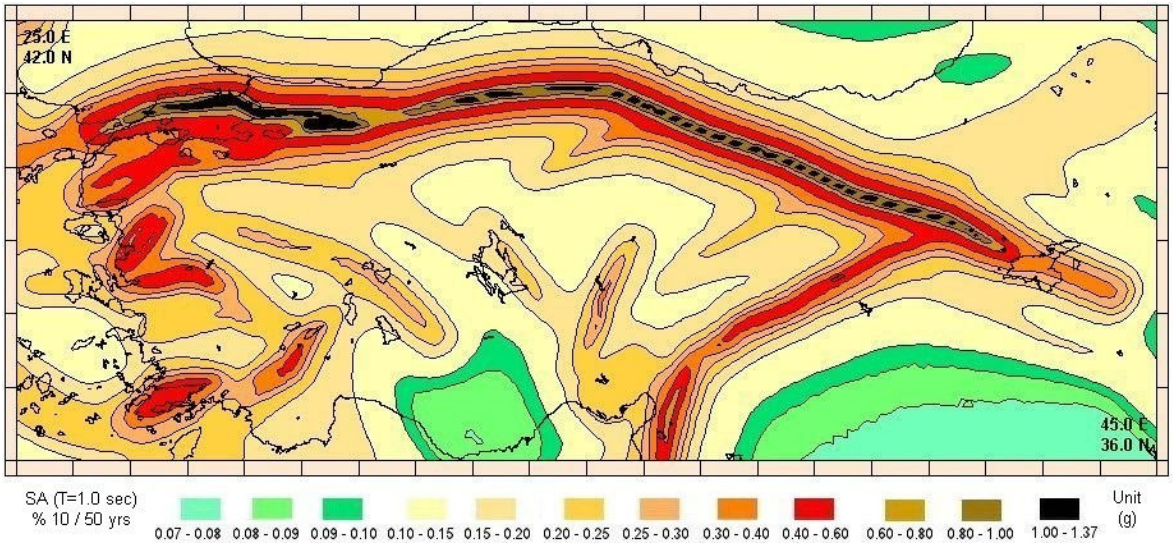

Figure 2.51. SA at T=1.0 sec for 10 per cent probability of exceedence in 50 years using previous GMPE

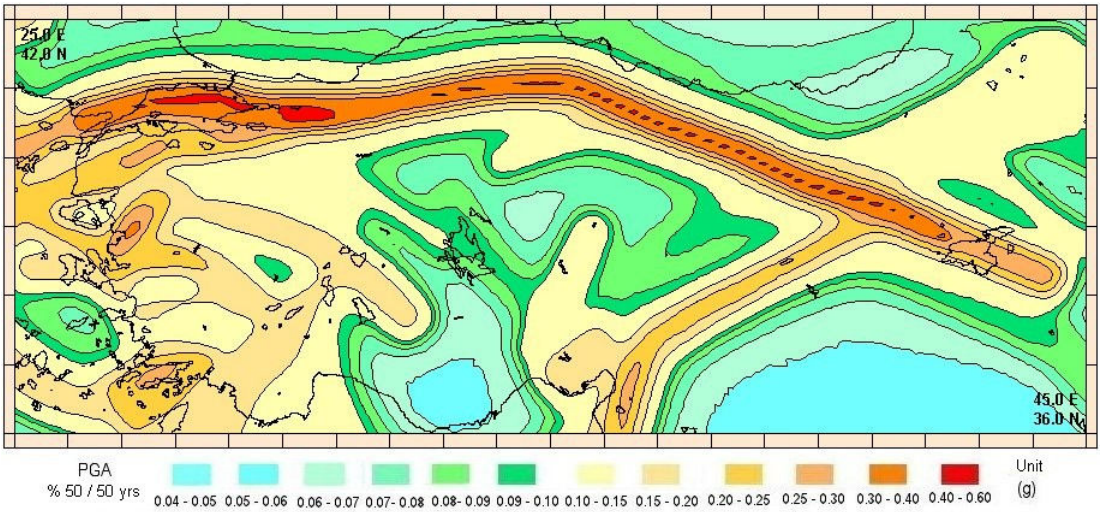

Figure 2.52. PGA for 50 per cent probability of exceedence in 50 years using previous GMPE

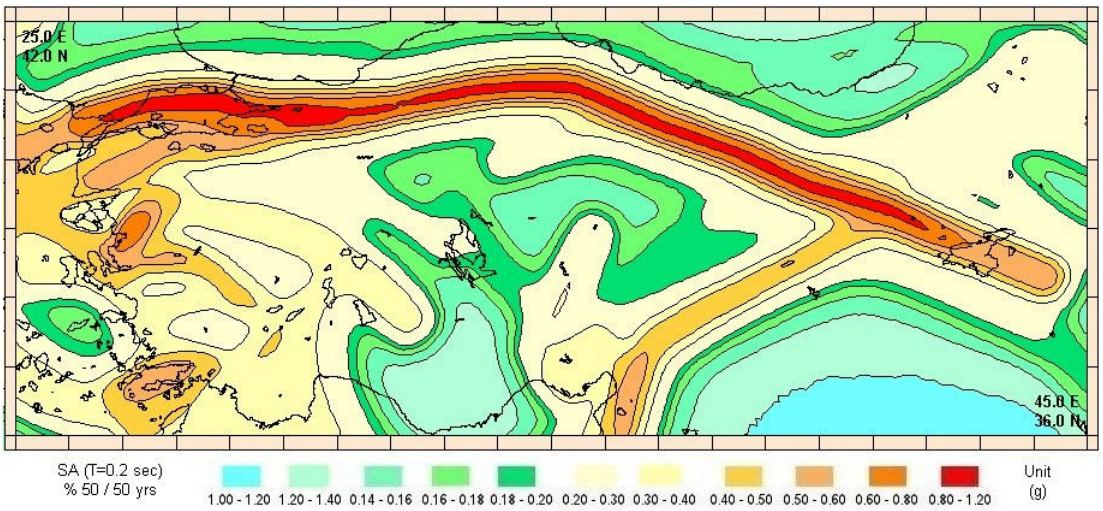

Figure 2.53. SA at T=0.2 sec for 50 per cent probability of exceedence in 50 years using previous GMPE

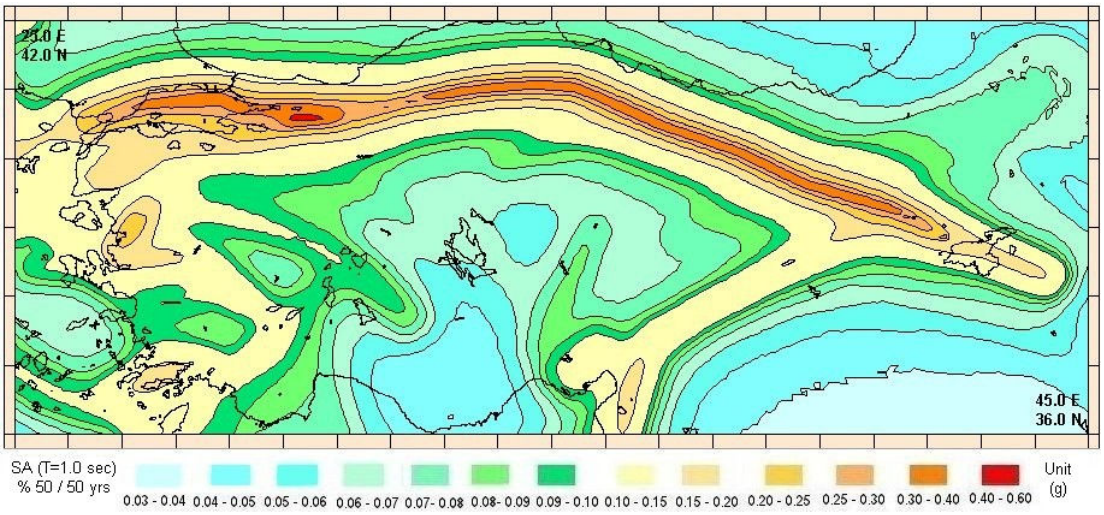

Figure 2.54. SA at T=1.0 sec for 50 per cent probability of exceedence in 50 years using previous GMPE

As a consequence of the change of paradigm in earthquake resistant design stronger design earthquakes now control the seismic design of important structures. These stronger earthquakes include the effects of near-field pulses, fault-normal motions, and near-field deep soil site motions. As a consequence, there is a strong need for the development of robust and reliable techniques for the assessment of long period earthquake ground motions especially for near field conditions. To provide an example to the assessment of long period ground motion a comparative study has been carried out for Turkey. The probabilistic earthquake hazard has been investigated using PEER-NGA (2008) new generation ground motion prediction equations for PGA and SA (0.2 sec, 1. sec, 2. sec, 4. sec, 5. sec, 7.5 sec) corresponding to 50 per cent, 10 per cent and 2. per cent probabilities of exceedance in 50 years. Generally, PGA values can be used to obtain the EuroCode whereas, SA (0.2 sec and 1. sec) can be used to obtain the NEHRP (2003) based response spectra. SA (0.2 sec, 1. sec, 2. sec, 4. sec, 5. sec, and 7.5 sec) values can be used to plot the equi-hazard spectrum. Furthermore associated hazard deaggregation has been conducted for several selected sites to obtain rational estimates of the deterministic long period spectral accelerations and the deterministic spectral shapes. Comparison of the findings indicates significant variation of long period spectral accelerations. The accuracy of seismic design spectra given in current codes is not sufficient for these periods. There is

also a need to develop guidelines for the selection of design basis ground motion for long period or highly nonlinear (softening) structure.

The results obtained from computations with the next generation ground motion prediction equations for earthquake engineering bedrock conditions are shown in Figure 2.55 through Figure 2.71. The average of Boore and Atkinson (2008), Chiou and Young (2008) and Campbell and Bozorgnia (2008) empirical equations for the PGA, the average of Boore *et al.* (2008) and Campbell and Bozorgnia (2008) empirical equations for Spectral Acceleration at 0.2 sec. and 1. sec. periods are utilized. The results are shown in Figure 2.55 through Figure 2.75.

To observe the effect of the new generation ground motion prediction equations on the hazard map, the comparison between the results obtained by using older and new generation ground motion prediction equations are presented in Figure 2.77.

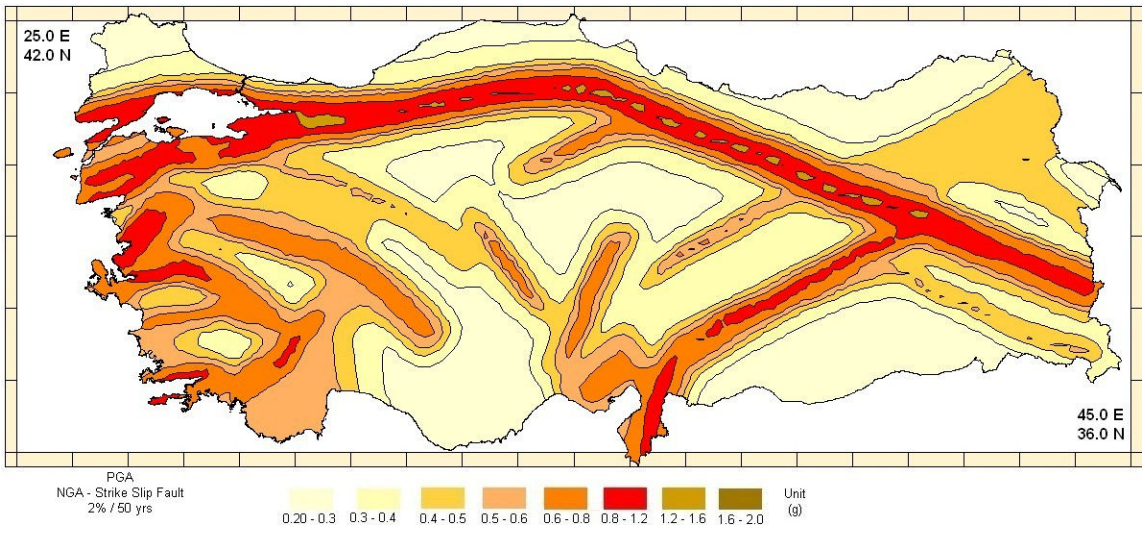

Figure 2.55. PGA for 2. per cent probability of exceedence in 50 years using NGA GMPE

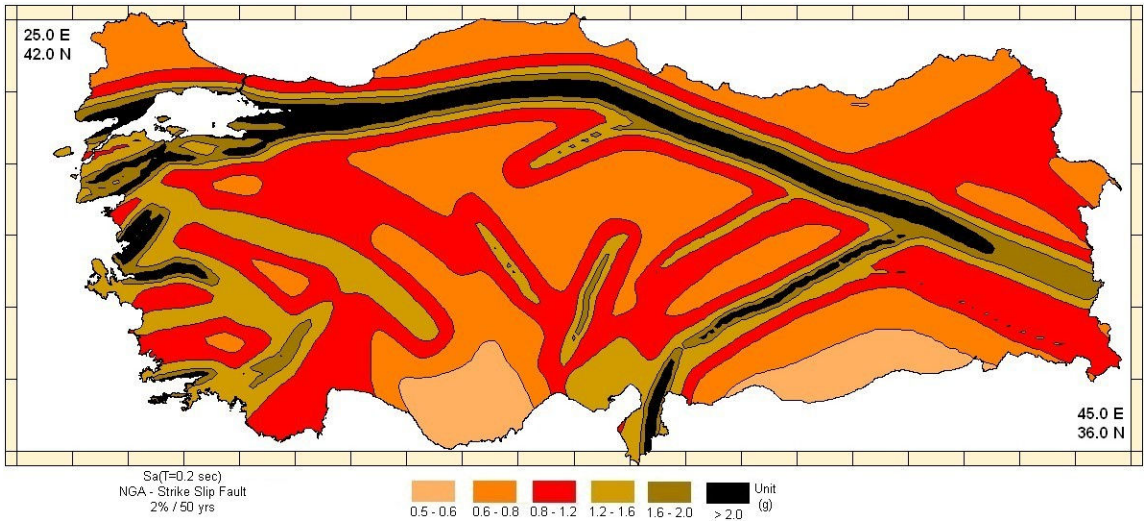

Figure 2.56. SA at T=0.2 sec for 2. per cent probability of exceedence in 50 years using NGA GMPE

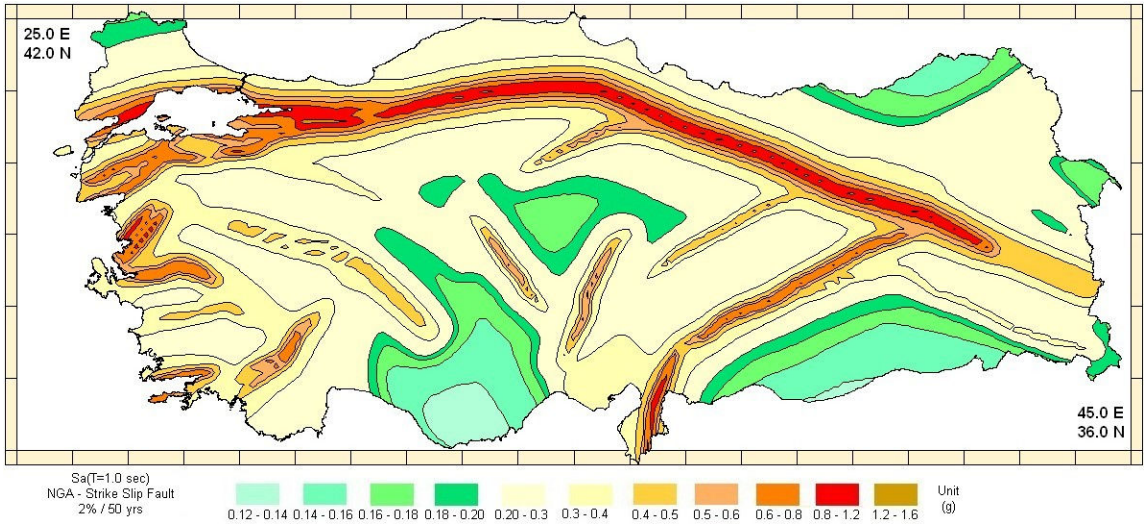

Figure 2.57. SA at T=1.0 sec for 2. per cent probability of exceedence in 50 years using NGA GMPE

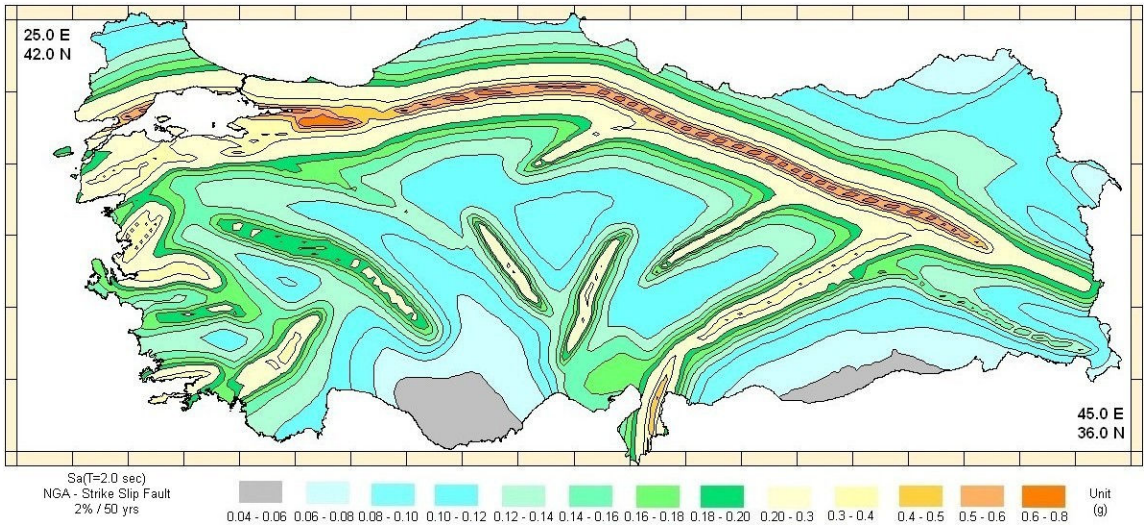

Figure 2.58. SA at T=2.0 sec for 2. per cent probability of exceedence in 50 years using NGA GMPE

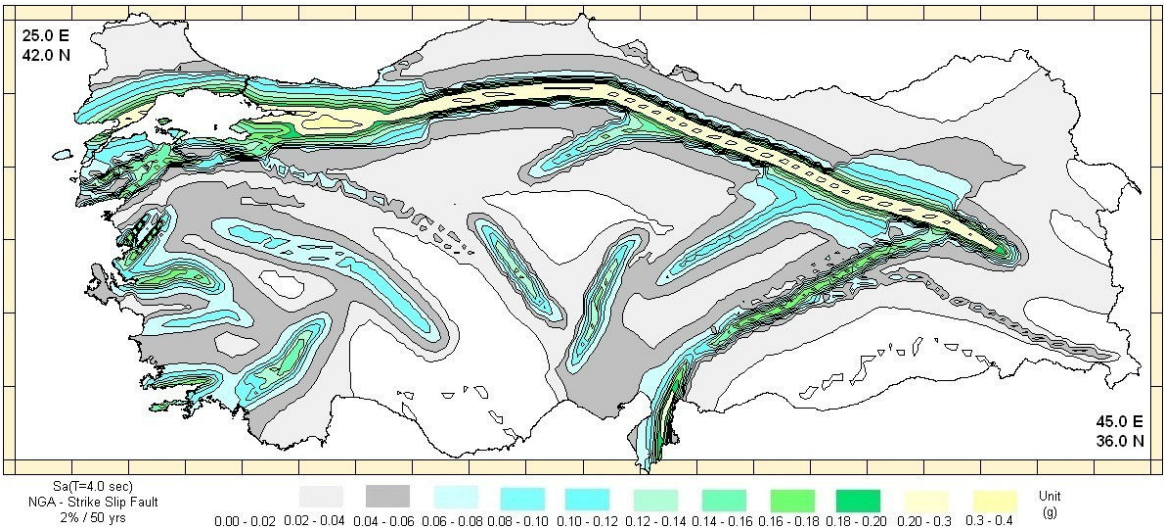

Figure 2.59. SA at T=4.0 sec for 2. per cent probability of exceedence in 50 years using NGA GMPE

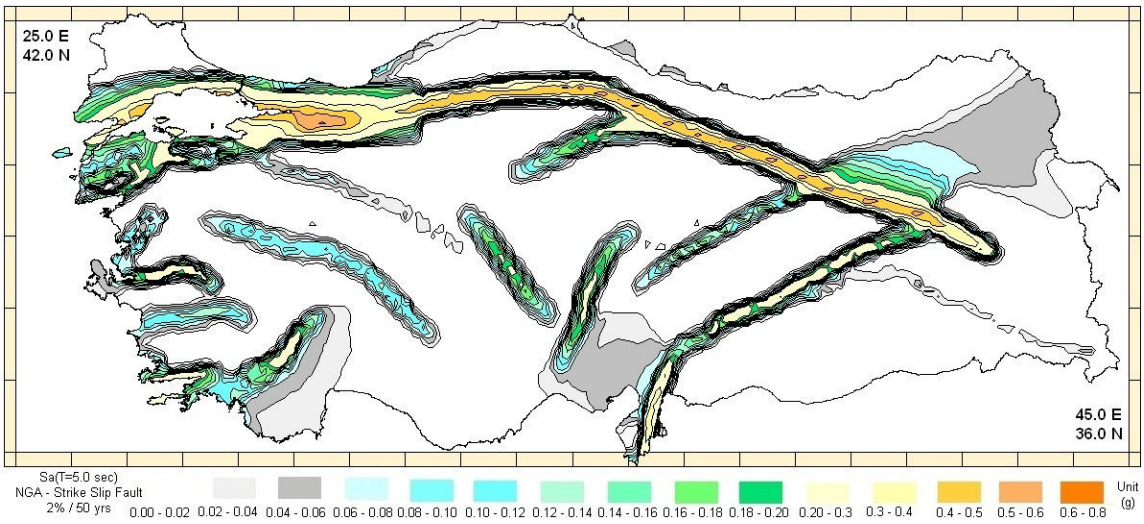

Figure 2.60. SA at T=5.0 sec for 2. per cent probability of exceedence in 50 years using NGA GMPE

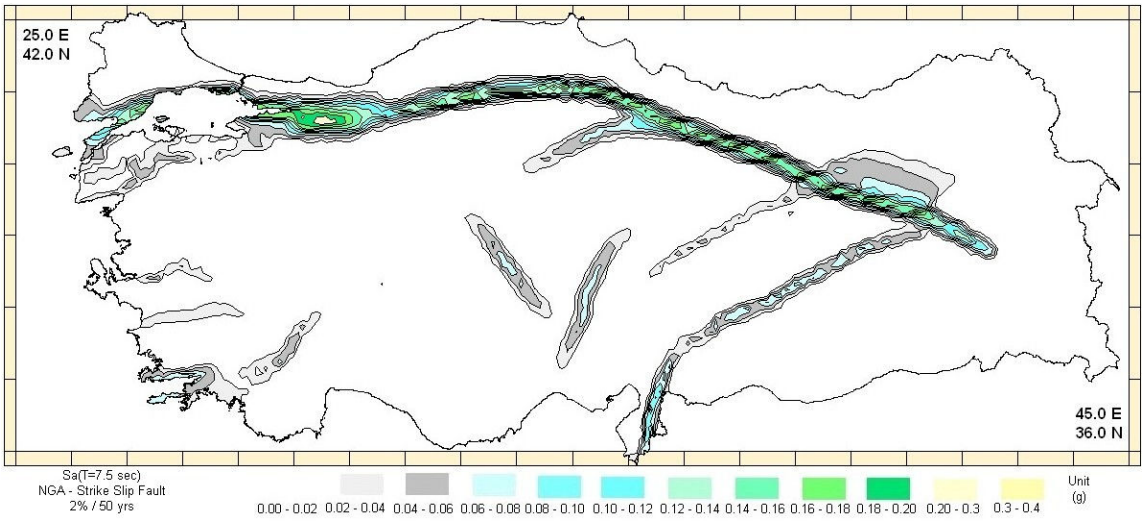

Figure 2.61. SA at T=7.5 sec for 2. per cent probability of exceedence in 50 years using NGA GMPE

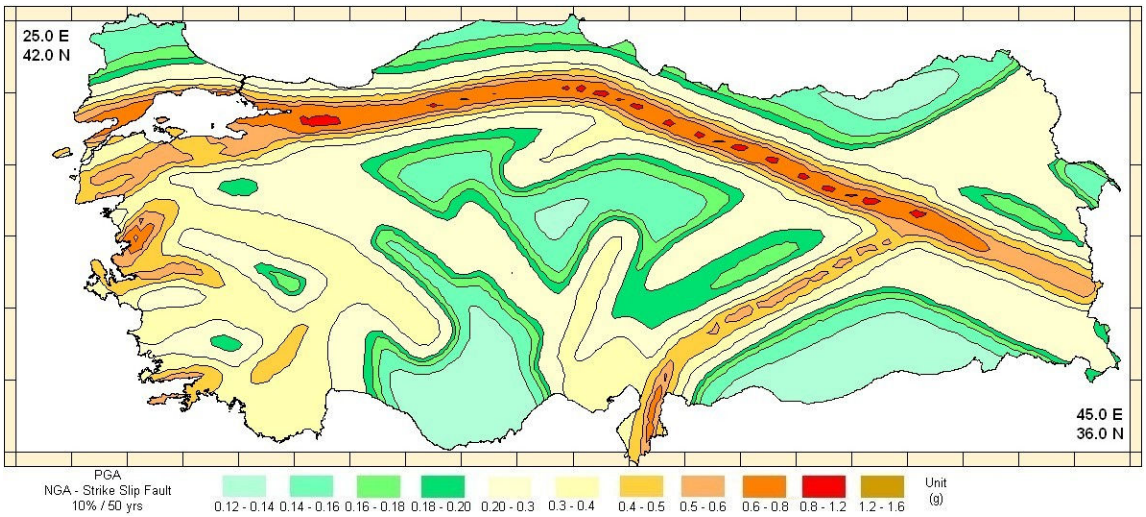

Figure 2.62. PGA for 10 per cent probability of exceedence in 50 years using NGA GMPE

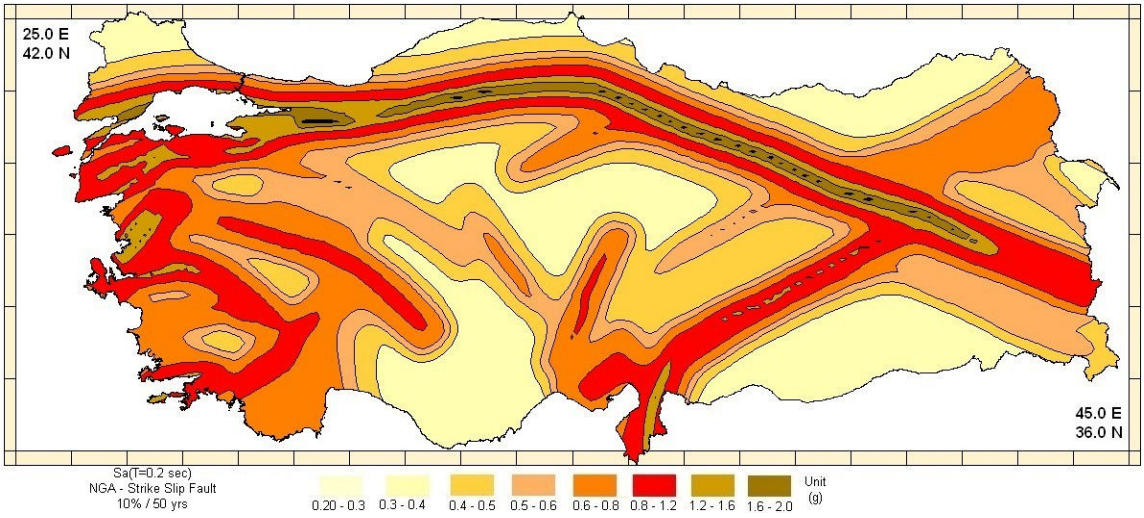

Figure 2.63. SA at T=0.2 sec for 10 per cent probability of exceedence in 50 years using NGA GMPE

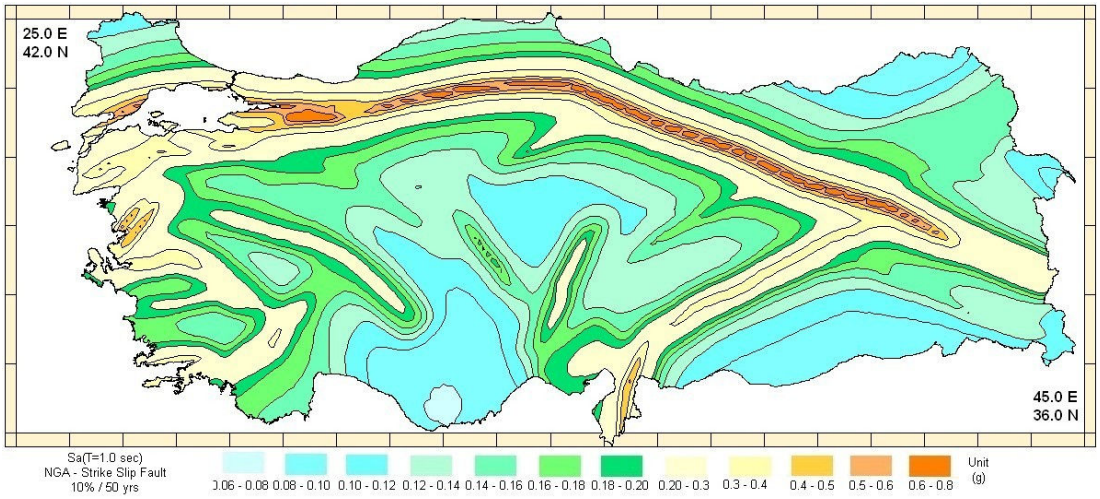

Figure 2.64. SA at T=1.0 sec for 10 per cent probability of exceedence in 50 years using NGA GMPE

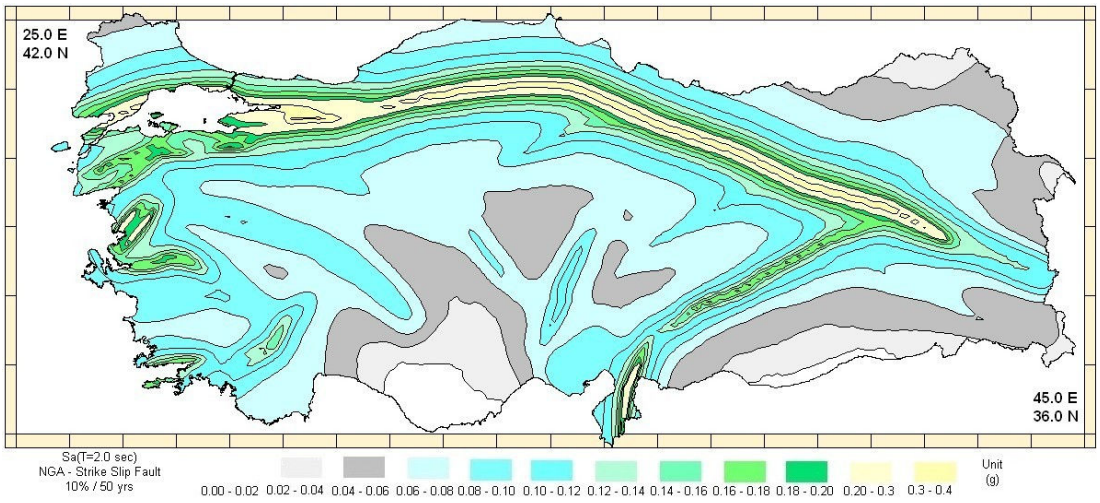

Figure 2.65. SA at T=2.0 sec for 10 per cent probability of exceedence in 50 years using NGA GMPE

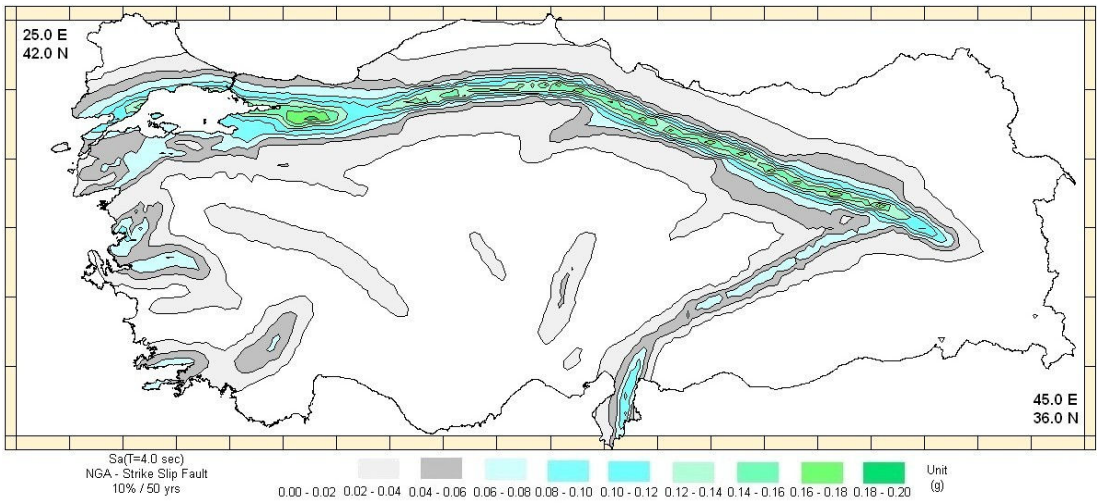

Figure 2.66. SA at T=4.0 sec for 10 per cent probability of exceedence in 50 years using NGA GMPE

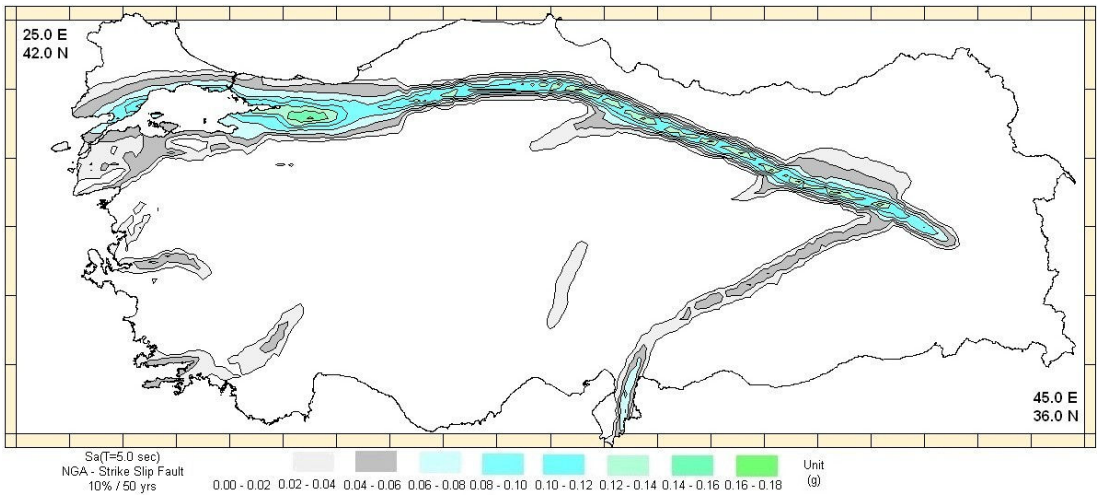

Figure 2.67. SA at T=5.0 sec for 10 per cent probability of exceedence in 50 years using NGA GMPE

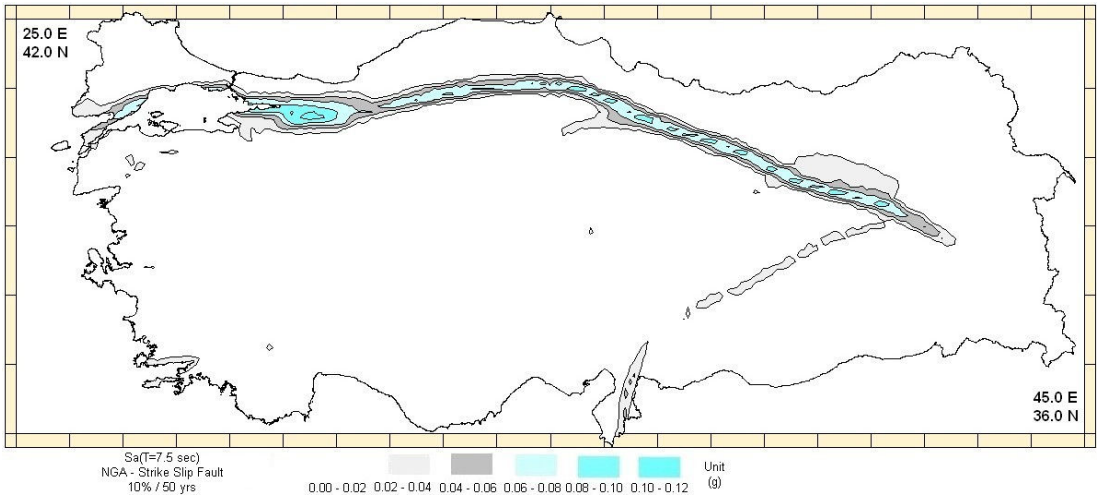

Figure 2.68. SA at T=7.5 sec for 10 per cent probability of exceedence in 50 years using NGA GMPE

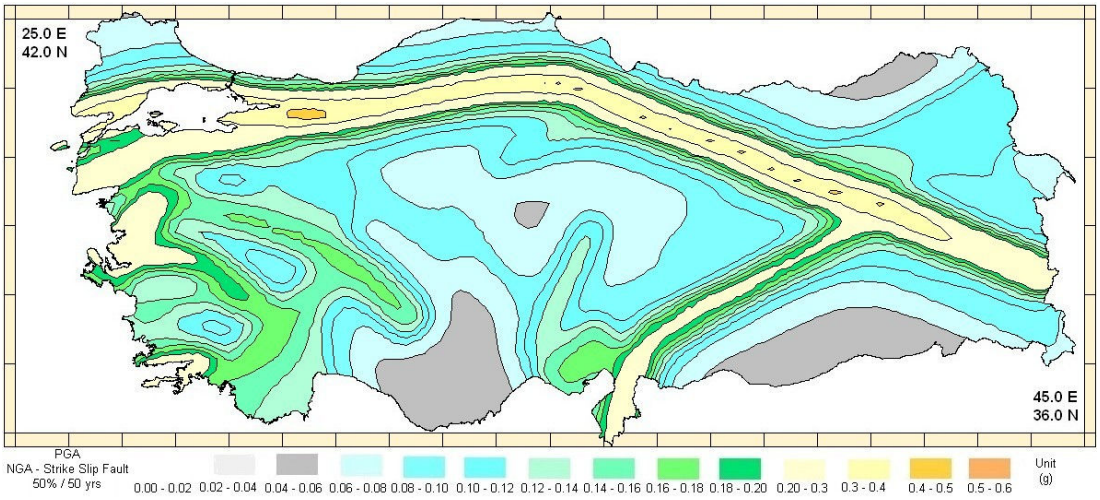

Figure 2.69. PGA for 50 per cent probability of exceedence in 50 years using NGA GMPE

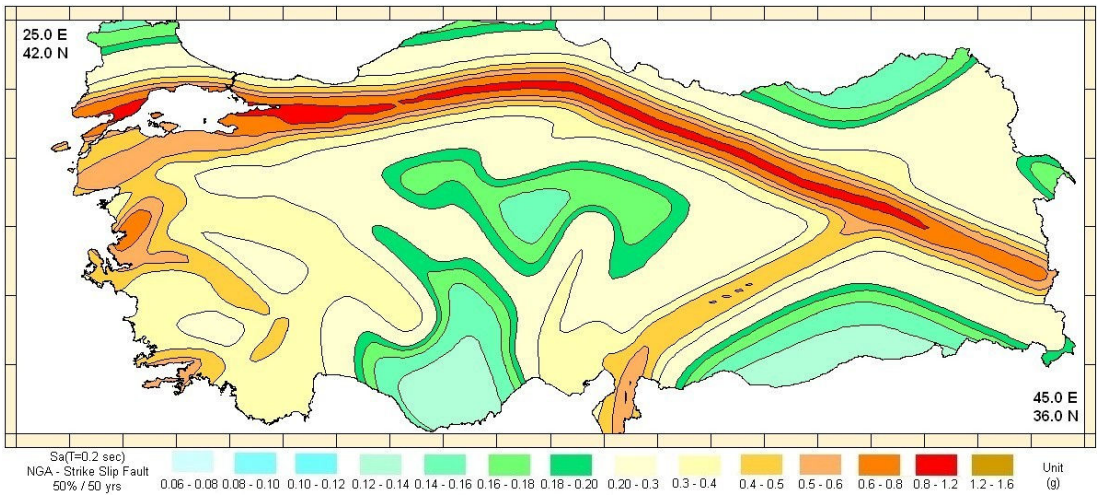

Figure 2.70. SA at T=0.2 sec for 50 per cent probability of exceedence in 50 years using NGA GMPE

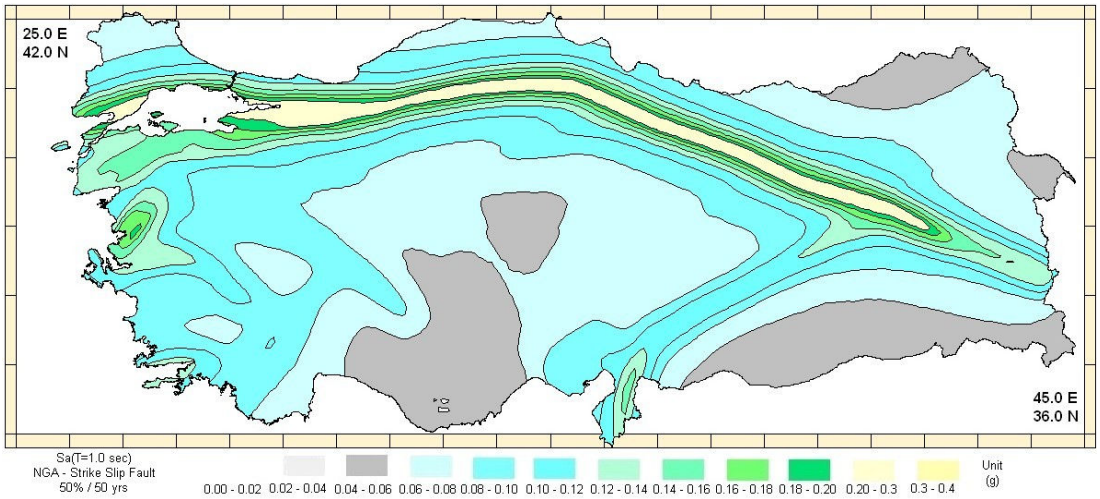

Figure 2.71. SA at T=1.0 sec for 50 per cent probability of exceedence in 50 years using NGA GMPE

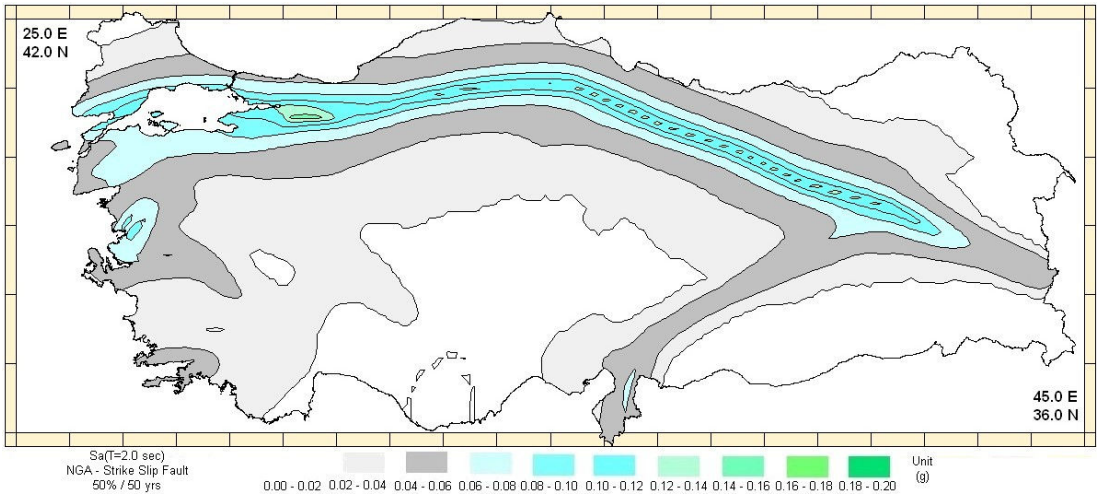

Figure 2.72. SA at T=2.0 sec for 50 per cent probability of exceedence in 50 years using NGA GMPE

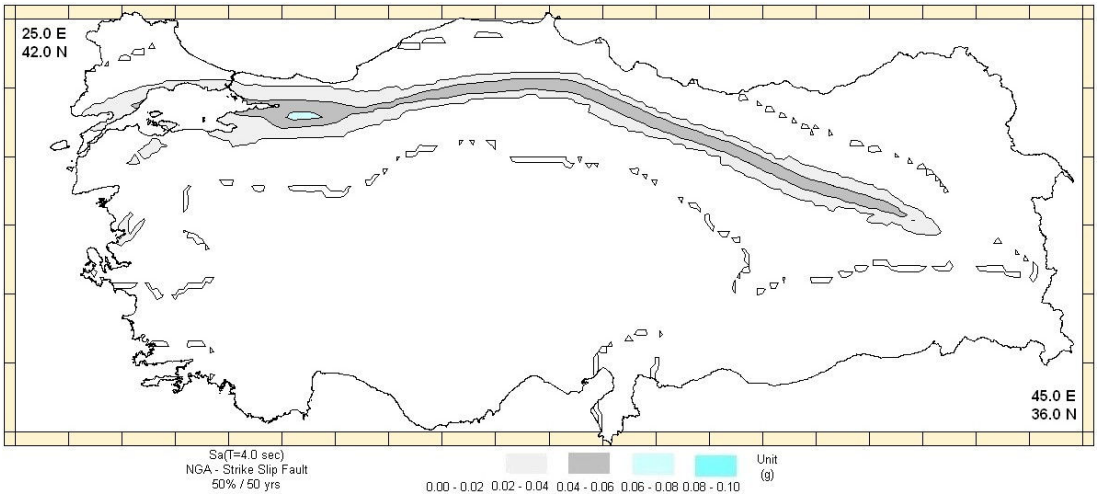

Figure 2.73. SA at T=4.0 sec for 50 per cent probability of exceedence in 50 years using NGA GMPE

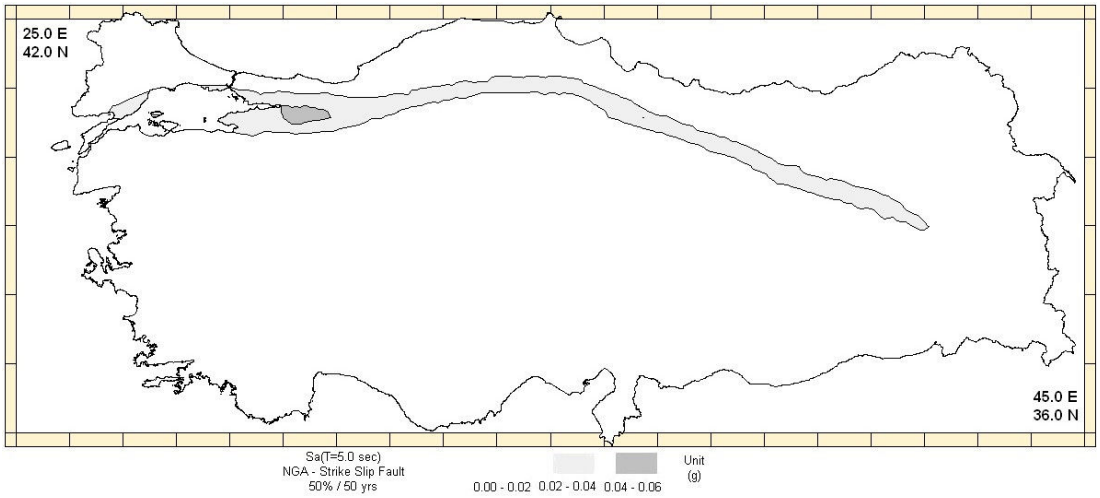

Figure 2.74. SA at T=5.0 sec for 50 per cent probability of exceedence in 50 years using NGA GMPE

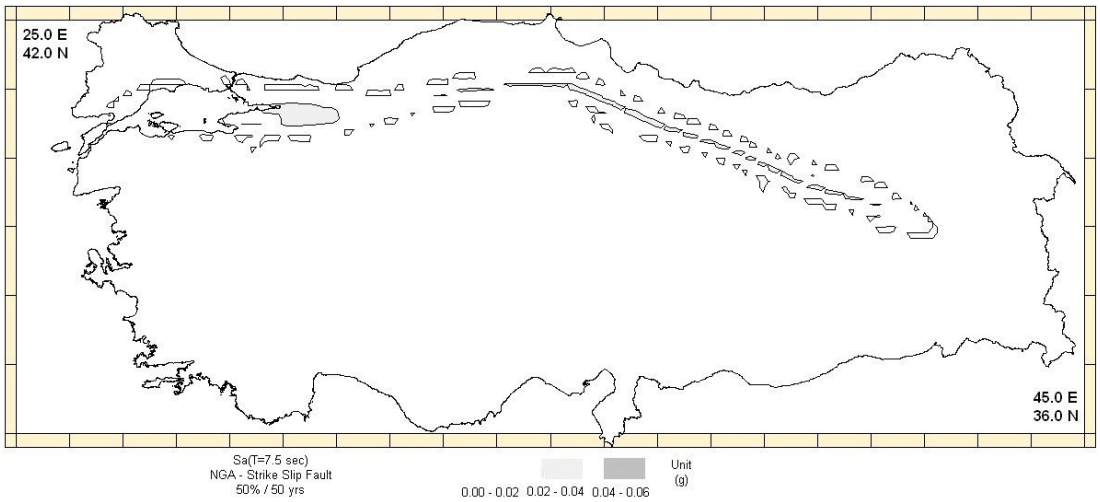

Figure 2.75. SA at T=7.5 sec for 50 per cent probability of exceedence in 50 years using NGA GMPE

Current studies in the United States Geological Survey (USGS) are released in the latest version of its National Seismic Hazard Maps in 2008. The earthquake hazard maps of USGS, previously updated in 2002, include the best available scientific data on fault slip rates, paleo-seismic data, earthquake catalogs and strong ground motion recordings from the global earthquakes. These maps define the latest scientific view of earthquake hazard

(*e.g.* using the NGA GMPE) at varying probability levels across the U.S. The new hazard maps are significantly different from the old maps (2002) showing a 10 per cents decrease in hazard for small residential buildings (Figure 2.76).

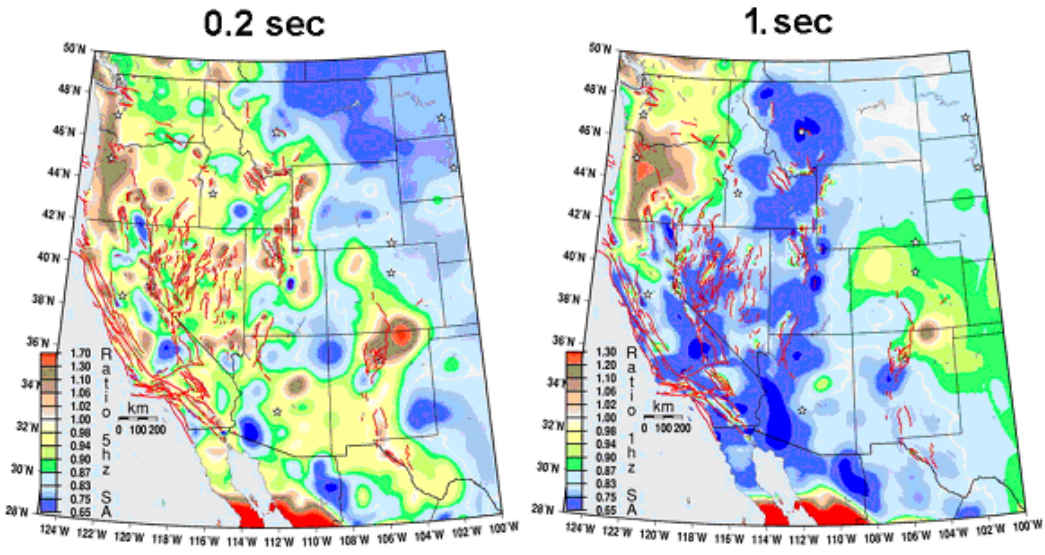

Figure 2.76. Change of earthquake hazard map from 2002 to 2008 in Western United States (taken from Y. Bozorgnia presentation)

Similar comparison is observed to generate a new hazard map for Turkey. As shown in Figure 2.77 and Figure 2.78, a decrease of about 10 per cent in the earthquake hazard levels are produced using NGA model especially in the vicinity of the active seismic regions of Turkey.

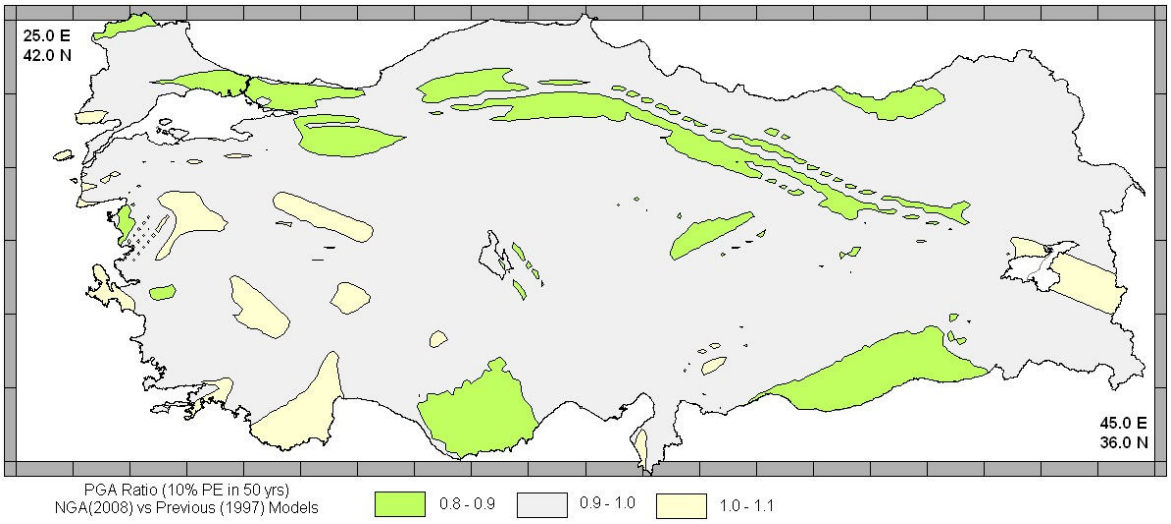

Figure 2.77. The ratio of PGA using the previous and the NGA ground motion prediction in the earthquake hazard analysis

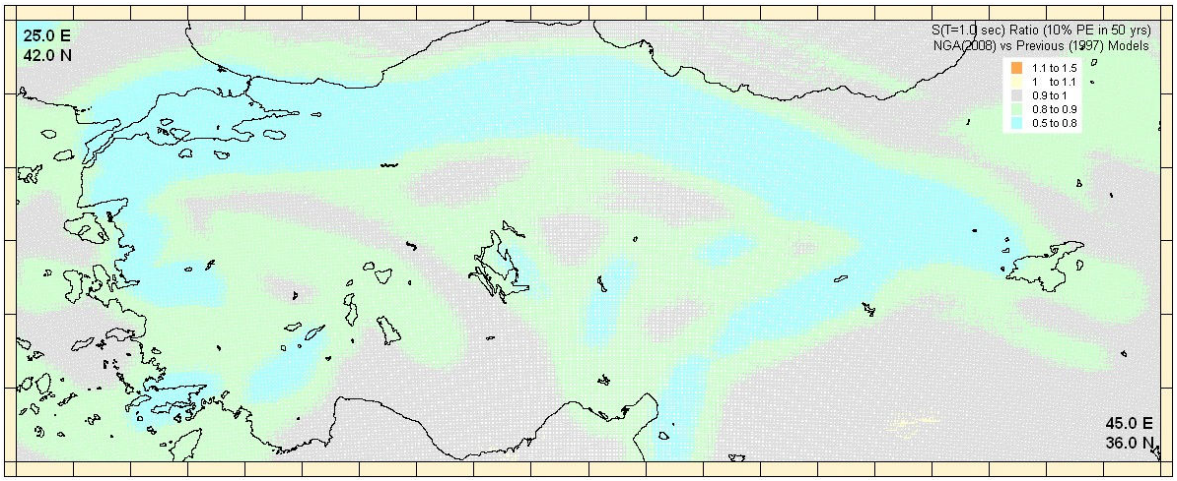

Figure 2.78. The ratio of SA (T=1.0s) ground motion using the previous and the NGA ground motion prediction in the earthquake hazard analysis

2.8.1. Intensity Based Hazard Maps

Macroseismic intensity has recently attracted attention as a tool for validating probabilistic seismic hazard assessment (PSHA) studies or as an alternative method for PSHA in countries where the historical catalog is much longer than the instrumental one.

In this study, a regional intensity based ground motion prediction equation (Sesetyan *et al*., 2005) is used as the selected ground motion parameter of analysis. The present analysis is conducted for return periods of 72, 475 and 2,475 years corresponding to 50 per cent, 90 per cent and 98 per cent probabilities of exceedence in 50 years, respectively. The iso-seismal maps are shown in Figure 2.79 through Figure 2.81. The seismic hazard map obtained for return period of 72 years is also utilized to estimate the building damage and the casualty.

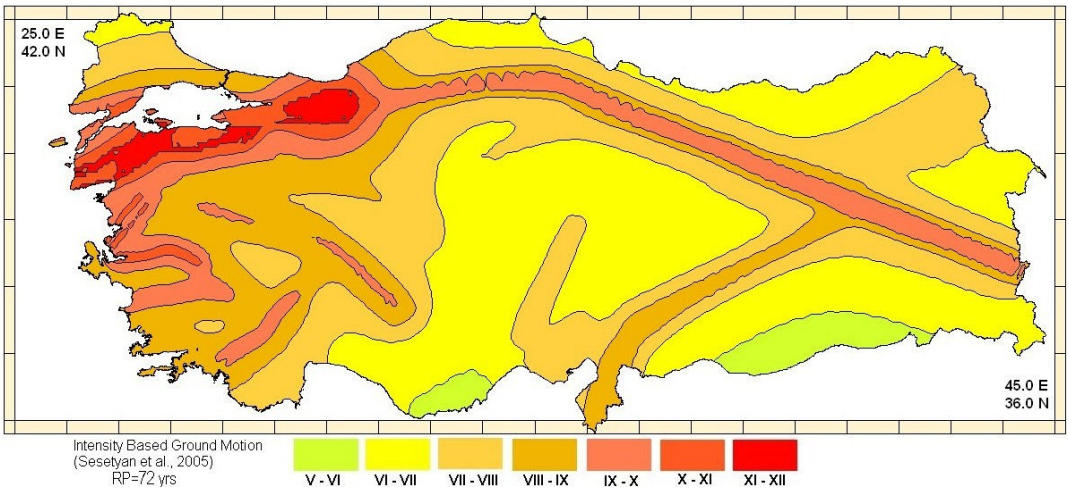

Figure 2.79. Intensity based ground motion for 50 per cent probability of exceedence in 50 years

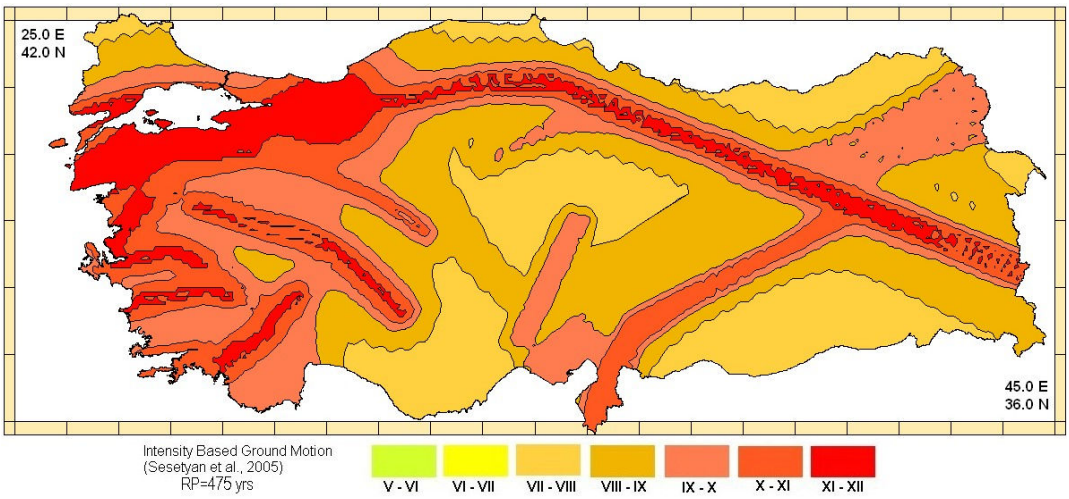

Figure 2.80. Intensity based ground motion for 10 per cent probability of exceedence in 50 years

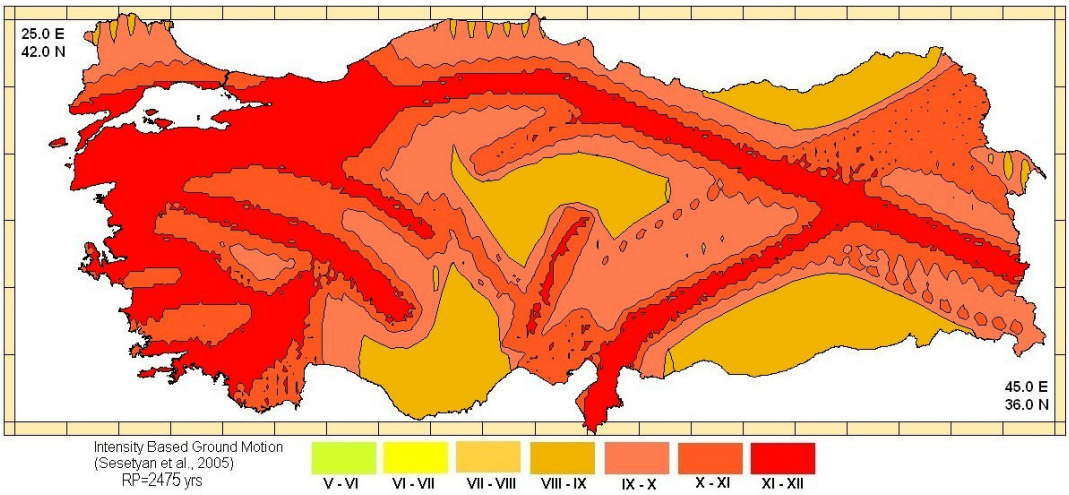

Figure 2.81. Intensity based ground motion for 2. per cent probability of exceedence in 50 years

2.9. Methodology of Site Dependent Seismic Hazard

The PSHA methodology being used today is in line with and assists to the current developments in performance based earthquake resistant design (*e.g.* Vision 2000, SEAOC, 1996, International Building Code - IBC, 2000, 2003; European Building Code - Eurocode-8, 2004), where descriptions of earthquake ground motion at different probabilities of exceedance are needed to meet specified set of buildings or structural performance objectives.

The earthquake hazard assessment is generally conducted for the free-field reference soil sites. Site dependence of the response spectrum found through such a hazard assessment can be accomplished by using site-dependent ground motion prediction equation, modifying on the basis of spectral modification factors (generally used in the earthquake resistant design codes) or by conducting rigorous site response analysis using a suite of spectrum compatible ground motion.

The influence of the local geological structure on damage distribution due to ground-motion amplification (also called site effects) has been well known in the literature (Borcherd, 1994). The construction of the design basis response spectrum for different Site Classes can be achieved through the modification of the spectral acceleration (SA at 0.2s

and at 1.0 sec) given by the hazard maps in Section 2.8. The Uniform Hazard Response Spectrum presented in NEHRP (2003) that is employed as the appropriate spectral shape for a site is constructed with two parameters: the site-specific short period (SMS); and medium-period (SM1).

The shape of the spectrum for five per cent damping is illustrated in Figure 2.82. The site-specific short-period spectral response acceleration parameter, S_{MS} and medium-period parameter S_{M1}can be obtained as follows:

$$S_{MS} = Fa * Ss \qquad \text{where} \quad Ss=SA(0.2sec)$$

$$S_{M1} = Fv * S1 \qquad \text{where} \quad S_1= SA(1.\ sec) \tag{2.8}$$

Where Ss and S_1 are represented by the spectral accelerations at T=0.2 sec and T=1.0 sec at reference soil site ($V_{s,30}$ ≥760m/s) obtained from the hazard analysis. Fa and Fv are respectively the applicable short and medium period amplification factors, defined in NEHRP (2003) (Table 2.6 and Table 2.7).

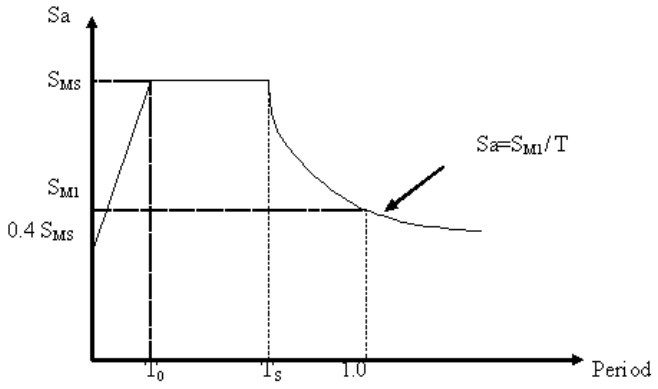

Figure 2.82. Standard shape of the response spectrum (NEHRP 2003)

Table 2.6. Values of Fa as a function of site class and 0.2 sec SA (at B/C boundary with Vs = 760 m/s)

Site Class	Ss≤0.25	Ss=0.50	Ss=0.75	Ss=1.0	Ss≥1.25
A	0.8	0.8	0.8	0.8	0.8
B	1	1	1	1	1
C	1.2	1.2	1.1	1	1
D	1.6	1.4	1.2	1.1	1
E	2.5	1.7	1.2	0.9	0.9
F	*	*	*	*	*

* Site-specific geotechnical investigation and dynamic site response analyses shall be performed.

Table 2.7. Values of Fv as a function of site class and 1.0 sec SA (at B/C boundary with Vs = 760 m/s)

Site Class	Ss≤0.1	Ss=0.20	Ss=0.3	Ss=0.4	Ss≥0.5
A	0.8	0.8	0.8	0.8	0.8
B	1	1	1	1	1
C	1.7	1.6	1.5	1.4	1.3
D	2.4	2.0	1.8	1.6	1.5
E	3.5	3.2	2.8	2.4	2.4
F	*	*	*	*	*

* Site-specific geo-technical investigation and dynamic site response analyses shall be performed.

In order to find the local site effects for Marmara region, earthquake ground motions in terms of intensity and spectral accelerations have been modified using the local geological map and NEHRP based site class map in Istanbul, respectively (Erdik *et al.*, 2004). Recently, a geologic map of Turkey including the geological age information as Quaternary, Mesozoic and Tertiary (QTM) has been produced in digital form by the General Directorate of Mineral Research and Exploration (MTA). In this study, this geological map for Turkey has been utilized to reflect local site effects in earthquake

hazard analysis. This approach involves using site classification and empirically derived adjustment factors. For southern California, the regional QTM classification was developed by Park and Elrick (1998) and used for site correction in the TriNet ShakeMap (Wald *et al*., 1999). Using the same approach the regional QTM classification map developed for Turkey (Figure 2.83) has been used in the intensity based study. Table 2.8 shows the average shear wave velocity values for each site type.

Table 2.8. QTM site correction

Site Type (Vs, m/s)	Corrections for Specified Input PGA			
	< 15 %g	15-25 %g	25-35 %g	> 35%g
Mesozoic (589 m/s)				
0.1 – 0.5 sec. period	1.0	1.0	1.0	1.0
0.5 – 2.0 sec. period	1.0	1.0	1.0	1.0
Tertiary (406 m/s)				
0.1 – 0.5 sec. period	1.14	1.10	1.04	0.98
0.5 – 2.0 sec. period	1.27	1.25	1.22	1.18
Quaternary (333 m/s)				
0.1 – 0.5 sec. period	1.22	1.15	1.06	0.97
0.5 – 2.0 sec. period	1.45	1.41	1.35	1.29

*This is a simplified table for average 30m depth site velocities by type. In the map of Park and Elrick (1998) surface velocity is mapped for the southern California region and it is possible to use more specific site velocity either known or inferred to produce period specific amplitude corrections following Borcherdt (1994).

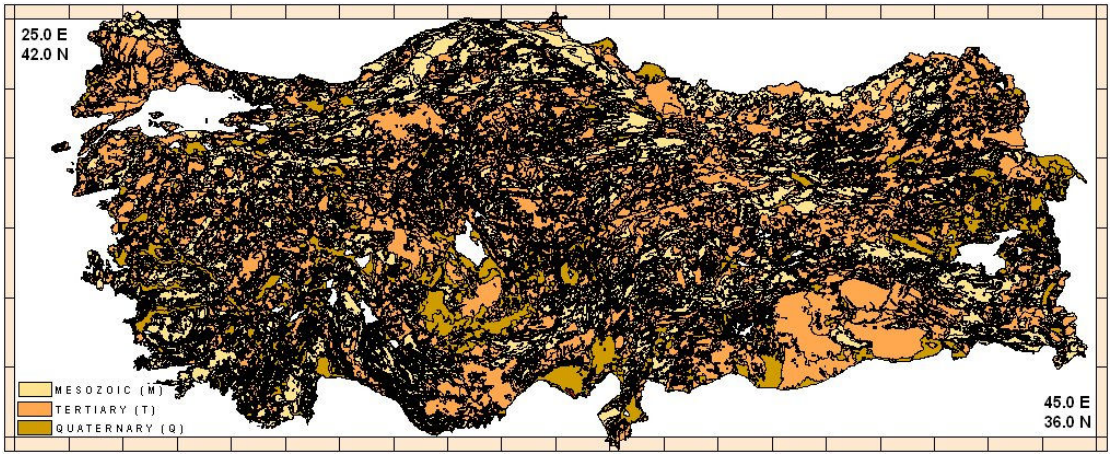

Figure 2.83. Regional map of QTM

For the quantification of the site effects in the urban earthquake hazard assessment or in earthquake microzonation maps, the results were used to produce the distribution of S-wave velocity averaged to 30 m depth for Turkey, since only this information is required to estimate site- dependent design spectra for use in building codes (*e.g.*, IBC 2006).

2.10. The Results of Site Dependent Seismic Hazard

Considering the effect of the ground motion prediction equation on the site specific hazard results obtained from seismic hazard analysis using the old and the next generation ground motion prediction equations (GMPE), the site dependent ground motion contour maps are presented in Figure 2.84 through Figure 2.89 and Figure 2.90 through Figure 2.95, respectively.

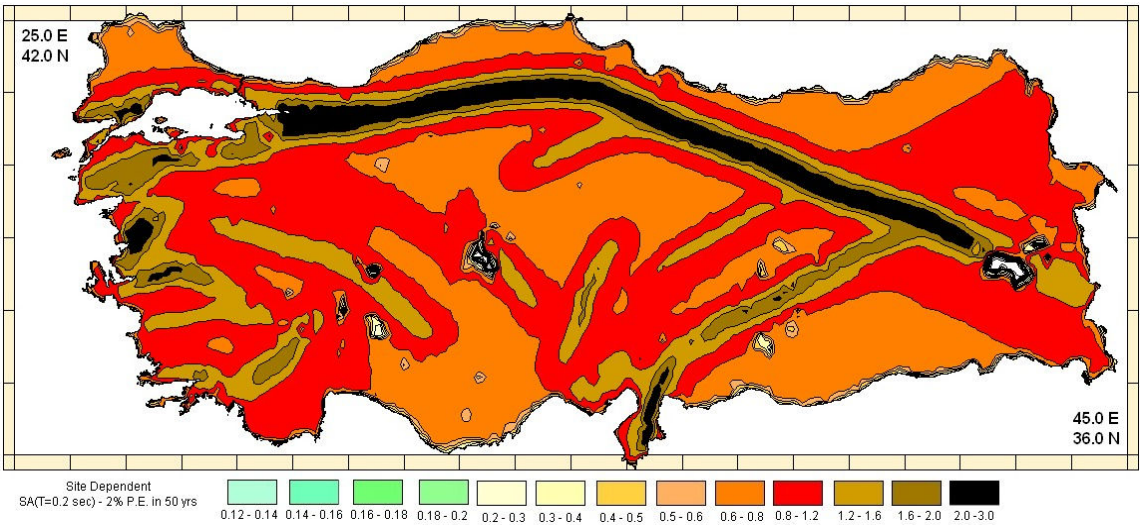

Figure 2.84. Site dependent SA at T=0.2 sec for 2. per cent probability of exceedence in 50 years using previous GMPE

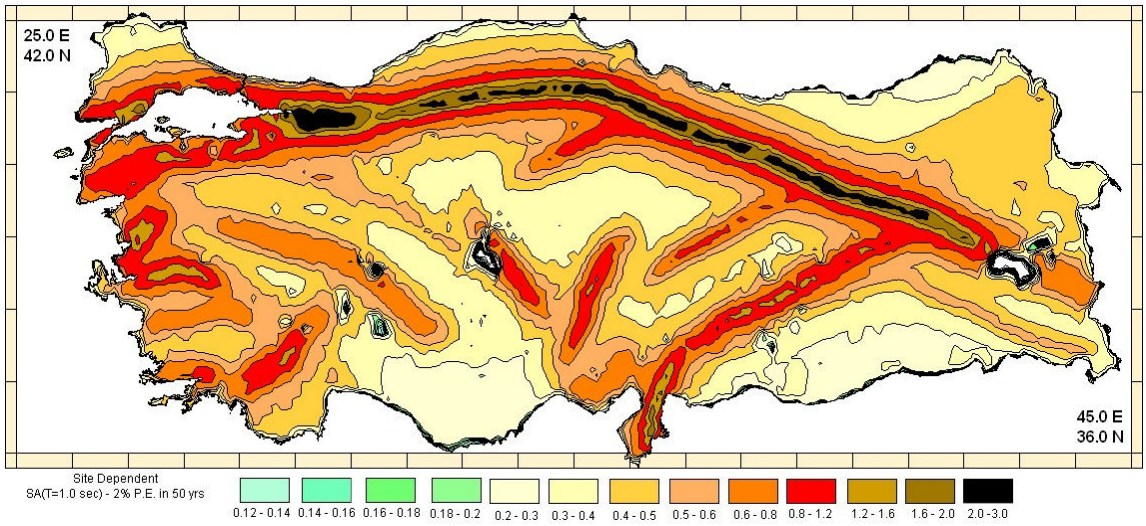

Figure 2.85. Site dependent SA at T=1.0 sec for 2. per cent probability of exceedence in 50 years using previous GMPE

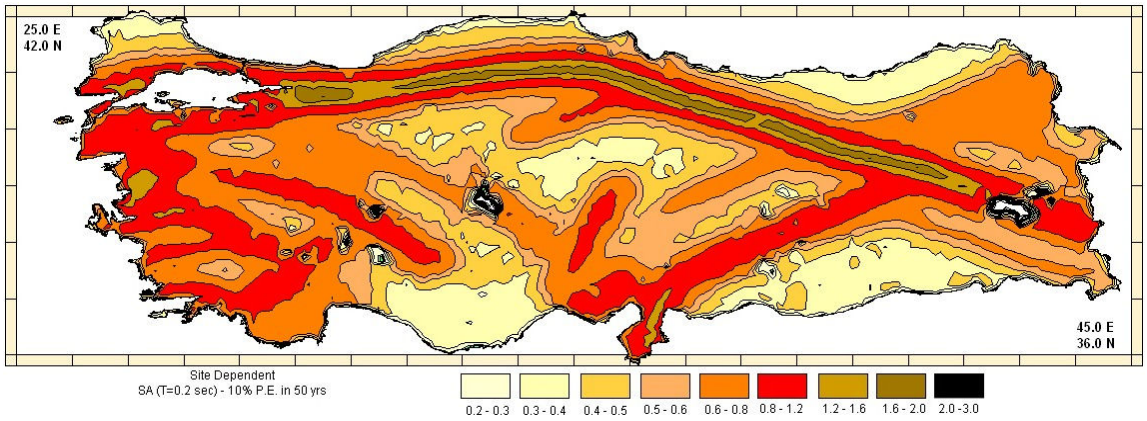

Figure 2.86. Site dependent SA at T=0.2 sec for 10 per cent probability of exceedence in 50 years using previous GMPE

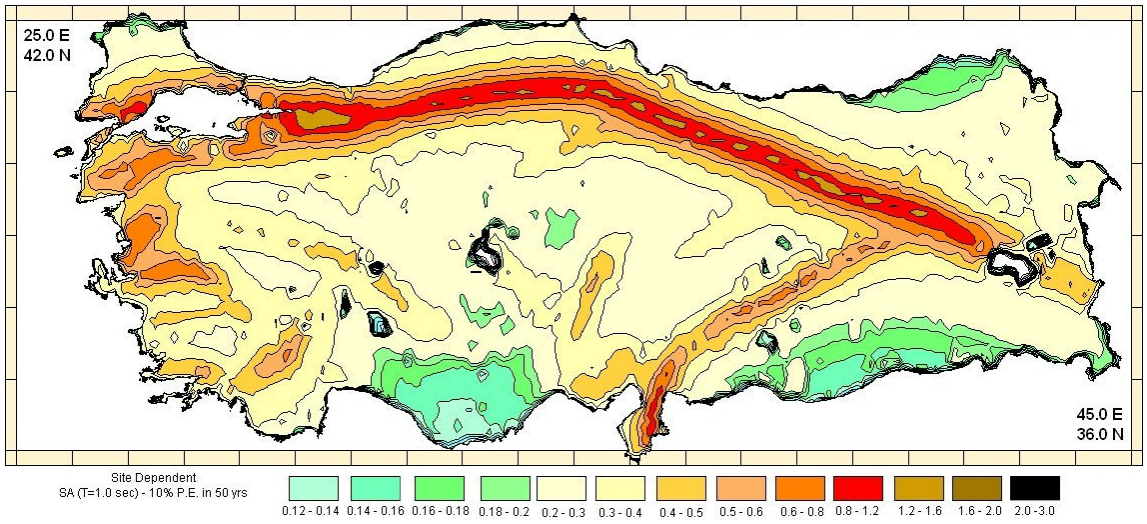

Figure 2.87. Site dependent SA at T=1.0 sec for 10 per cent probability of exceedence in 50 years using previous GMPE

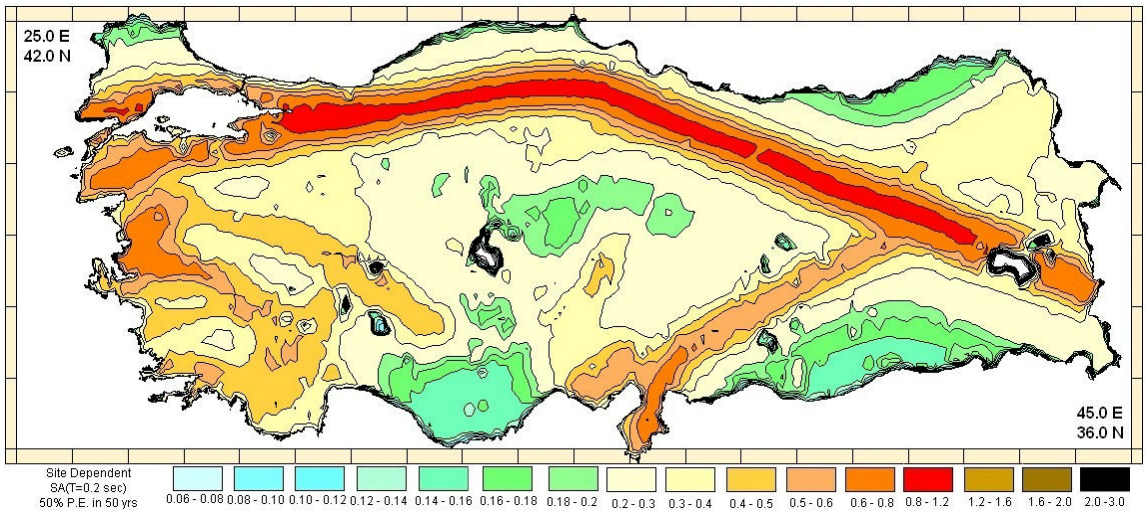

Figure 2.88. Site dependent SA at T=0.2 sec for 50 per cent probability of exceedence in 50 years using previous GMPE

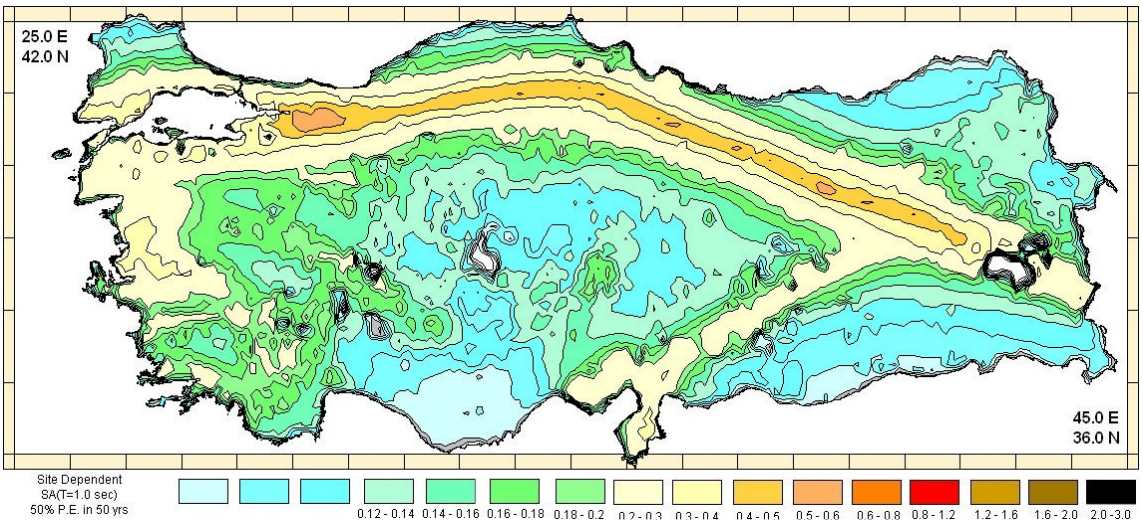

Figure 2.89. Site dependent SA at T=1.0 sec for 50 per cent probability of exceedence in 50 years using previous GMPE

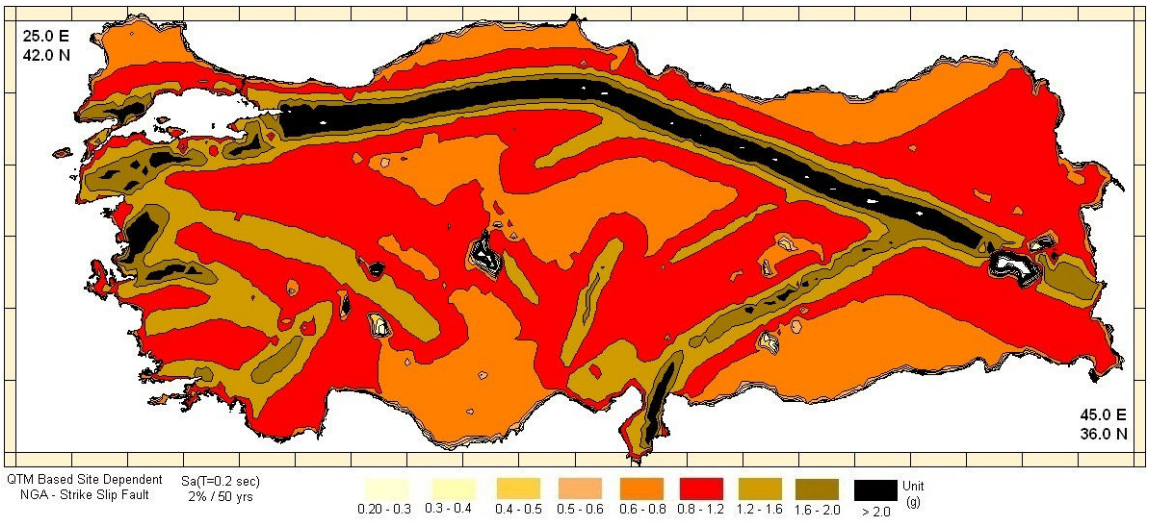

Figure 2.90. Site dependent SA at T=0.2 sec for 2. per cent probability of exceedence in 50 years using the NGA GMPE

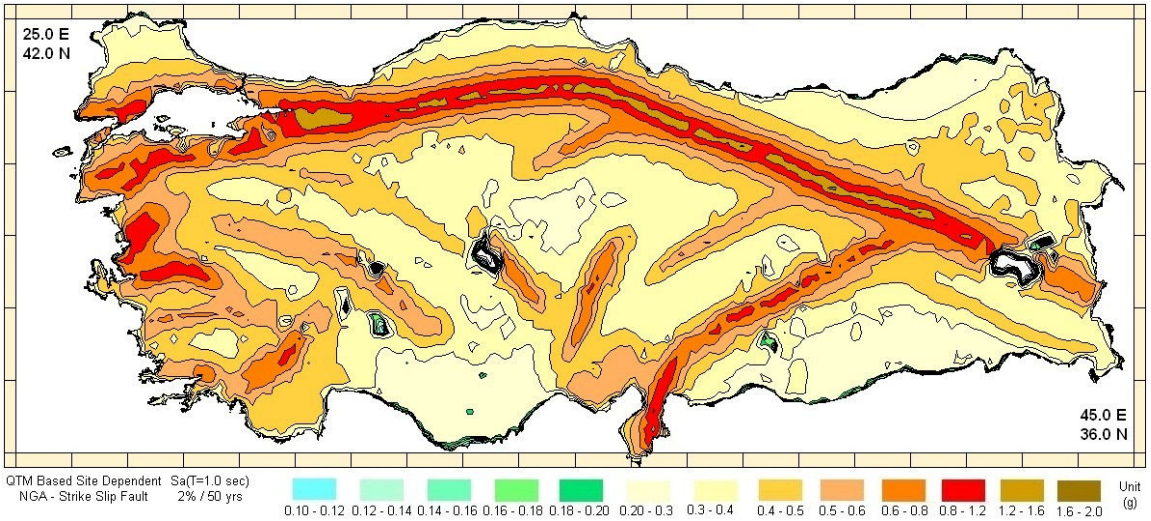

Figure 2.91. Site dependent SA at T=1.0 sec for 2. per cent probability of exceedence in 50 years using the NGA GMPE

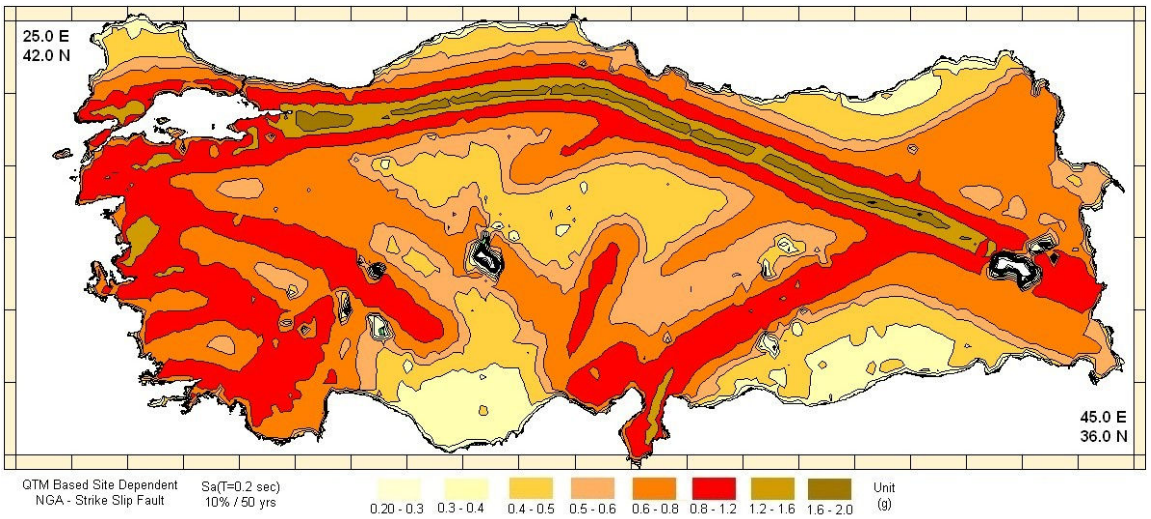

Figure 2.92. Site dependent SA at T=0.2 sec for 10 per cent probability of exceedence in 50 years using the NGA GMPE

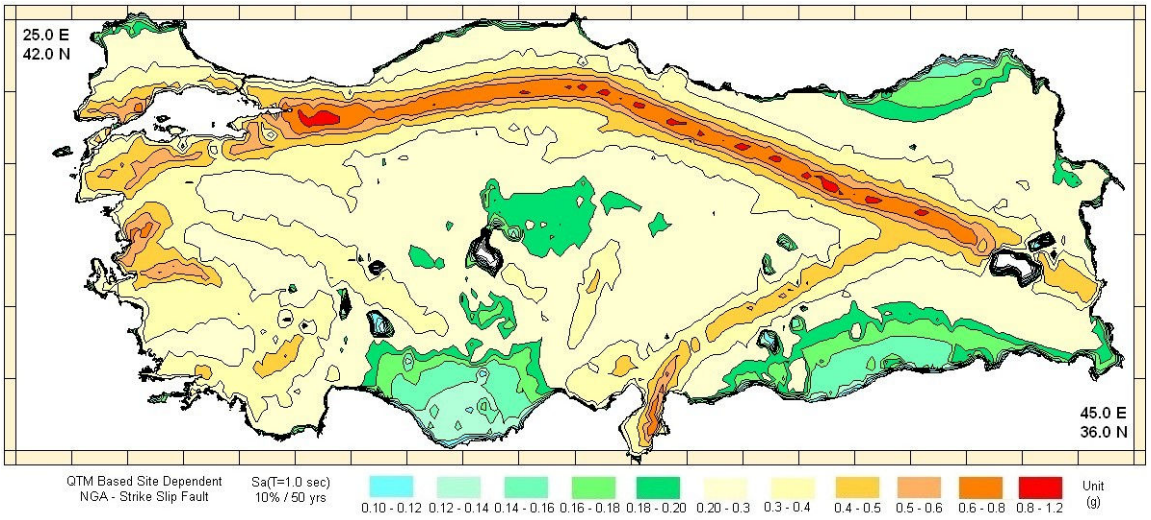

Figure 2.93. Site dependent SA at T=1.0 sec for 10 per cent probability of exceedence in 50 years using the NGA GMPE

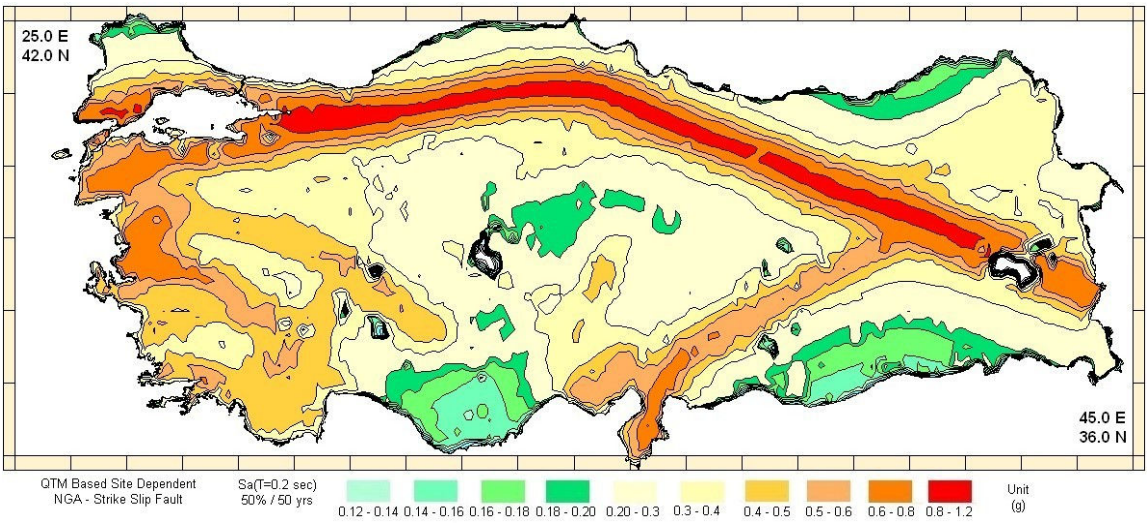

Figure 2.94. Site dependent SA at T=0.2 sec for 50 per cent probability of exceedence in 50 years using the NGA GMPE

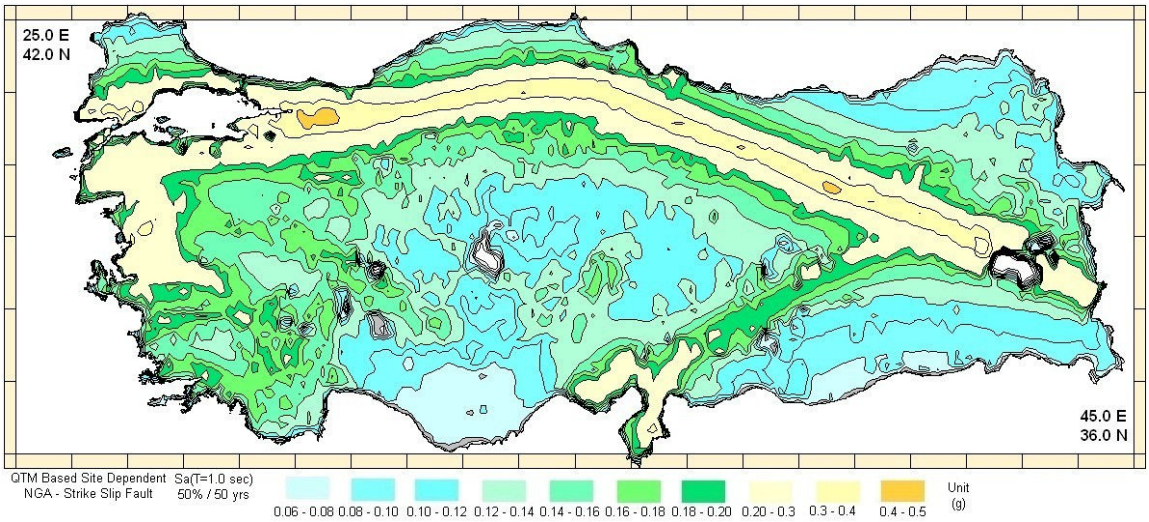

Figure 2.95. Site dependent SA at T=1.0 sec for 50 per cent probability of exceedence in 50 years using the NGA GMPE

3. EARTHQUAKE RISK ASSESSMENT

Probabilistic seismic risk assessments (PSRA) are used to quantify the seismic damage probability of complex engineering structures due to seismic events. Combination of the seismic hazard and vulnerability analyses in a mathematical formulation is defined the seismic risk assessment.

The vulnerability is expressed as the probability of a specified degree of damage from a specified shaking as well as the hazard is expressed as the probability of the specified shaking. Then, earthquake risk is expressed as the combined probability. This simple relation provides a mathematical framework for assessing damage and losses from an earthquake quantitatively. General equation for the calculation of risk related to the earthquake vulnerability and hazard can be given as (Figure 3.1):

$$\left[R_{i,j}\right]=\left[H_j\right]\left[V_{i,j}\right] \tag{3.1}$$

Where, for an element at risk (*e.g.* an individual building) i:

$\left[R_{i,j}\right]$ is the risk, the probability or average rate of loss to element *I* due to earthquake ground motion of severity *j*.

$\left[H_j\right]$ is the hazard, the probability or average expected rate of experiencing earthquake ground motion (or other earthquake related damaging event) of severity *j*.

$\left[V_{i,j}\right]$ is the vulnerability, the level of loss that would be caused to element *I* as a result of experiencing earthquake ground motion of severity *j* (where loss is the specific loss; loss as a proportion of the total value of element *i*).

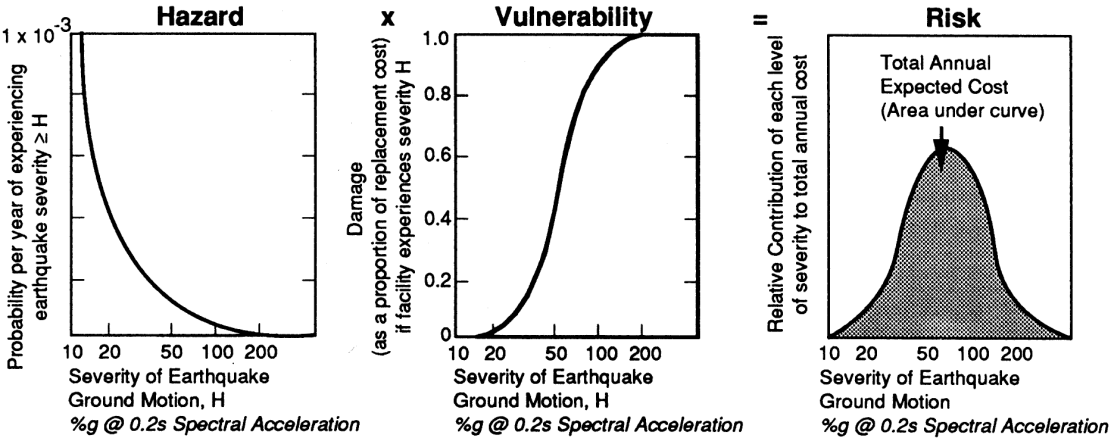

Figure 3.1. Risk is a product of hazard and vulnerability: typical curve shapes (Coburn & Spence, 2002)

Earthquake risk analysis requires measuring the likely damage, casualties and cost of earthquakes within a specified geographical area over certain periods of time. A comprehensive risk analysis assesses various levels of hazard (72, 475 and 2475 years – return period corresponding to 50 per cent, 10 per cent and 2. per cent probabilities of exceedence in 50 years), as well as the consequences to structures and population.

The risk studies can be deterministic or probabilistic, depending upon the requirements of the particular study. Practical techniques for probabilistic risk analysis in the earthquake-resistant design of structures have become highly developed. Probabilistic analyses allow for uncertainties in the locations and rates of earthquake occurrence and levels of ground motion on contrary to using a single scenario earthquake of a specific size and location. For that reason, in this study, a probabilistic seismic risk analysis is used to integrate the earthquake hazard which is performed by the potential effects of earthquakes of varying magnitude and frequencies for Turkey. In Section 2, the subject of the probabilistic seismic hazard analysis is widely investigated.

As an input of the vulnerability analysis, the building inventory, population distribution for Turkey have been compiled and classified. Considering the Landscan population distribution data shown in Figure 3.3 (30 sec arc), grid based population distribution has been obtained as population inventory for Turkey.

3.1. Building Inventory Data

One of the major concerns to perform an effective vulnerability assessment, loss estimation, relief planning and assess insurance liability is having access to accurate database of existing structures. Compiling a comprehensive database of buildings and facilities are primary inputs for vulnerability exposure and loss estimation models. They are also utilized as planning tools prior to an event and as a response tool once an event has occurred. Although current methods of inventory development are often not standardized and frequently not available in electronic format, GRM Company has prepared the recent building inventory dataset compiled from Istanbul Metropolitan Municipality (IMM), Turkish Statistical Institute (TurkStat), Department of Housing and Urban Development, Department of Earthquake Risk Management and Urban Development in Turkey.

Classification of buildings in Turkey is essential to ensure a uniform interpretation of data and results. The building inventory is classified using three basic categories on structural systems, number of stories and year of construction. Each category is further subdivided into groups to yield 24 different building classes. Turkey was divided into grids as 0.005° x 0.005° (approximately 400 m x 600 m) cells for aggregation of hazard and physical inventory data (Figure 3.2). The Landscan population were utilized, and then assigned to the geo-cells in order to calculate the human losses in Turkey due to a major earthquake. The building data as well as the population census for Turkey have been obtained from the study of GRM Company.

The primary consideration in developing a classification scheme is the differences in the resistance of various buildings to damage during ground shaking. Some of the factors taken into account are the type of structural system, the materials of construction, the size of the buildings, and the degree to which structural features limiting damage have been provided during design and construction. The age of a building is sometimes used as an indirect indicator of seismic design level in areas where seismic code have been adopted, and it can indicate typical construction practice in a given region.

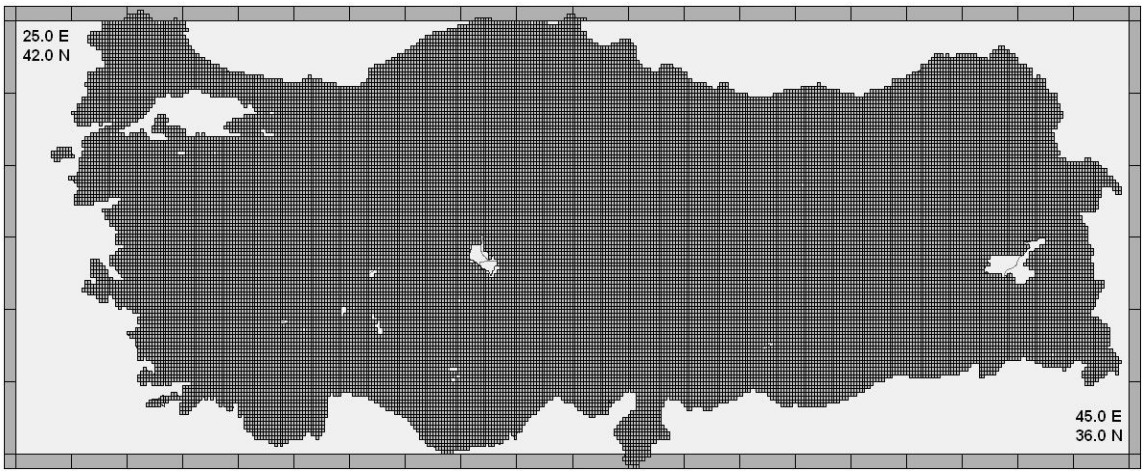

Figure 3.2. Grids as 0.005° x 0.005° (approximately 400 m x 600 m) cells

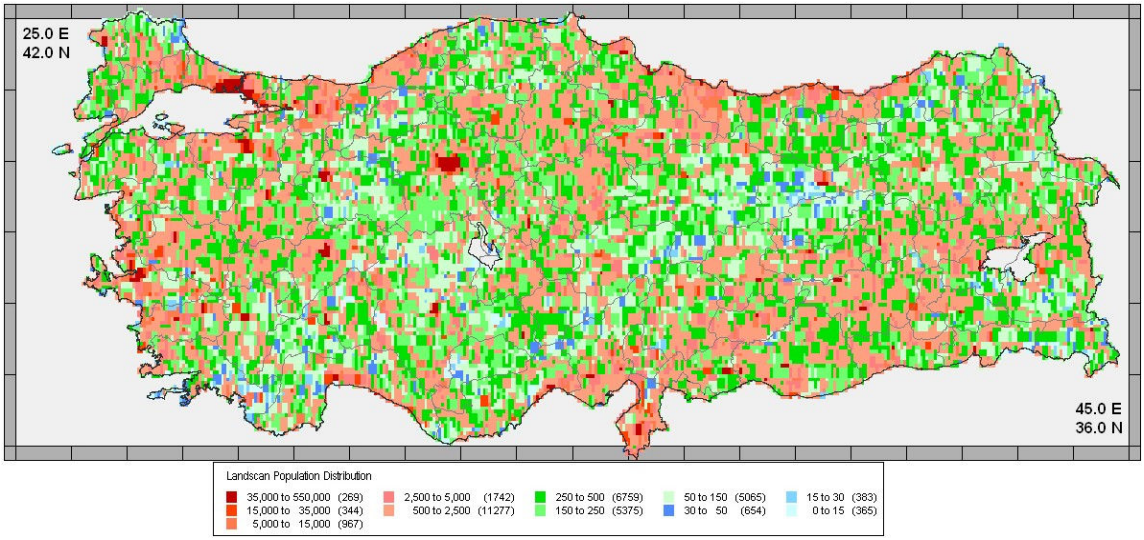

Figure 3.3. Distribution of population in Turkey on the basis of Landscan data

The building inventory is classified separately such as construction types, number of stories and construction year considering the European Building Taxonomy.

Taking the construction type into consideration (Figure 3.4 through Figure 3.7):

1. Reinforce concrete (RC1- Moderate)
2. Unreinforced masonry (M5)
3. Adobe (M2)

4. Rubble stone (M1)

Taking the number of stories into consideration (Figure 3.8 through Figure 3.10):

1. Low rise (1-3 stories + unknown data)
2. Mid rise (4-6 stories)
3. High rise (7-16)

Taking construction date into consideration (Figure 3.11 through Figure 3.12):

1. Construction year: Pre-1980
2. Construction year: Post-1980

Table 3.1. Distribution of the buildings classification

Construction Type		Number of Stories		Construction Date	
RC1-Moderate	3,837,576	Low Rise	6,647,014	Pre-1979	3,167,482
M5	2,977,263	Mid Rise	763,143	Post -1979	4,345,890
M2	472,562	High Rise	103,223	-	
M1	225,976	-		-	
TOTAL	7,513,377		7,513,380	-	7,513,371

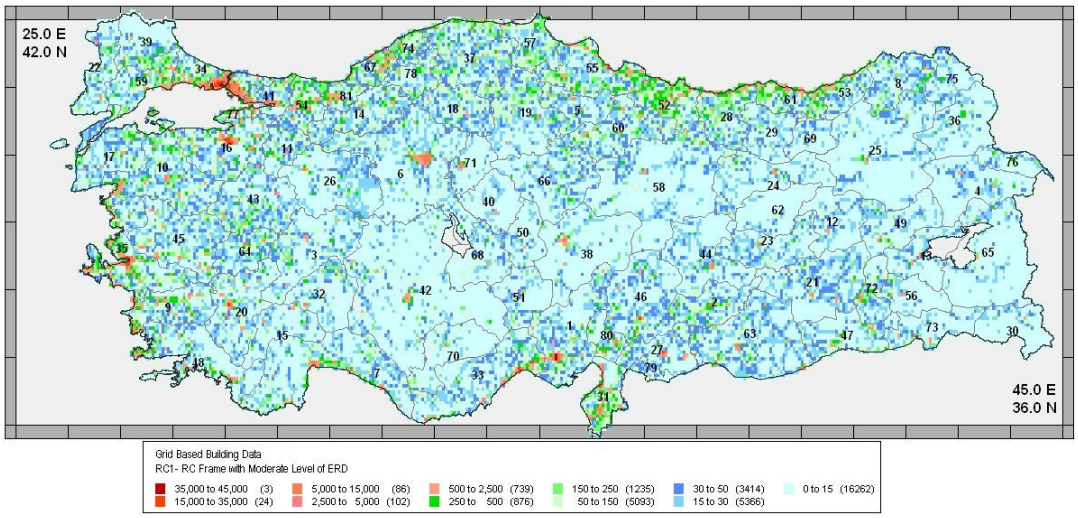

Figure 3.4. RC1 moderate building distribution

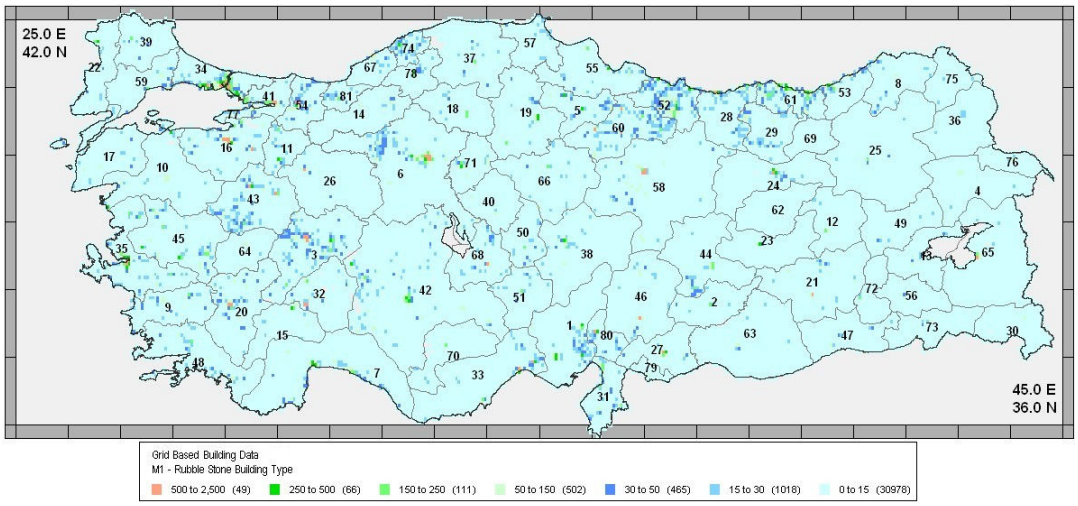

Figure 3.5. M1 rubble stone building distribution

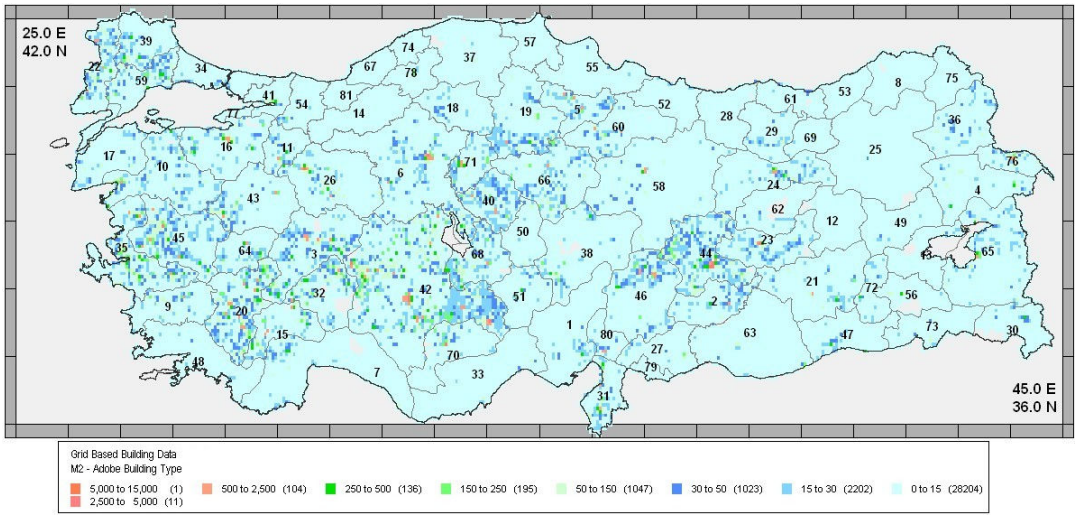

Figure 3.6. M2 adobe building distribution

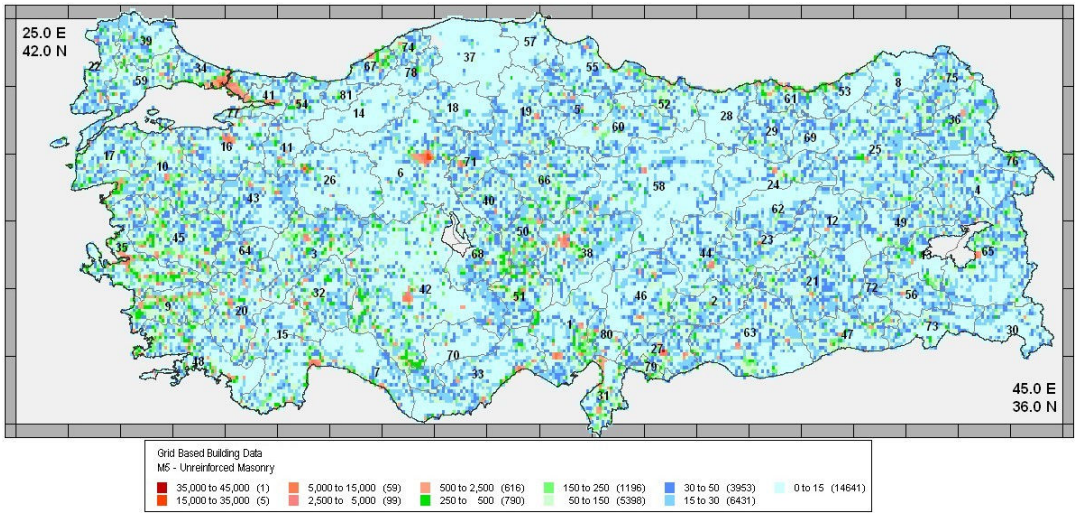

Figure 3.7. M5 unreinforced masonry building distribution

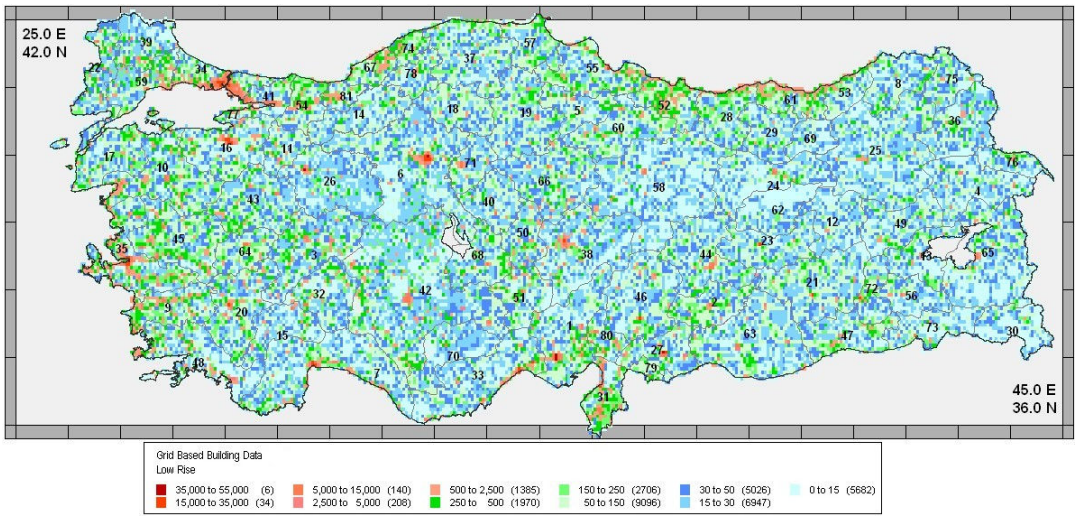

Figure 3.8. Low rise building distribution

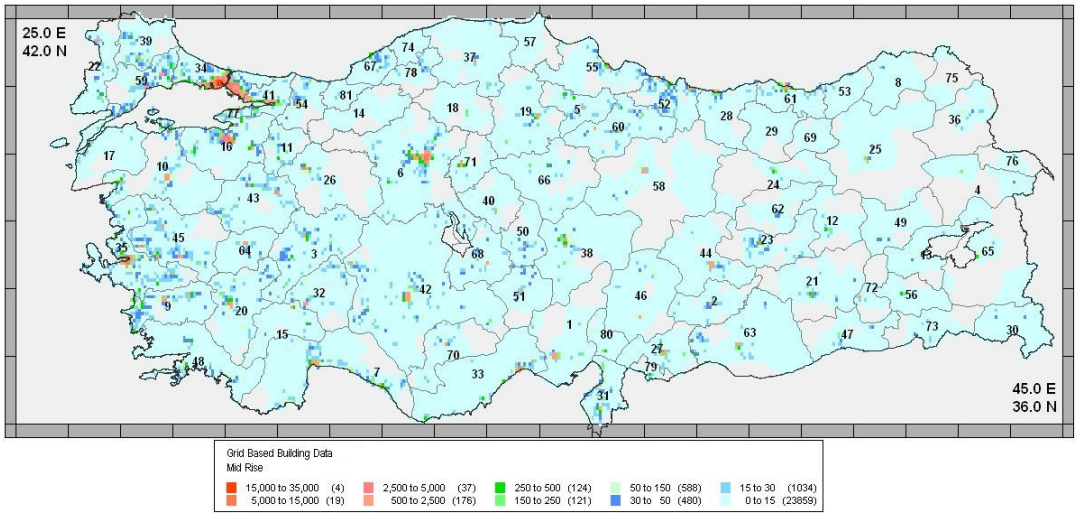

Figure 3.9. Mid rise building distribution

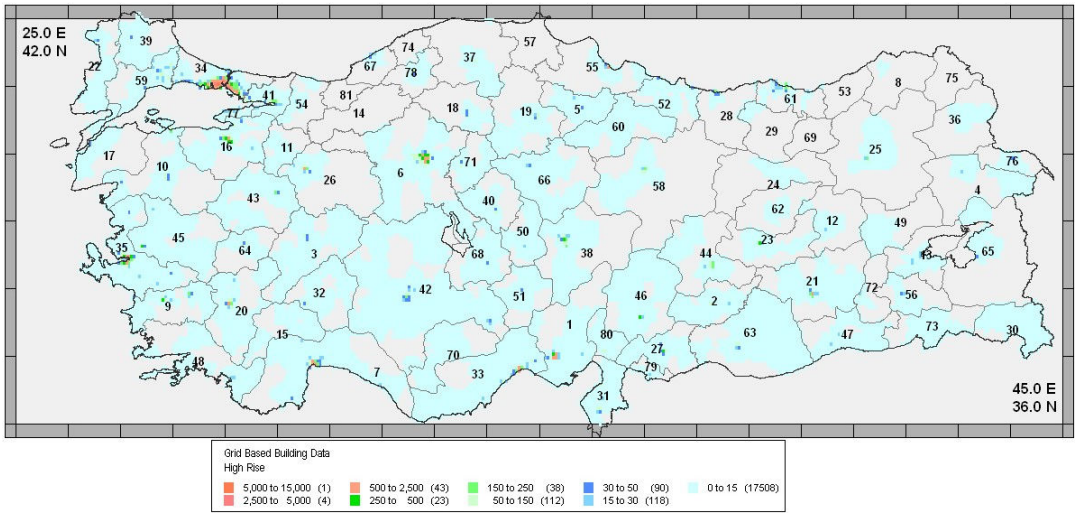

Figure 3.10. High rise building distribution

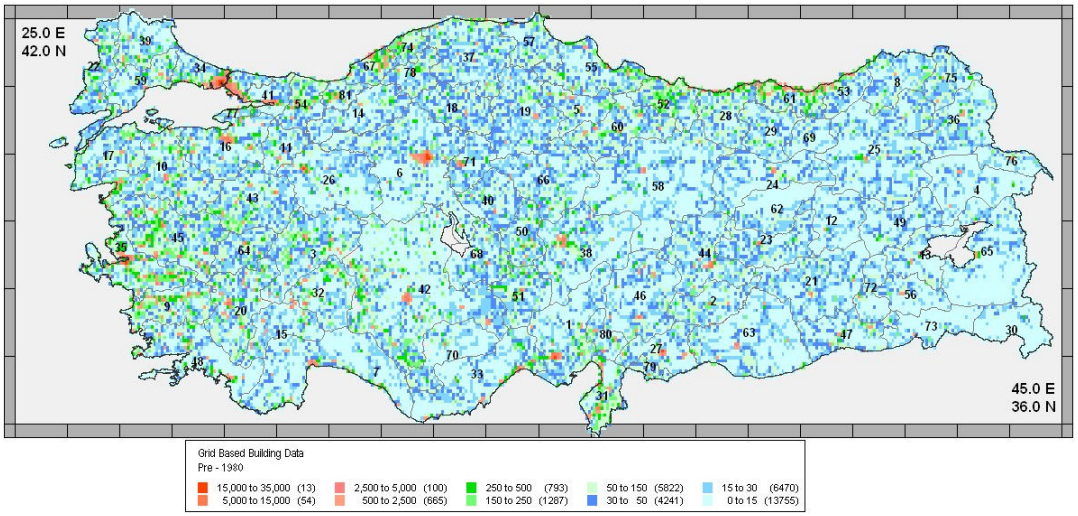

Figure 3.11. Pre – 1980 building distribution

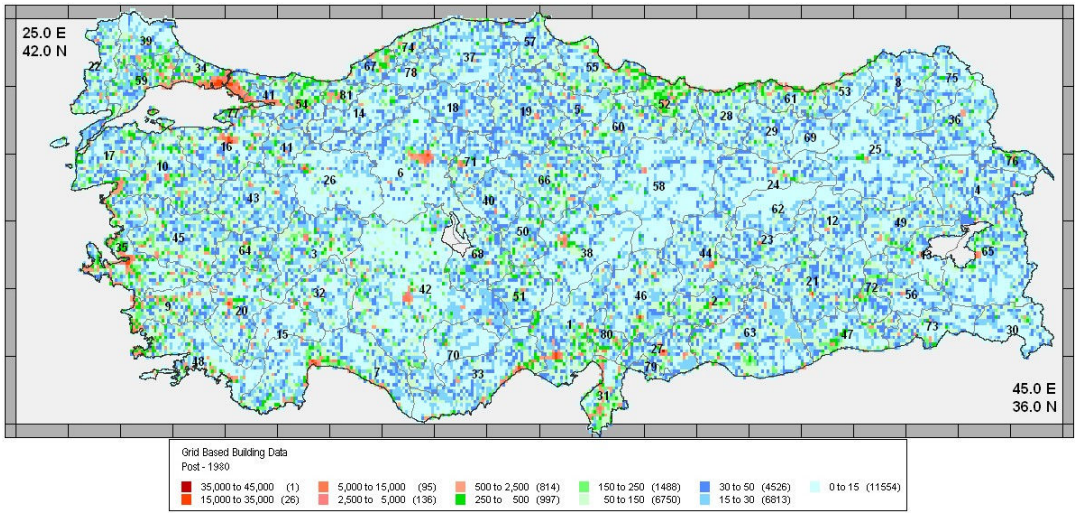

Figure 3.12. Post – 1980 building distribution

Considering the grid based building inventory, the logic tree approach is utilized to determine the percentage of the construction type, the story number of buildings and construction year for each cell and then, according to that ratio, the building inventory is determined for each building type, the story number of building and construction date for each cell.

Table 3.2. Logic tree scheme

Construction Type	The story Number of Buildings	Construction Year
RC1	Low Rise	Pre – 1980
M1- Rubble	Mid Rise	Post - 1980
M2- Adobe	High Rise	
M5 – Unreinforced Masonry		

However, the building inventory for Turkey should be rearranged and rechecked according to the total number of buildings for each district in the Turk Stat database.

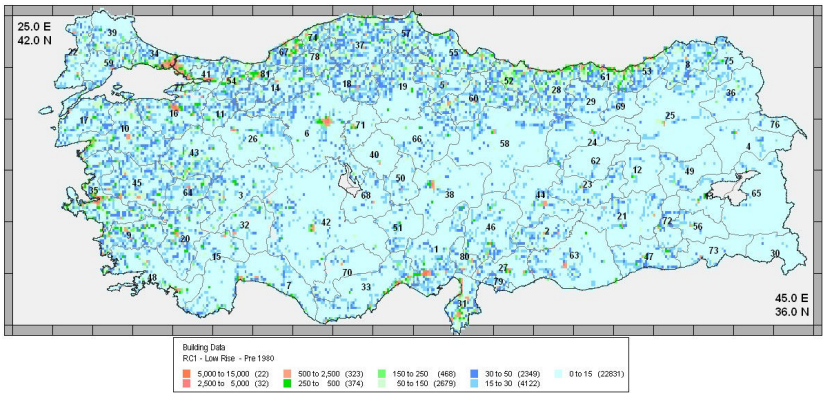

Figure 3.13. Number of buildings of type of reinforced concrete, low rise and pre1980

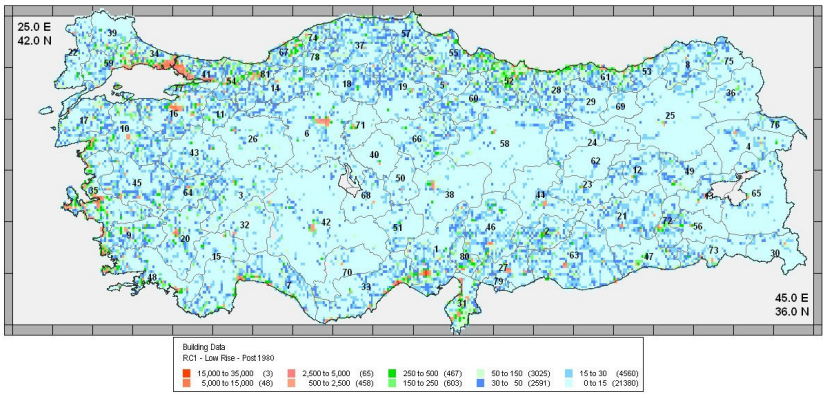

Figure 3.14. Number of buildings of type of reinforced concrete, low rise and post1980

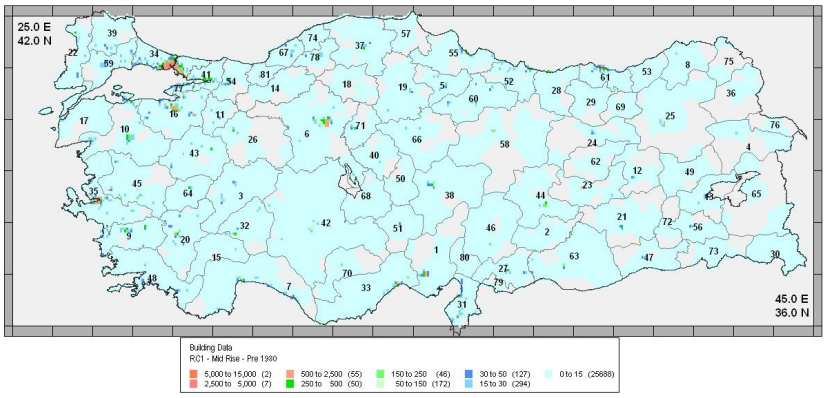

Figure 3.15. Number of buildings of type of reinforced concrete, mid rise and pre1980

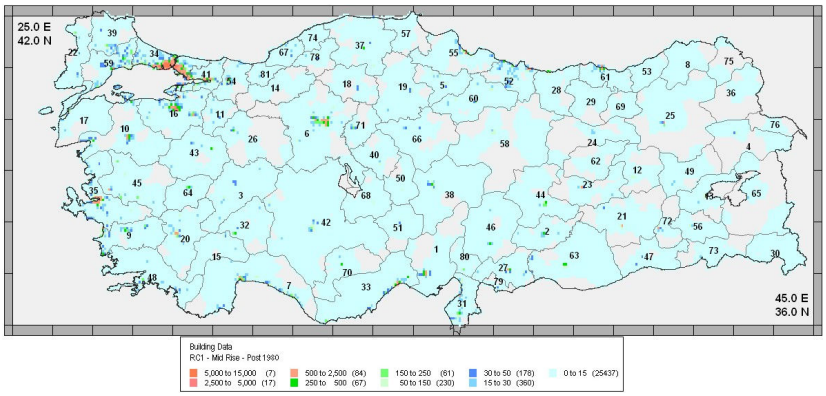

Figure 3.16. Number of buildings of type of reinforced concrete, mid rise and post1980

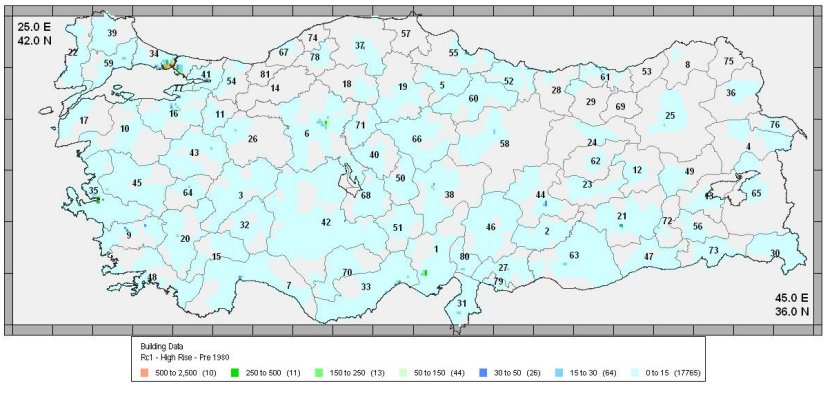

Figure 3.17. Number of buildings of type of reinforced concrete, high rise and pre1980

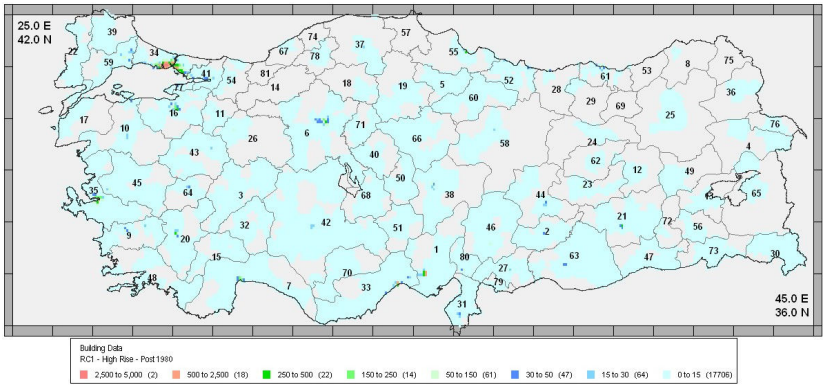

Figure 3.18. Number of buildings of type of reinforced concrete, high rise and post1980

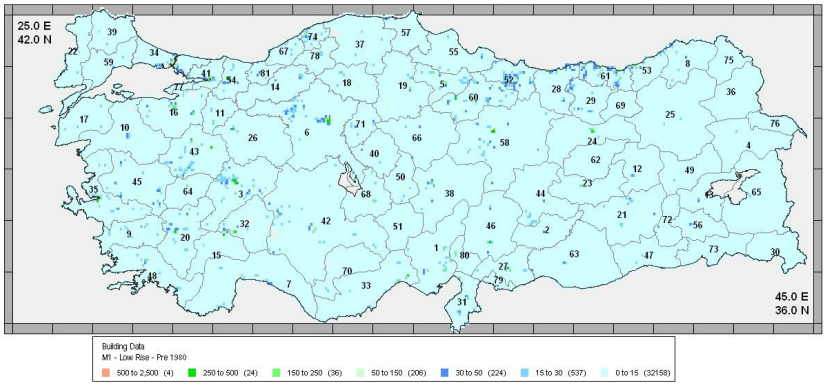

Figure 3.19. Number of buildings of type of rubble stone (M1), low rise and pre1980

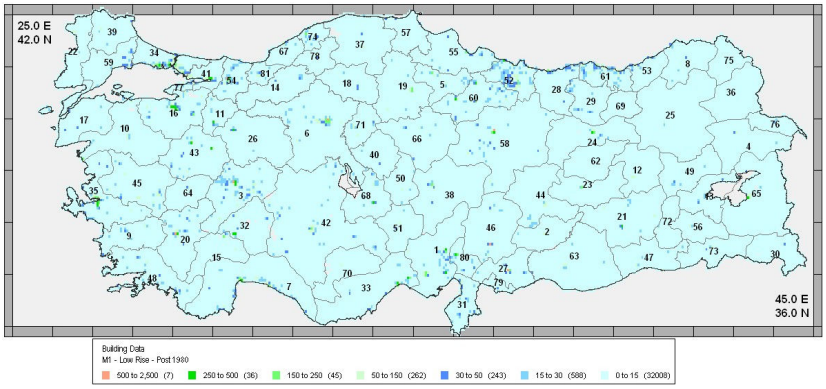

Figure 3.20. Number of buildings of type of rubble stone (M1), low rise and post1980

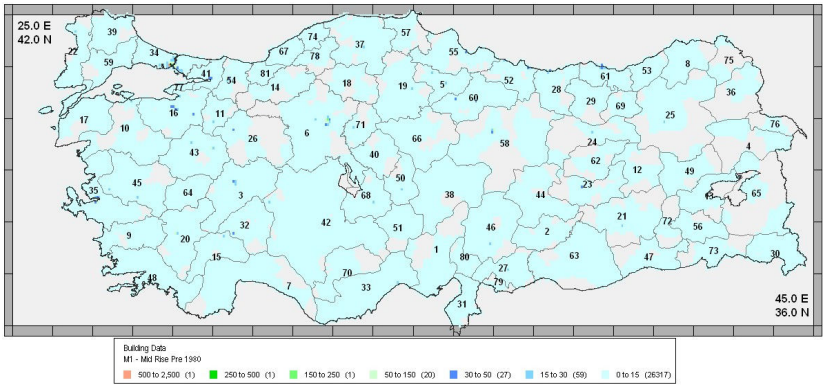

Figure 3.21. Number of buildings of type of rubble stone (M1), mid rise and pre1980

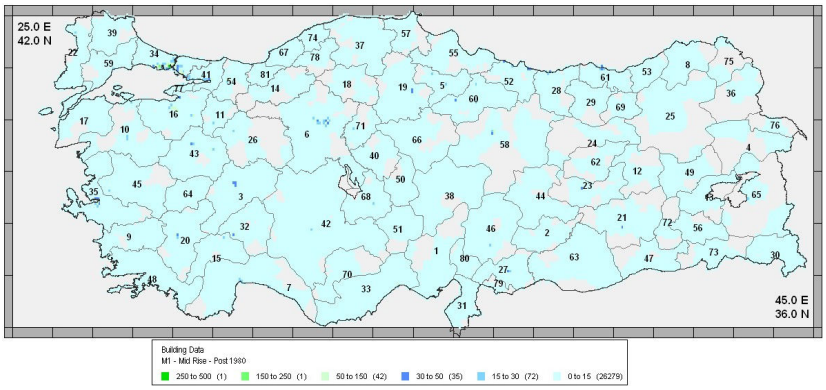

Figure 3.22. Number of buildings of type of rubble stone (M1), mid rise and post1980

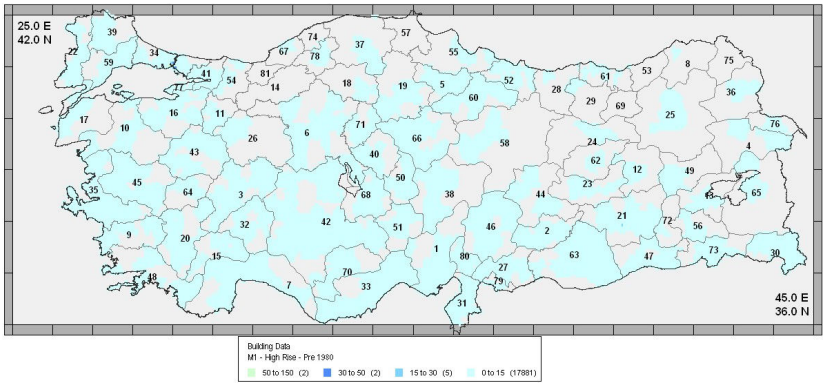

Figure 3.23. Number of buildings of type of rubble stone (M1), high rise and pre1980

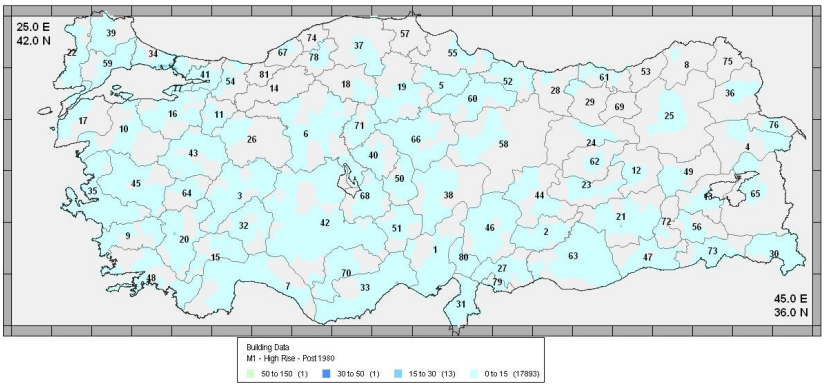

Figure 3.24. Number of buildings of type of rubble stone (M1), high rise and post1980

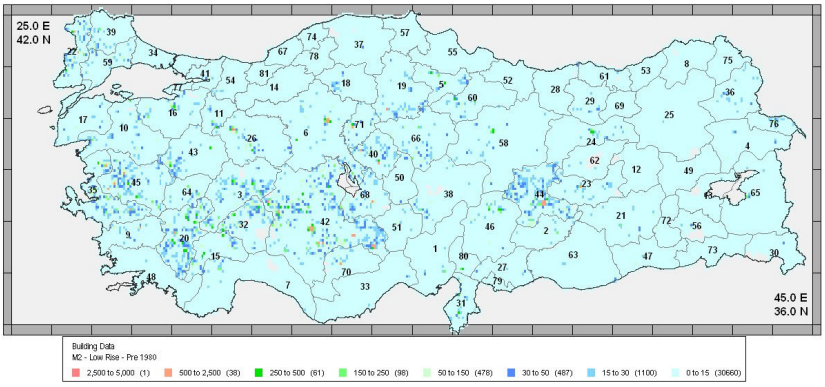

Figure 3.25. Number of buildings of type of adobe (M2), low rise and pre1980

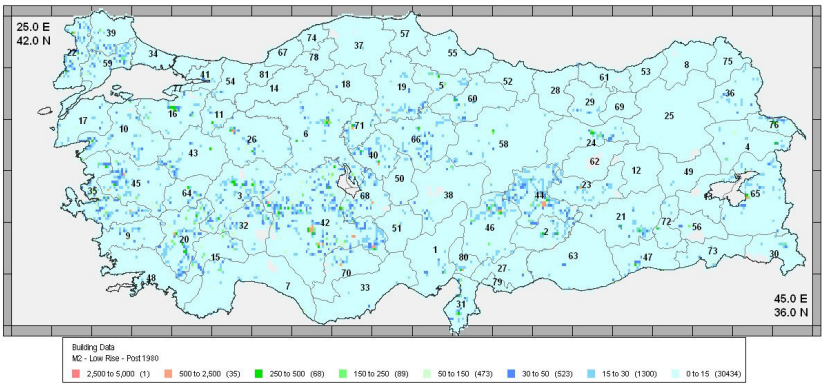

Figure 3.26. Number of buildings of type of adobe (M2), low rise and post1980

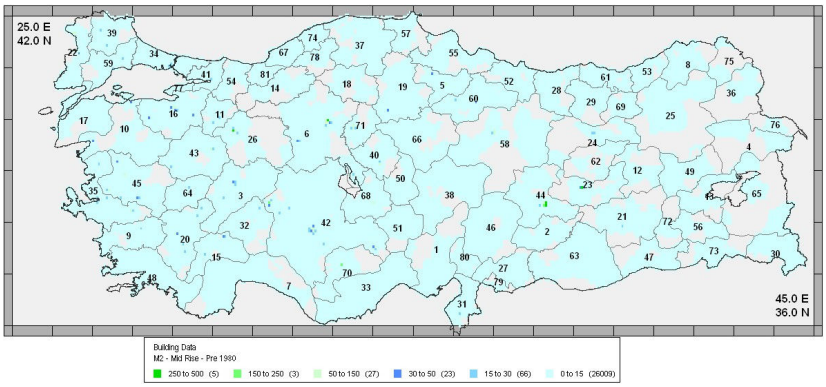

Figure 3.27. Number of buildings of type of adobe (M2), mid rise and pre1980

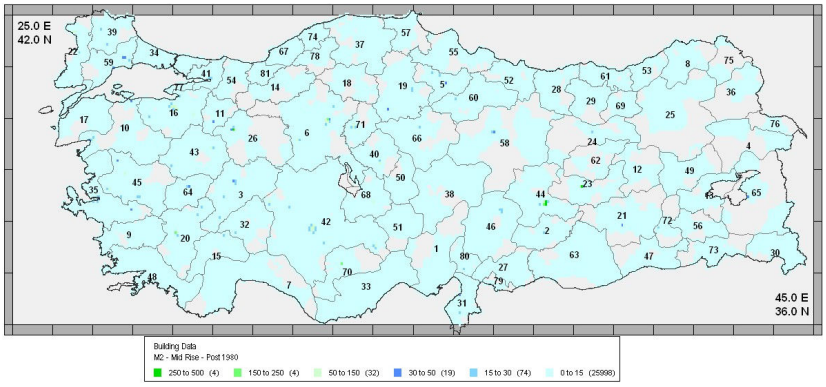

Figure 3.28. Number of buildings of type of adobe (M2), mid rise and post1980

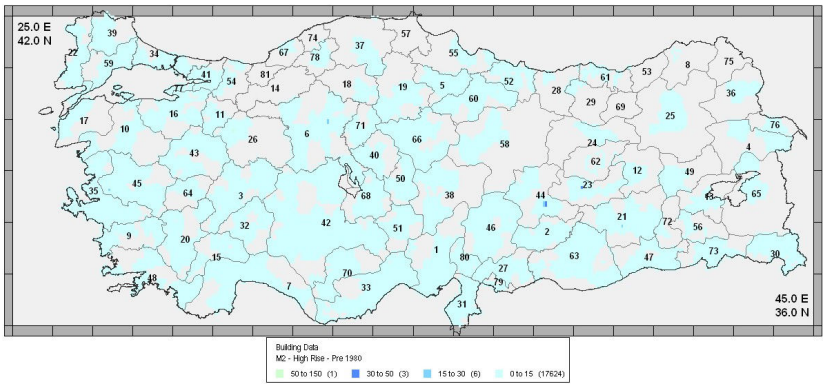

Figure 3.29. Number of buildings of type of adobe (M2), high rise and pre1980

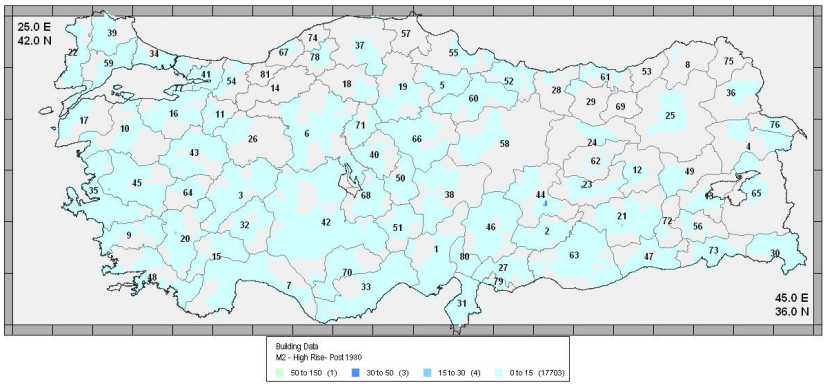

Figure 3.30. Number of buildings of type of adobe (M2), high rise and post1980

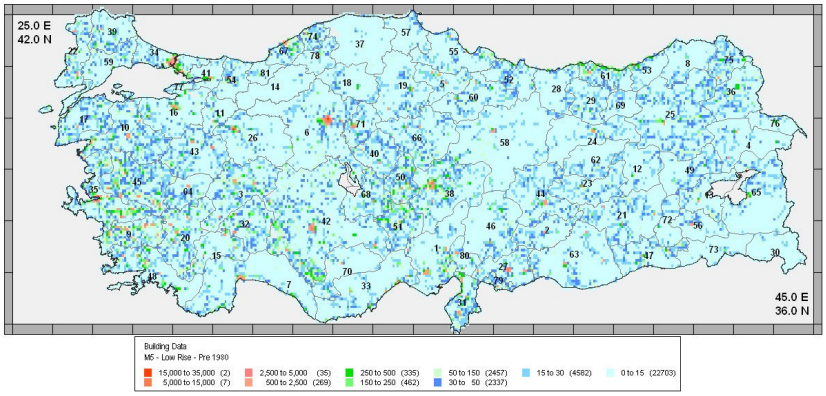

Figure 3.31. Number of buildings of type of unreinforced masonry (M5), low rise and pre1980

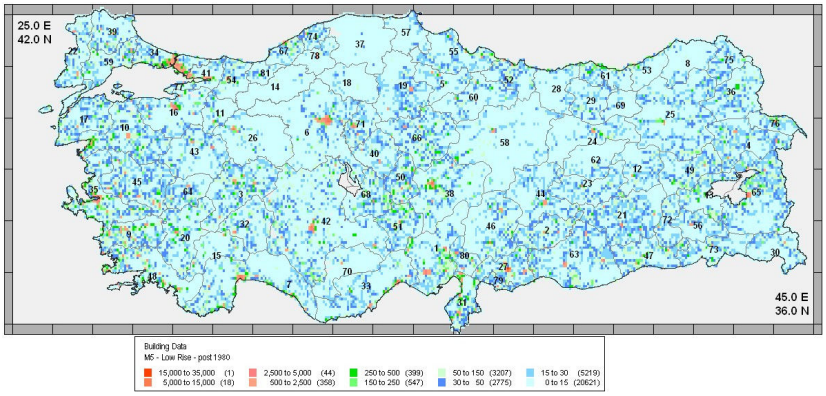

Figure 3.32. Number of buildings of type of unreinforced masonry (M5), low rise and post1980

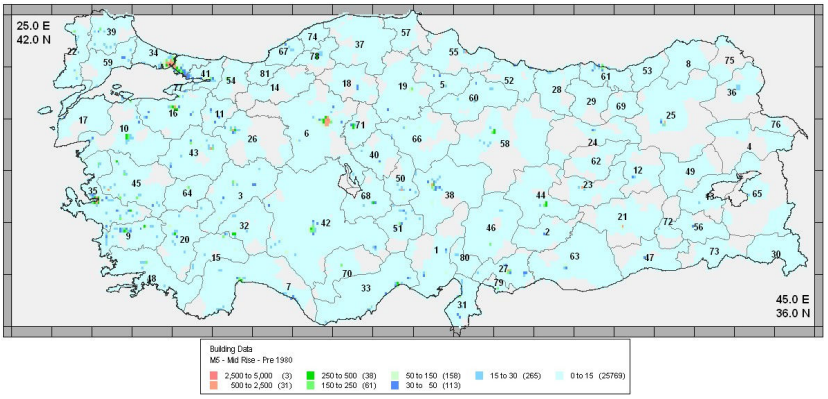

Figure 3.33. Number of buildings of type of unreinforced masonry (M5), mid rise and pre1980

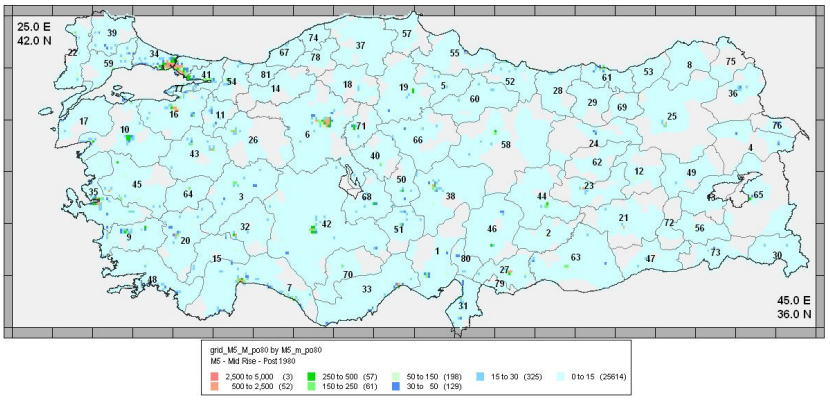

Figure 3.34. Number of buildings of type of unreinforced masonry (M5), mid rise and post1980

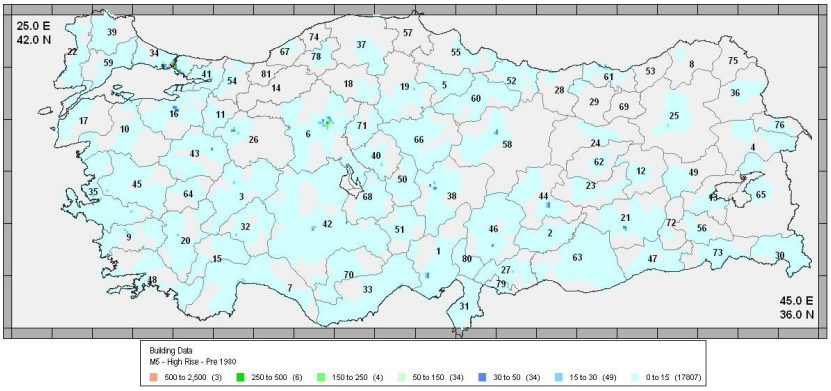

Figure 3.35. Number of buildings of type of unreinforced masonry (M5), high rise and pre1980

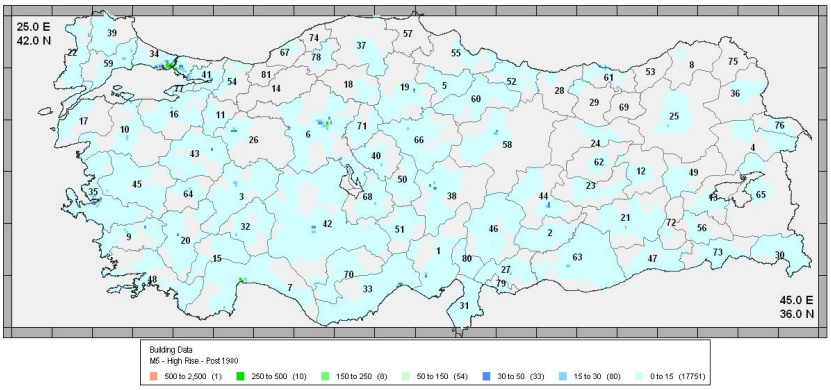

Figure 3.36. Number of buildings of type of unreinforced masonry (M5), high rise and post1980

3.2. Earthquake Loss Assessment

Earthquake loss estimation models have found a variety of application in the primary insurance and reinsurance markets and, more recently, in capital markets and also in emergency planning and also in seismic code drafting committees (Bommer *et al*., 2005). The models can also be useful in the area of seismic risk mitigation by providing cost-benefit analyses of the impact of various mitigation strategies.

The basic ingredients for earthquake loss estimation are the estimated building damage using the regional building inventory (and/or portfolio) and building

vulnerabilities associated with typical construction systems; the estimated casualty using the regional population distribution and the estimated building damage; and estimations of building replacement costs for different damage levels.

Combining the inventory with motion damage relationships goes ahead directly to estimate for property losses, although it is necessary to be careful and explicit as to what value of buildings- replacement cost or market value is used in the calculation. Although it is also necessary to estimate numbers of casualties, the data on which to predict deaths and injuries are very sparse, and considerable judgment is necessary in organizing available information to estimate casualties. There are three methods used in this study to estimate casualties: Coburn and Spence (1992A, 1992B), Risk UE (Bramerini *et al.*, 1995) and KOERI 2002 (DEE-KOERI, 2003), definition of damage states and casualty rates are based on KOERI 2002, (DEE-KOERI, 2003) and ATC13, respectively. The detailed information about methods is given in Section 3.4.1 through Section 3.4.3.

3.3. Building Damage Estimation

Building damage estimation leads to the knowledge/ awareness of the extent of damage due to an earthquake. It is possible to know not only the total amount of the damage but also the lack of the city / country which has a high possibility to occur a destructive earthquake.

This section provides damage estimates for each of the building classification based on the level of exposure and the vulnerability of structures, which is a potential for damage at different ground shaking levels.

Identifying the relationships between the intensity of ground shaking and the damage experienced by a group of generally similar structures, or a construction class, is essential to vulnerability analyses. Several methods for the vulnerability assessment have been developed and proposed in recent years. Different states of art of vulnerability methodologies lead to this following classification: typological methods (such as categorization methods, statistical methods); inspection and rating methods (indirect, expert judgment); mechanical methods (analytical). These approaches are differently

described by positive features and limitations so that recent experiences have also provided the applicability of hybrid techniques.

Comprehensive frameworks for damage scenarios and seismic risk analysis have been proposed and developed as part of major international programs as HAZUS (1999); RADIUS (1999); Risk-UE (2004). The aim of these projects is to build the alternative methods to adopt for the seismic vulnerability assessment of building at territorial scale based on: a) actual damage observation b) expert judgment, c) simplified- mechanical and analytical models. By doing this, an accepted definition of seismic risk (*i.e.* convolution of hazard, expose, vulnerability analyses and cost evaluation) has been developed.

The so-called Macroseismic Method of Giovinazzi and Lagomarsino (2004) and Giovinazzi (2005) developed to be employed for hazard description in terms of macroseismic intensity is utilized in this study. This observed vulnerability approach have been evaluated in terms of EMS98 intensities and damage grades for the set of EMS98 vulnerability classes and building taxonomies. Fuzzy set theory, which can be defined as the association of numerical values to linguistic definitions of the damage distribution, constitutes an important tool in this vulnerability analysis.

3.3.1. Empirical Approach for Determination of Physical Vulnerability (Giovinazzi and Lagomarsino, 2005; 2006)

A vulnerability curve is needed to estimate the probabilities of a population of structures reaching or exceeding various limit states at given levels of ground shaking severity.

The recent vulnerability model proposed by Giovinazzi and Lagomarsino (2005) encompasses both macroseismic and mechanical approaches. In this study, the observed vulnerability approach referred to as “macroseismic one” (Giovinazzi and Lagomarsino 2004, Giovinazzi 2005) is utilized. According to that approach, the intensity based vulnerability has been derived from the definitions provided by the EMS98 macroseismic scale (Grünthal 1998) making use of classical probability theory and of the fuzzy-set theory.

The method is derived in a theoretically rigorous way; starting from EMS98 macroseismic scale (Grünthal, 1998) definitions overcome the distinction between typological and rating methods and allow carrying out a vulnerability analysis with a single approach, graded to different levels according to the quantity and quality of the available data and the size of the territory. The method, which is applicable to all European regions, has been verified on the basis of data observed after earthquakes occurred in different countries.

3.3.2. EMS Damage Matrices

The recent methodology proposed in this study makes reference to the EMS98 scale. It is the most recent and probably most extensively used at the European level particularly, for the quality and the detail with which the building taxonomies, the degree of damage and the quantities are defined.

The EMS98 scale provides a measure of the earthquake shaking based on structural and non-structural damage suffered by buildings as well as what human beings and animals felt. In EMS98, buildings are classified into 6 vulnerability classes A-F (A being most vulnerable and F being most resistant to earthquakes) and 5 damage grades (D1 corresponding to negligible damage and D5 corresponding to collapse). Through damage matrices, distribution of damage corresponding to different intensity levels are described with use of three different qualitative terms *few*, *many*, *most* (Figure 3.37). Quantitative descriptions to these terms are also provided, which overlap with each other to a certain degree (Figure 3.38).

In addition, a correspondence between vulnerability classes and building typologies is described in EMS98. Each type of structure is characterized by a prevailing vulnerability class however as it is possible to find buildings with a better or worse seismic behavior depending on their constructive and structural characteristics, different building types are associated with a range of vulnerability classes rather than a single vulnerability class. The different belongings of a building type to various vulnerability classes are depicted through

linguistic terms such as *most possible class, possible class and unlikely class*. These are summarized below (Table 3.3).

	Class A				
I	D_1	D_2	D_3	D_4	D_5
V	Few				
VI	Many	Few			
VII			Many	Few	
VIII				Many	Few
IX					Many
X					Most
XI					
XII					

	Class B				
I	D_1	D_2	D_3	D_4	D_5
V	Few				
VI	Many	Few			
VII		Many	Few		
VIII			Many	Few	
IX				Many	Few
X					Many
XI					Most
XII					

	Class C				
I	D_1	D_2	D_3	D_4	D_5
V					
VI	Few				
VII		Few			
VIII		Many	Few		
IX			Many	Few	
X				Many	Few
XI					Many
XII					Most

	Class D				
I	D_1	D_2	D_3	D_4	D_5
V					
VI					
VII	Few				
VIII		Few			
IX		Many	Few		
X			Many	Few	
XI				Many	Few
XII					Most

	Class E				
I	D_1	D_2	D_3	D_4	D_5
V					
VI					
VII					
VIII					
IX		Few			
X		Many	Few		
XI			Many	Few	
XII					

	Class F				
I	D_1	D_2	D_3	D_4	D_5
V					
VI					
VII					
VIII					
IX					
X		Few			
XI		Many	Few		
XII					

Figure 3.37. Damage distribution for different vulnerability classes and different intensity degrees according to EMS98 macroseismic scales

Table 3.3. EMS98 building typologies and identification of their seismic behavior by vulnerability classes

Type of Structure		Vulnerability Class					
		A	B	C	D	E	F
MASONRY	Rubble stone, fieldstone						
	Adobe (earth brick)						
	Simple stone						
	Massive stone						
	Unreinforced, with manufactured stone units						
	Unreinforced, with RC floors						
	Reinforced or confined						
REINFORCED CONCRETE (RC)	Frame without earthquake-resistant design						
	Frame with moderate level of ERD						
	Frame with high level of ERD						
	Walls without ERD						
	Walls with moderate level of ERD						
	Walls with high level of ERD						
STEEL	Steel structures						
WOOD	Timber structures						

Most possible

Possible

Not likely

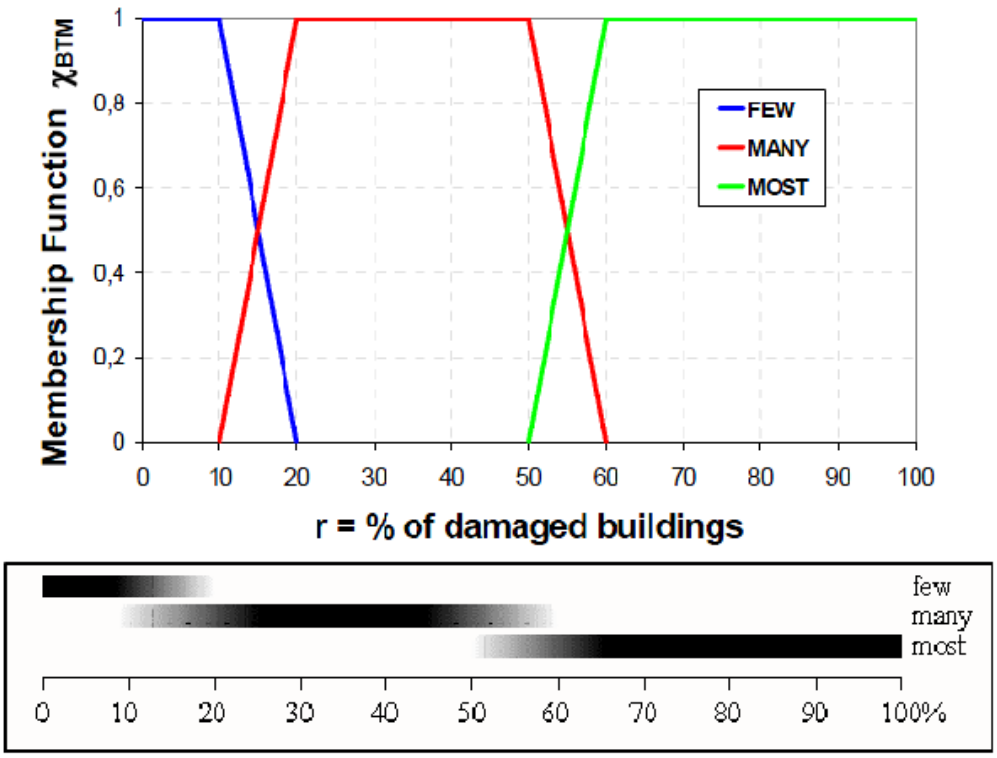

Figure 3.38. Quantitative description of terms few, many, most

3.3.3. Complete Damage Probability Distribution

The EMS98 scale provides a damage matrix that contains the probability of the buildings belonging to a certain vulnerability class suffering a certain damage level under a given intensity. However these damage matrices can only provide a vague and incomplete vulnerability model. As the damage probabilities are provided in a fuzzy way through three narrowly overlapping percentage ranges and as the damage matrices are incomplete considering only the most common and easily observable situations. In the study of Giovinazzi (Giovinazzi, 2005), the incompleteness matter was solved by introducing beta and binomial distributions to model damage grade variation. This enabled the development of an analytical expression for the relationship between mean damage grade, μ_D (mean of the discrete beta distribution) – intensity, I and vulnerability index, V as shown in Equation (3.2), allowing estimation of the building damage distribution once vulnerability index V dominant in the area of interest is known.

$$\mu_D = 2.5\left[1+\tanh\left(\frac{I+6.5V-13.1}{2.3}\right)\right] \tag{3.2}$$

The vulnerability and ductility indices obtained for different building types are given into Equation (3.2) allows the estimation of the mean damage value μ_D ($0 < \mu_D < 5$) of the expected discrete damage distribution.

$$\mu_D = \sum_{k=0}^{5} p_k k \tag{3.3}$$

Damage distributions of earthquakes occurred in the past has been considered to solve the incompleteness matter. A possible distribution to represent building damage is the binomial and the beta distribution.

Binomial Distribution: The probabilistic assessment for the mean damage value μ_D evaluated in relation to Equation (3.2) is found by assuming a binomial distribution. However, the probability pk of having each damage grade D_k (k=0:5), for a certain mean damage μ_D, is evaluated using to the Probability Mass Function (PMF) of the binomial distribution as shown in Equation (3.4).

$$PMF: p_k = \frac{5!}{k!(5-k)!}\left(\frac{\mu_D}{5}\right)^k\left(1-\frac{\mu_D}{5}\right)^{5-k} \tag{3.4}$$

Where "!" represents the factorial operator.

The scatter for the expected damage distribution Eq. (4) is defined as a function of the mean damage value μ_D, the only free parameter for the assumed binomial distribution.

$$\sigma_D = \sqrt{\mu_D\left(1 - \frac{\mu_D}{5}\right)} \tag{3.5}$$

Beta Distribution Function: The mean damage grade values (Equation (3.2)) are then connected to the two parameters r and t (Equation (3.11)) required to fully describe the continuous beta distribution with a 3rd degree polynomial of the form shown below (Equation (3.6)). The t parameter governs the dispersion of beta distribution, where increasing t decreases the scatter. In this study based on empirical data, t values were assigned to different building types (Table 3.4). So the only unknown parameter required to describe the damage distribution is r. Parameters t and r (or equivalently the mean and the variance) control the shape of the distribution. The parameter t affects the scatter of the distribution. A reduction of scatter is observed increasing the value of the parameter t for the same damage state (Figure 3.39). If the parameter t is 8., the beta distribution looks very similar to the binomial distribution.

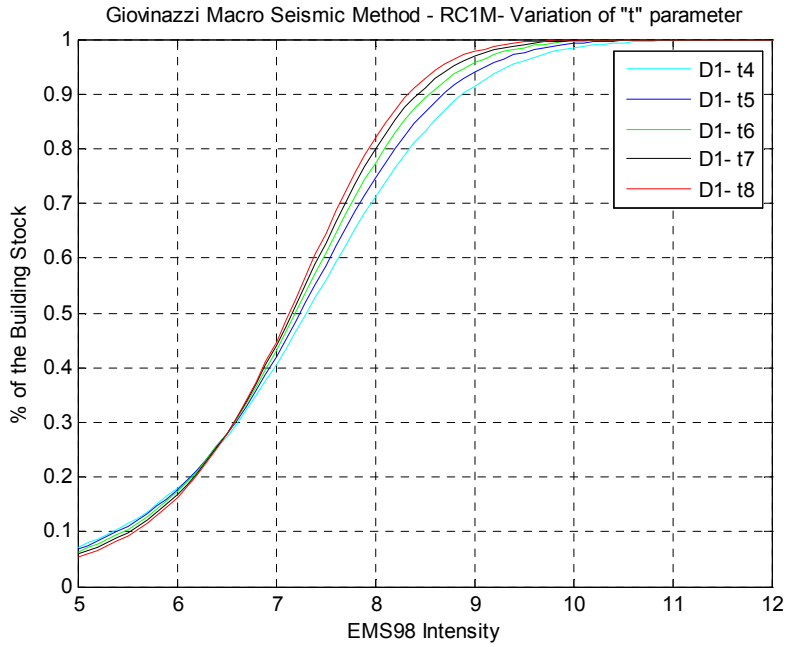

Figure 3.39. The effects of the parameter t

$$pdf_{\beta}(x) = \frac{\Gamma(t)}{\Gamma(r)\Gamma(t-r)} \frac{(x-a)^{r-1}(b-x)^{t-r-1}}{(b-a)^{t-1}} \quad a \le x \le b \tag{3.6}$$

$$CDF_{\beta} = \int_{a}^{x} pdf_{\beta}(y)dy \tag{3.7}$$

Where a, b, t and r are the parameters of the distributions and Γ is the gamma function. As a function of the same parameters the mean value μ_x of the continues variable x, which ranges between a and b and its variance are σ_x^2 so defined,

$$\begin{aligned} \mu_x &= a + \frac{r}{t}(b-a) \\ \sigma_x^2 &= (b-a)^2 \frac{r(t-r)}{t^2(t+1)} \end{aligned} \tag{3.8}$$

Considering the beta distribution, it is necessary to make a reference to damage grade D, which is a discrete variable, characterized by 6 damage grades (including the absence of damage). For that reason, it is advisable to assign value 0 to the parameter a and value 6 to the parameter b. Beginning from this assumption, it is possible to calculate the probability associated with damage grade k (k=0, 1, 2, 3, 4, 5) as follows;

$$p_k = pdf_{\beta}(k+1) - pdf_{\beta}(k) \tag{3.9}$$

Following this equation, the mean damage grade, mean value of the discrete distribution, and the mean value of the beta distribution can be correlated through a third degree polynomial:

$$\mu_x = 0.042\mu_D^3 - 0.315\mu_D^2 - 1.725\mu_D = \frac{6\,r}{t} \quad \text{(for } a\text{=0 and } b\text{=6)} \tag{3.10}$$

It is possible to correlate the two parameters of the beta distribution with the mean damage grade:

$$r = t(0.007\mu_D{}^3 - 0.0525\mu_D{}^2 + 0.2875\mu_D) \tag{3.11}$$

Using the statistical analysis of data collected after the 1980 Irpina (Italy) earthquake (Braga *et al*., 1982), the binomial distribution to represent the building damage has been adopted for the macroseismic approach (Giovinazzi , 2005). However, the bionomial distribution does not allow defining a different scatter around the mean value μ_D (Equation. (3.5)). Thus, a beta distribution based on a fuzzy random approach has been used as an alternative model to have different scattered damage distributions, depending on the number of cognitive uncertainties affecting the vulnerability assessment.

Table 3.4. *t* values for different building typologies (Giovinazzi and Lagomarsino, 2004)

t		
Building Typologies	M1, M2, M3	6
	M4, M5, M6, M7, RC4, RC5, RC6	4
	RC1, RC2, RC3, S, W	3

Besides the building type, there are several other factors that affect the overall vulnerability of a structure caused by both the variety of the constructive methods and the structural details and materials used in different regions. Thus, a regional vulnerability factor should be defined to obtain a more reliable evaluation. On the basis of the historical data or the experience, the V_r value is allowed to modify the typological vulnerability index. If regional intensity based vulnerability curves or sufficient observed damage data

are available, the average curve can be shifted to obtain a better approximation of the regional data (Figure 3.40, Giovinazzi and Lagomarsino, 2004). However, in this study, we have no need to use any regional vulnerability factor.

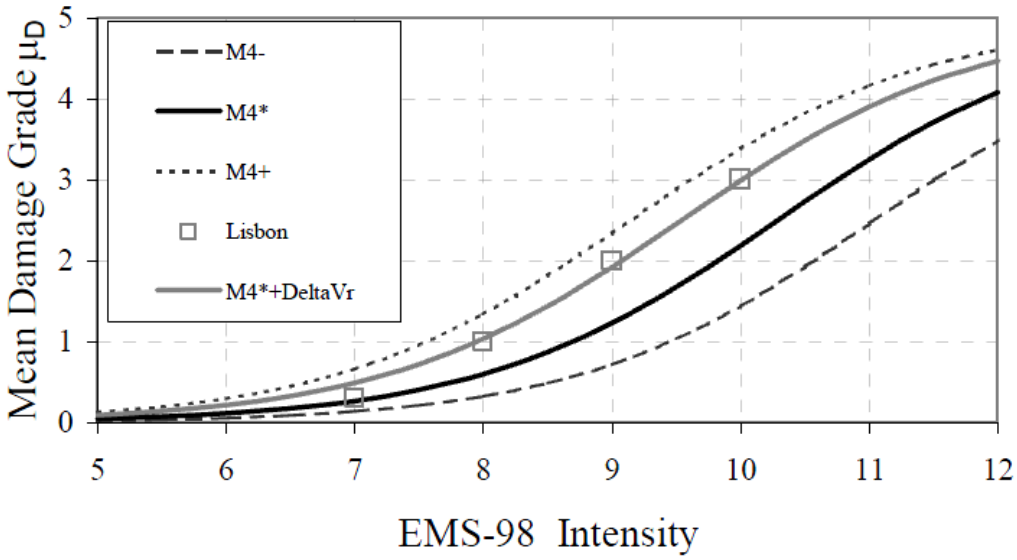

Figure 3.40. Massive stone shows a better behavior (Oliveira *et al*., 1984) than the average for M4 in Lisbon; ΔV_r=0.12 is applied

As mentioned in Section 3.3.2, the translation of the qualitative terms has been tackled assuming for the linguistic terms ("few", "many", "most") the quantitative meaning suggested by the scale in a graphical fuzzy manner as overlapping intervals of frequency in the range 0 - 100.

Considering the fuzzy set theory (Dubois and Parade, 1980), the overlapping intervals of frequencies have been defined as trapezoid memberships function χ (Figure 3.38). A complete and full membership has been define into the definite ranges $\chi(r)=1$ (Few $0 \le r \le 10$;Many $20 \le r \le 50$; Most $60 \le r \le 100$). The boundary between Few and Many or Many and Most has been represented by overlapping ranges $0 \le \chi(r) \le 1$. In other words, χ is 1 when the degree of belonging is plausible (that is to say almost sure), while a

membership between zero and one indicates that the value of the parameter is rare but possible; if χ is zero, the parameter does not belong to using the fuzzy sets theory and starting from EMS98 definitions. The study of Lagomorsino and Giovinazzi (2006) has been explained in an example for building class A and intensity $I_{EMS98}=VIII$ to assume for the translation of the linguistic terms using the binomial probability density function. Using parameters such as plausible and possible upper and lower values assumed for EMS98 linguistic terms and damage probability distributions and mean damage values resulting from the numerical translation of the linguistic definition for class A and intensity $I_{EMS98}=VIII$ has been tabulated in Table 3.5.

Table 3.5. Derivation of the macroseismic method from EMS98 implicit DPM

		Few	Many	Most
α=0 - upper	++	20	60	100
α=1 - upper	+	10	50	100
α=1 – lower	-	0	20	60
α=0 - lower	--	0	10	50

According to EMS98 damage description for "*A"* vulnerability class and member ships functions for the linguistic term (Figure 3.37), the probability p_k of having each damage grade damage D_k (k=0:5) has been evaluated using the probability mass function (PMF) of the binomial distribution (Equation (3.4)). The bold value has been defined regarding the EMS98 description. Using the bold value, the value of μ_D in Equation (3.4) has been determined and then using the Equation (3.4), the value of p_k for the other damage grade has been evaluated. The upper and lower bounds of the mean damages grades related to plausible and possible have been calculated according to the Equation (3.3).

Table 3.6. Damage probability distributions and mean damage values resulting from the numerical translation of the linguistic definition for A class and intensity $I_{EMS98}=VIII$

A Class I =VIII	*D0*	*D1*	*D2*	*D3*	*D4*	*D5*	
	-	-	-	-	Many	Few	μ_D
A++	0	2	11	29	38	**20**	3.6
A+	1	6	20	34	29	**10**	3.2
A-	2	12	28	33	**20**	5	2.7
A--	6	22	34	26	**10**	2	2.2

Due to this procedure has been repeated point by point for each intensity value, it is possible to obtain the plausible and possible bound of the mean damage grade for each vulnerability class (Table 3.7).

Table 3.7. EMS98 building types and identification of the seismic behaviour by vulnerability classes (Giovinazzi and Lagomarsino, 2003)

A^+ - upper plausibility bound

Damage / Intensity	1	2	3	4	5	μ_D
V	**10**	1.6	0.2	0.0	0.0	0.25
VI	32.0	**10**	1.9	0.2	0.0	0.68
VII	22.4	35.6	**27.6**	**10**	0.8	2.18
VIII	4.1	17.7	34.2	**33.9**	**10**	3.30
IX	0.2	2.5	12.2	35.0	**50**	4.23
X	0	0	0	0	**100**	5
XI	0	0	0	0	100	5
XII	0	0	0	0	100	5

A^- - lower plausibility bound

damage / Intensity	1	2	3	4	5	μ_D
V	**0**	0	0	0	0	0
VI	**20**	4.3	0.6	0.0	0.0	0.43
VII	31.3	35.2	**20**	5.2	0.3	1.81
VIII	11.8	29.6	34.9	**20**	2.9	2.71
IX	1.7	10.3	27.7	40.2	**20**	3.67
X	0.1	1.5	8.6	29.8	**60**	4.37
XI	0	0	0	0	100	5
XII	0	0	0	0	100	5

A^{++} - upper possibility bound

damage / Intensity	1	2	3	4	5	μ_D
V	**20**	4.3	0.6	0.0	0.0	0.43
VI	40.6	**20**	5.5	0.7	0.0	1.04
VII	11.8	29.6	34.9	**20**	2.9	2.71
VIII	1.7	10.3	27.7	40.2	**20**	3.67
IX	0.1	1.5	8.6	29.8	**60**	4.37
X	0	0	0	0	**100**	5
XI	0	0	0	0	100	5
XII	0	0	0	0	100	5

A^{--} - lower possibility bound

damage / Intensity	1	2	3	4	5	μ_D
V	**0**	0	0	0	0	0
VI	**10**	1.6	0.2	0.0	0.0	0.25
VII	40.4	27.4	**10**	1.6	0.0	1.31
VIII	22.4	35.6	27.6	**10**	0.8	2.18
IX	4.1	17.7	34.2	33.9	**10**	3.30
X	0.2	2.5	12.2	35.0	**50**	4.23
XI	0	0	0	0	100	5
XII	0	0	0	0	100	5

By connecting these points, curves have been obtained, which define the plausibility and possibility areas for each vulnerability class as function of the macroseismic intensity (Figure 3.41). At that Figure 3.41, each vulnerability class is divided into four levels; for instance, for class A such levels are termed A-- (…), A- (…), A+ (…) and A++ (…).

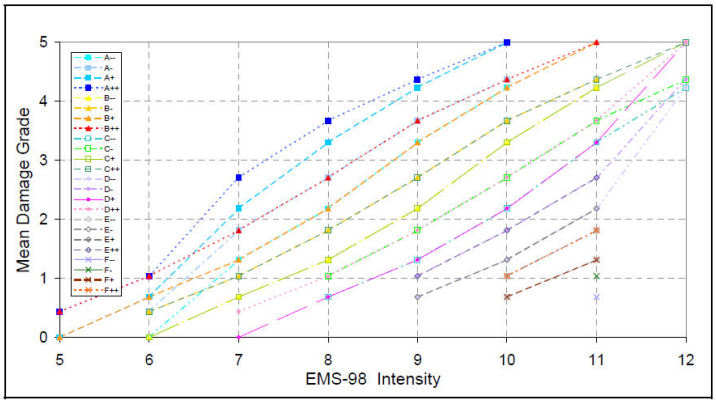

Figure 3.41. Plausible and possible behavior for each vulnerability class (Multinovic and Trendafiloski, 2003)

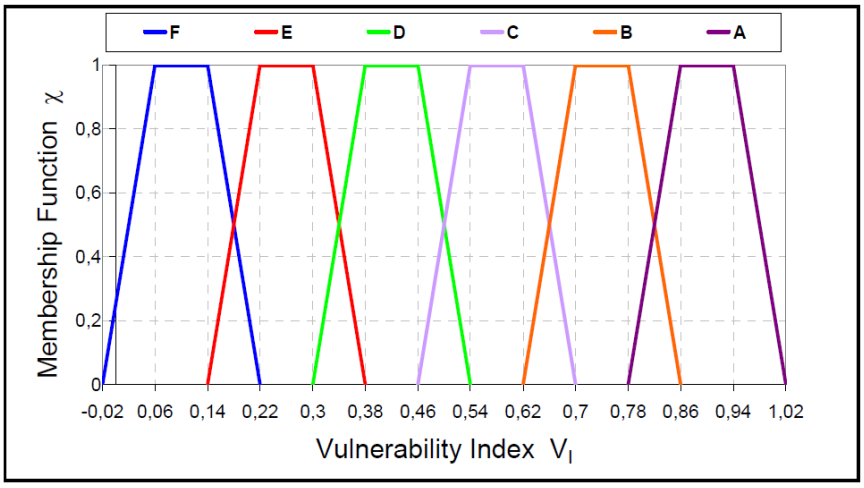

Figure 3.42. Membership function of the vulnerability index for each vulnerability class (Multinovic and Trendafiloski, 2003)

Considering the diagram of Figure 3.41 and Figure 3.42, Giovinazzi and Lagomarsino (2005) have been explicated the issue as following:

- The area between B+ and B- is distinctive of class B, while there is a contiguous area in which the best building of class B and the worse of class C coexists (the B- curve coincides with C++ one; the B—curve coincides with C+ one).

- The curves are more or less parallel because the damage produced by an intensity to buildings of certain vulnerability class is the same caused by the intensity degree to buildings of the subsequent vulnerability class (Figure 3.37 and Figure 3.38).

The capable of interpolating the curves (Figure 2.42) the mean damage grade μ_D in the proposed Equation (3.2) has been given as a function of the macroseismic intensity I, only depending from the parameter V_I (vulnerability index) as shown in Equation (3.2).

The vulnerability index represents a measure of the weakness of a building to the earthquake. It changes between zero and one in order to cover all the area of possible behavior, being value closed to one those of the most vulnerable buildings and value close to zero the ones of high-code designed structures (Figure 3.43).

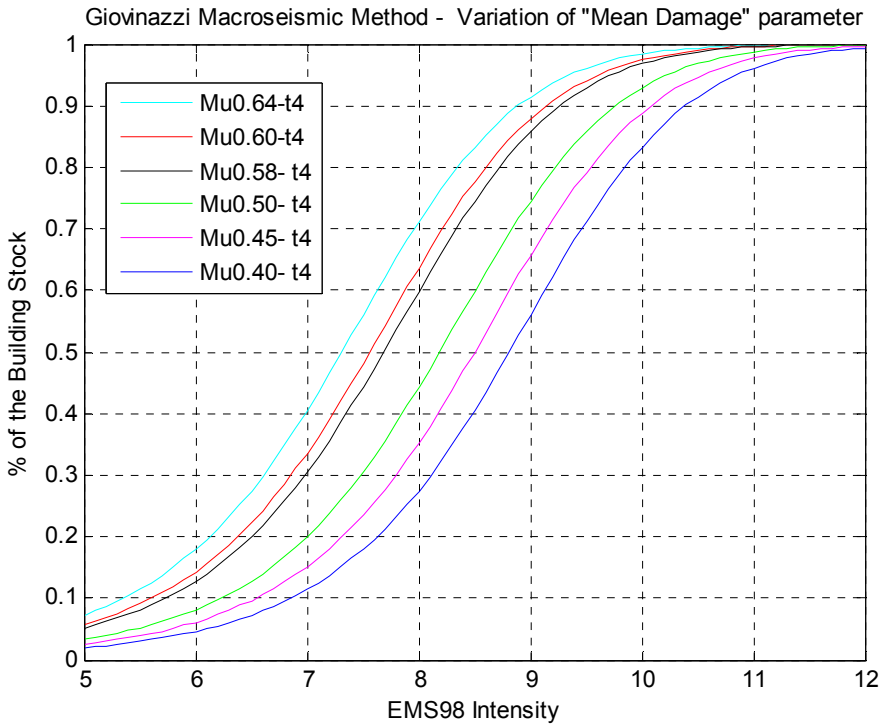

Figure 3.43. Variation of "mean damage" parameter

Therefore, the membership of a building to a specific vulnerability class can be defined by this vulnerability index (Figure 3.42) through a linear combination of the vulnerability class membership functions (Figure 3.41). As an example, the membership function of the massive stone masonry (M4) is shown in Table 3.3 and so defined:

$$\chi_{M4}(V_I) = \chi_C(V_I) + 0.6\chi_B(V_I) + 0.2\chi_D(V_I) \tag{3.12}$$

For the membership function of each typology, five representative values of V_I have been defined through a de-fuzzification process (Ross, 1995) as shown in Figure 3.44.

These values are represented in Figure 3.44 for Massive Stone masonry taxonomy and reported in Table 3.8 for all the EMS98 building taxonomies; replacing the values of V^*_I , V^-_I , V^+_I inside the given analytical function ((3.2) vulnerability curves has been found.

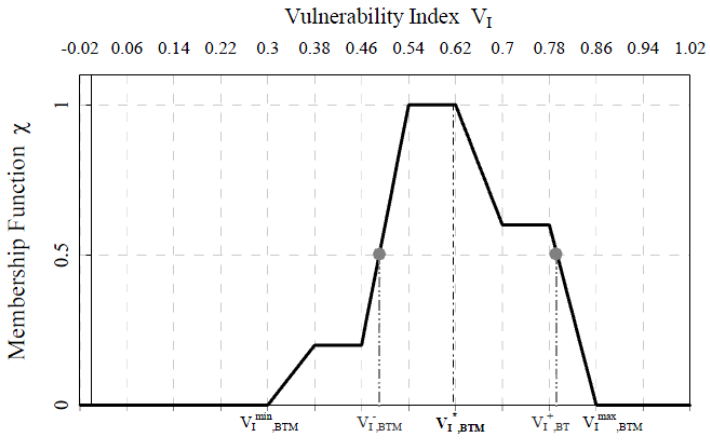

Figure 3.44. Vulnerability index membership function fro M4 massive stone typology and V_I values

Table 3.8. The values of vulnerability index for the European building taxonomy

Taxonomy		Building Type	V−−	V−	V	V+	V++
Masonry	M1	Rubble	0.62	0.81	0.873	0.98	1.02
	M2	Adobe (earth bricks)	0.62	0.687	0.84	0.98	1.02
	M3	Simple Stone	0.46	0.65	0.74	0.83	1.02
	M4	Massive Stone	0.3	0.49	0.616	0.793	0.86
	M5	U Masonry (old brick)	0.46	0.65	0.74	0.83	1.02
	M6	U Masonry * R.C. Floors	0.3	0.49	0.616	0.79	0.86
	M7	Reinforced / confined masonry	0.14	0.33	0.451	0.633	0.7
Reinforced Concrete	RC1	Frame in R.C. (without E.R.D)	0.3	0.49	0.644	0.8	1.02
		Frame in R.C. (moderate E.R.D)	0.14	0.33	0.484	0.64	0.86
		Frame in R.C. (high E.R.D)	−0.02	0.17	0.324	0.48	0.7
	RC2	Shear walls (without E.R.D)	0.3	0.367	0.544	0.67	0.86
		Shear walls (moderate E.R.D)	0.14	0.21	0.384	0.51	0.7
		Shear walls (high E.R.D)	−0.02	0.047	0.224	0.35	0.54

The study of Lagomarsino and Giovinazi (2006) has been given the proposed parameters defining vulnerability curves after cross-validation for masonry taxonomy, reinforced concrete taxonomies designed without seismic code prescription , reinforced concrete taxonomy designed according to seismic code prescription of different ductility classes, low (DCL), medium (DCM) and high (DCH).

This method has also been compared with the observed damage data and a good agreement has been observed between the proposed Macroseimic Method and observed damage data. Giovinazzi (2005) has used the Turkish observed damage data such as Gediz (1970), Bingol (1970), Burdur (1971), Lice (1975) Erzincan (1992). Figure 3.45 shows the vulnerability curves from the Macroseismic method for different masonry building taxonomies and comparison with observed damage data (Giovinazzi, 2005).

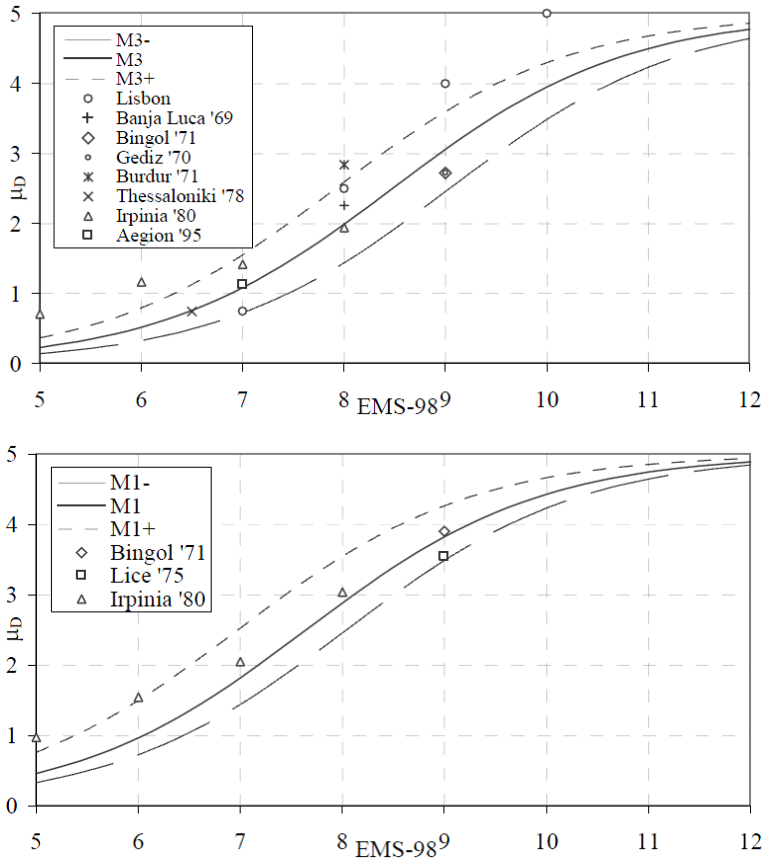

Figure 3.45. Vulnerability curves from macroseismic method for different masonry building taxonomies and compared with observed data (Giovinazzi, 2005)

According to the building taxonomy of Turkey, these parameters have been adopted to estimate the building vulnerability curve. Based on the observation of a good agreement between the proposed Macroseismic Method and observed damage data of Turkey, it was decided to use the Macroseismic method in this study in order to estimate the building damage.

Considering the previous studies for Turkey, the empirical vulnerability relationships for Mid-Rise R/C framed buildings obtained from 1999 Kocaeli Earthquake damage distribution are given in Figure 3.46 (Coburn and Spence, 2002). Based on available empirical data, harmonization from referenced works, the vulnerability curves for the general mid rise (4-8 storey) R/C frame type buildings in Turkey are provided in Figure 3.47 (DEE-KOERI, 2003). The horizontal and vertical axese indicate the range of MSK

intensities and the percentage loss for the five different damage grade (D1 through D5, as defined in Figure 3.37), respectively.

Giovinazzi (2005) has deduced that PSI intensity ψ (shown in Coburn and Spence, 2002), relates to the EMS98 macroseismic intensity I according to the following linear correlation:

$$I = 0.54 \cdot \psi + 3.25 \tag{3.13}$$

If a parameter t=4 has been used, Figure 3.48 demonstrates a very good matching between two curves to describe the distribution of building damage. This means that, PSI scale methods provides more scattered results in comparison to the ones obtained employing the macroseismic.

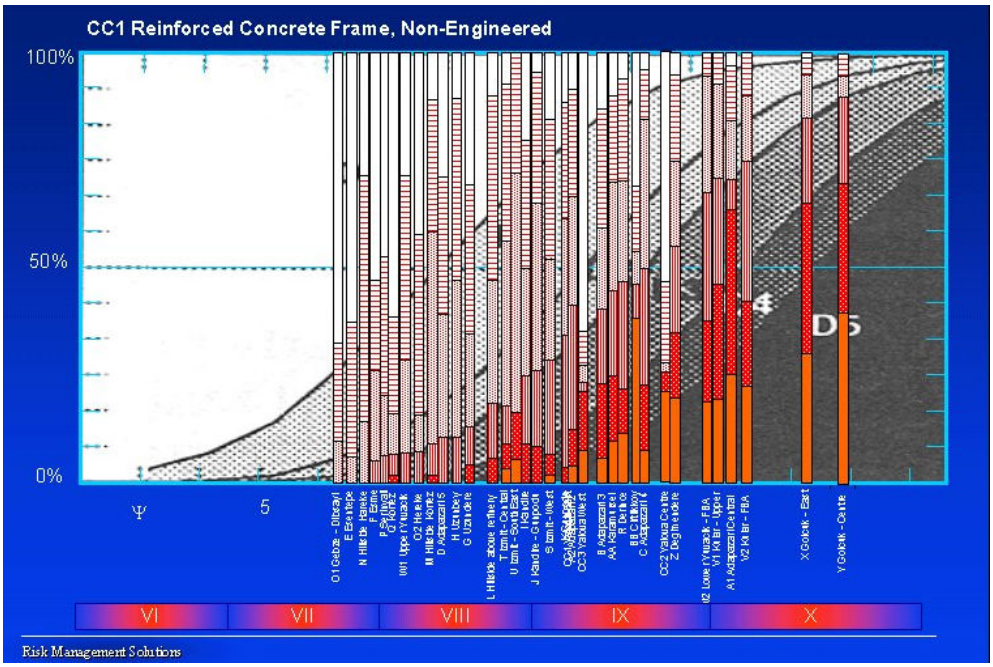

Figure 3.46. The empirical vulnerability relationships for mid-rise R/C framed buildings obtained from 1999 Kocaeli Earthquake damage distribution (Coburn and Spence, 2002)

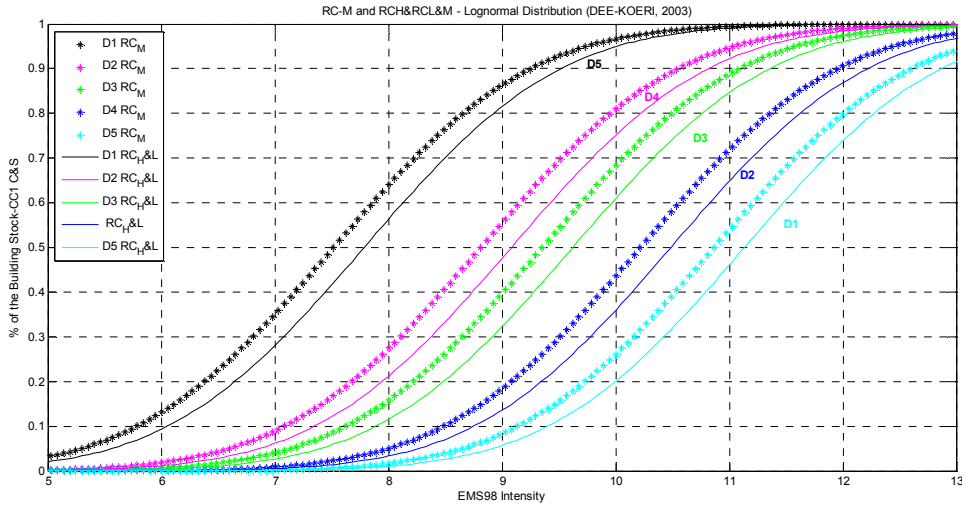

Figure 3.47. The vulnerability curves for the general mid rise, high-rise, and low-rise R/C frame type and masonry buildings in Turkey

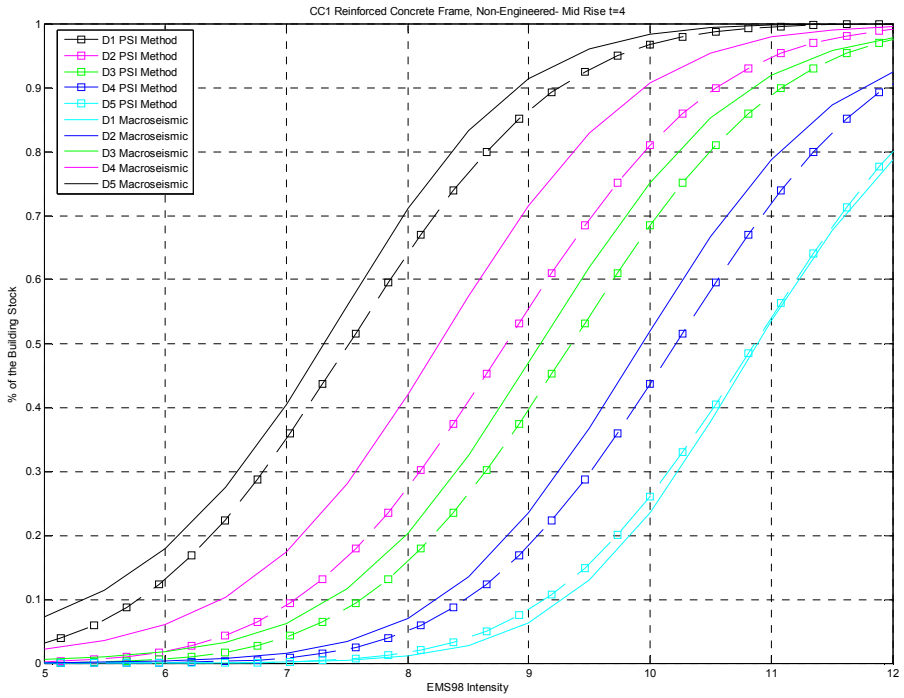

Figure 3.48. Comparison between the EMS98 damage fragility curves and PSI damage fragility curves for building type of CC1 (RC1_W_ERD RC Frame non seismic)

Seven earthquakes (Denizli-1976; Bingol-1971; Erzincan-1992; Dinar-1995; Adana-1998; Kocaeli-1999; Bingol-2003) have occurred in several provinces of Turkey since

1975. Detailed damage surveys of these earthquakes were evaluated. The damage data compiled based on the surveys and observations after these destructive earthquakes are evaluated with two probability models; (a) lognormal distribution have been used in KOERI model (DEE-KOERI,2003) (b) beta and binomial distribution have been used in Macroseismic method (Giovinazzi and Lagomarsino, 2005). Figure 3.49 shows a good correlation between the damage surveys and empirical models. The earthquakes used in Figure 3.49 are listed in Table 3.9.

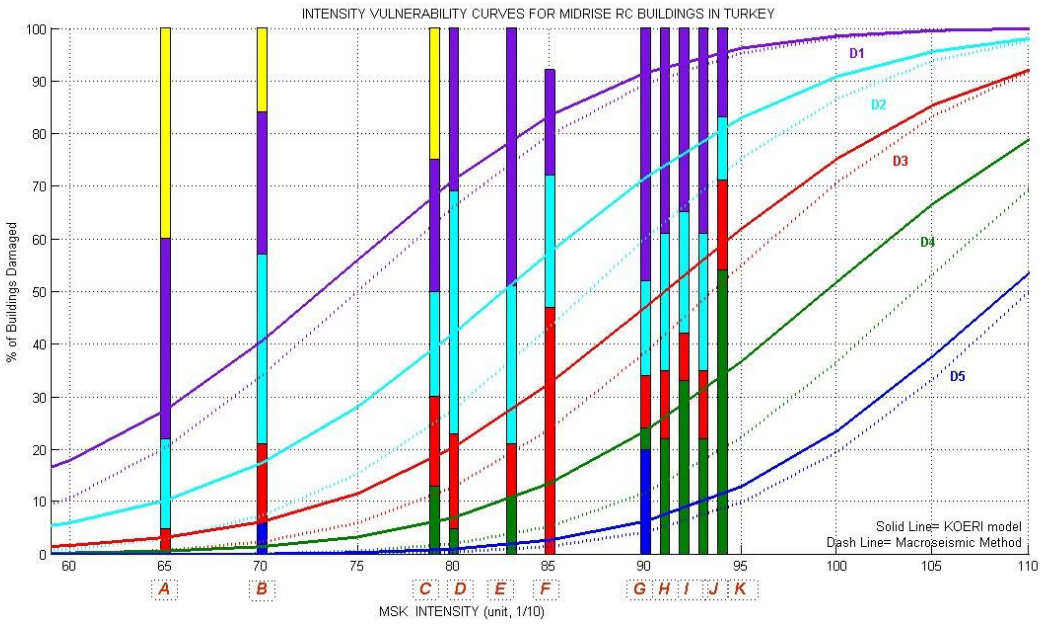

Figure 3.49. Intensity based vulnerability curves for mid rise RC building for Turkey (dash line and solid line represent macroseismic and KOERI methods (DEE-KOERI, 2003), respectively)

Table 3.9. The earthquakes used in Figure 3.49

	Earthquakes	References
A	1976,Denizli	ERD
B	1971, Bingol	ERD
C	1992, Erzincan	ERD
D	1998, Adana	Wenk *et al*., 1998)
E	2003, Bingol	Ellul and D'Ayala, 2003

F	1995, Dinar	Ansal *et al*., 1997
G	1999, Kocaeli	AIJ, 2000
H	1999, Kocaeli - Cumhuriyet	Sancio *et al*., 2002
I	1999, Kocaeli - Semerciler	Sancio *et al*., 2002
J	1999, Kocaeli - Orta	Sancio *et al*., 2002
K	1999, Kocaeli - Tığcılar	Sancio *et al*., 2002

Considering the intensity based vulnerability methodology (Giovinazzi and Lagomarsino, 2005), in this study, two different vulnerability relationships are taken into consideration. "Result 1" is represented by the Modified KOERILoss Vulnerability curves (DEE-KOERI, 2003) between low-rise, mid-rise and high-rise RC Frame and masonry structures. In this approach, the vulnerability curves for low-rise and high-rise RC frame type buildings are obtained by half a unit left shifting of the intensity scale in the horizontal axis of the vulnerability curves of the medium rise RC frame buildings. Medium-rise RC frame is also similar to the CC1 Reinforced concrete frame non engineered type of buildings defined in the study of Coburn and Spence (2002). The vulnerability and ductility indexes for CC1 type of building are obtained in the Giovinazzi's theses (Giovinazzi, S, 2005). As a result, the vulnerability and ductility indexes and by using this parameter the comparison with the KOERILoss vulnerability curves are presented in the Figure 3.50. Using the Macroseismic method for each type of building in Turkey, "Result 2" is considered. Based on the European building taxonomy, Turkey building inventory is classified as defined in Section 3.1.

Table 3.10. The vulnerability and ductility indexes for "Result 1" and "Result 2"

		Modified KOERI model			Giovinazzi & Lagomarsino model		
	Definition	*V*	*Q*	*t*	*V*	*Q*	*t*
RC1_L	RC Frame with moderate level of ERD – LR	0.6	2.3	4	0.62	2.3	4
RC1_M	RC Frame with moderate level of ERD. – MR	0.64	2.3	4	0.64	2.3	4
RC1_H	RC Frame with moderate level of ERD – HR	0.6	2.3	4	0.68	2.3	4
M1_L	Rubble- Low Rise (LR)	0.6	2.3	4	0.79	2.3	6
M1_M	Rubble – Mid Rise (MR)	0.6	2.3	4	0.87	2.3	6

M1_H	Rubble – High Rise (HR)	0.6	2.3	4	0.87	2.3	6
M2_L	Adobe – Low Rise (LR)	0.6	2.3	4	0.84	2.3	6
M2_M	Adobe – Mid Rise (MR)	0.6	2.3	4	0.84	2.3	6
M2_H	Adobe – High Rise (HR)	0.6	2.3	4	0.84	2.3	6
M5_L	Unreinforced Masonry – Low Rise (LR)	0.6	2.3	4	0.62	2.3	5
M5_M	Unreinforced Masonry – Mid Rise (MR)	0.6	2.3	4	0.72	2.3	5
M5_H	Unreinforced Masonry – High Rise (HR)	0.6	2.3	4	0.8	2.3	5

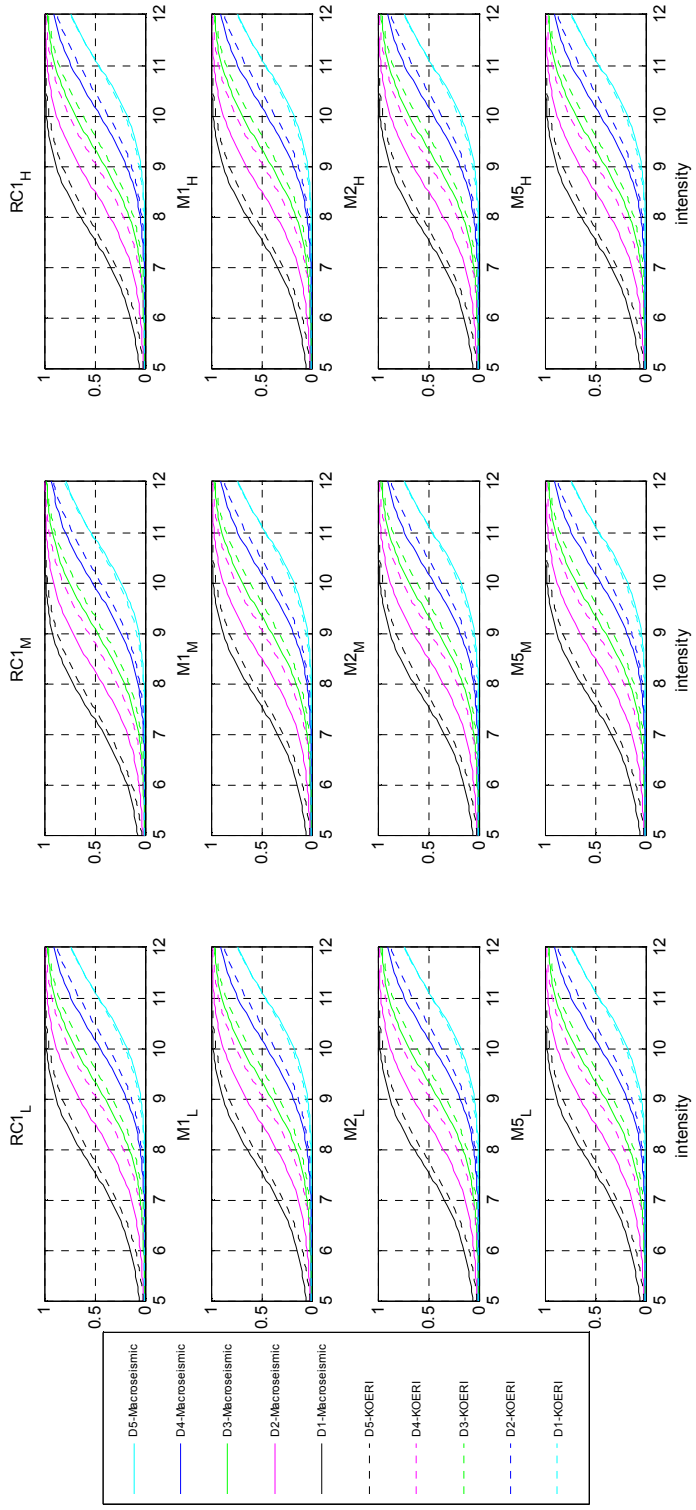

Figure 3.50. Intensity based vulnerability curves using the KOERI model (DEE-KOERI, 2003) and modified KOERI model with Giovinazzi and Lagomarsino Methodology

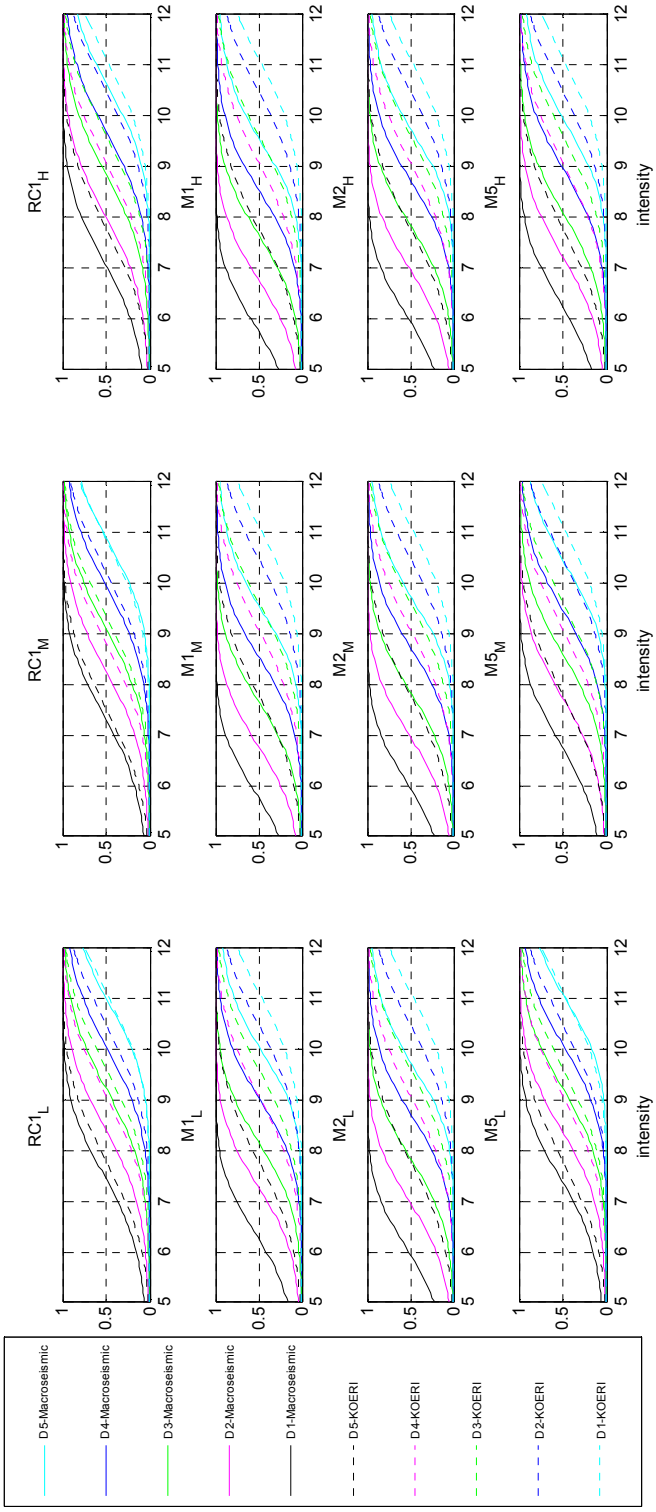

Figure 3.51. Intensity based vulnerability curves using the KOERI (DEE-KOERI, 2003) and Giovinazzi and Lagomarsino methodology for each type of buildings in Turkey

3.3.4. Estimation of Building Damage Distribution

The total estimated building damage results of the "Modified KOERI model - Result 1" and the "Giovinazzi and Lagomarsino - Result 2" for 50 per cent, 10 per cent and 2. per cent probability of exceedence in 50 years are presented in Figure 3.52 through Figure 3.81 for the range of five different damage grades, D1 through D5 as, described in EMS98, respectively.

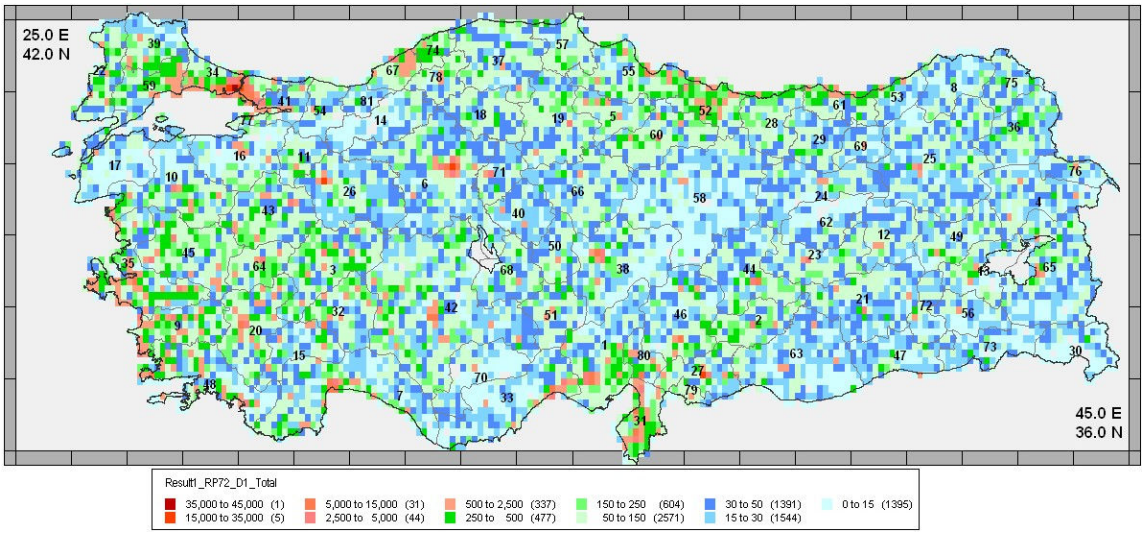

Figure 3.52. Intensity based probabilistic estimated building damage distribution of slight damage (D1) for all type of building in Turkey corresponding to 50 per cent probability of exceedence in 50 years (modified KOERI model – Result 1)

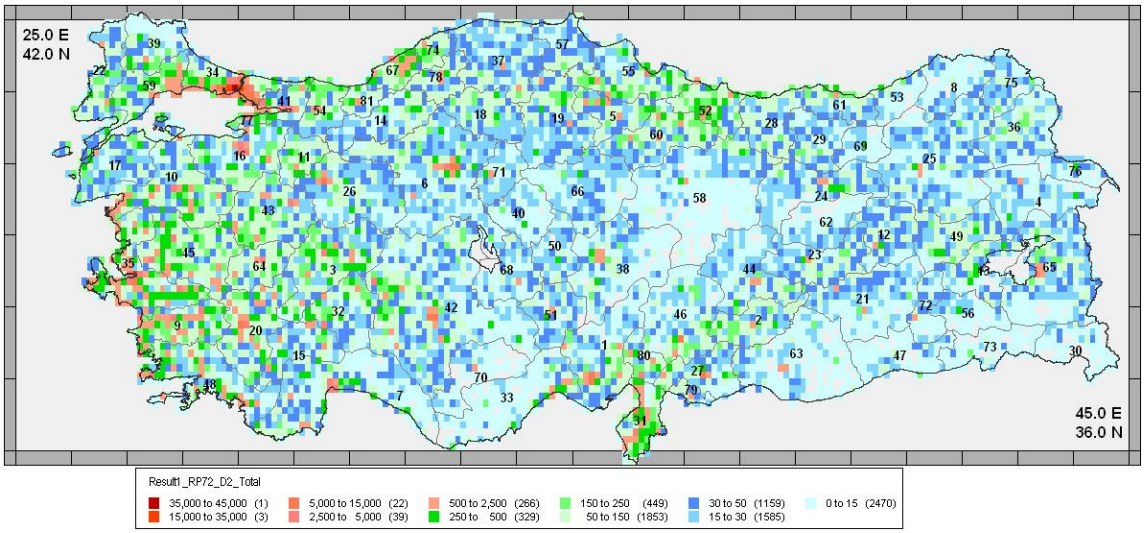

Figure 3.53. Intensity based probabilistic estimated building damage distribution of moderate damage (D2) for all type of building in Turkey corresponding to 50 per cent probability of exceedence in 50 years (modified KOERI model - Result 1)

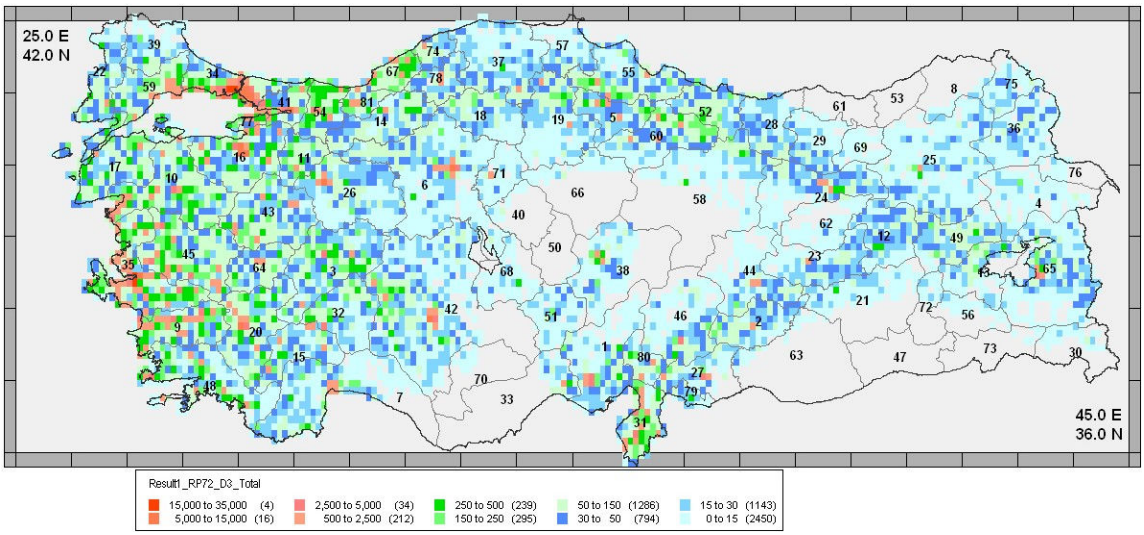

Figure 3.54. Intensity based probabilistic estimated building damage distribution of heavy damage (D3) for all type of building in Turkey corresponding to 50 per cent probability of exceedence in 50 years (modified KOERI model - Result 1)

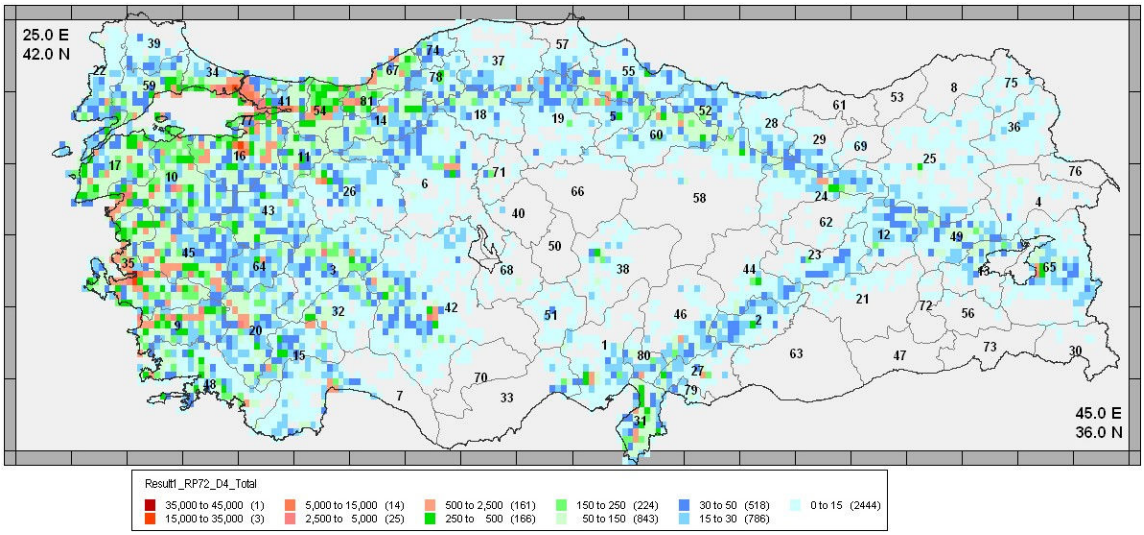

Figure 3.55. Intensity based probabilistic estimated building damage distribution of partial destruction damage (D4) for all type of building in Turkey corresponding to 50 per cent probability of exceedence in 50 years (modified KOERI model - Result 1)

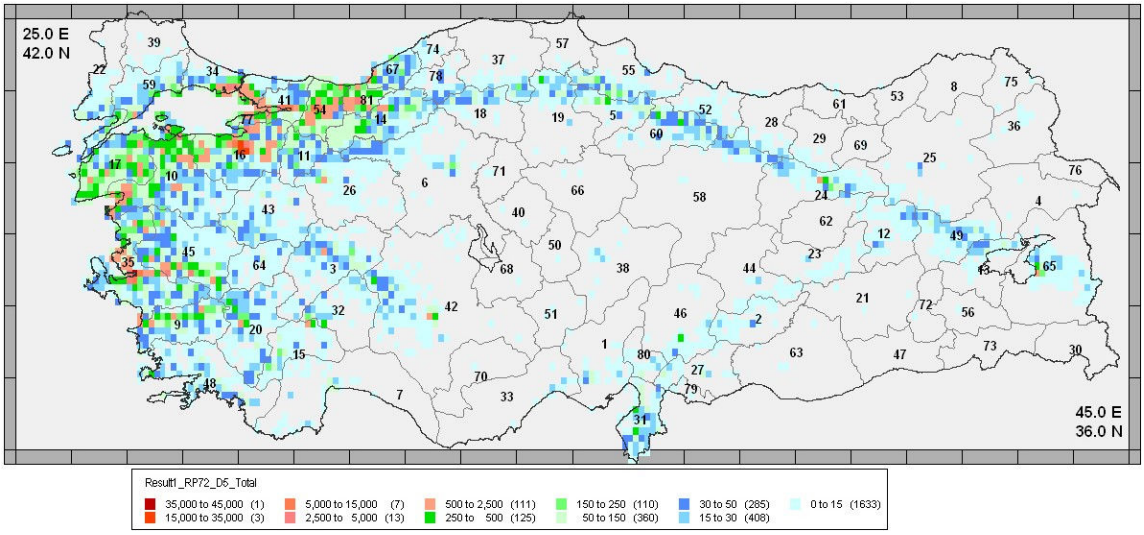

Figure 3.56. Intensity based probabilistic estimated building damage distribution of collapse damage (D5) for all type of building in Turkey corresponding to 50 per cent probability of exceedence in 50 years (modified KOERI model - Result 1)

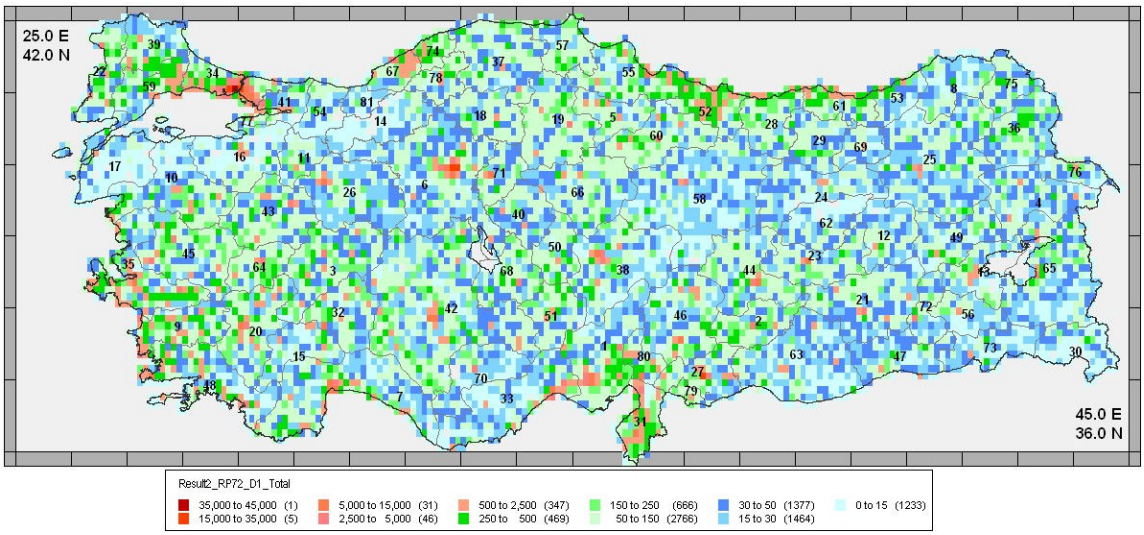

Figure 3.57. Intensity based probabilistic estimated building damage distribution of slight damage (D1) for all type of building in Turkey corresponding to 50 per cent probability of exceedence in 50 years (Giovinazzi and Lagomarsino model - Result 2)

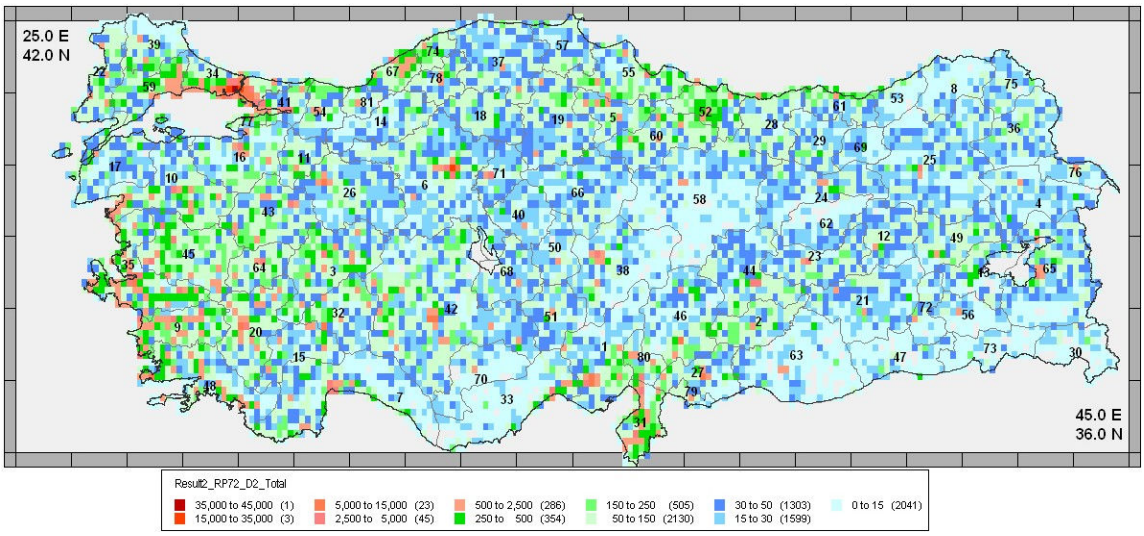

Figure 3.58. Intensity based probabilistic estimated building damage distribution of moderate damage (D2) for all type of building in Turkey corresponding 50 per cent probability of exceedence in 50 years (Giovinazzi and Lagomarsino model - Result 2)

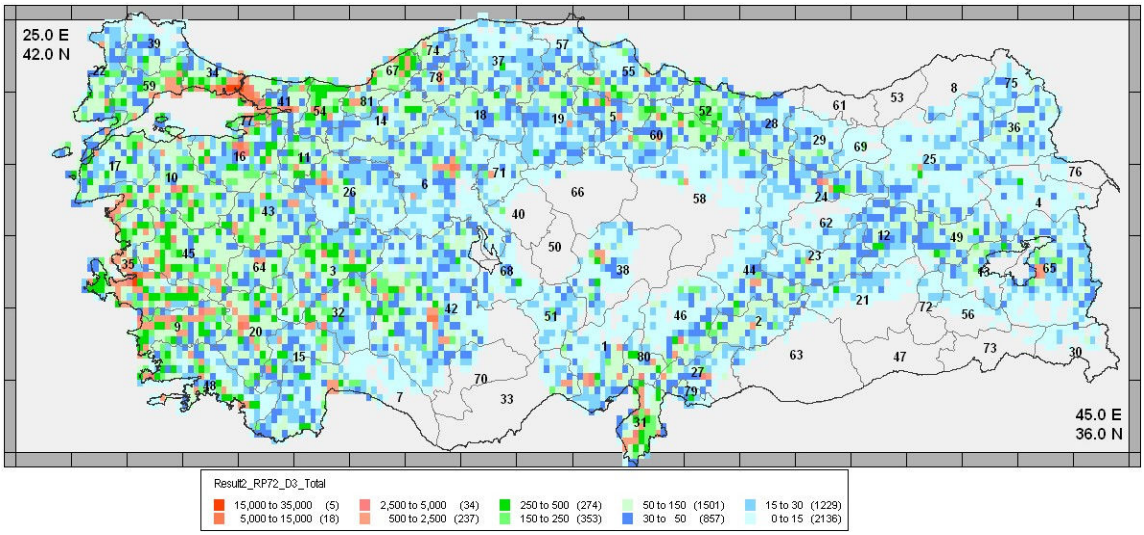

Figure 3.59. Intensity based probabilistic estimated building damage distribution of heavy damage (D3) for all type of building in Turkey corresponding to 50 per cent probability of exceedence in 50 years (Giovinazzi and Lagomarsino model - Result 2)

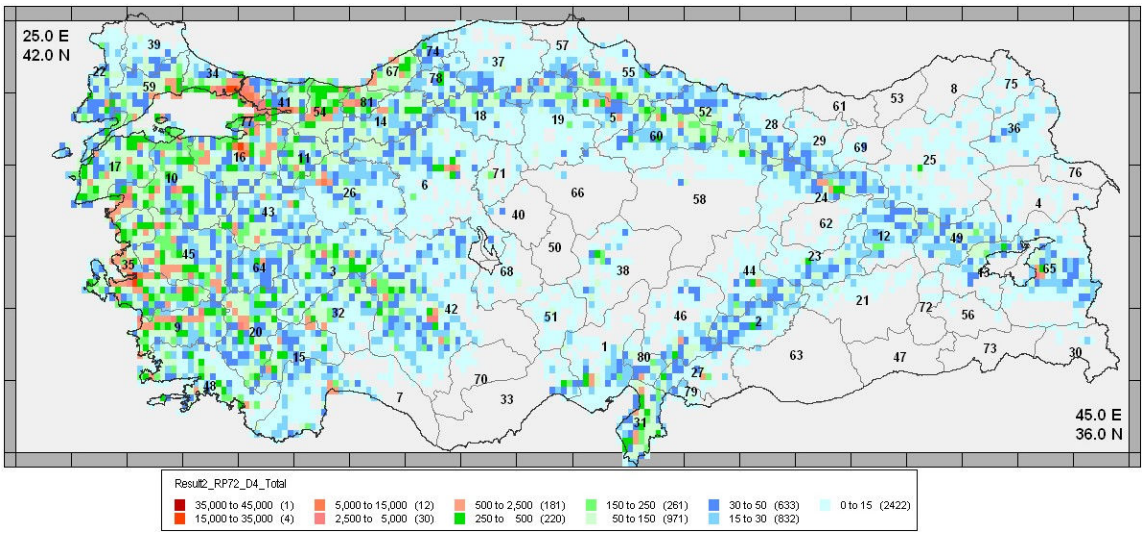

Figure 3.60. Intensity based probabilistic estimated building damage distribution of partial destruction damage (D4) for all type of building in Turkey corresponding to 50 per cent probability of exceedence in 50 years (Giovinazzi and Lagomarsino model - Result 2)

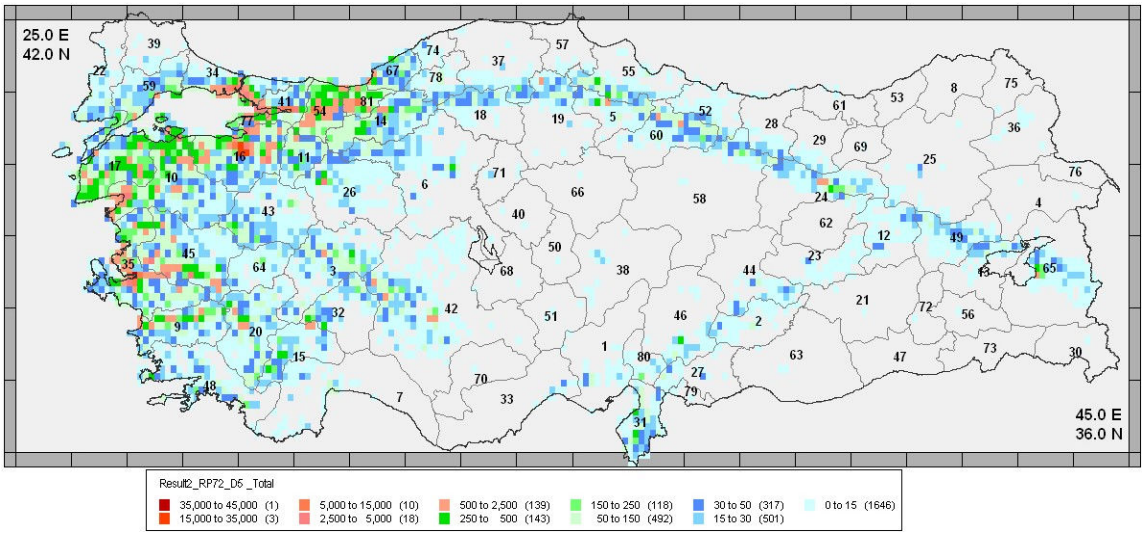

Figure 3.61. Intensity based probabilistic estimated building damage distribution of collapse damage (D5) for all type of building in Turkey corresponding to 50 per cent probability of exceedence in 50 years (Giovinazzi and Lagomarsino model- Result 2)

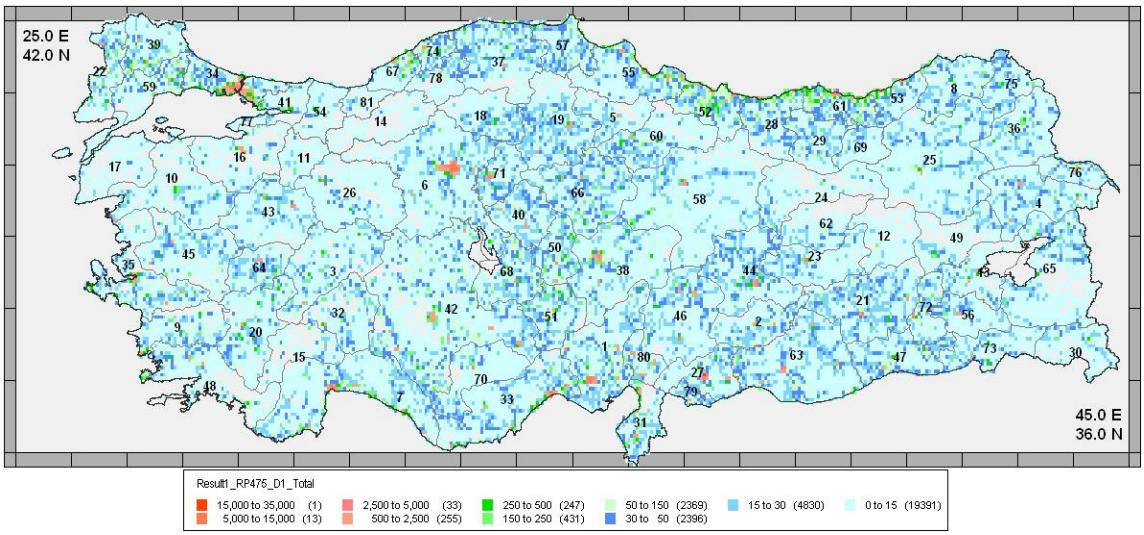

Figure 3.62. Intensity based probabilistic estimated building damage distribution of slight damage (D1) for all type of building in Turkey corresponding to 10 per cent probability of exceedence in 50 years (modified KOERI model – Result 1)

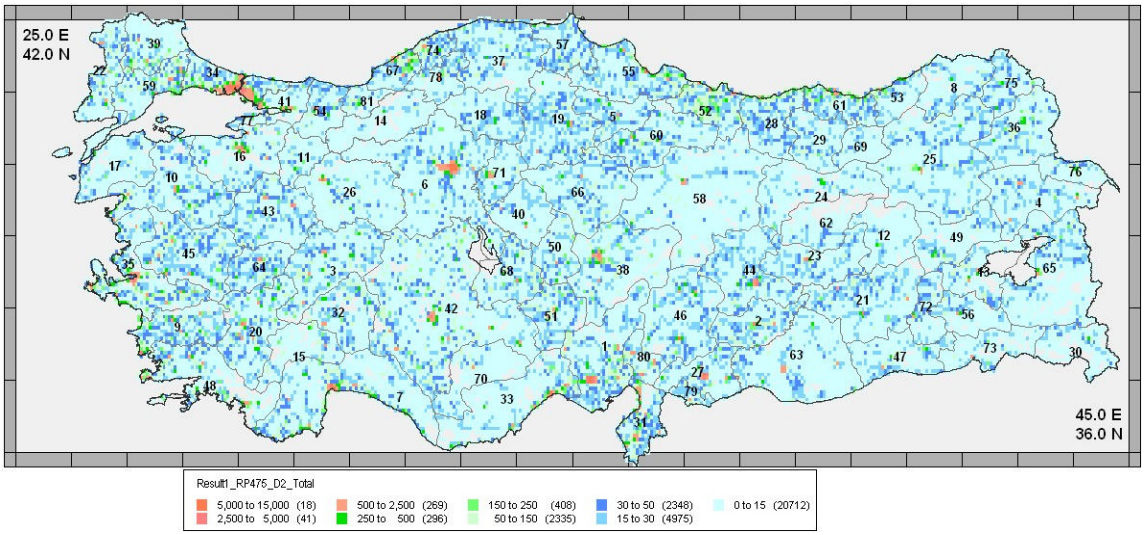

Figure 3.63. Intensity based probabilistic estimated building damage distribution of moderate damage (D2) for all type of building in Turkey corresponding to 10 per cent probability of exceedence in 50 years (modified KOERI model – Result 1)

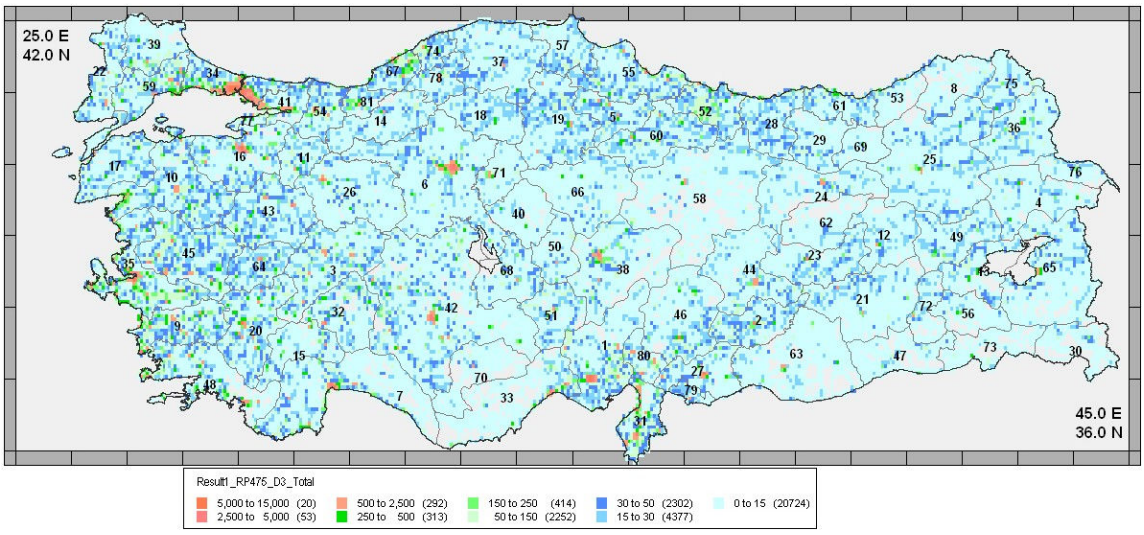

Figure 3.64. Intensity based probabilistic estimated building damage distribution of heavy damage (D3) for all type of building in Turkey corresponding to 10 per cent probability of exceedence in 50 years (modified KOERI model – Result 1)

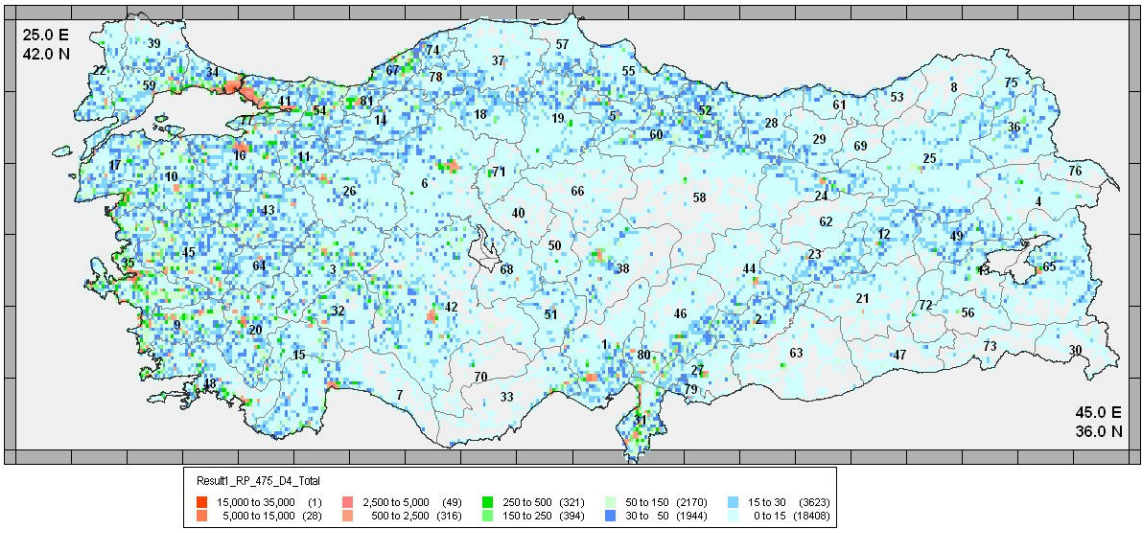

Figure 3.65. Intensity based probabilistic estimated building damage distribution of partial destruction damage (D4) for all type of building in Turkey corresponding to 10 per cent probability of exceedence in 50 years (modified KOERI model – Result 1)

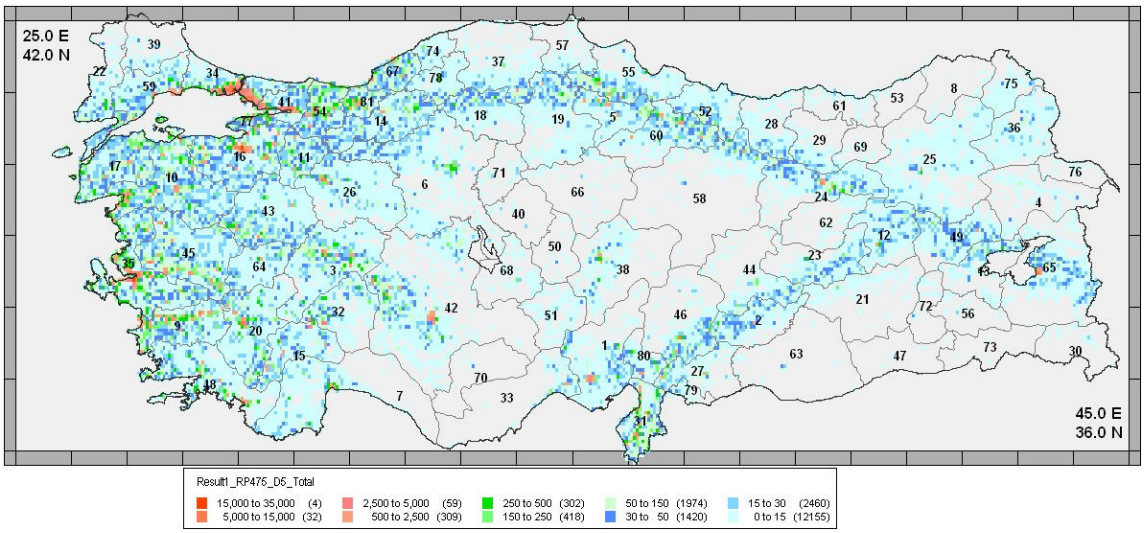

Figure 3.66. Intensity based probabilistic estimated building damage distribution of collapse damage (D5) for all type of building in Turkey corresponding to 10 per cent probability of exceedence in 50 years (modified KOERI model – Result 1)

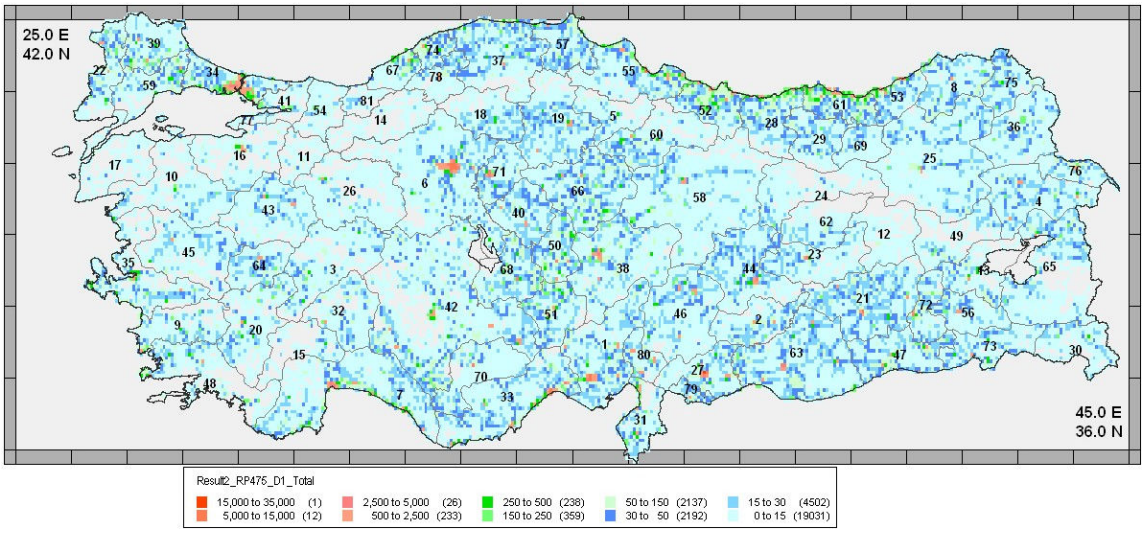

Figure 3.67. Intensity based probabilistic estimated building damage distribution of slight damage (D1) for all type of building in Turkey corresponding to 10 per cent probability of exceedence in 50 years (Giovinazzi and Lagomarsino model - Result 2)

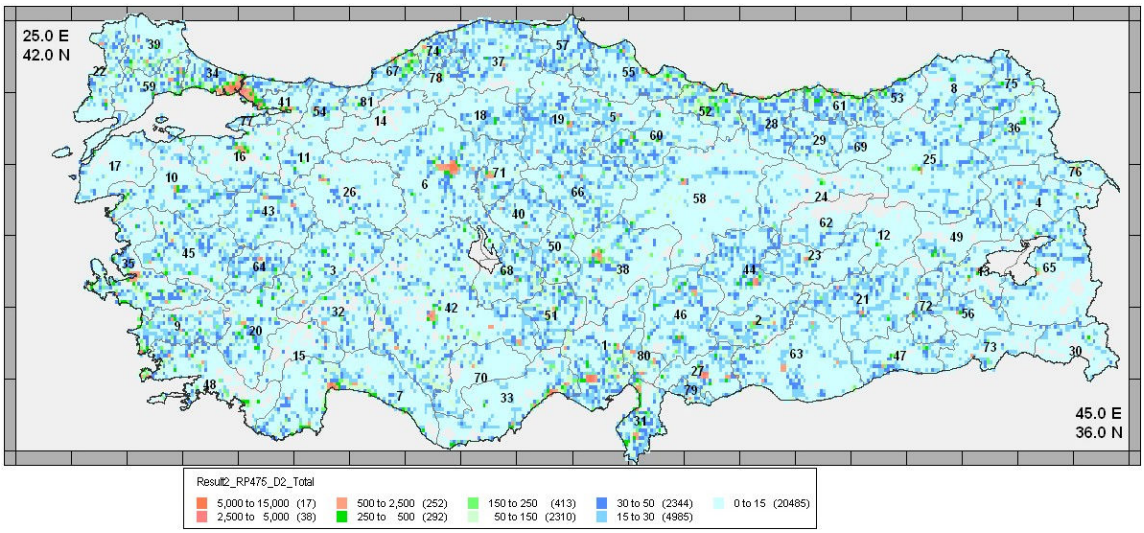

Figure 3.68. Intensity based probabilistic estimated building damage distribution of moderate damage (D2) for all type of building in Turkey corresponding to 10 per cent probability of exceedence in 50 years (Giovinazzi and Lagomarsino model - Result 2)

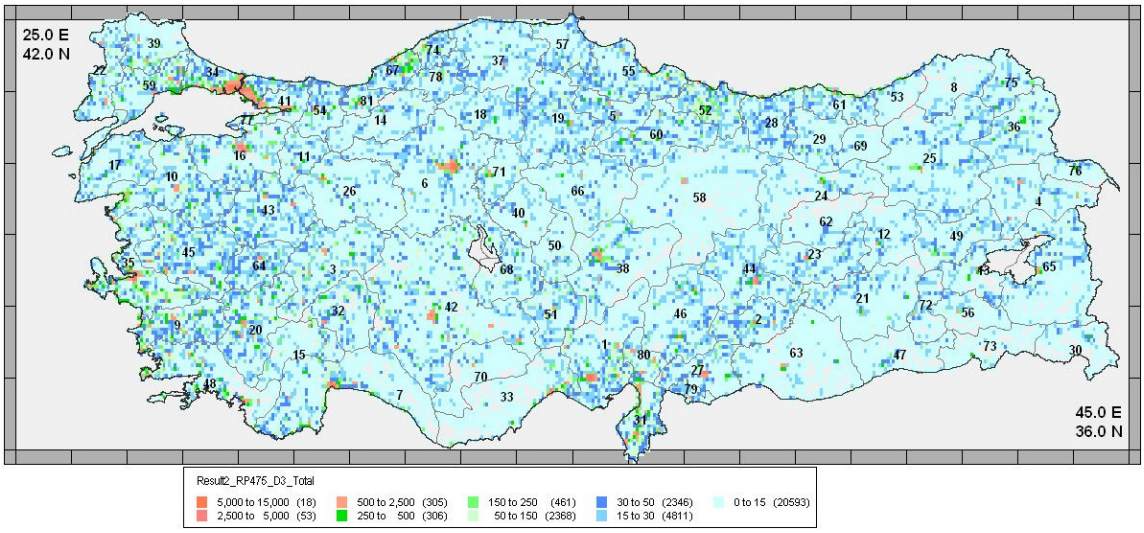

Figure 3.69. Intensity based probabilistic estimated building damage distribution of heavy damage (D3) for all type of building in Turkey corresponding to 10 per cent probability of exceedence in 50 years (Giovinazzi and Lagomarsino model - Result 2)

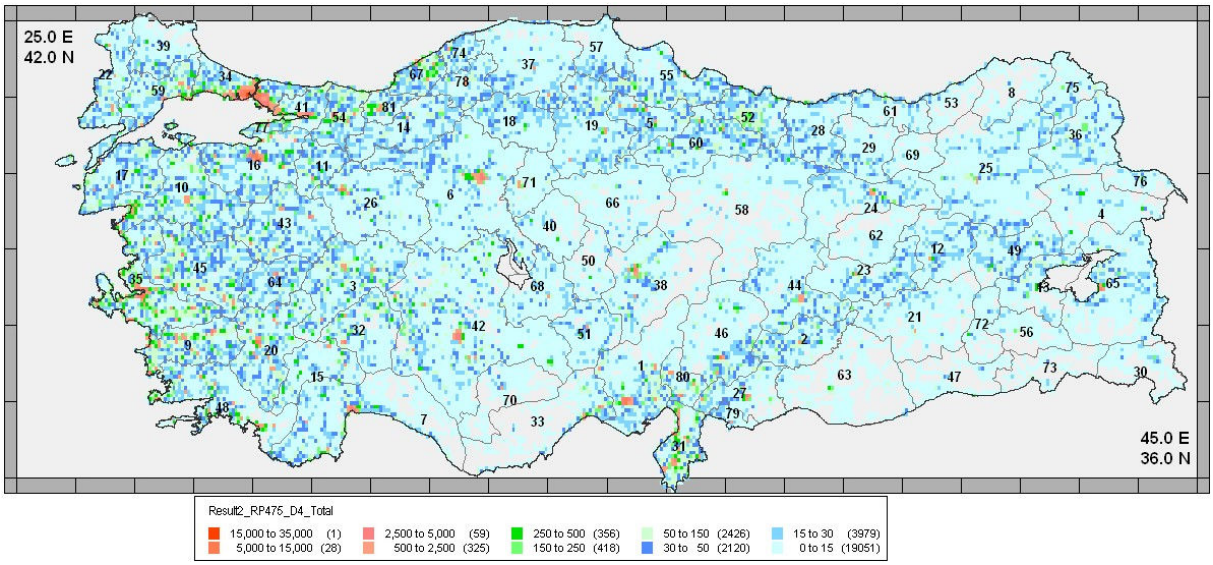

Figure 3.70. Intensity based probabilistic estimated building damage distribution of partial destruction damage (D4) for all type of building in Turkey corresponding to 10 per cent probability of exceedence in 50 years (Giovinazzi and Lagomarsino model - Result 2)

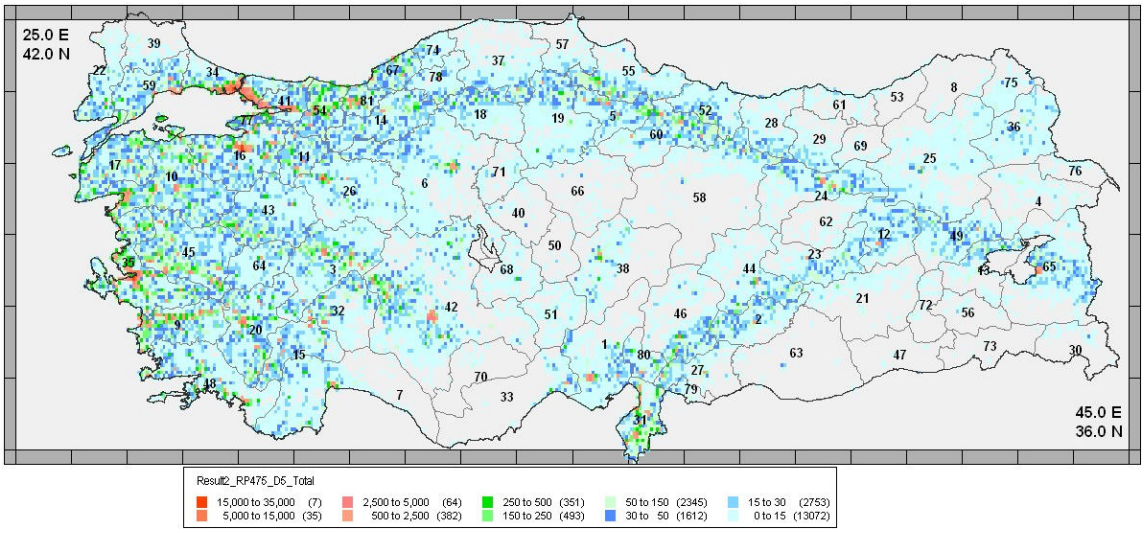

Figure 3.71. Intensity based probabilistic estimated building damage distribution of collapse damage (D5) for all type of building in Turkey corresponding to 10 per cent probability of exceedence in 50 years (Giovinazzi and Lagomarsino model - Result 2)

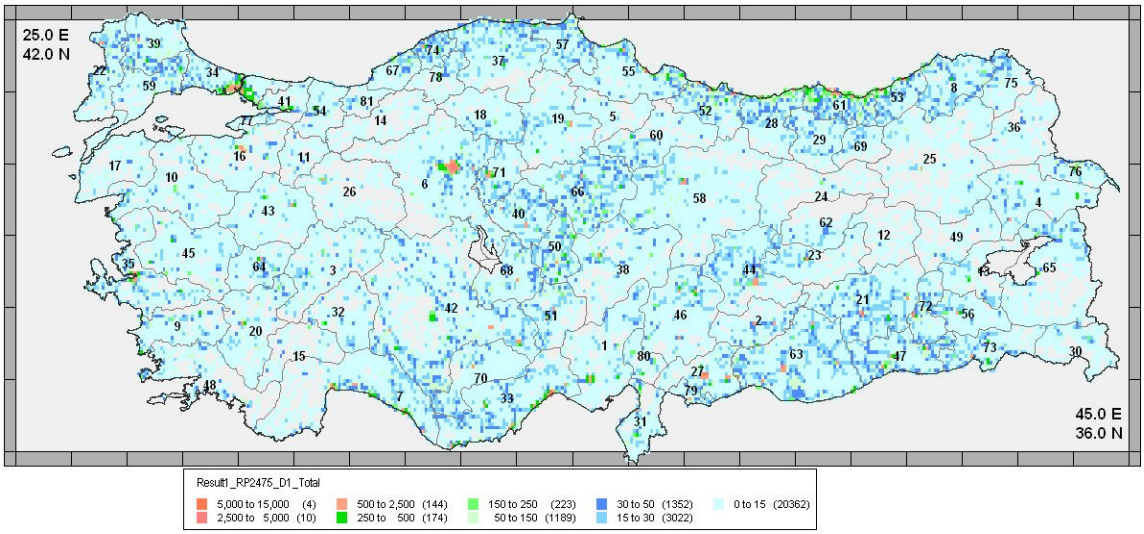

Figure 3.72. Intensity based probabilistic estimated building damage distribution of slight damage (D1) for all type of building in Turkey corresponding to 2. per cent probability of exceedence in 50 years (modified KOERI model – Result 1)

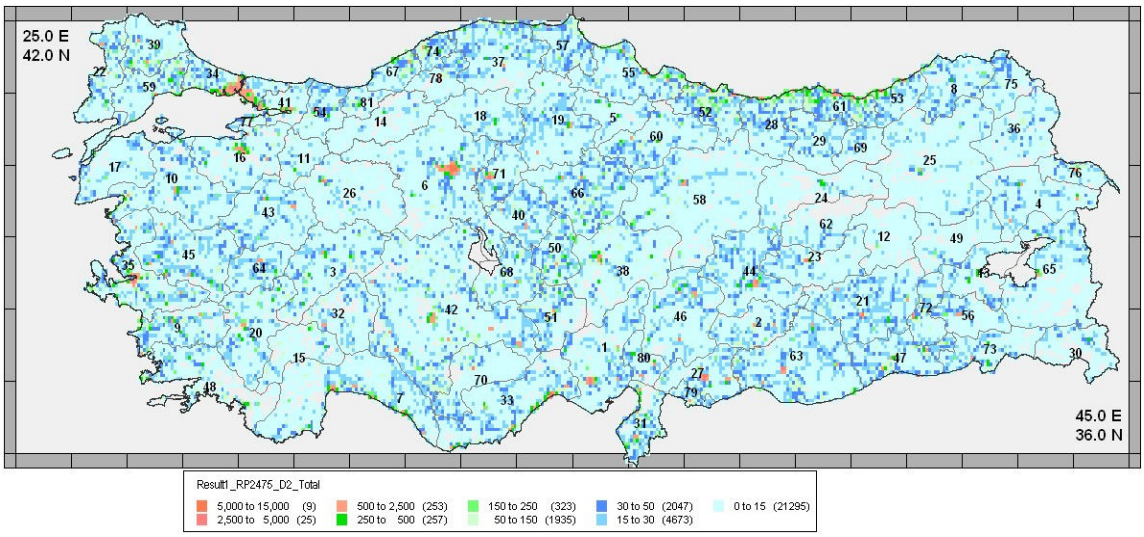

Figure 3.73. Intensity based probabilistic estimated building damage distribution of moderate damage (D2) for all type of building in Turkey corresponding to 2. per cent probability of exceedence in 50 years (modified KOERI model – Result 1)

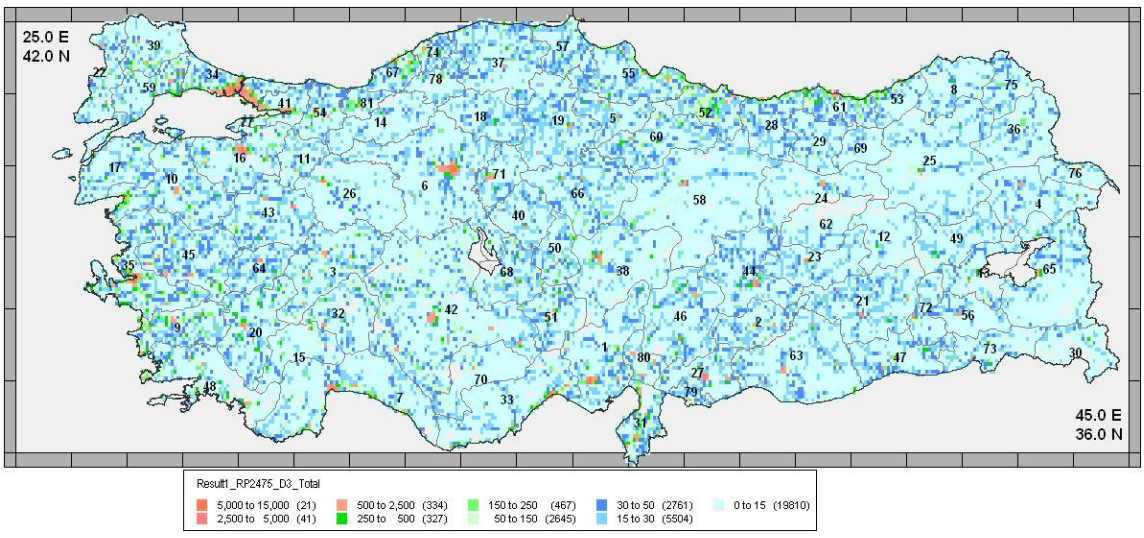

Figure 3.74. Intensity based probabilistic estimated building damage distribution of heavy damage (D3) for all type of building in Turkey corresponding to 2. per cent probability of exceedence in 50 years (modified KOERI model – Result 1)

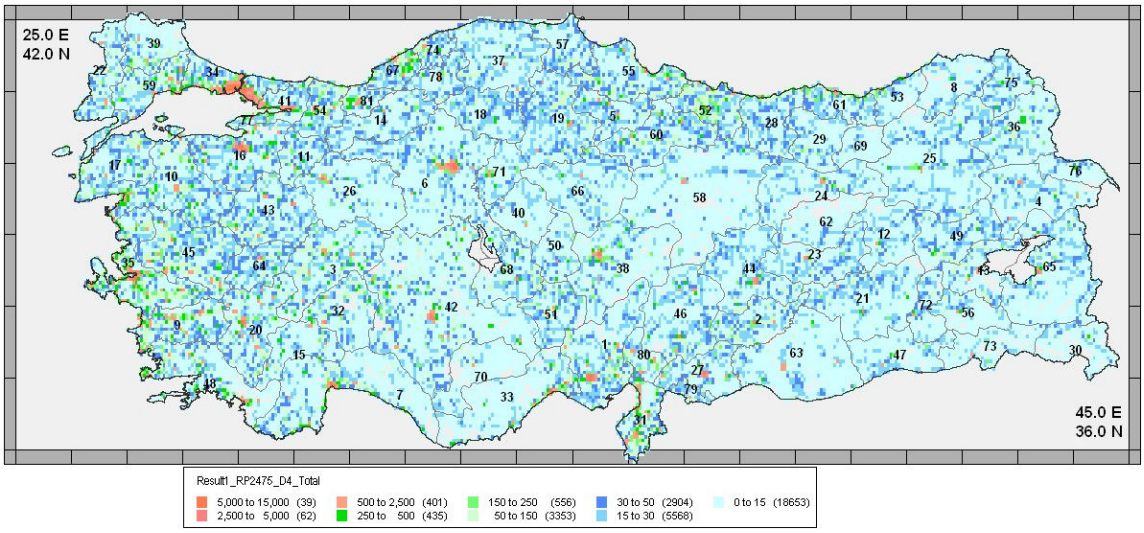

Figure 3.75. Intensity based probabilistic estimated building damage distribution of partial destruction damage (D4) for all type of building in Turkey corresponding to 2. per cent probability of exceedence in 50 years (modified KOERI model – Result 1)

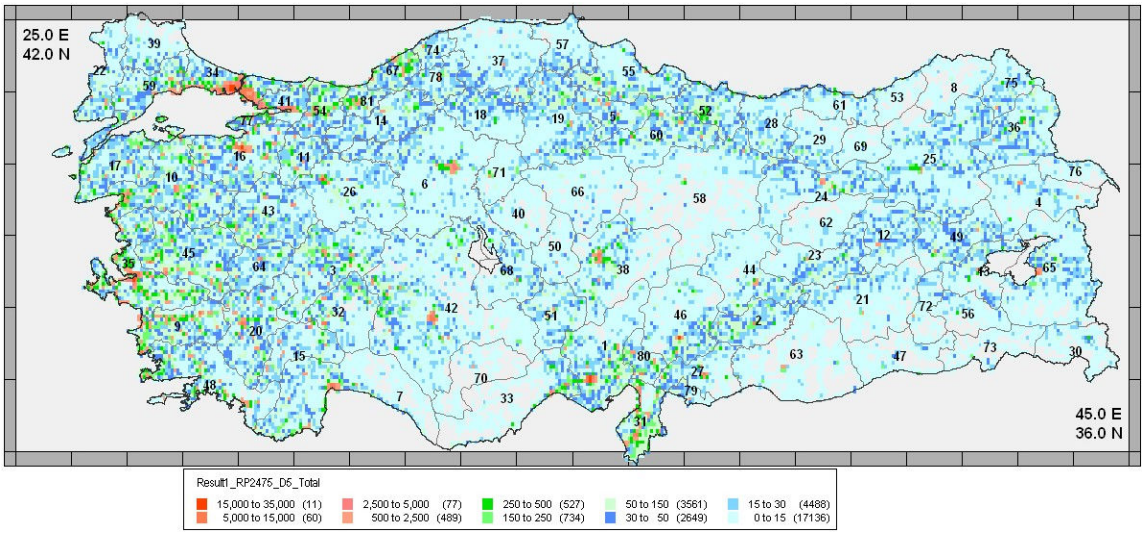

Figure 3.76. Intensity based probabilistic estimated building damage distribution of collapse damage (D5) for all type of building in Turkey corresponding to 2. per cent probability of exceedence in 50 years (modified KOERI model – Result 1)

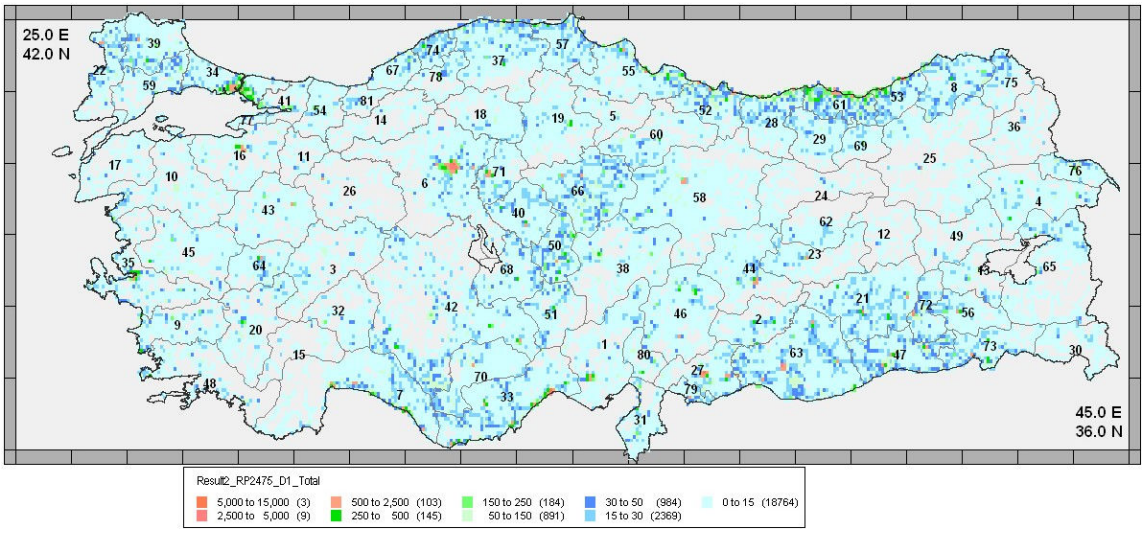

Figure 3.77. Intensity based probabilistic estimated building damage distribution of slight damage (D1) for all type of building in Turkey corresponding to 2. per cent probability of exceedence in 50 years (Giovinazzi and Lagomarsino model - Result 2)

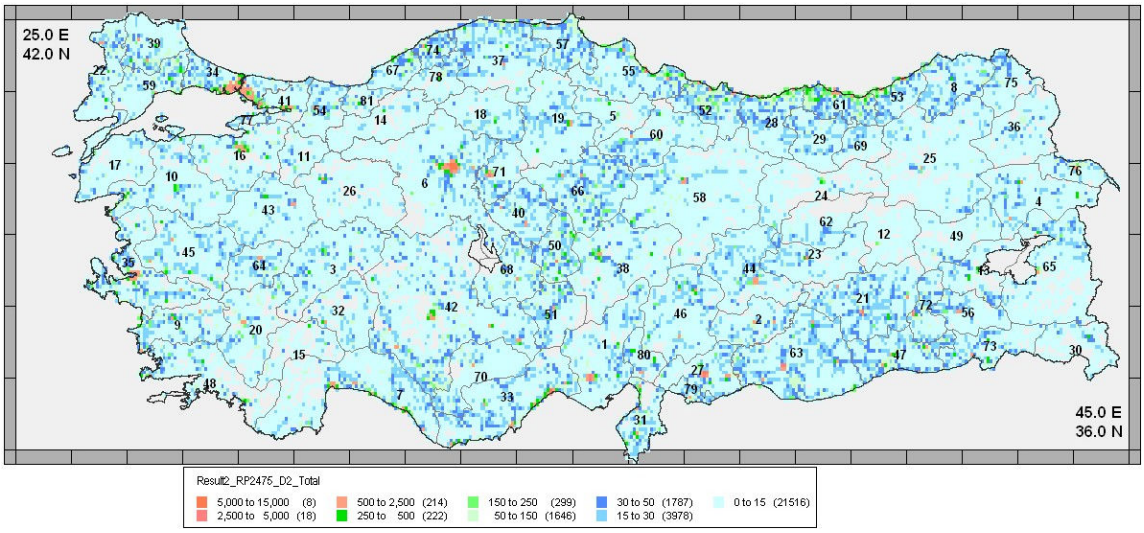

Figure 3.78. Intensity based probabilistic estimated building damage distribution of moderate damage (D2) for all type of building in Turkey corresponding to 2. per cent probability of exceedence in 50 years (Giovinazzi and Lagomarsino model - Result 2)

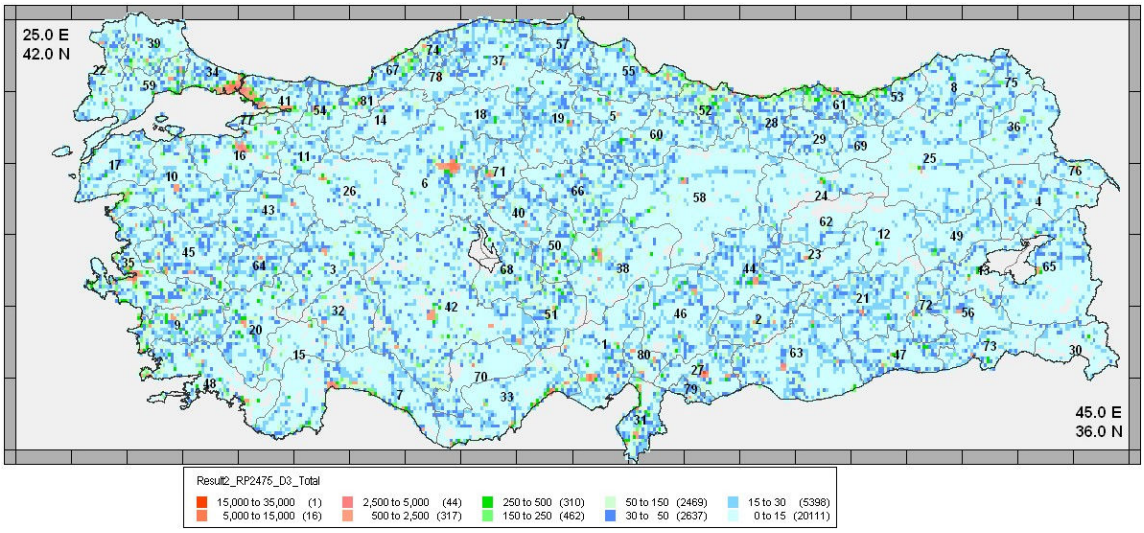

Figure 3.79. Intensity based probabilistic estimated building damage distribution of heavy damage (D3) for all type of building in Turkey corresponding to 2. per cent probability of exceedence in 50 years (Giovinazzi and Lagomarsino model - Result 2)

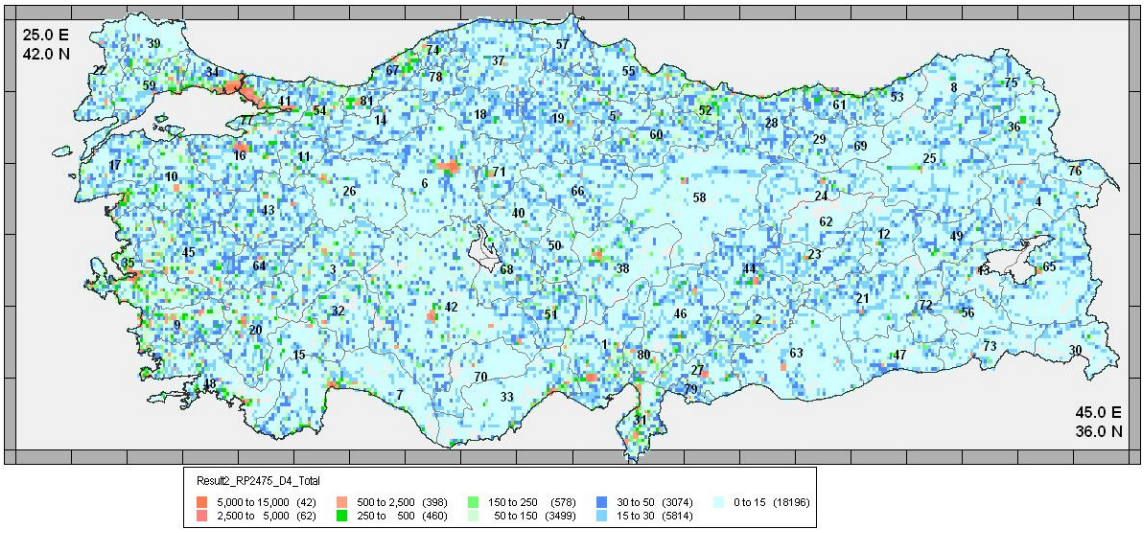

Figure 3.80. Intensity based probabilistic estimated building damage distribution of partial destruction damage (D4) for all type of building in Turkey corresponding to 2. per cent probability of exceedence in 50 years (Giovinazzi and Lagomarsino model - Result 2)

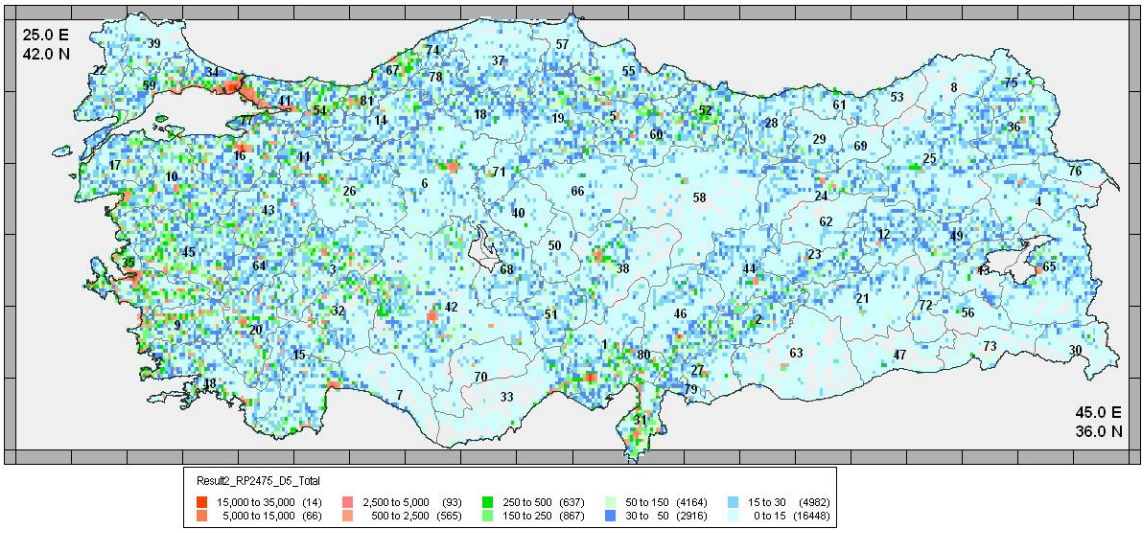

Figure 3.81. Intensity based probabilistic estimated building damage distribution of collapse damage (D5) for all type of building in Turkey corresponding to 2. per cent probability of exceedence in 50 years (Giovinazzi and Lagomarsino model - Result 2)

3.3.5. Verification of the Building Damage Estimation for Turkey

Turkey lies at the centre of an earthquake-prone region, resulting from the jostling of the tectonic plates of Africa, which are pushing northwards into Europe; and the Arabian Plate, which is squeezing Eastern Turkey. Much of Turkey has a history of destructive seismic activity, going back to the earliest days of recorded history. In recent 50 years, many destructive earthquakes hit Turkey measured greater than 5.0 on the Richter scale. Table 3.11 summarizes the information about these earthquakes (prepared by General Directorate of Disaster Affairs Earthquake Research Department; ERD, http://www.deprem.gov.tr/haber.htm).

In this study, the building damage information of the destructive earthquakes in Turkey listed in Table 3.11 has been utilized to calibrate the reported building damage distribution obtained from the probabilistic seismic hazard analysis (PSHA) for Turkey. In this analysis, the annual population growth rate (per cent) is the main parameter to calculate the expected population at the date of each destructive earthquake listed in Table 3.11. Population growth rate (PGR) is the increase or decrease in a country's population

during a period of time, usually one year, expressed as a percentage of the population at the start of that period.

Annual growth rate of population in the period between two census dates is the population increase per 1000 population per year. The expected population is calculated by natural growth correlation.

$$P_{n+t} = P_n * e^{rt} \quad (3.14)$$

Where;

Pn : Population at n date (at the initial period)

Pn+t : Population at n+t date (t years later)

e : Natural Logarithm

r : Annual growth rate of population

t : The time period between two dates (in years)

Depending on the general population census for each district between years 1970 and 2008, the population growth rates listed in Figure 3.82 are calculated by applying the above equation. For pre-1970 period, the population growth rate for each district is estimated based on the total population growth rates given for Turkey as the ratio of the population growth rate for each district from 1970-1975 Census to the total population growth rate given in Figure 3.82. The ratio of estimated population at earthquake local time to 2008 population of the district is used to estimate the building damage of destructive earthquake as if it had happened in 2008 by multiplying building damage given for earthquake local time by this ratio. Since the knowledge of the building damage taken from the General Directorate of Disaster Affairs Earthquake Research Department is generally based on the number of households, the number of reported building damage is adjusted by multiplying the number of average household for each district. The results are compared with the ones obtained from the PSHA for the return period of 72 years.

Table 3.11. Many destructive earthquakes in Turkey

Location	Day	Month	Year	Lon	Lat	Ms	Collapsed & Heavy Damage	Moderate Damage	Slight Damage
Erzincan	26	12	1939			8	116,720		
Erbaa(Tokat)	20	12	1942			7	32,000		
Ladik	26	11	1943			7	40,000		
Gerede	1	2	1944			7	20,865		
Varto/ Muş	19	8	1966			7	20,007		
Gediz	28	3	1970			7	19,291		
Lice/ Diyarbakır	6	9	1975			7	8,149		
Muradiye/Van	24	11	1976			8	9,232		
Denizli	19	8	1976	37.67	29.17	5	887	2,833	3,887
İzmir	9	12	1977	38.56	27.47	5	11		
İzmir	16	12	1977	38.4	27.19	6	40		
Antakya /Hatay	30	6	1981	36.17	35.89	4	2		
Biga / Çanakkale	5	7	1983	40.33	27.21	6	85		
Erzurum-Kars	30	10	1983	40.2	42.1	7	3,241	3,007	4,085
Sürgü-Malatya	5	5	1986	37.95	37.8	6	824	2,539	4,705
Sürgü-Malatya	6	6	1986	38.01	37.91	6	1,174	313	458
Erzincan	13	3	1992	39.68	39.56	7	6,702	9,108	15,384
Kuşadası-İzmir	6	11	1992	38.07	26.6	6			
Dinar / Afyon	11	10	1995	38.18	30.02	6	4,909	3,276	6,709
Çorum-Amasya	14	8	1996	40.73	35.28	5	707	789	2,080
Antakya/Hatay	22	1	1997	36.25	36	6		2,709	
Karlıova / Bingöl	13	4	1998	39.32	41.05	5	69	79	878
Adana-Ceyhan	27	6	1998	36.85	35.55	6	10,675	20,788	50,663
Gölcük-Kocaeli	17	8	1999	40.7	29.91	8	66,491		

Düzce / Bolu	12	11	1999	40.79	31.21	8	15,389	13,548	13,381
Bolvadin-Afyon	15	12	2000	38.6	31.2	5.6*	250		
Sultandayı-Afyon	3	2	2002	38.46	31.3	6.1*	4,401	1,733	9,785
Pülümür-Tunceli	27	1	2003	39.41	39.8	6.4*	67	179	859
Bingöl	1	5	2003	38.94	40.51	6.0*	8,142	4,483	13,277
Aşkale-Erzurum	25	3	2004	39.74	40.88	5.1*	1,212		
Merkez-Hakkari	25	1	2005	37.64	43.82	5.4*	82		
Karlıova-Bingöl	12	3	2005	39.42	40.87	5.6*	760		
Urla-Izmir	17	10	2005	38.22	26.66	5.8*	96		
Seferihisar-Izmir	20	10	2005	38.15	26.67	5.9*	100		

* symbol represents Md

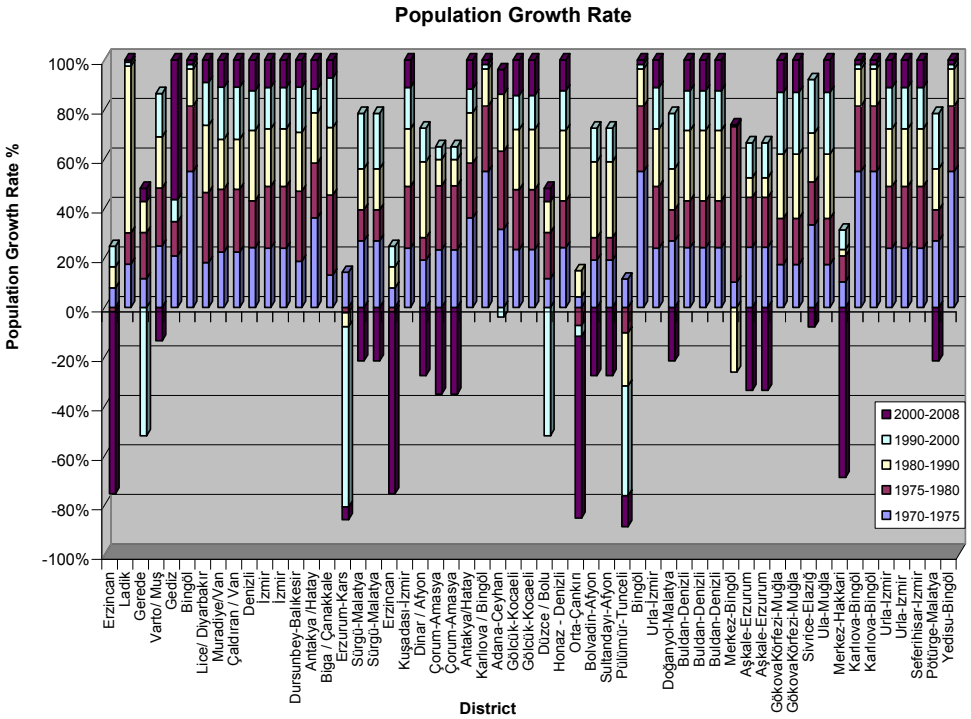

Figure 3.82. Population growh rate for each earthquake location between years 1970 and 2008

Table 3.12. Average population growth rate in Turkey for pre-1970 period

Period (year)	Annual Population Growth Rate (‰)
1927 - 1935	21.1
1935 - 1940	17.0
1940 - 1945	10.6
1945 - 1950	21.7
1950 - 1955	27.8
1955 - 1960	28.5
1960 - 1965	24.6
1965 - 1970	25.2

Table 3.13. Estimated population for each district at earthquake time

Location	**Earthquake**	**Day**	**Month**	**Year**	**Population at Earthquake occured time**	**Average size of household**
Erzincan	Erzincan-26121939	26	12	1939	236,895	4.78
Erbaa	Tokat-20121942	20	12	1942	464,018	4.98
Ladik	Samsun-26111943	26	11	1943	40,101	4.09
Gerede	Bolu-121944	1	2	1944	295,712	3.93
Varto	Muş-1981966	19	8	1966	199,899	7.15
Gediz	Kutahya-2831970	28	3	1970	62,222	3.88
Bingöl	Bingöl-2251971	22	5	1971	184,084	3.65
Lice	Diyarbakır-691975	6	9	1975	651,233	6.23
Muradiye	Van-24111976	24	11	1976	401,533	6.64
Çaldıran	Van-24111976	24	11	1976	401,533	6.64
Denizli	Denizli-1981976	19	8	1976	569,155	3.66
İzmir	İzmir-9121977	9	12	1977	1,789,080	3.54
İzmir	İzmir-16121977	16	12	1977	1,789,080	3.54

Dursunbey	Balıkesir-1871979	18	7	1979	792,334	3.33
Antakya	Hatay-3061981	30	6	1981	878,765	4.63
Biga	Çanakkale-571983	5	7	1983	392,861	3.24
Erzurum	Kars-30101983	30	10	1983	698,934	5.05
Sürgü	Malatya-551986	5	5	1986	608,470	4.81
Sürgü	Malatya-661986	6	6	1986	608,470	4.81
Erzincan	Erzincan-1331992	13	3	1992	300,107	4.78
Kuşadası	İzmir-6111992	6	11	1992	2,725,102	3.54
Dinar	Afyon-11101995	11	10	1995	740,620	4.34
Çorum	Amasya-1481996	14	8	1996	357,324	4.03
Antakya	Hatay-2211997	22	1	1997	1,111,690	4.63
Karlıova	Bingöl-1341998	13	4	1998	251,000	3.65
Ceyhan	Adana-2761998	27	6	1998	1,933,815	4.51
Gölcük	Kocaeli-1781999	17	8	1999	938,802	4.00
Gölcük	Kocaeli-1391999	13	9	1999	938,802	4.00
Düzce	Bolu-12111999	12	11	1999	533,684	3.93
Honaz	Denizli-2142000	21	4	2000	850,029	3.66
Orta	Çankırı-662000	6	6	2000	270,355	4.70
Bolvadin	Afyon-15122000	15	12	2000	812,416	4.34
Sultandayı	Afyon-322002	3	2	2002	804,699	4.34
Pülümür	Tunceli-2712003	27	1	2003	93,275	4.59
Bingöl	Tunceli-152003	1	5	2003	253,837	4.59
Urla	İzmir-1042003	10	4	2003	3,387,589	3.54
Doğanyol	Malatya-1372003	13	7	2003	848,293	4.81
Buldan	Denizli-2372003	23	7	2003	852,752	3.66
Buldan	Denizli-2672003	26	7	2003	852,752	3.66
Merkez	Bingöl-332004	3	3	2004	253,812	3.65
Aşkale	Erzurum-2532004	25	3	2004	931,832	5.31
Aşkale	Erzurum-2832004	28	3	2004	931,832	5.31
GökovaKörfezi	Muğla-482004	4	8	2004	717,591	3.37
Sivrice	Elazığ-1182004	11	8	2004	568,914	4.77
Ula	Muğla-20122004	20	12	2004	717,591	3.37
Merkez	Hakkari-2512005	25	1	2005	220,769	7.51

Karlıova	Bingöl-1232005	12	3	2005	253,798	3.65
Karlıova	Bingöl-1432005	14	3	2005	253,798	3.65
Urla	İzmir-17102005	17	10	2005	3,380,890	3.54
Seferihisar	İzmir-20102005	20	10	2005	3,380,890	3.54
Pötürge	Malatya-26112005	26	11	2005	850,435	4.81
Yedisu	Bingöl-10122005	10	12	2005	253,798	3.93

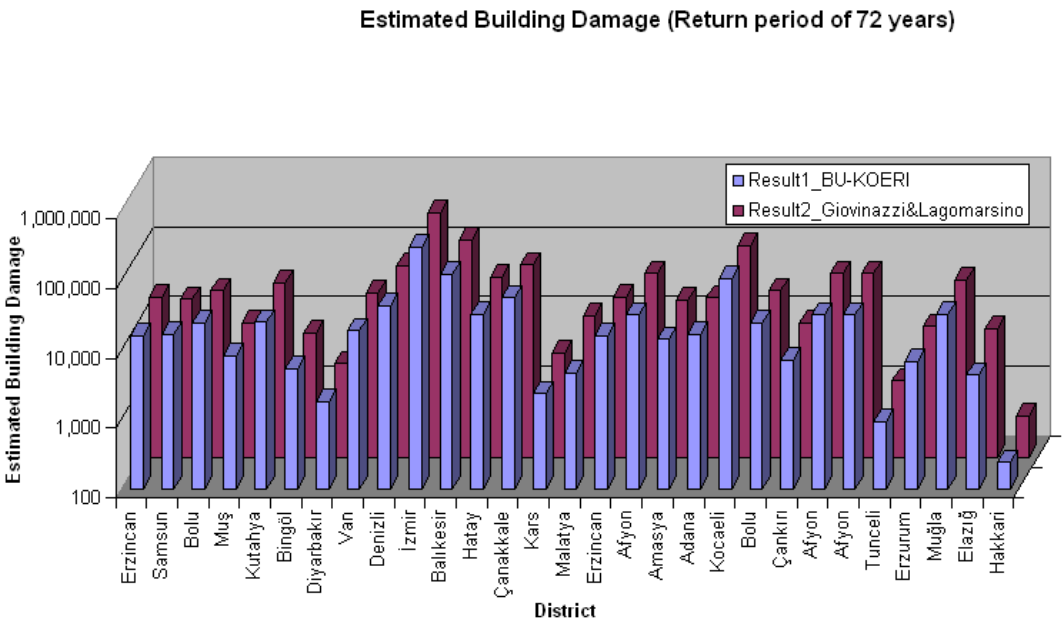

Figure 3.83. Based on the probabilistic seismic hazard analysis at return period of 72 years, the observed building damage (D3+D4+D5) using the two alternative vulnerability relationships for each destructive earthquake locations

Table 3.14. Based on the probabilistic seismic hazard analysis at return period of 72 years, the estimated building damage (D3+D4+D5) using the two alternative vulnerability relationships for each destructive earthquake locations

		Vulnerability Relationships	
Building Damage Level	Observed Building Damage for destructive earthquakes adapted to present day population and building inventories	Giovinazzi & Lagomarsino (2005)	DEE-KOERI, 2003

Collapsed and Heavy Damage (D3+D4+D5)	914,341	1,159,396	995,783
Moderate and Slight Damage (D1+D2)	787,910	1,097,933	1,106,968

The calibration between the reported and the estimated building damage distribution in Turkey showed that the probabilistic approach is reliable to estimate the building damage in Turkey.

3.4. Estimation of Casualty Distribution

Different techniques are utilized to perform earthquake casualty/loss estimation at local or regional levels and advocated various approaches depending upon type of data, spatial applicability, and modeling principles. These different techniques can be classified into variants of three distinct approaches, namely empirical, analytical, and hybrid (or semi-empirical) approaches. Analytical human loss models utilize building damage and consequential physical damage (*e.g*. post-earthquake fire, explosion, hazmat release) as the starting point for the evaluation of casualties. This casualty assessment approach requires the knowledge of building occupancy data and the probability of several levels of injury and death for different building types with given states of building damage. This however, is not easily attainable due to the limited quality and lack of information on earthquake casualty data. There are three analytical approaches used in this intensity based study.

3.4.1. Coburn and Spence (1992) Method

For the estimation of the fatalities due to structural damage (the K_s parameter), which is the controlling factor for most destructive earthquakes, Coburn and Spence (1992) proposed the equation given below:

$$K_{sb} = TC_b\left[M_1 M_2 M_3 \left(M_4 + M_5\left(1 - M_4\right)\right)\right] \tag{3.15}$$

where TC_b is the total number of collapsed buildings of type B, M_1 is the factor taking into account regional variation of population per building, M_2 is the factor taking into account variation of occupancy depending on the time (Figure 3.84), M_3 is the factor taking into account percentage of trapped occupants under collapsed buildings (Table 3.15), M_4 is the factor taking into account different injury levels of trapped people (Table 3.16), and M_5 is the factor taking into account change of injury levels of trapped people with time (Table 3.16). Using Equation (3.15) and Table 3.15 through Table 3.17, the casualty rates applicable immediately after the earthquake for masonry and reinforced concrete buildings corresponding to different severity levels are calculated (Table 3.18 and Table 3.19). For severity level S_4, final casualty levels corresponding to level 3 type emergency responses described in Table 3.16 are also given in Table 3.18 and Table 3.19.

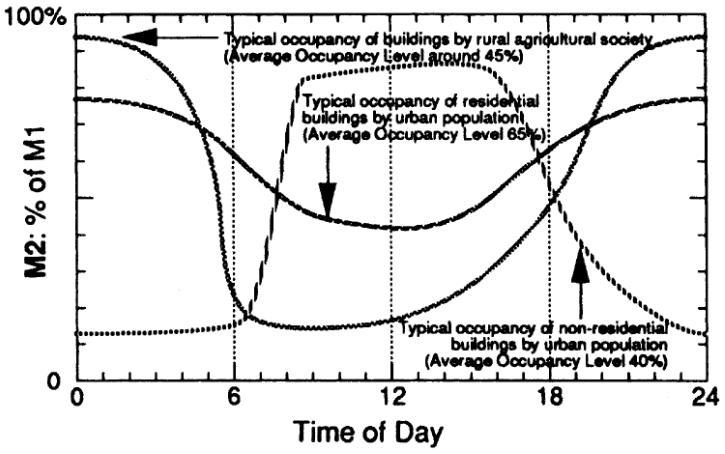

Figure 3.84. Variation of occupancy with time

Table 3.15. Factor M_3 for masonry and RC structures

Collapsed Masonry Buildings (up to 3 storeys)				
MSK Intensity	VII	VIII	IX	X
	5%	30%	60%	70%
Collapsed RC Structures (3-5 storeys)				
Near-field, high-frequency ground motion			70%	
Distant, long period ground motion			50%	

Table 3.16. Factor M_4 for masonry and RC structures

Injury Category	***Masonry***	***RC***
Light Injury (S_1)	20%	10%
Injury requiring hospital treatment (S_2)	30%	40%
Severe Injury (S_3)	30%	10%
Dead or unsaveable (S_4)	20%	40%

Table 3.17. Factor M_5 for masonry and RC structures

Situation	Masonry	RC
Level 1: Community incapacitated by high casualty rate	95%	-
Level 2: Community capable of organizing rescue activity	60%	90%
Level 3: Community + emergency squads after 12 hours	50%	80%
Level 4: Community + emergency squads+SAR experts after 36 hours	45%	70%

Table 3.18. Casualty rates for masonry structures

	Intensity	Injury distribution at collapse				Post
		S_1	S_2	S_3	S_4	S_4
Masonry Building	VII	0.01	0.015	0.015	0.01	0.03
	VIII	0.06	0.09	0.09	0.06	0.18
	IX	0.12	0.18	0.18	0.12	0.36
	X	0.14	0.21	0.21	0.14	0.42

Table 3.19. Casualty rates for reinforced concrete structures

	Frequency Content	Injury distribution at collapse				Post
		S_1	S_2	S_3	S_4	S_4
Reinforced Concrete Building	Near-field, high frequency ground motion	0.07	0.28	0.07	0.28	0.62
	Distant, long period ground motion	0.05	0.2	0.05	0.2	0.44

The number of buildings and population in each cell are the main parameters to estimate casualties. To obtain casualty estimations from the number of buildings in different damage states, an average number of populations per building should be known. To estimate this, the user should define an average number of dwelling units per building type, which is usually a function of the number of floors. Using the user-defined average number of dwellings per building type and the grid based population data entered by the user, or the default Landscan population data of the region, the program computes an average number of population per dwelling unit, which in turn can be used to check if the estimated number of dwellings per building type were correct. The analysis of population and building census tracks of Turkey revealed an average of three people per dwelling unit (Table 3.20) in Turkey as used for Istanbul in the study of Erdik *et al.* (2002).

Table 3.20. Population for different building types in Istanbul

Building Type	Number of floors	Number of dwelling units	Population
Low Rise	1 -4	2	6
Mid Rise	5-8	7	21
High Rise	>=9	24	72

3.4.2. Risk-UE Casualty Vulnerability Relationships

The casualty vulnerability relationships used in the Risk-UE project are based on the findings of Bramerini *et al*. (1995), which studied the statistics on casualties, severely injured and homeless people in Italy. The study of Bramerini resulted in the correlations given in Table 3.21 between damage grades and effects of these on population:

Table 3.21. Correlation between damage grades and their effects on the built environment and population

Effects to people and impact on the built environment		
BUILDINGS	Unusuable	40% of buildings with damage grade 3 and 100% of buildings with damage grades 4 and 5
	Collapsed	Buildings with damage grade 5
PEOPLE	Homeless	100% of the population living in unusable buildings – casualties and severely injured
	Casualties and severely injured	30% of the population living in collapsed buildings

3.4.3. KOERI 2002 (DEE-KOERI, 2003) Method

Casualty rates, especially deaths, depend largely on the probability of the building being in the "complete" damage state. Casualty data in urbanized areas from Turkish earthquakes indicate much higher fatalities in heavily damaged multi-storey R/C buildings. Data from the 1992 Erzincan Earthquake indicate 1 death and 3 hospitalized injures per collapsed or heavily damaged R/C building (Erdik, 1994) Similar statistics are also valid for the 1999 Kocaeli Earthquake. About 20,000 R/C buildings were collapsed or heavily damaged and the total casualty was around 19,000. The death to hospitalized injury ratio in this earthquake was 1:2.5. For the assessment of human casualties from damage data computed from intensity based vulnerabilities we have assumed that the number of deaths will be equal to the number of buildings with damages in D_4 and D_5 level. The number of

hospitalized injuries is found by multiplying the death figure by 4 based on ATC-13 recommendations (Table 3.22).

Table 3.22. ATC-13 casualty rates (* for light steel and wood-frame construction, multiply all numerators by 0.1)

Damage State	Range	Minor Injuries	Serios Injuries	Deaths
Slight	0-1	3/100,000	1/250,000	1/1,000,000
Light	1-10	3-10,000	1/25,000	1/100,000
Moderate	10-30	3/1,000	1/2,500	1/10,000
Heavy	30-60	3/100	1/250	1/1,000
Major	30-100	3/10	1/25	1/100
Destroyed	100	2/5	2/5	1/5
		RATE=30A	RATE=4A	RATE=A

3.4.4. Estimated Casualty Results

Considering the estimated building damage using two different vulnerability relationships, three analytical casualty estimation models are utilized to perform earthquake casualty/loss estimation for Turkey. The total estimated casualty results corresponding to 50 per cent, 10 per cent and 2. per cent probability of exceedence in 50 years for both the “Result 1” and the “Result 2” intensity based vulnerability models are shown in Figure 3.52 through Figure 3.102, respectively.

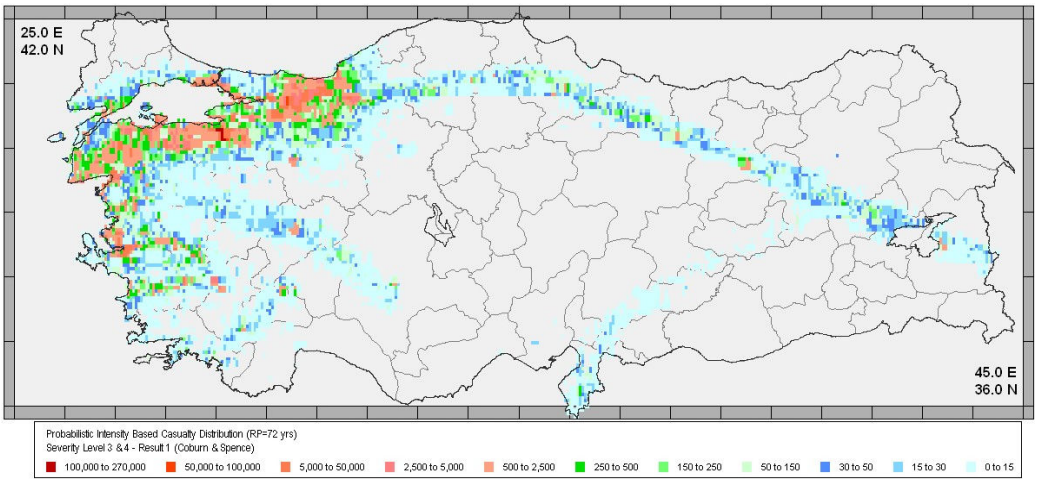

Figure 3.85. Probabilistic intensity based casualty distribution corresponding to the return period of 72 years for modified KOERI model - Result 1- Coburn & Spence model

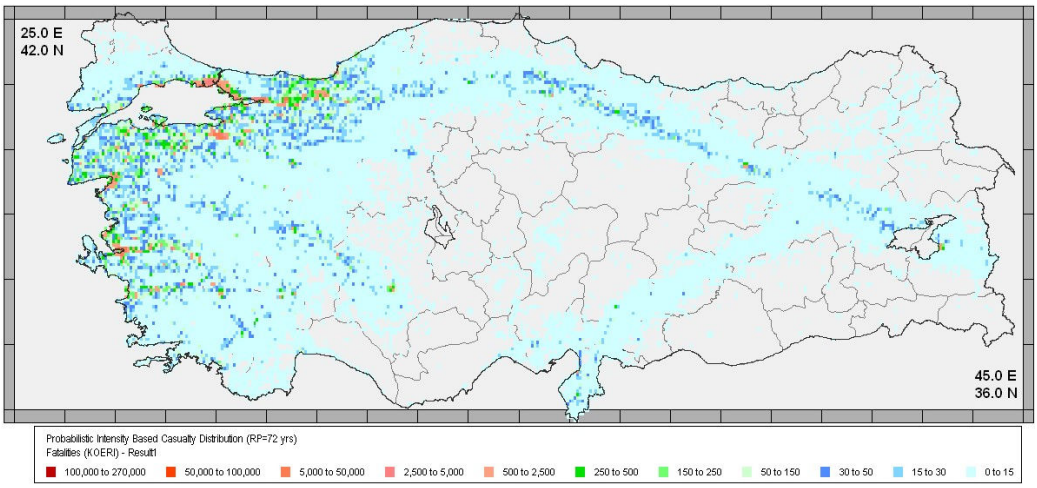

Figure 3.86. Probabilistic intensity based casualty distribution corresponding to the return period of 72 years for modified KOERI model - Result 1 – Risk-UE model

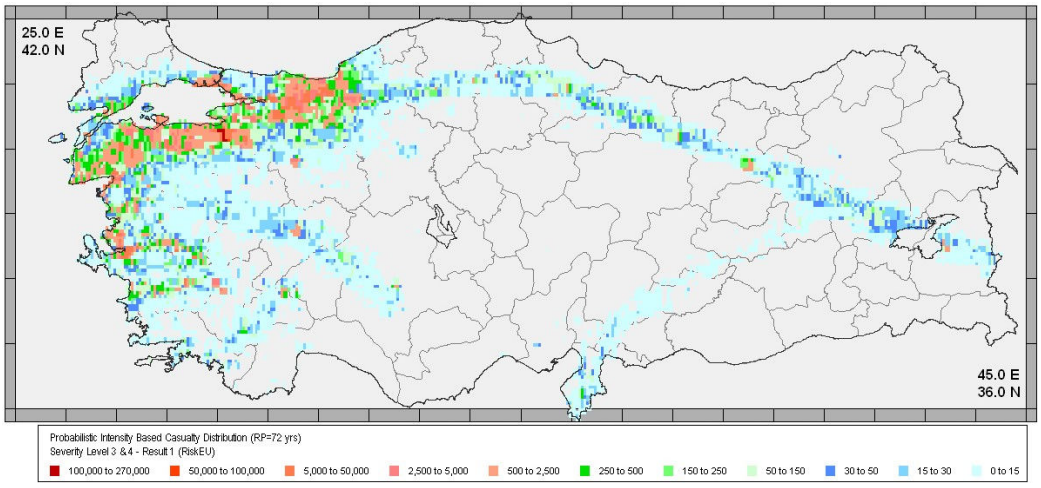

Figure 3.87. Probabilistic intensity based casualty distribution corresponding to the return period of 72 years for modified KOERI model - Result 1 –KOERI model

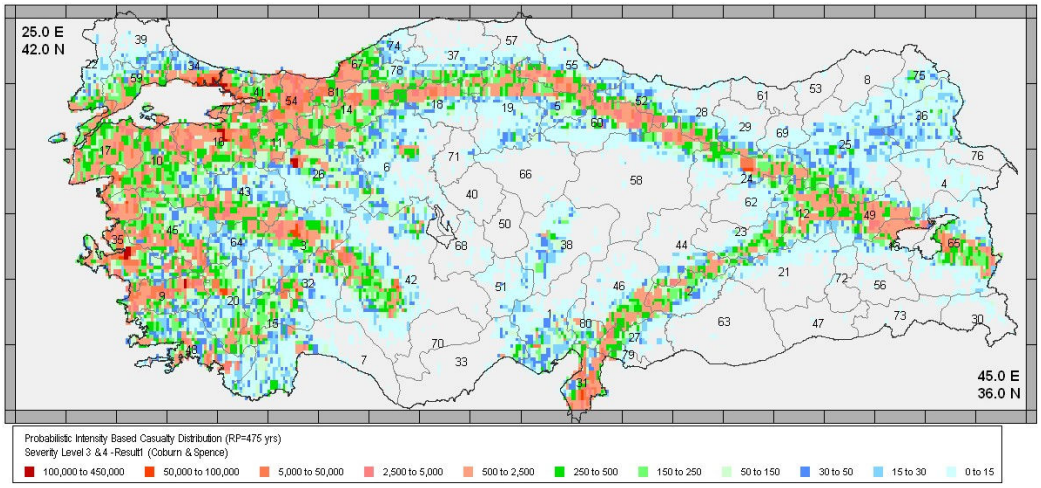

Figure 3.88. Probabilistic intensity based casualty distribution corresponding to the return period of 475 years for modified KOERI model - Result 1- Coburn & Spence model

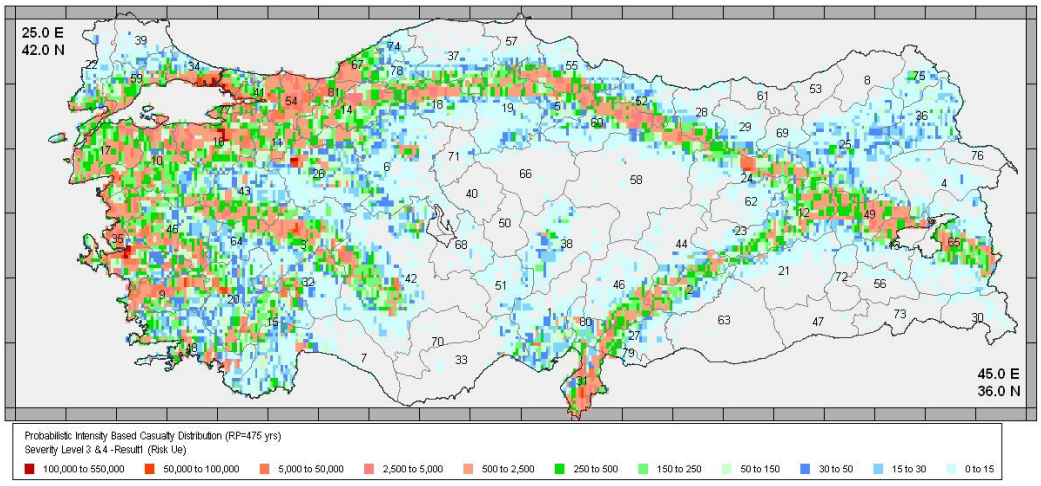

Figure 3.89. Probabilistic intensity based casualty distribution corresponding to the return period of 475 years for modified KOERI model - Result 1 – Risk-UE model

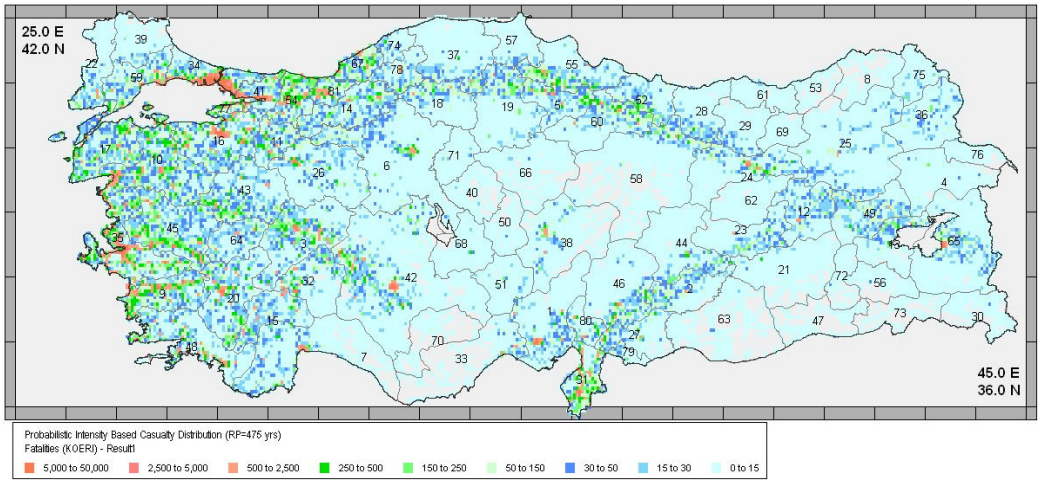

Figure 3.90. Probabilistic intensity based casualty distribution corresponding to the return period of 475 years for modified KOERI model - Result 1 –KOERI model

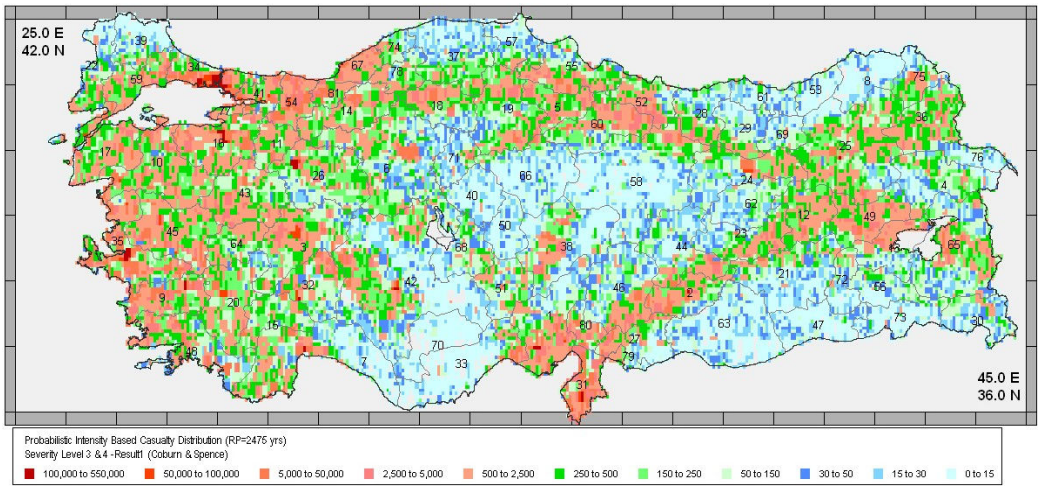

Figure 3.91. Probabilistic intensity based casualty distribution corresponding to the return period of 2475 years for modified KOERI model - Result 1- Coburn & Spence model

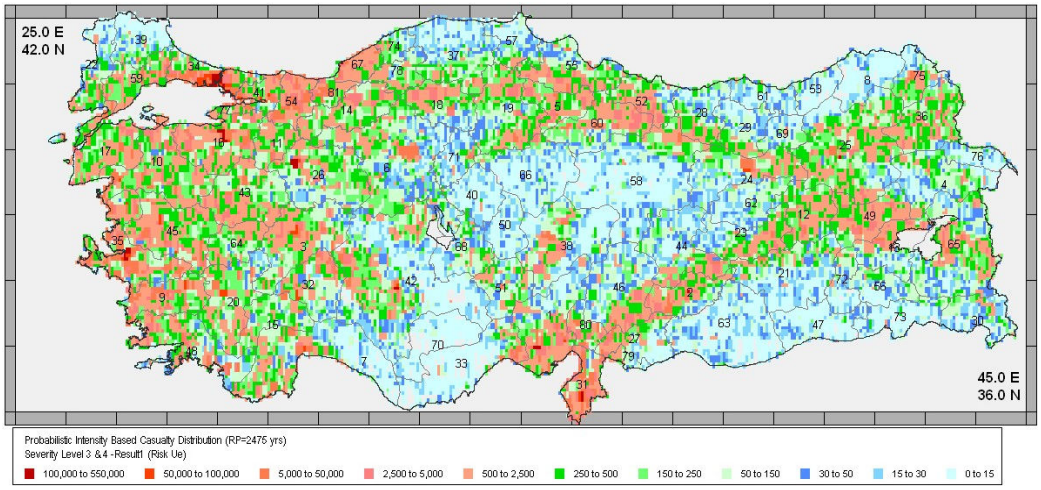

Figure 3.92. Probabilistic intensity based casualty distribution corresponding to the return period of 2475 years for modified KOERI model - Result 1 – Risk-UE model

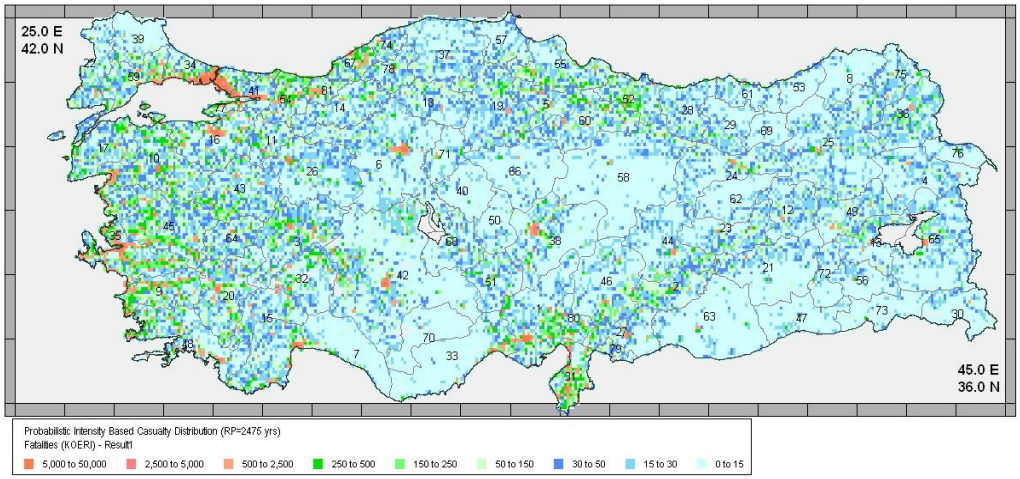

Figure 3.93. Probabilistic intensity based casualty distribution corresponding to the return period of 2475 years for modified KOERI model - Result 1 –KOERI model

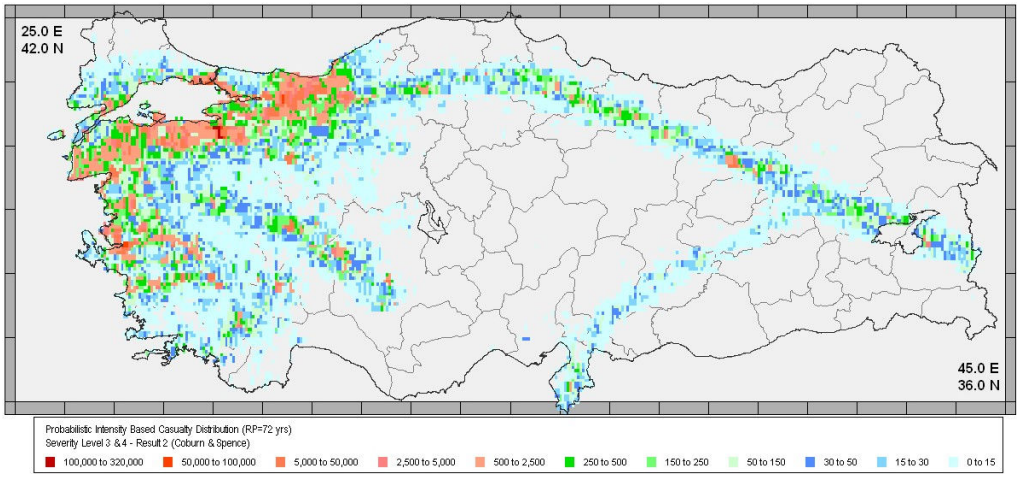

Figure 3.94. Probabilistic intensity based casualty distribution corresponding to the return period of 72 years for Giovinazzi and Lagomarsino – Result 2 - Coburn & Spence model

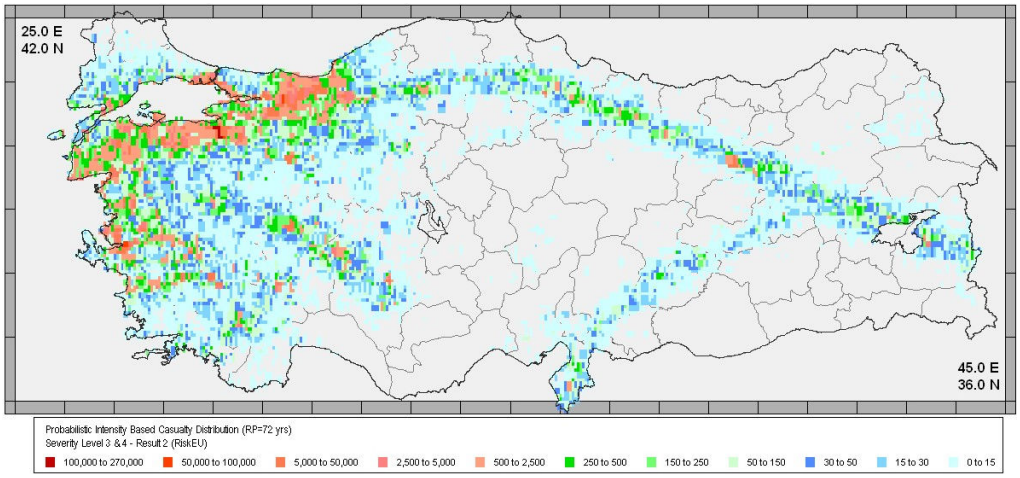

Figure 3.95. Probabilistic intensity based casualty distribution corresponding to the return period of 72 years for Giovinazzi and Lagomarsino – Result 2 – Risk-UE model

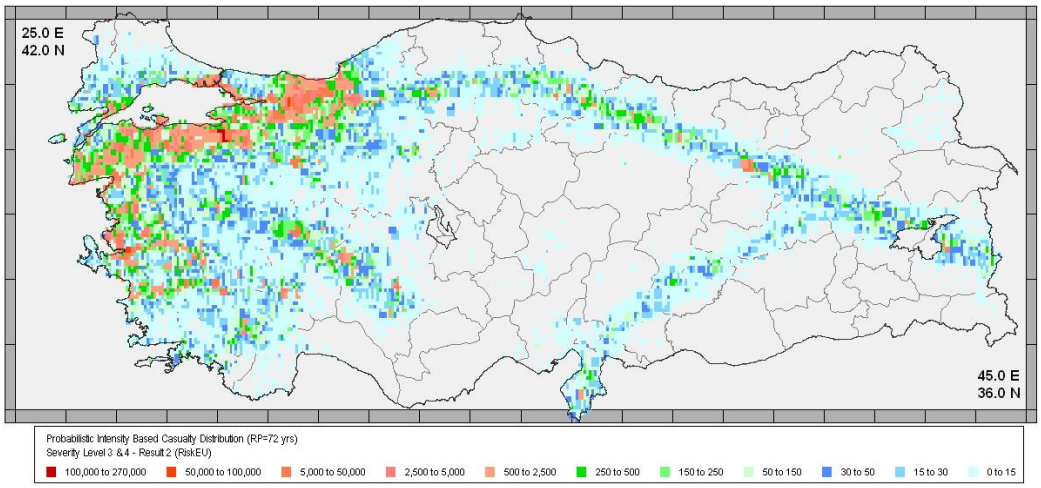

Figure 3.96. Probabilistic intensity based casualty distribution corresponding to the return period of 72 years for Giovinazzi and Lagomarsino – Result 2 –KOERI model

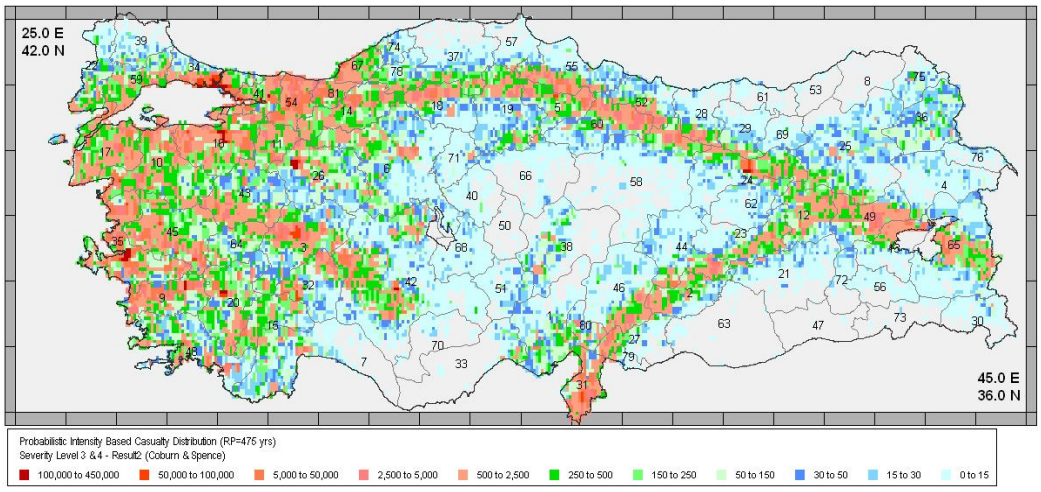

Figure 3.97. Probabilistic intensity based casualty distribution corresponding to the return period of 475 years for Giovinazzi and Lagomarsino – Result 2- Coburn & Spence model

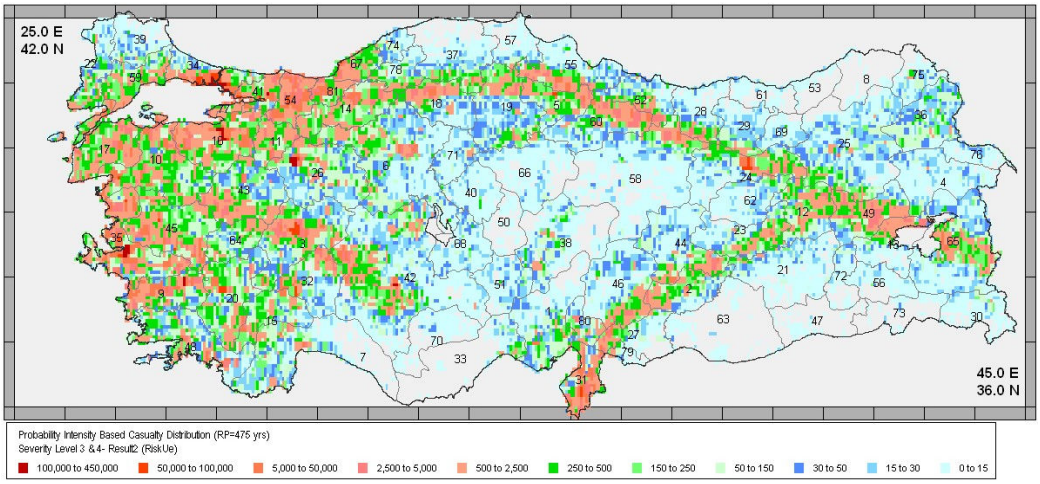

Figure 3.98. Probabilistic intensity based casualty distribution corresponding to the return period of 475 years for Giovinazzi and Lagomarsino – Result 2 – Risk-UE model

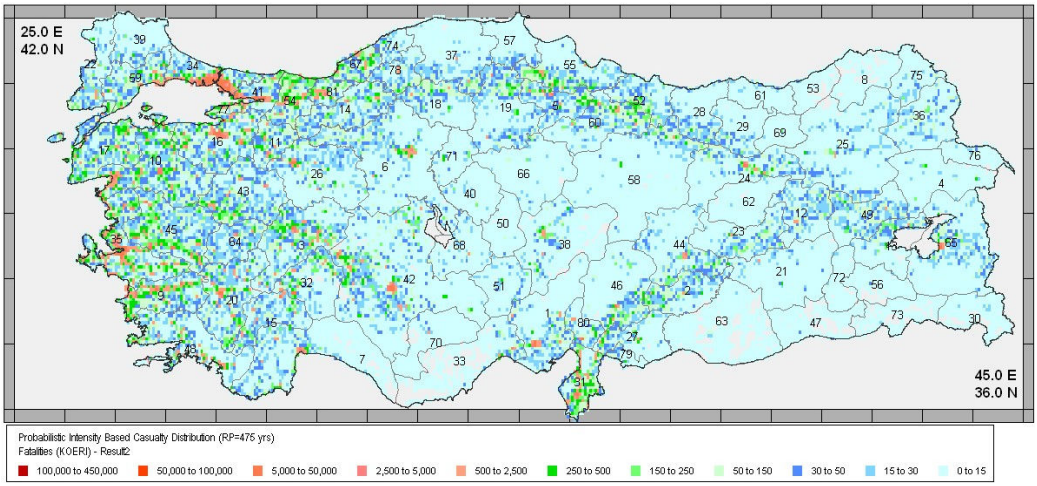

Figure 3.99. Probabilistic intensity based casualty distribution corresponding to the return period of 475 years for Giovinazzi and Lagomarsino – Result 2 –KOERI model

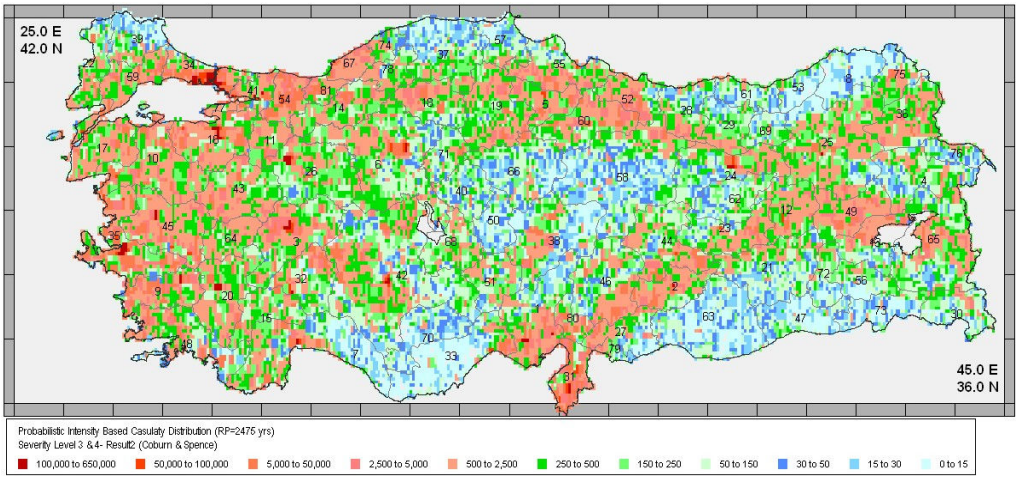

Figure 3.100. Probabilistic intensity based casualty distribution corresponding to the return period of 2475 years for Giovinazzi and Lagomarsino – Result 2- Coburn & Spence model

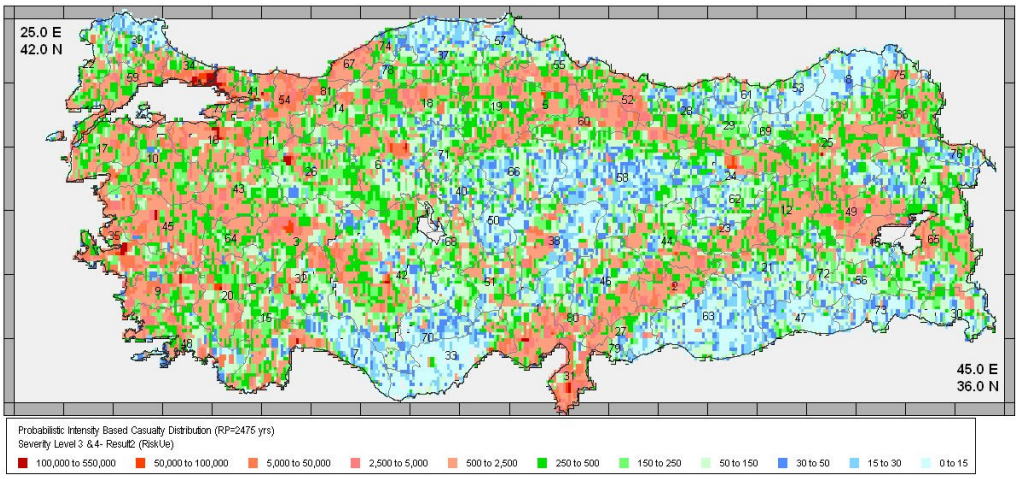

Figure 3.101. Probabilistic intensity based casualty distribution corresponding to the return period of 2475 years for Giovinazzi and Lagomarsino – Result 2 – Risk-UE model

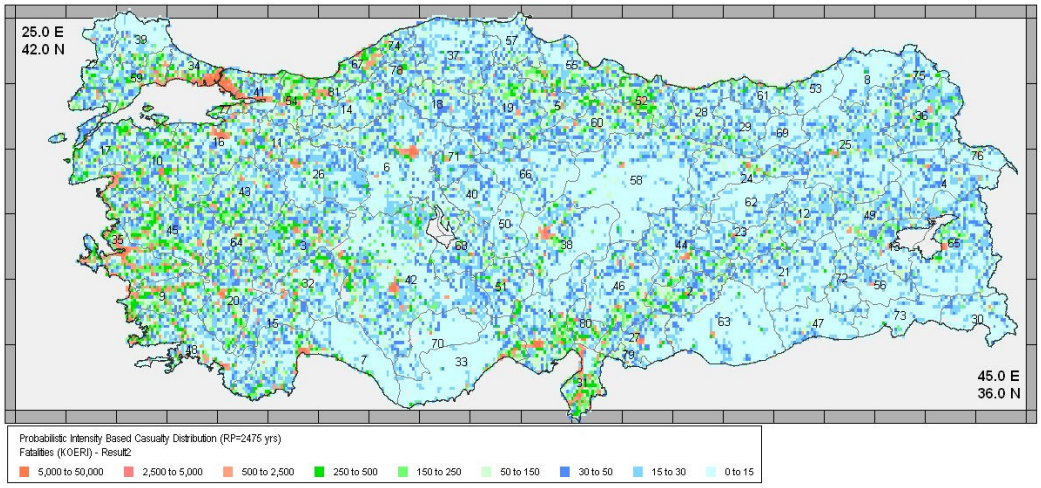

Figure 3.102. Probabilistic intensity based casualty distribution corresponding to the return period of 2475 years for Giovinazzi and Lagomarsino – Result 2 –KOERI model

3.4.5. Verification of the Casualty Estimations for Turkey

The estimated casualties were performed using three different intensity based approaches: Coburn and Spence (1992), Risk-UE (Bramerini *et al*., 1995) and KOERI (2002). For each method, the results have been compared with the reported ones. For that purpose, the knowledge of the number of casualty and fatality related to the each destructive earthquake listed in Table 3.11 have been used to compare with the results obtained from the PSHA for the return period of 72 years. The database used in this analysis is listed in Table 3.23 and the methodology for converting these databases from the local time of the historical earthquakes to the present time period (Table 3.25) has been explained in Section 3.3.5).

Table 3.23. The number of casualties and fatalities related to the each destructive earthquake (reported by ERD)

			Historical Building Damage		
Location	Province	Year	Dead	Casualty	Dead+Casualty
Erzincan	Erzincan	26.12.1939	32,968		32,968
Erbaa(Tokat)	Tokat	20.12.1942	3,000		3,000
Ladik	Samsun	26.11.1943	4,000		4,000
Gerede	Bolu	01.02.1944	3,959		3,959
Varto/ Muş	Muş	19.08.1966	2,396	1,500	3,896
Gediz	Kutahya	28.03.1970	1,086		1,086
Lice/ Diyarbakır	Diyarbakır	06.09.1975	2,385		2,385
Muradiye/Van	Van	24.11.1976	3,840		3,840
Denizli	Denizli	19.08.1976	4	28	32
Biga / Çanakkale	Çanakkale	05.07.1983	3		3
Erzurum-Kars	Kars	30.10.1983	1,155	1,142	2,297
Sürgü-Malatya	Malatya	05.05.1986	8	24	32
Sürgü-Malatya	Malatya	06.06.1986	1	20	21
Erzincan	Erzincan	13.03.1992	653	3,850	4,503
Dinar / Afyon	Afyon	01.10.1995	94	240	334
Çorum-Amasya	Amasya	14.08.1996		6	6
Gölcük-Kocaeli	Kocaeli	17.08.1999	17,408		17,408
Düzce / Bolu	Bolu	12.11.1999	845	4,948	5,793
Bolvadin-Afyon	Afyon	15.12.2000	6	82	88
Sultandayı-Afyon	Afyon	03.02.2002	42	325	367
Pülümür-Tunceli	Tunceli	27.01.2003	1		1
Bingöl	Tunceli	01.05.2003	184	515	699
Aşkale-Erzurum	Erzurum	25.03.2004	10		10
Merkez-Hakkari	Hakkari	25.01.2005	3		3
TOTAL			74,051	12,680	86,731

Table 3.24. The population ratio based on province of Turkey

Location	Year	Year / Population	2008 Population (provincel)	Population Ratio %	Average size of house hold
Erzincan	26.12.1939	236,895	210,645	0.89	4.78
Erbaa(Tokat)	20.12.1942	464,018	617,158	1.33	4.98
Ladik	26.11.1943	40,101	1,233,677	30.76	4.09
Gerede	01.02.1944	295,712	328,611	1.11	3.93
Varto/ Muş	19.08.1966	199,899	404,309	2.02	7.15
Gediz	28.03.1970	62,222	565,884	9.09	3.88
Lice/ Diyarbakır	06.09.1975	651,233	1,492,828	2.29	6.23
Muradiye/Van	24.11.1976	401,533	1,004,369	2.50	6.64
Denizli	19.08.1976	569,155	917,836	1.61	3.66
Biga / Çanakkale	05.07.1983	392,861	474,791	1.21	3.24
Erzurum-Kars	30.10.1983	698,934	312,128	0.45	5.05
Sürgü-Malatya	05.05.1986	608,470	733,789	1.21	4.81
Sürgü-Malatya	06.06.1986	608,470	733,789	1.21	4.81
Erzincan	13.03.1992	300,107	210,645	0.70	4.78
Kuşadası-İzmir	06.11.1992	2,725,102	3,795,978	1.39	3.54
Dinar / Afyon	01.10.1995	740,620	697,365	0.94	4.34
Çorum-Amasya	14.08.1996	357,324	323,675	0.91	4.03
Gölcük-Kocaeli	17.08.1999	938,802	1,490,358	1.59	4.00
Düzce / Bolu	12.11.1999	533,684	328,611	0.62	3.93
Bolvadin-Afyon	15.12.2000	812,416	697,365	0.86	4.34
Sultandayı-Afyon	03.02.2002	804,699	697,365	0.87	4.34
Pülümür-Tunceli	27.01.2003	93,275	86,449	0.93	4.59
Bingöl	01.05.2003	253,837	256,091	1.01	4.59
Aşkale-Erzurum	25.03.2004	931,832	774,967	0.83	5.31
Merkez-Hakkari	25.01.2005	220,769	25,859	0.12	7.51

Table 3.25. The number of casualties and fatalities related to the each destructive earthquake (adopted information to present time)

-		Reported Building Damage		
Location	Year	Dead	Casualty	Dead+Casualty
Erzincan	26.12.1939	140,125	0	140,125
Erbaa(Tokat)	20.12.1942	19,871	0	19,871
Ladik	26.11.1943	503,306	0	503,306
Gerede	01.02.1944	17,290	0	17,290
Varto/ Muş	19.08.1966	34,649	21,692	56,341
Gediz	28.03.1970	38,322	0	38,322
Lice/ Diyarbakır	06.09.1975	34,060	0	34,060
Muradiye/Van	24.11.1976	63,778	0	63,778
Denizli	19.08.1976	24	165	189
Erzurum-Kars	30.10.1983	2,605	2,575	5,180
Sürgü-Malatya	05.05.1986	46	139	186
Sürgü-Malatya	06.06.1986	6	116	122
Erzincan	13.03.1992	2,191	12,917	15,108
Dinar / Afyon	01.10.1995	384	981	1,365
Çorum-Amasya	14.08.1996	0	22	22
Gölcük-Kocaeli	17.08.1999	110,542	0	110,542
Düzce / Bolu	12.11.1999	2,045	11,973	14,018
Bolvadin-Afyon	15.12.2000	22	305	328
Sultandayı-Afyon	03.02.2002	158	1,222	1,380
Pülümür-Tunceli	27.01.2003	4	0	4
Bingöl	01.05.2003	852	2,385	3,237
Aşkale-Erzurum	25.03.2004	44	0	44
Merkez-Hakkari	25.01.2005	3	0	3
TOTAL		970,326	54,494	1,024,820

The estimated casualties based on the two alternative vulnerability relationships are shown in Figure 3.103 and Figure 3.104, respectively.

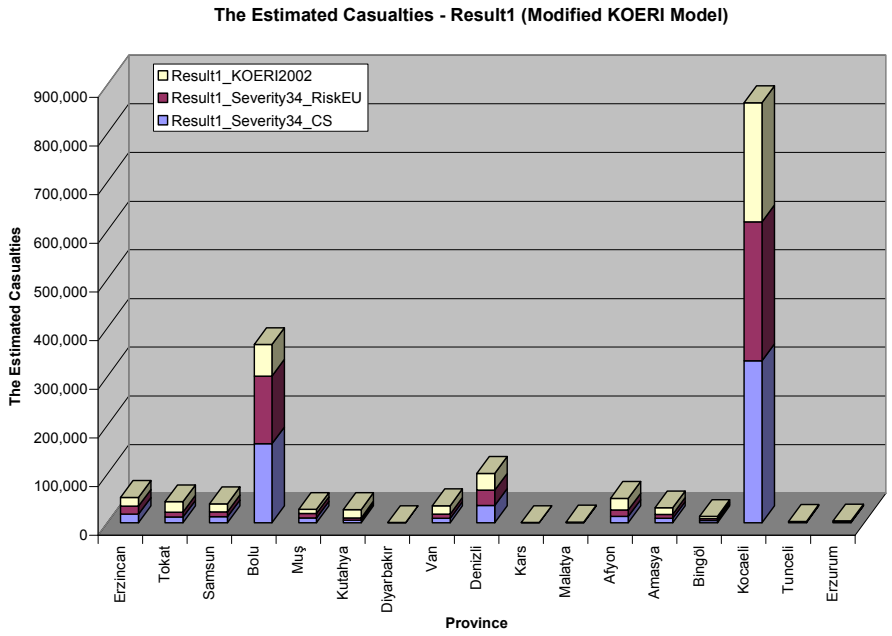

Figure 3.103. The estimated casualties corresponding to the Result 1 (Modified KOERI) vulnerability relationship

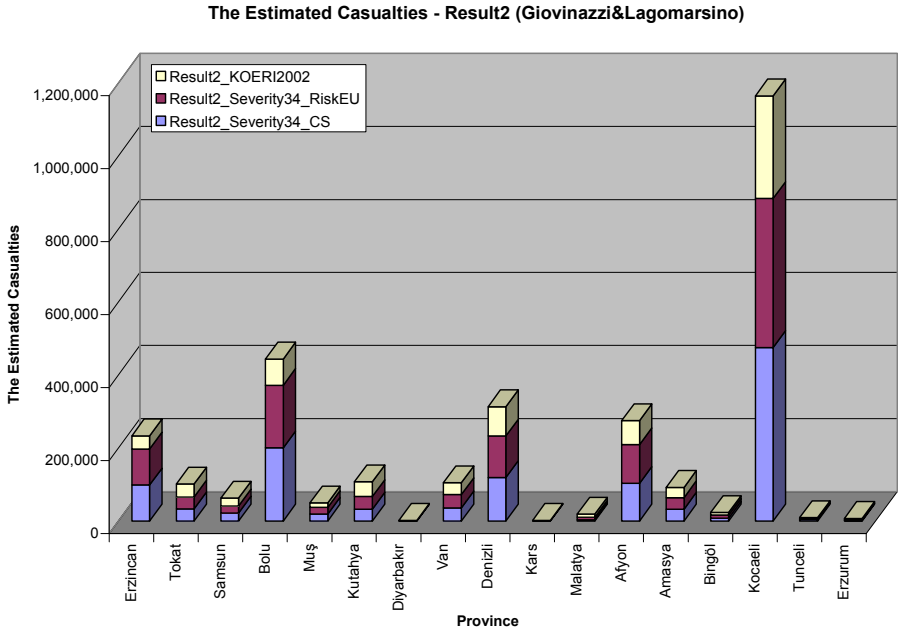

Figure 3.104. The estimated casualties corresponding to the Result 2 (Giovinazzi and Lagomarsino) vulnerability relationship

For the preliminary assessment of human life losses due to the occurrence of a relatively strong earthquake, a quantitative model consisting of a correlation between the number of casualties and the estimated building damage caused by earthquakes as a function of earthquake intensity have been utilized in this study. Prognostic estimations of the expected number of killed or injured people associated with the damages caused by probabilistically, for all significant earthquakes are performed to compare with various vulnerability relationships and casualty methodologies as described in Table 3.26.

The calibration between the reported and the estimated casualties in Turkey showed that the probabilistic approach is reliable to estimate the casualties in Turkey. Especially, Coburn and Spence and Risk-UE methods with using the Result 1 vulnerability relationship have been very comparable to the reported one as presented in Table 3.26.

Table 3.26. The estimated casualty models

		Casualty Severity Level 3&4		
Building Damage Level	Dead & Casualties	Coburn & Spence	Risk-UE	KOERI2002 Fatalities
Observed Building Damage for destructive earthquakes adapted to present day population and building inventories	1,024,832			
Result 2 - Giovinazzi & Lagomarsino (2005)		1,729,207	1,559,650	1,320,658
Result 1 – KOERI 2002 (DEE-KOERI,2003)		1,045,295	905,890	1,109,000

4. AVERAGE ANNUALIZED EARTHQUAKE AND EARTHQUAKE LOSS RATIO

Recently earthquakes around the world indicate a pattern of steadily increasing damages and losses. The significant growth in urban areas that are prone to earthquakes and the weak vulnerability of the older building stock are the main two reasons of these increases. Understanding the importance of estimation of the varying degrees of seismic risk throughout the world, recent developments in loss estimation technologies have impacted the way insurance and reinsurance industries to develop their business strategies in recent years.

HAZUS (FEMA 366, 2000) and HAZUS-MH (FEMA, 2008) have been prepared to assess levels of seismic risk in The United States. These are PC-based standardized tool that utilizes a uniform engineering-based approach to measure damages, casualties and economic losses from earthquakes nationwide. The basic ingredients for loss estimation are earthquake hazard, regional building inventory, building vulnerabilities associated with typical construction systems in Turkey and estimations of building replacement costs for different damage states. These first three subjects are mentioned widely in Section 2 and Section 3, respectively. The estimation of replacement costs which is the last part of loss estimation is taken into consideration in this chapter.

The procedure documented in FEMA 366 (FEMA, 2008) to produce subsequently the average annual loss (AAL) at a collection of sites has been adapted to allow the use of the Macroseismic vulnerability method of Giovinazzi and Lagomarsino (2005).

The ratio of the cost of repair of the damage to the cost of reconstruction can be expressed as the Repair Cost Ratio corresponding to the damage grades D_1 through D_5 (defined in European Macro-seismic Scale- EMS98). When multiplied with the corresponding percent damages in a geo-cell found from the combined analysis of earthquake hazard and building vulnerabilities, they yield the loss ratio in that zone.

There are several studies to determine the replacement cost ratio for Turkey. These ratios are used to find to set the quantitative basis of the compulsory earthquake insurance scheme in Turkey (Table 4.1).

Table 4.1. The widely used repair cost ratios for Turkey

REPAIR COST RATIO (Replacement Cost Ratio)	D_1	D_2	D_3	D_4	D_5	D_4 & D_5
A. Durukal *et al*., (2006)	0.1	0.3	0.5	-	-	1
B. DEE-KOERI, (2003)	0.05	0.20	0.50	0.80	1	1
C. Bommer *et al*., (2002)	0	0.02	0.1	0.5	1	1

The variability associated with the repair cost ratio for Turkey has been observed in the study of Durukal *et al*. (2006). They have utilized two different dataset in the loss estimation for Istanbul. One of them is the priory known damage levels and the other is the damage levels as they are assigned by the experts to the damage cases. Eventually, the adopted replacement cost ratio in the loss estimations is accepted as 10 per cent, 30 per cent, 50 per cent and 100 per cent for D_1, D_2, D_3 and D_4 plus D_5, respectively. Using the new building repair costs for different levels of damage, earthquake hazard based on probabilistic and deterministic approaches, building inventory information of Istanbul, building vulnerability associated with typical construction system in Turkey; average annualized loss (AAL) and probable maximum loss (PML) estimations in Istanbul due to regional earthquake hazard have been provided. They have found that the estimated AAL associated with the Istanbul building stock was 0.47 per cent. It is changeable between 0.31 per cent and 0.62 per cent. Because the reinforced concrete structures represent the majority of the building inventory in Turkey, the compulsory earthquake insurance premiums in the highest earthquake hazard zone was 0.22 per cent.

Bommer *et al*. (2006) have studied on the development of the earthquake risk model for the TEFER project. They have developed an earthquake loss model for the Turkish Catastrophe Insurance Pools (TCIP) to serve as a basis for the decision process with respect to the pricing of its insure policy, risk control, the purchase of reinsure, and the transfer of seismic risk. An event based probabilistic loss estimation model has been built

to determine economic losses and loses to TCIP from earthquakes loss estimation. Assumed damage ratios for TEFER are shown in Table 4.1 and used for all building types in the absence of detailed local data on claims rates for the different damage level of distinct building types. As a result, the Annualized Earthquake Damage Ratio (AEDR) for residential buildings at province level has been calculated. High values of AEDR have been observed in the south-western parts of Turkey and provinces which were affected by the 1999 Kocaeli and Düzce events.

The Average Annual Loss Ratio (AALR) and Probable Maximum Loss Ratio (*PMLR*) are using two interrelated risk indicators.

Firstly, the Mean Damage Ratio (MDR, Table 4.2) is computed as the sum of the ratio of the numbers of damaged buildings in each damage class to the total number of buildings to multiply by the corresponding repair cost ratios.

Table 4.2. Mean damage ratios for each model

		Mean Damage Ratio (MDR)					
		Durukal *et al*., 2006		DEE-KOERI, 2003		Bommer *et al*., 2002	
Annual Rate of Exceedence	Return Period (years)	Result1	Result2	Result1	Result2	Result1	Result2
0.0139	72	0.14	0.31	0.12	0.27	0.08	0.19
0.0021	475	0.51	0.56	0.47	0.527	0.38	0.43
0.0004	2475	0.70	0.75	0.67	0.72	0.58	0.64

The Annualized Earthquake Loss Ratio (AELR, Table 4.4) shows the level of earthquake risk in relation to the insured value of property. The average annual loss (AAL) is computed as the area under the best-fit curve for the points corresponding to the three loss- probability pairs using a logarithmic relationship. The equations produced with the best fit curve for the points are shown in Table 4.3.

Table 4.3. The equations produced with the best fit curve for the points

Repair Cost Ratio	Result 1	Result 2
A. Durukal *et al.*, (2006)	y=-0.1599 ln(x)-0.5184 (R^2=0.98)	y=-0.1256ln(x)-0.2226 R^2=0.99
B. DEE-KOERI, (2003)	y=-0.1555 ln(x)-0.5215 (R^2=0.98)	y=-0.1276 ln(x)-0.2723 (R^2=1)
C. Bommer *et al.*, (2002)	y=-0.1418 ln(x)-0.52 (R^2=0.99)	y=-0.1279 ln(x)-0.3562 (R^2=1)

x=mean damage ratio (%)

y= annual rate of exceedence

By the integrating the logarithmic curve between annual rate of exceedence limits of 0.0004 and 0.0140, the average building loss is computed for Turkey as follows:

Table 4.4. AALR for each replacement cost ratio

REPAIR COST RATIO (Replacement Cost Ratio) Model	*Average Annual Loss Ratio (AALR): (%)*	
	Result 1	Result 2
A. Durukal *et al.*, (2006)	0.42	0.58
B. DEE-KOERI, (2003)	0.38	0.53
C. Bommer *et al.*, (2002)	0.30	0.41

As a comparison to California, the state average of AAL is 0.18 per cent. It can be varying between 0.05 per cent and 0.26 per cent.

The PML ratio is defined as the ratio of probable maximum loss to the building replacement value. The PML associated with 475 year return period as shown in Table 4.4 is used as a standard by the insurance sector. The average MDR for each return period and each building vulnerability model is presented in Table 4.5. The average PML vary between 0.45 and 0.51.

Table 4.5. Average mean damage ratio (per cent)

	Mean Damage Ratio (MDR)	
Return Period (yrs)	Result 1 (Average)	Result 2 (Average)
72	0.11	0.26
475	0.45	0.51
2475	0.65	0.70

Durukal *et al*. (2006) have found that the PML ratios are estimated as 19 per cent in the occurrence of a scenario event using the intensity based vulnerabilities and 22 per cent using the spectral-displacement based vulnerabilities. Using the probabilistic approach, they estimate the 72, 100, 475 year return periods PML ratio as 28 per cent, per cent 32, 31 per cent, respectively.

As a comparison in Kingston, Jamaica (Chandler *et al*., 2001), the upper bound of earthquake PML of a round 3. per cent occurs for Risk 1 and 2, with a 50 year return period and a PE of only 2. per cent. In San Francisco Bay Area, their preliminary estimate for the expected direct economic annualized losses to building for the ten countries San Francisco Bay Area (Alameda, Contra Costa, Marin, Napa, San Francisco, San Matea, Santa Clara, Santa Cruz, Solano, Sonoma) is $754 million. It corresponds to an average annual per-capital loss of $121 and the average annual loss ratio of roughly 0.2 per cent**.** The annualized building damage resulting from the integrated effects of ground motion shaking emanating from the potential earthquakes is estimated using HAZUS, with the same building inventory that they have used for the scenario calculations.

5. UNCERTAINTY

All of the inputs or /and outputs to an earthquake loss model have included large uncertainties, and the identification, quantification and incorporation of these uncertainties into the calculations form an integral part of establishing a loss model (Bommer *et al*., 2005). It is convenient to categorize the character of uncertainties as either aleatory or epistemic. An aleatoric uncertainty is one that is presumed to be the intrinsic randomness of a phenomenon, on the other hand, an epistemic uncertainty is one that is presumed as being caused by lack of knowledge or data (Reiter, 1990, McGuire, 2004). The epistemic uncertainty gives an opportunity to solve the same problem with alternative input parameters. There are several alternatives for representing epistemic uncertainty (Helton and Oberkampf 2004). The most commonly used method to reduce the epistemic uncertainty in the concept of the probability is a term of logic trees which is an implementation of a probability model of uncertainties and is related to the interpretations of the branch weights in logic trees (Abrahamson and Bommer 2005, McGuire *et al*., 2005, Musson 2005).

The purpose of a logic tree is to capture and quantify the epistemic uncertainty. To reduce the epistemic uncertainty, average ground motion parameter obtained from each of the attenuation relationships in hazard calculation, average estimated building damage obtained from each of the two types of vulnerabilities, and average of estimated earthquake loss obtained from each of three different repair cost ratios are utilized in this study. The scheme of logic tree used in this study is tabulated in Table 5.1.

Table 5.1. The scheme of logic tree used in this study

<table>
<tr><th colspan="2">Hazard</th><th>Vulnerability</th><th>Loss</th></tr>
<tr><td colspan="2">Ground Motion Prediction Equation
(GMPE)</td><td>Building Vulnerability
(Intensity based)</td><td>Repair Cost Ratio</td></tr>
<tr><td colspan="2">Intensity Based Regional GMPE
(Mean value)
(Sesetyan et al., 2005)</td><td>Average of
Modified KOERI model
Giovinazzi & Lagomarsino
model</td><td>Average of
Durukal et al. (2006)

DEE-KOERI (2003)
Bommer et al. (2002)</td></tr>
<tr><td>PGA</td><td>Average of
Boore et al. (1997)
Sadigh et al. (1997)
Campbell (1997)</td><td colspan="2" rowspan="4">-</td></tr>
<tr><td>SS</td><td>Average of
Boore et al. (1997)
Sadigh et al. (1997)</td></tr>
<tr><td>PGA</td><td>Average of
CB (2008)
BA (2008)
CY (2008)</td></tr>
<tr><td>SS</td><td>Average of
CB (2008)
BA (2008)</td></tr>
</table>

*Campbell and Bozorgnia (2008)

**Boore and Atkinson (2008)

***Chiou and Young (2008)

Based on site dependent and site independent, the average of earthquake ground motion parameter for each return period has been shown in Section 2.8 and 2.10, respectively. The average of estimated building damages and estimated casualties for each return period are shown in Figure 5.1 through Figure 5.24.

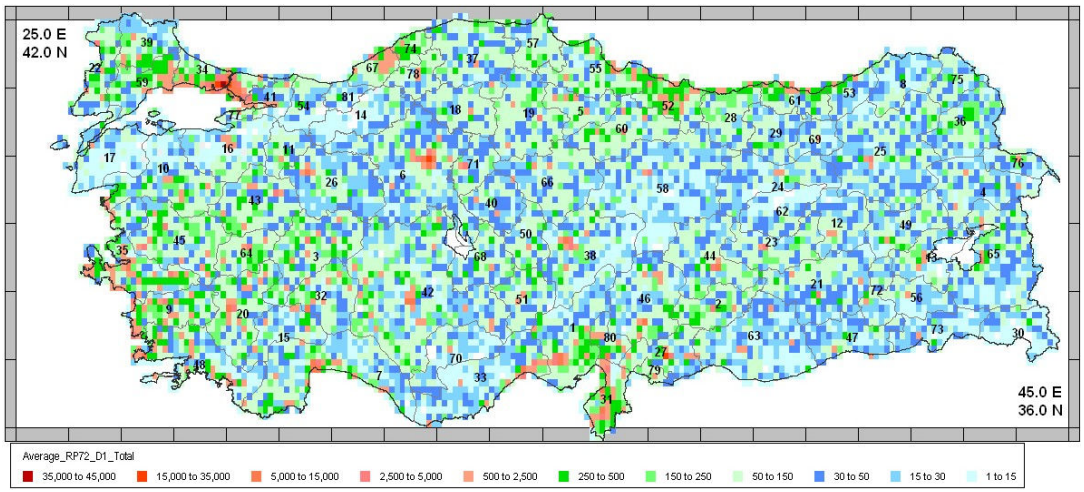

Figure 5.1. Intensity based probabilistic estimated building damage distribution of slight damage (D1) for all type of building in Turkey corresponding to 50 per cent probability of exceedence in 50 years (average of two vulnerability models)

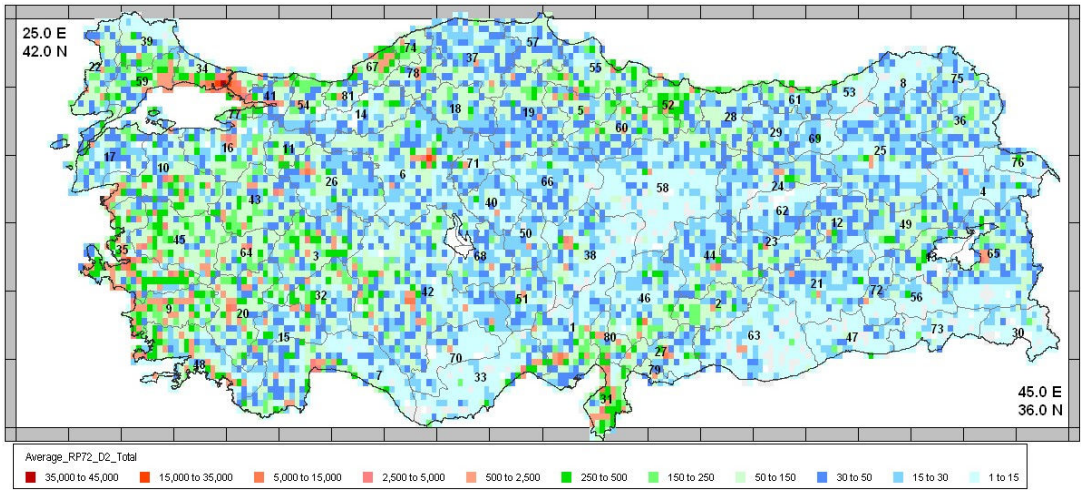

Figure 5.2. Intensity based probabilistic estimated building damage distribution of moderate damage (D2) for all type of building in Turkey corresponding to 50 per cent probability of exceedence in 50 years (average of two vulnerability models)

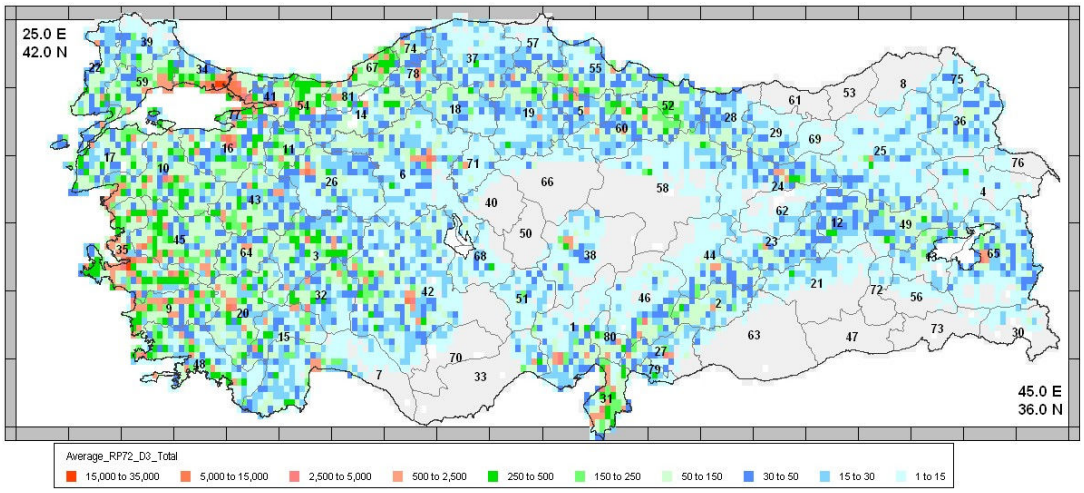

Figure 5.3. Intensity based probabilistic estimated building damage distribution of heavy damage (D3) for all type of building in Turkey corresponding to 50 per cent probability of exceedence in 50 years (average of two vulnerability models)

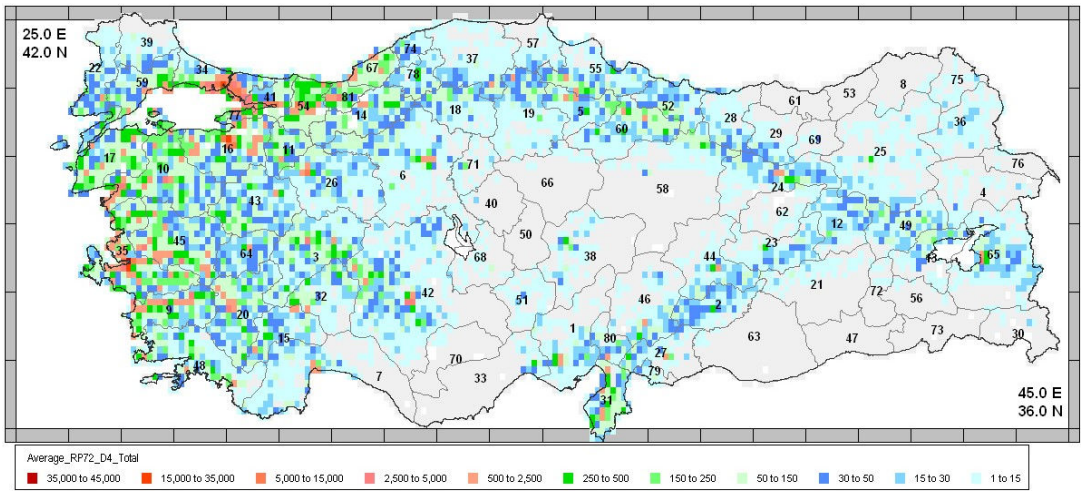

Figure 5.4. Intensity based probabilistic estimated building damage distribution of partial destruction damage (D4) for all type of building in Turkey corresponding to 50 per cent probability of exceedence in 50 years (average of two vulnerability models)

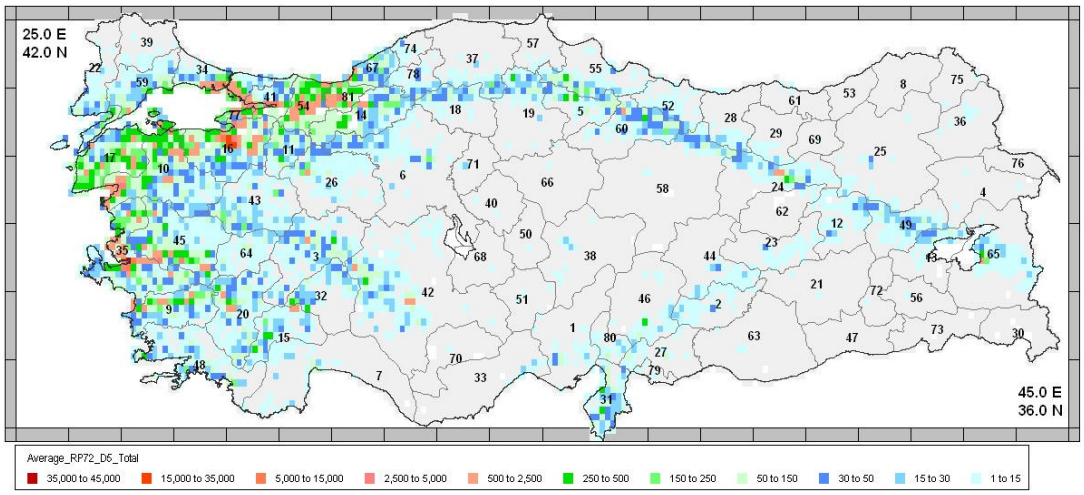

Figure 5.5. Intensity based probabilistic estimated building damage distribution of collapse damage (D5) for all type of building in Turkey corresponding to 50 per cent probability of exceedence in 50 years (average of two vulnerability models)

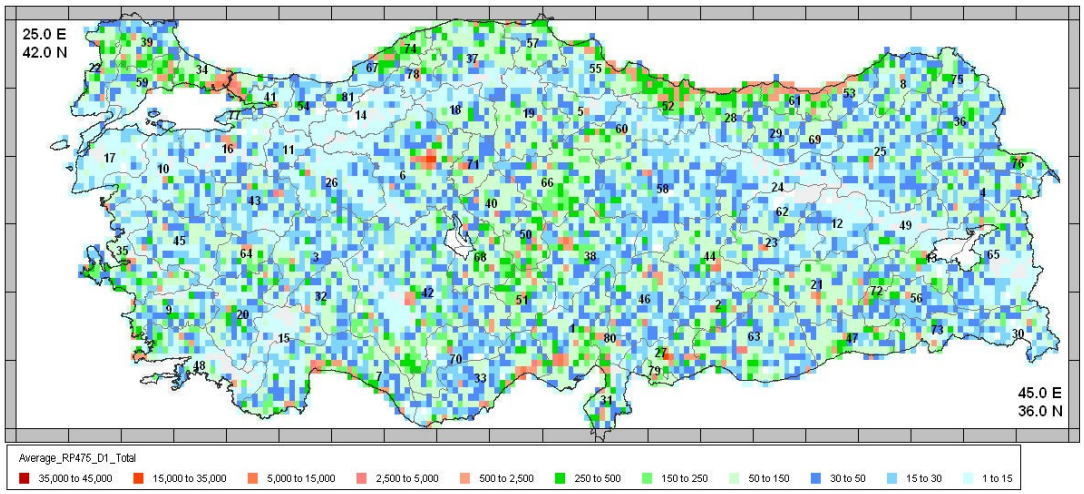

Figure 5.6. Intensity based probabilistic estimated building damage distribution of slight damage (D1) for all type of building in Turkey corresponding to 10 per cent probability of exceedence in 50 years (average of two vulnerability models)

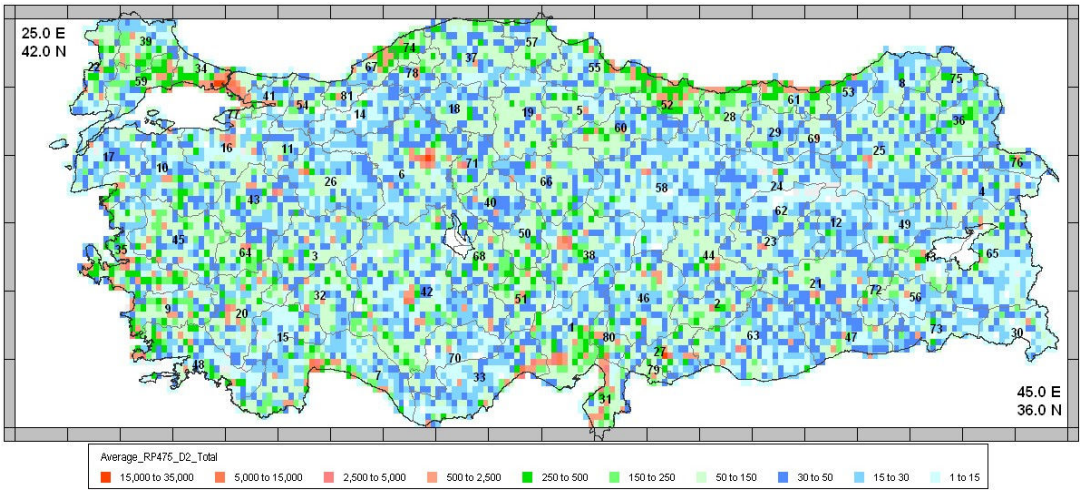

Figure 5.7. Intensity based probabilistic estimated building damage distribution of moderate damage (D2) for all type of building in Turkey corresponding to 10 per cent probability of exceedence in 50 years (average of two vulnerability models)

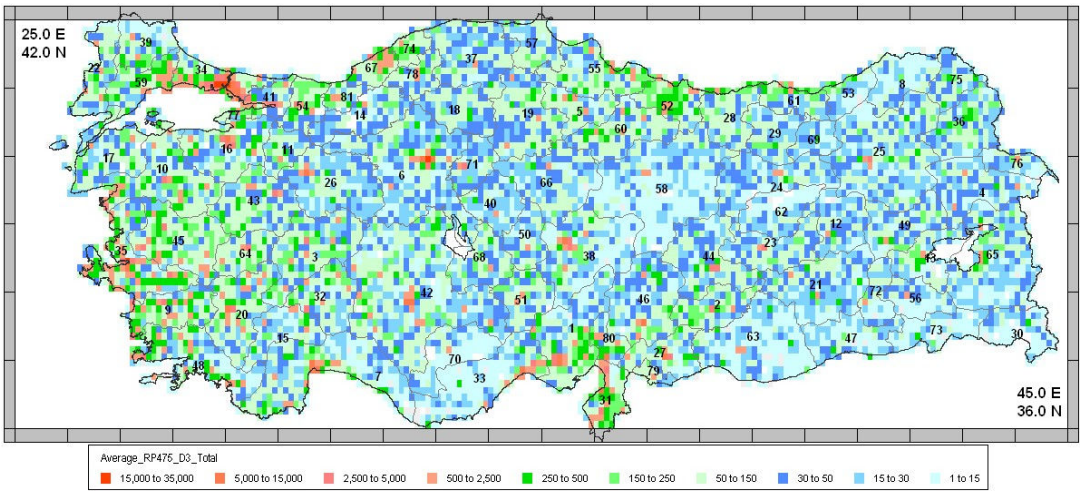

Figure 5.8. Intensity based probabilistic estimated building damage distribution of heavy damage (D3) for all type of building in Turkey corresponding to 10 per cent probability of exceedence in 50 years (average of two vulnerability models)

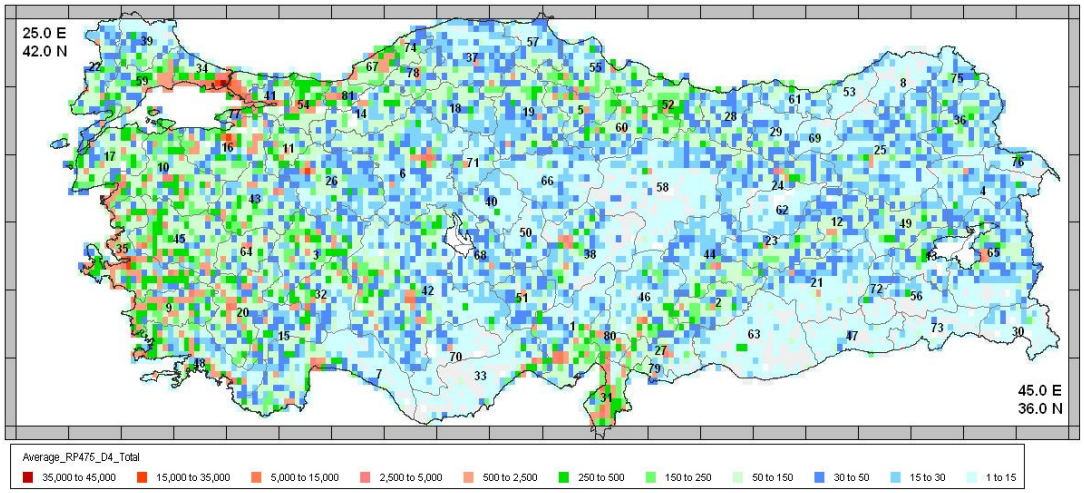

Figure 5.9. Intensity based probabilistic estimated building damage distribution of partial destruction damage (D4) for all type of building in Turkey corresponding to 10 per cent probability of exceedence in 50 years (average of two vulnerability models)

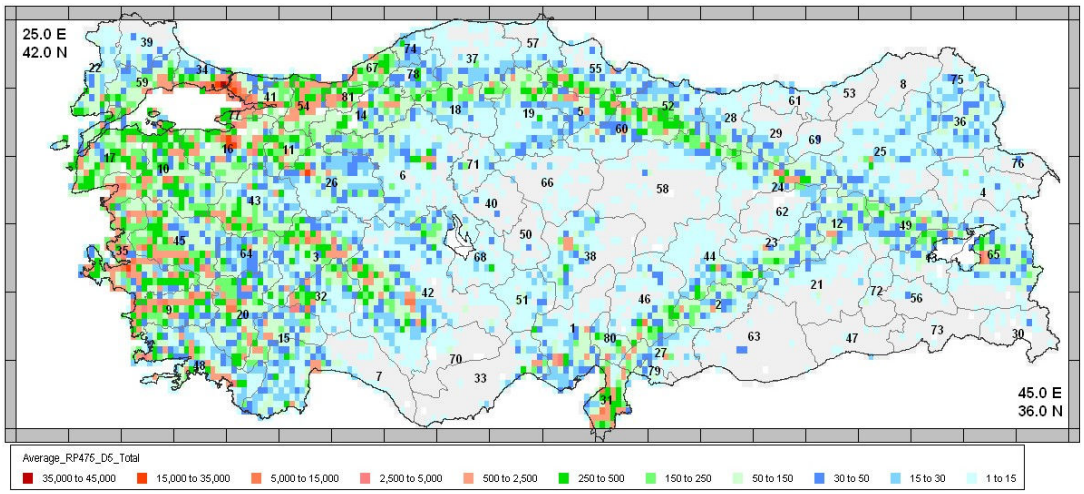

Figure 5.10. Intensity based probabilistic estimated building damage distribution of collapse damage (D5) for all type of building in Turkey corresponding to 10 per cent probability of exceedence in 50 years (average of two vulnerability models)

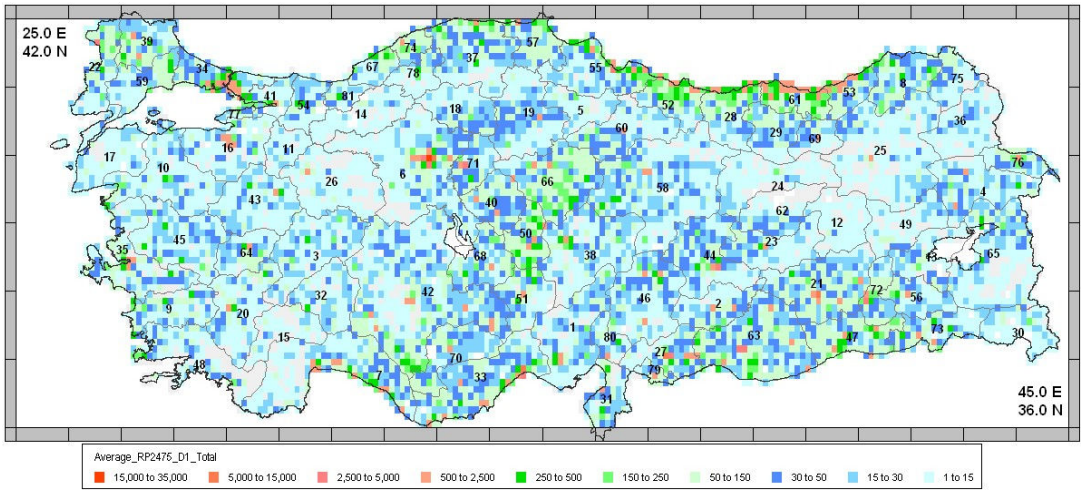

Figure 5.11. Intensity based probabilistic estimated building damage distribution of slight damage (D1) for all type of building in Turkey corresponding to 2. per cent probability of exceedence in 50 years (average of two vulnerability models)

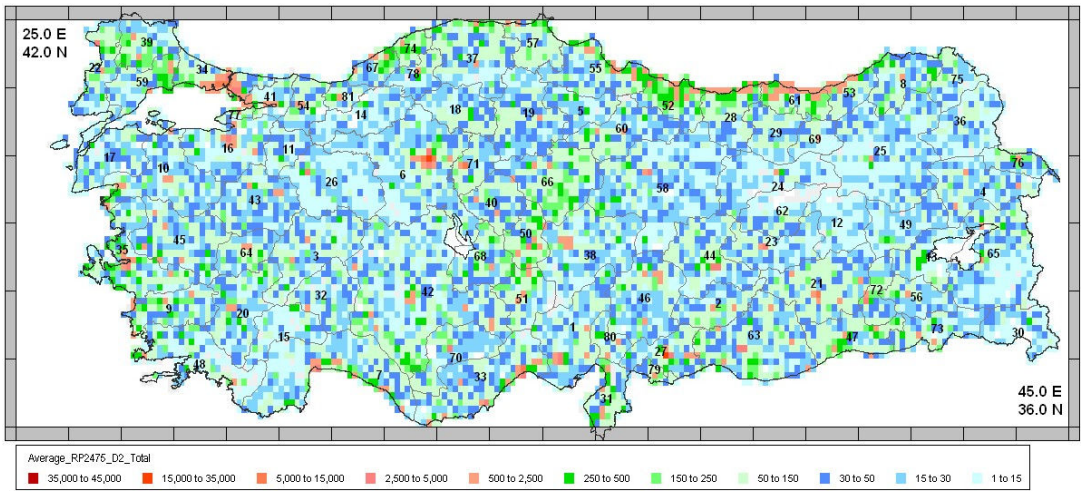

Figure 5.12. Intensity based probabilistic estimated building damage distribution of moderate damage (D2) for all type of building in Turkey corresponding to 2. per cent probability of exceedence in 50 years (average of two vulnerability models)

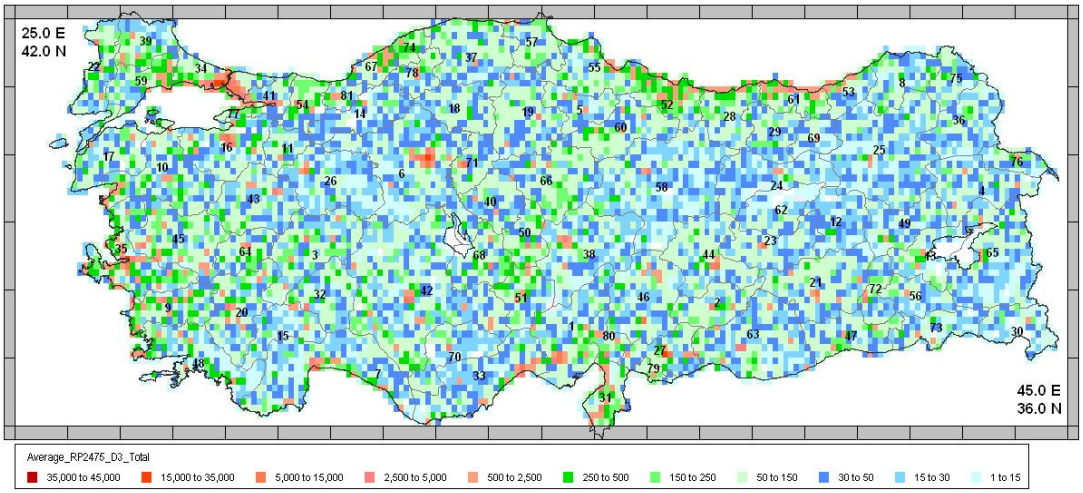

Figure 5.13. Intensity based probabilistic estimated building damage distribution of heavy damage (D3) for all type of building in Turkey corresponding to 2. per cent probability of exceedence in 50 years (average of two vulnerability models)

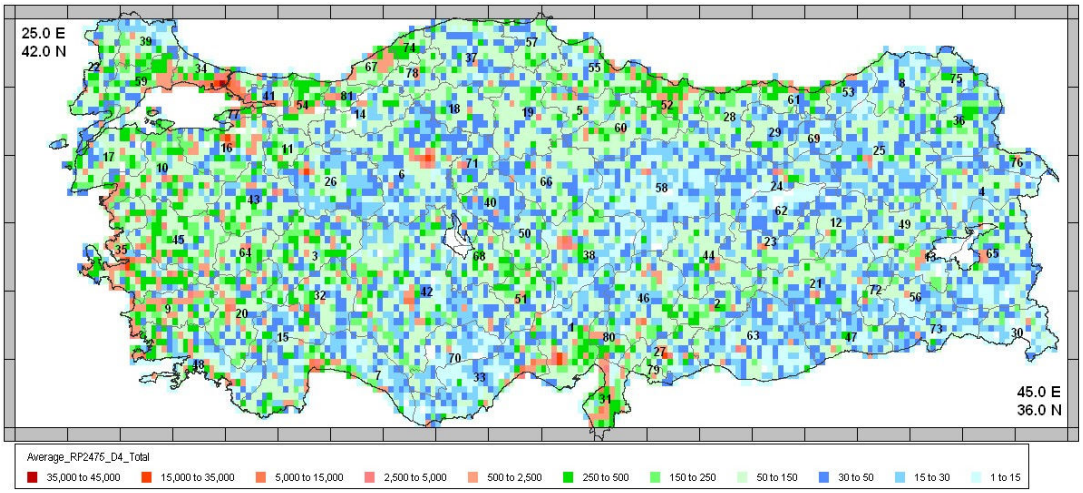

Figure 5.14. Intensity based probabilistic estimated building damage distribution of partial destruction damage (D4) for all type of building in Turkey corresponding to 2. per cent probability of exceedence in 50 years (average of two vulnerability models)

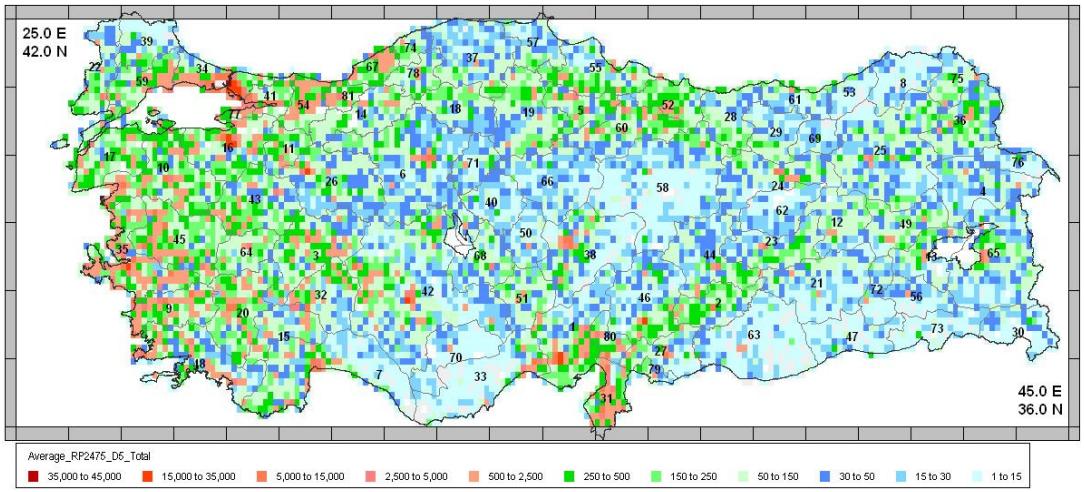

Figure 5.15. Intensity based probabilistic estimated building damage distribution of collapse damage (D5) for all type of building in Turkey corresponding to 2. per cent probability of exceedence in 50 years (average of two vulnerability models)

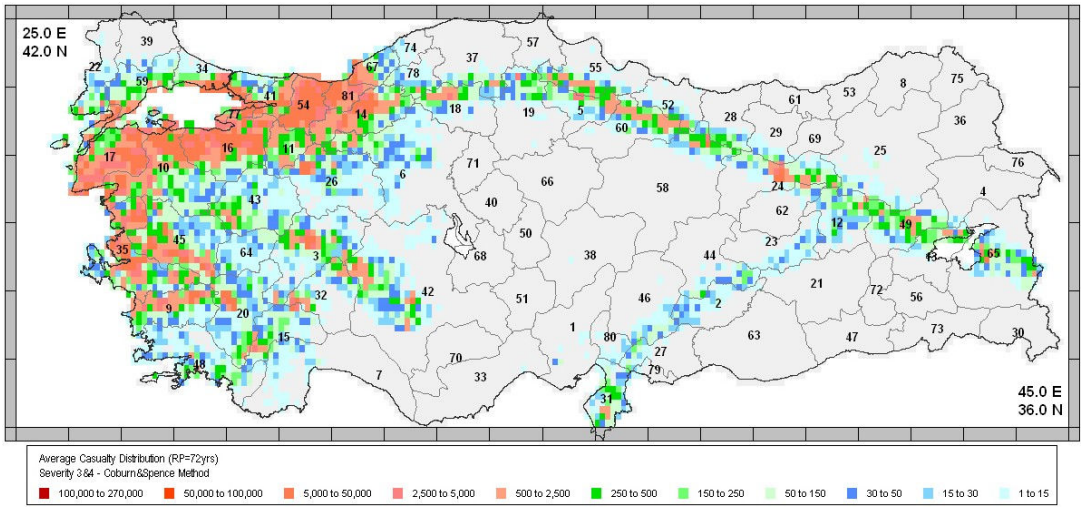

Figure 5.16. Probabilistic intensity based casualty distribution corresponding to the return period of 72 years - Coburn & Spence model

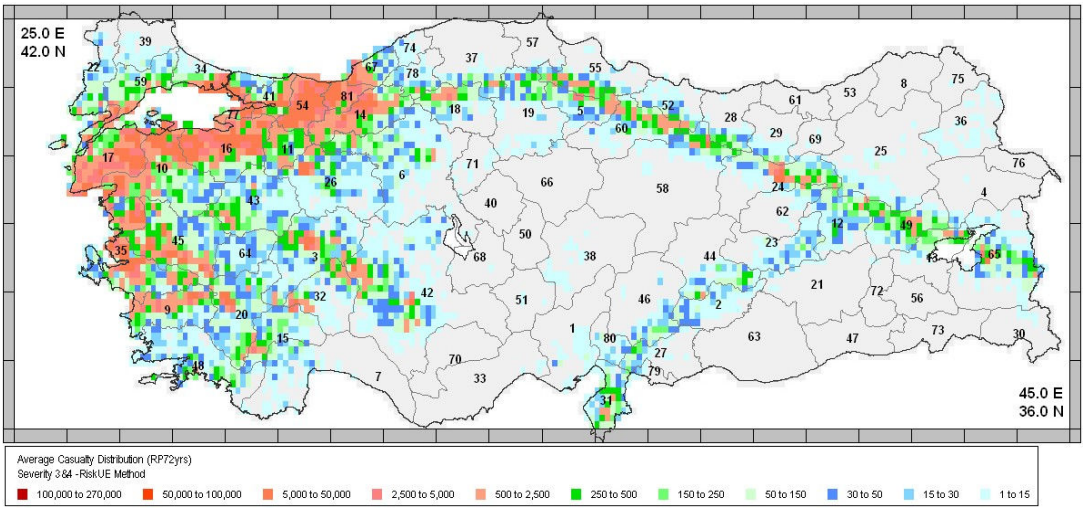

Figure 5.17. Probabilistic intensity based casualty distribution corresponding to the return period of 72 years – Risk UE model

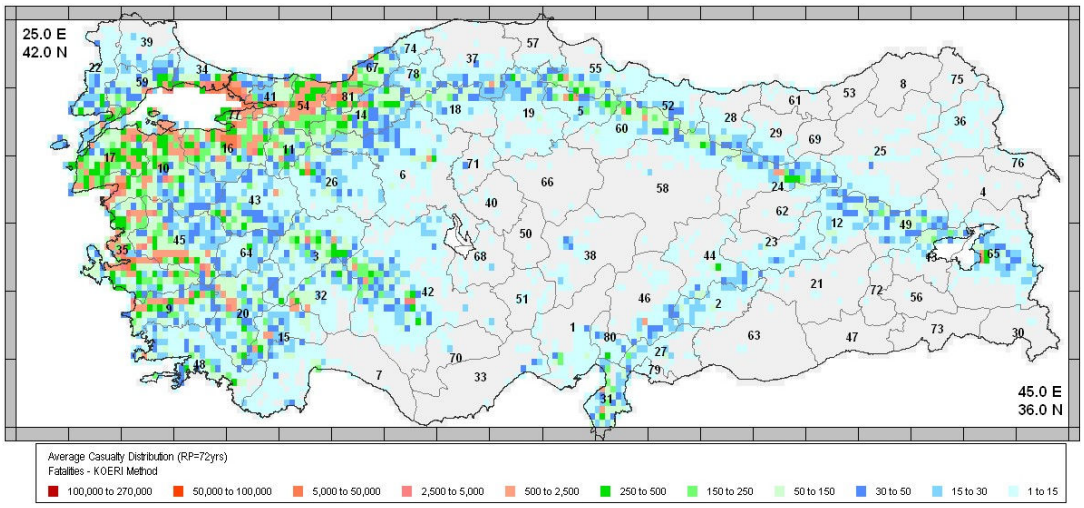

Figure 5.18. Probabilistic intensity based casualty distribution corresponding to the return period of 72 years – KOERI model

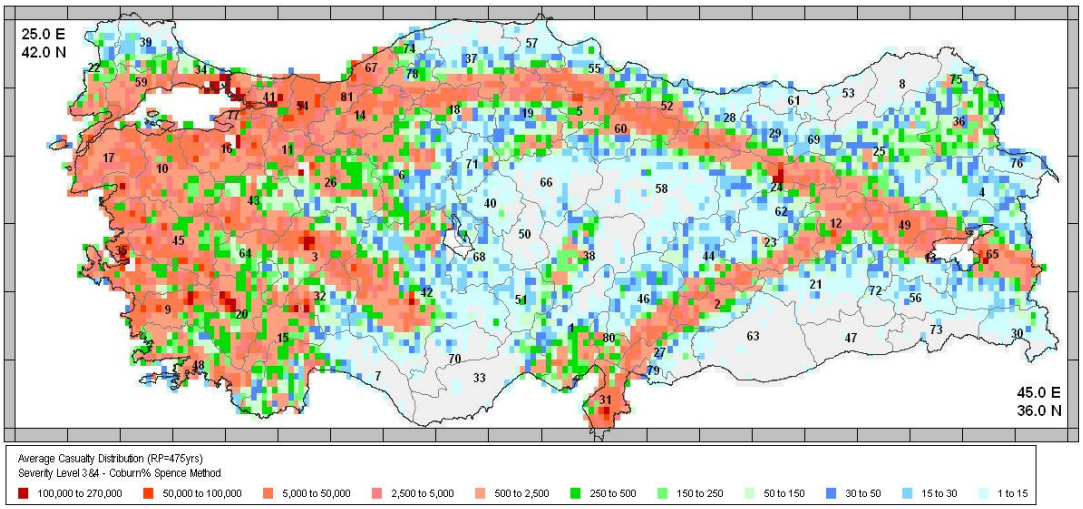

Figure 5.19. Probabilistic intensity based casualty distribution corresponding to the return period of 475 years - Coburn & Spence model

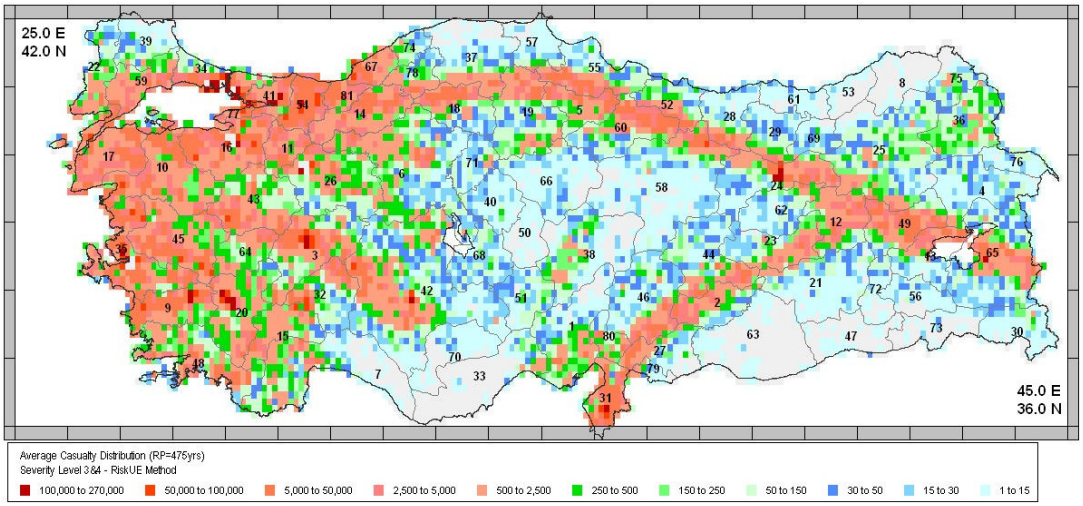

Figure 5.20. Probabilistic intensity based casualty distribution corresponding to the return period of 475 years – Risk UE model

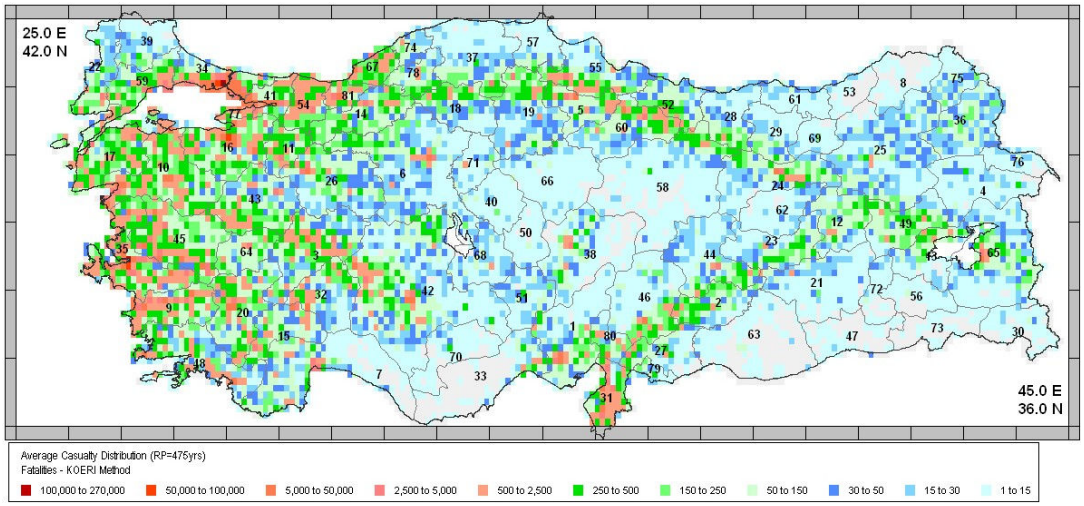

Figure 5.21. Probabilistic intensity based casualty distribution corresponding to the return period of 475 years – KOERI model

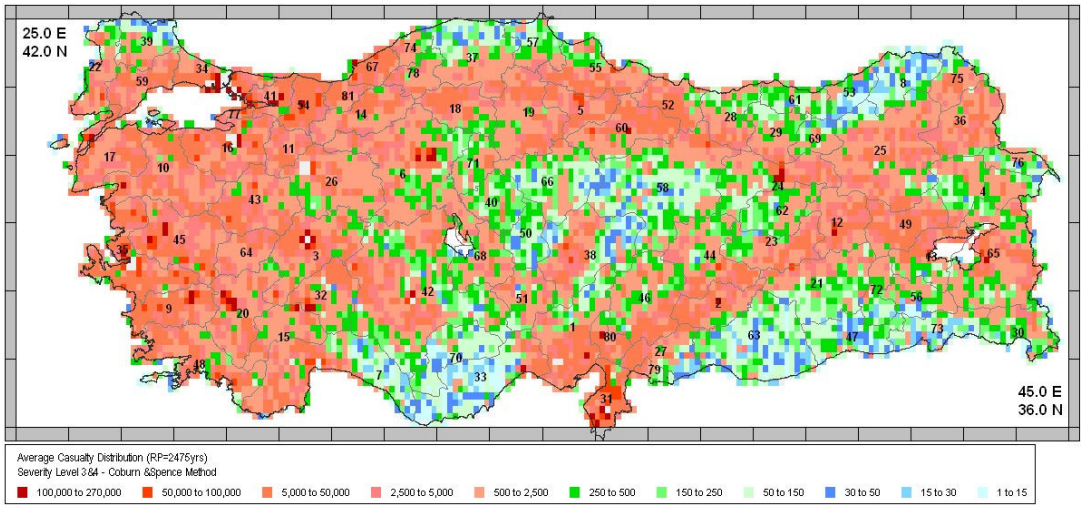

Figure 5.22. Probabilistic intensity based casualty distribution corresponding to the return period of 2475 years - Coburn & Spence model

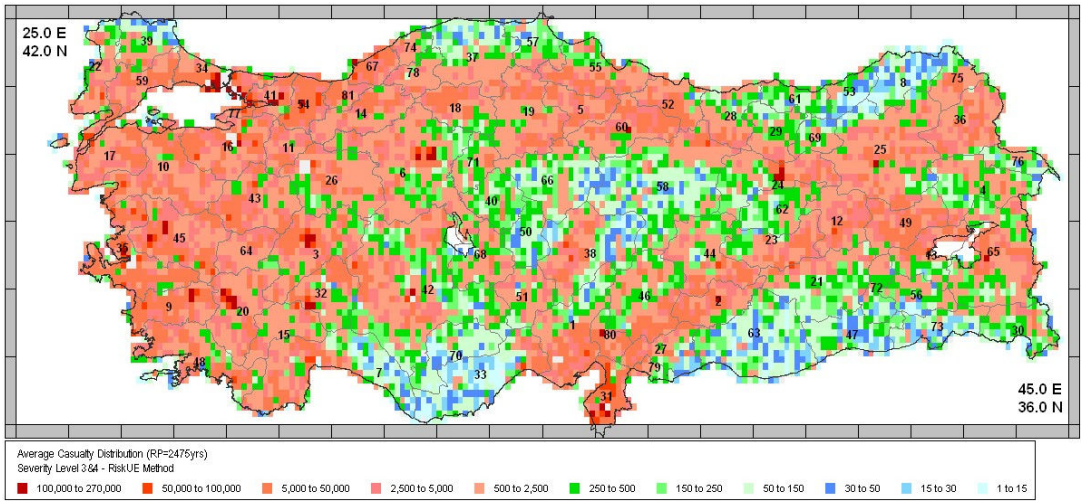

Figure 5.23. Probabilistic intensity based casualty distribution corresponding to the return period of 2475 years – Risk UE model

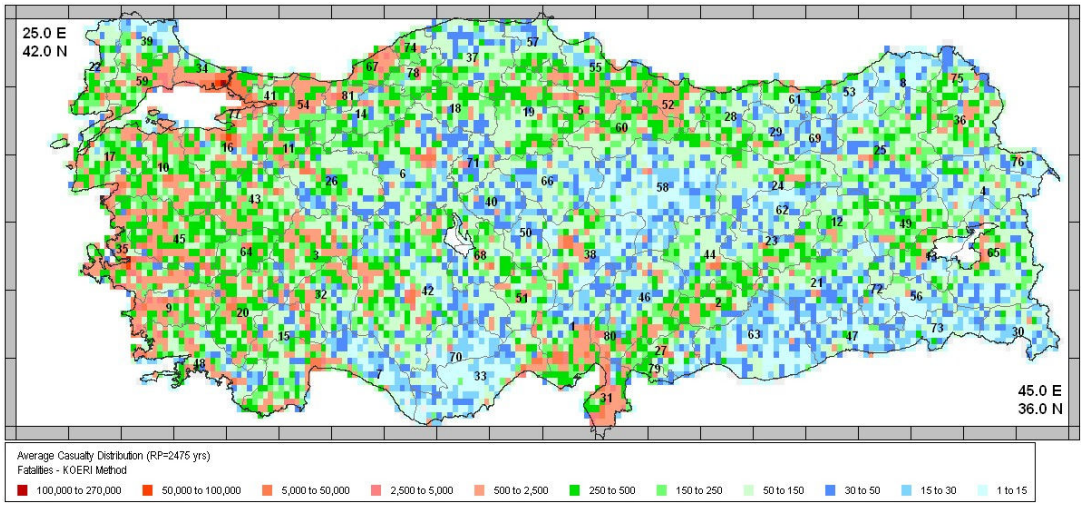

Figure 5.24. Probabilistic intensity based casualty distribution corresponding to the return period of 2475 years – KOERI model

6. CONCLUSIONS

Turkey is one of the most earthquake-prone countries in the world. For that reason, the study of the earthquake hazard and risk assessment is very crucial and required for national earthquake resistant design of structures, to prioritize risk mitigation actions, to prepare for emergency response and recovery from earthquakes and to provide input for risk transfer modalities. Generally, using a GIS environment, seismic risk analysis builds on the ingredients of seismic hazard, regional inventory of buildings and vulnerability analysis. Earthquake loss estimation models have found a variety of applications in the primary insurance and reinsurance markets and, more recently, in capital markets. These models can also be useful in the area of seismic risk mitigation by providing cost-benefit analyses of the impact of various mitigation strategies.

This study had two main objectives. The first objective was to carry out a state of the knowledge assessment of the country wide earthquake hazard based on the NGA ground motion prediction models and the comparison of the results with the previous models. In this study, probabilistic hazard approach was used to estimate the site independent earthquake hazard corresponding to 50 per cent, 10 per cent and 2. per cent probabilities of exceedence in 50 years for various ground motion parameters such as PGA, intensity and SA at various periods. Additionally, the geological units based QTM map of Turkey has been utilized to reflect the effects of local site condition on these hazard parameters to yield the site-dependent results. The site independent earthquake hazard based on NGA models is found to be 10 per cent less than the hazard obtained using the previous generation of ground motion prediction models. A comparable difference has also observed between the two models of Western California prepared by USGS in 2002 and 2008 (Bozorgnia, presentation, 2009, http://www.adea.metu.edu.tr/lecturers.htm)

The second objective was the evaluation of intensity based probabilistic seismic risk for Turkey. For the assessment of structural vulnerabilities, the so-called European Macroseismic approach developed by Giovinazzi and Lagomarsino (2005) has been used. This method has been derived from EMS98 macroseismic scale definition by the use of the probability and of the fuzzy set within the context of Risk-UE (www.RISK-UE.net) project

and is recognized to be applicable throughout the European regions. In this study, this method has been utilized to produce the intensity based vulnerability models for European building taxonomy corresponding to each damage state described in EMS98. Two alternative vulnerability relationships were considered to estimate the building damage. modified KOERI - Result1 model is based on the vulnerability relationships of Coburn and Spence (2002) for the building type of non seismic reinforced concrete (CC1). In this approach, the vulnerability curves for low-rise and high-rise RC frame type buildings are obtained by a half unit left shifting of the intensity scale in the horizontal axis of the vulnerability curves of the medium rise RC frame buildings. Medium-rise RC frame is also similar to the CC1 Reinforced Concrete Frame Non Engineered type of buildings defined in the study of Coburn and Spence (2002). The vulnerability and ductility indices for CC1 type of building were taken from the study of Giovinazzi (2005).

Based on the European building taxonomy, the Turkish building inventory was classified in twelve groups. The second vulnerability model (Result 2) used in this study was based on the vulnerability and ductility indices for all building classes of Turkish database obtained according to the Macroseismic method of Giovinazzi and Lagomarsino (2005). These two vulnerability models have been compared with the observed earthquake damage database. A good agreement between these curves has been clearly observed. Additionally, the building damage and casualty estimations for each return period and for each vulnerability relationships have been used for the assessment of the earthquake losses.

Due to the philosophy behind the probabilistic method used for assessment of earthquake hazard, earthquakes of any size can occur randomly at any time. As such, the loss figure in each cell is associated with indicated probabilities. To arrive that total expected loss figure for Turkey, it would be misleading to sum these figures at individual cells since they will not take place simultaneously at the same time.

Finally, the building replacement costs for different damage states have been estimated. There are several studies to determine the replacement cost ratio for Turkey. These ratios are used to set a quantitative basis for the compulsory earthquake insurance scheme in Turkey. In this study, the variability associated with the repair cost ratio for Turkey has been obtained by use of the studies of Durukal *et al.* (2006), DEE-KOERI

(2003) and Bommer *et al*. (2002). The ratio of the cost of repair of the damage to the cost of reconstruction can be expressed as the Repair Cost Ratio corresponding to the damage grades D_1 through D_5 (defined in European Macro-seismic Scale- EMS98). When multiplied with the corresponding percent damages in a geo-cell found from the combined analysis of earthquake hazard and building vulnerabilities, they yield the loss ratio in that zone. These loss ratios are used to obtain the average annual loss (AAL) and the probable maximum loss ratio (PMLR). The average annual loss (AAL) is computed as the area under the best-fit curve for the points corresponding to the three loss- probability pairs using a logarithmic relationship. The average annual loss ratio has been found to be in the ranges of 0.30 per cent and 0.58 per cent. In California, this range varied between 0.005 per cent and 0.26 per cent.

6.1. Future Research

1. The median value is used to quantify the estimated building damage and building loss. The standard deviation of ground motions and vulnerability parameters should be considered in order to assess the uncertainties.

2. The intensity based hazard maps provided in the study are site independent. Regional geological map can be used to determine the site dependent intensity increments.

3. Monte Carlo simulations based on the seismicity model could be used as an alternative model. It involves the use of multiple earthquake scenarios to generate the ground motions at all sites of interest. It could be better to determine the uncertainty when a number of sites are considered simultaneously in earthquake hazard and loss model.

4. Instead of the regional intensity ground motion prediction equation, the seismic hazard values computed in terms of PGA are converted to MMI scale and for this conversion the empirical relationships given by Trifunac and Brady (1975) and Wald *et al*. (1999) are utilized and /or using the earthquake data occurred in Turkey, a new relationship between PGA and earthquake intensity (MMI or EMS98) can be produced.

5. The economic loss parameter is calculated as a ratio. However, the loss value can be calculated as a monetary value.

7. REFERENCES

Abrahamson N. A. and J. J. Bommer, 2005, "Uncertainty and Probability in Seismic Hazard Analysis", *Earthquake Spectra*, Vol. 21, No.2, pp. 603–607.

Abrahamson, N. A. and W. J. Silva, 2008, "Summary of the Abrahamson and Silva NGA Ground Motion Relations", *Earthquake Spectra*, Vol. 24, pp. 45–66.

Aksu, A. E., T. J. Calon, R. N. Hiscott, and D. Yasar, 2000, "Anatomy of the North Anatolian Fault Zone in the Marmara Sea, Western Turkey: Extensional Basins above a Continental Transform*", Geological Society of America (GSA Today*), June 3-7.

Akyuz, H. S., E. Altunel, E. V. Karabacak, and C.C. Yalcıner, 2006, "Historical Earthquake Activity of the Northern Part of the Dead Sea Fault Zone, Southern Turkey", *Tectonophysics*, Vol. 426, pp.281–93.

Allen, C. R., 1969, *Active Faulting in Northern Turkey", Division of Geological Sciences*, California Institute of Technology, Contribution No. 1577, pp.32, California.

Allen, T. I., and D. J. Wald, 2007, *Topographic Slope as a Proxy for Seismic Site Conditions (Vs30) and Amplification around the Globe*", U.S. Geological Survey, Open File Report, pp. 1357.

Alpar B. and C. Yaltirak, 2002, "Characteristic Features of the North Anatolian Fault in the Eastern Marmara Region and its Tectonic Evolution", *Marine Geology*, Vol. 190, pp. 329-350.

Alpar, B., Yaltırak, C., 2002, "North Anatolian Fault in the Eastern Marmara Region and its Tectonic Evolution", *Marine Geology*, Vol. 190, pp. 493-529.

Alptekin, O., 1973, *Focal Mechanism of Earthquakes in Western Turkey and their Tectonic Implications*, PhD Thesis, New Mexico Institute of Mining and Technology.

Ambraseys N. N. and C. F. Finkel, 1987, "Seismicity of the Northeast Mediterranean Region During Early 20th Century", *Annals Geophysics*, Vol. 5B, pp.701-726.

Ambraseys N. N., 1995, "The Prediction of Earthquake Peak Ground Acceleration in Europe", *Journal of Earthquake Engineering and Structural Dynamics*, Vol. 24, pp. 467-490.

Ambraseys, N. N. ve C. F. Finkel, 1991, "Long-term Seismicity of Istanbul and of the Marmara Sea region", *Terra Nova*, Vol. 3, pp. 527-539.

Ambraseys, N. N., 1989, "Temporary Seismic Quiescence: SE Turkey", *Geophysics Journal International*, Vol. 96, pp: 311-331.

Ambraseys, N. N., M. Barazangi, 1989, "The 1759 Earthquake in the Bekaa Valley: Implications for Earthquake Hazard Assessment in the Eastern Mediterranean Region", *Journal of Geophysical Research*, Vol. 94, pp. 4004-4013.

Ambraseys, N., 1988, "Engineering Seismology", *Journal of Earthquake Engineering and Structural Dynamics*, Vol. 17, pp.1-105.

Ambraseys, N. N. and C. P. Melville, 1995, "Historical Evidence of Faulting in Eastern Anatolia and Northern Syria", *Annali di Geofisica*, Vol: 38, No: 3-4.

Ambraseys, N. N. and J. A. Jackson, 1998, "Faulting Associated with Historical and Recent Earthquakes in the Eastern Mediterranean Region", *Geophysics Journal International*, Vol 133, pp. 390-406.

Ambraseys, N. N., 1970, "Some Characteristic Features of the North Anatolian Fault Zone", *Tectonophysics*, Vol.9, pp. 143– 165.

Ambraseys, N. N., 1988, "Engineering Seismology", *Journal of Earthquake Engineering and Structural Dynamics*, Vol. 17, pp. 1-105.

Ambraseys, N. N., 1989, "Temporary Seismic Quiescence in SE Turkey", *Geophysics Journal International*, Vol. 96, pp. 311-331.

Ambraseys, N. and C.Finkel, 1995, *The Seismicity of Turkey and Adjacent Areas*, EREN Publications, İstanbul.

Ansal, A. M., Iyisan, R. and Ozkan, M., 1997, "A Microzonation Study for the Town of Dinar", *Proceedings of Special Technical Session on Earthquake Geotechnical Engineering During 14th ICSMFE*, Hamburg, 6-12 September, pp. 3-9, Germany.

Armijo, R. N. Pondard, B. Meyer, B. Mercier de Lepinay, G. Ucarkus, J. Malavieille, S. Dominguez, M-A Beck Gustcher, M-A. Beck, N. Çagatay, Z. Cakir, C. Imren, E. Kadir and Natalin, and MARMARASCARPS cruise party, 2005, "Submarine Fault Scarps in the Sea of Marmara Pull-apart (North Anatolian Fault): Implications for Seismic Hazard in Istanbul", *Geochemisty Geophysics Geosystems*, pp. 1-29.

Armijo, R., B. Meyer, A. Hubert, A. Barka, 1999, "Westward Propagation of the North Anatolian Fault into the Northern Aegean: Timing and Kinematics", *Geology*, Vol. 27, pp. 267–270.

Arpat E, F. Şaroğlu, 1972, "East Anatolian Fault System; thoughts on its Development", *Bull. Min. Res. Expl. Inst,* Vol. 78, pp. 33–39.

Atabey, E., N. Tarhan, B. Akarsu, and M.A. Taskıran, 1987, *Sereflikoçhisar, Panlı (Ankara) –Acıpınar (Nigde) Yöresinin Jeolojisi*, Ankara, General Directorate for Mineral Research and Exploration (MTA), Report No:8155.

ATC 13, 1987, *Earthquake Damage Evaluation Data for California,* Applied Technology Council, Redwood City, California.

ATC 40, 1996, *Seismic Evaluation and Retrofit of Concrete Buildings*, Applied Technology Council, Redwood City, California.

ATC-36, 1997, *Earthquake Loss Evaluation Methodology and Databases for UTAH*, Applied Technology Council, Redwood City, California

Barka A. A. and K. Kadinsky-Cade, 1988, "Strike-Slip Fault Geometry in Turkey and its Influence on Earthquake Activity", *Tectonics*, Vol. 7, No. 3, pp: 663-684.

Barka, A. and R. Reilinger, 1997, "Active Tectonics of Eastern Mediterranean Region: Deduced from GPS, Neotectonic and Seismicity Data", *Annali Di Geofisica*, Vol.X2, No.3, pp. 587–610.

Barka, A., 1992, "The North Anatolian Fault Zone," *Annales Tectonicae*, Special Issue – Supplement to Vol. VI, pp: 164-195.

Barka, A., 1996, "Slip Distribution Along the North Anatolian Fault Associated with the Large Earthquakes of the Period 1939 to 1967", *Bulletin of the Seismological Society of America*, Vol. 86, pp. 1238-1254.

Barka, A., E. Yigitbas, F. Saroglu and E. Altunel, 2000, *Baku-Ceyhan Pipeline Project: A Preliminary Report on Active Faults and Earthquake Potentials*, ENVY Inc., Ankara.

Barka, A., S. Akyüz and E. Altunel, 1999, *Active Tectonics of the Adana Region and the 1998 Adana Earthquake (in Turkish)*, Aktif Tektonik Araştırma Grubu, 2. Toplantısı Makaleler Kitabı, I.T.U. Avrasya Yerbilimleri Enstitüsü.

Beekman, P. H., 1966, "The Volcanic Activity of Pliocene and Quaternary Era in Hasandagi-Melendizdagi Regions", MTA Publications, Vol. 66, pp. 88–104 (in Turkish).

Bellier, O. and M. Zoback, 1995, "Recent State of Stress Change in theWalker Lane Zone Western Basin and Range Province-USA", *Tectonics*, Vol. 14, pp. 564–593.

Bellier, O., S. Over, A. Poisson, and J. Andrieux, 1997, "Recent Temporal Change in the Stress State and Modern Stress Field along North Anatolian Fault Zone (Turkey)", *Geophysics Journal International*, Vol. 131, pp. 61–86.

Beloussov V. V. and B.S. Volvovsky, Editors, 1989, *Structure and Evolution of the Earth's Crust and Upper Mantle of the Black Sea*, Nauka, Moscow, Russia.

Bender, B. and D.M. Perkins, 1987, "SEISRISK III: A Computer Program for Seismic Hazard Estimation", *USGS Bulletin 1772*, U.S Government Printing Office.

Boatwright, J., H. Bundock, J. Luetgert, L. Seekins, L. Gee and P. Lombard, 2003, "The Dependence of PGA and PGV on Distance and Magnitude Inferred from Northern California ShakeMap Data", *Bulletin of the Seismological Society of America*, Vol. 93, No. 5, pp. 2043-2055.

Bommer J. J., 2002, "Deterministic vs. Probabilistic Seismic Hazard Assessment: an Exaggerated and Obstructive Dichotomy", *Journal of Earthquake Engineering*, (Special Issue 1), No. 6, pp.43–73.

Bommer J. J., F. Scherbaum, H. Bungum, F Cotton, F. Sabetta, N. A. Abrahamson, 2005, "On the use of Logic Trees for Ground Motion Prediction Equations in Seismic Hazard Analysis", *Bulletin of the Seismological Society of America*, Vol. 95, No.2, pp.377–389.

Bommer J. J., J. Douglas, F. O. Strasser, 2003, "Style-of-faulting in Ground Motion Prediction Equations", *Bulletin of Earthquake Engineering*, Vol. 1, No. 2, pp. 171–203.

Bommer J. J., R. Mendis, 2005, "Scaling of Spectral Displacement Ordinates with Damping Ratios", *Earthquake Engineering and Structural Dynamics*, Vol. 34, No.2, pp. 145–165.

Bommer, J., R. Spence, M. Erdik, S. Tabuchi, N. Aydinoglu, E. Booth, D. del Re, O. Peterken, 2002, "Development of an Earthquake Loss Model For Turkish Catastrophe Insurance", *Journal of Seismology*, Vol. 6, pp. 431-466.

Bommer, J. J., and H. Crownley, 2006, "The Influence of Ground Motion Variability in Earthquake Loss Modelling", *Bulletin of Earthquake Engineering*, Volume 4, Number 3, pp. 231-248.

Boore, D. M., and G. M. Atkinson, 2008, "Ground Motion Prediction Equations for the Average Horizontal Component of PGA, PGV, and 5% - damped PSA at Spectral Periods between 0.01 s and 10.0 s", *Earthquake Spectra*, Vol. 24, pp. 99 –138.

Boore, D. M., W. B. Joyner, and T. E. Fumal, 1997, "Equations for Estimating Horizontal Response Spectra and Peak Accelerations from Western North American

Earthquakes: A Summary of Recent Work", *Seismological Research Letter*, Vol. 68, pp.128-153.

Boore, D. M., 2003, "Simulation of Ground Motion Using the Stochastic Method," *Pure and Applied Geophysics*, Vol. 160, pp. 635 - 676.

Borcherdt, R. D., 1994, "Estimates of Site-dependent Response Spectra for Design (Methodology and Justification)", *Earthquake Spectra*, Vol. 10, pp. 617-654.

Borcherdt, R. D., 1997, "Spatial Ground Motion Amplification Analysis", *Proceedings of Geo-Logan*, July 15-19 1997, No.68, pp. 56–69, Utah.

Bozkurt E., 2001, "Neotectonics of Turkey – a Synthesis", *Geodinamica Acta*, Vol. 14, pp. 3-30.

Braga F, Dolce M, Liberatored, 1982, "A Statistical Study on Damaged Buildings and an Ensuing Review of the M.S.K76 Scale", *Proc. 7th European Conference on Earthquake Engineering*, Athens, September, publ. II-394.

Bramerini F., Di Pasquale G., Orsini A., Pugliese A., Romeo R., Sabetta F., 1995, *Rischio Sismico del Territorio Italiano,* Proposta per Una metodologia e Risultati Preliminari. Rapporto Tecnico del Servizio Sismico Nazionale SSN/RT/95/01, Roma (In Italian).

Burton,P. W, R. W. McGonigle, R. W. Macropoulos and S. B. Üçer, 1984, "Seismic Risk in Turkey, the Aegean, and the Eastern Mediterranean: the Occurrence of large Magnitude Earthquakes", *Geophys.J.R.Astr.Soc*., Vol. 78, pp. 475-506.

Campbell, K. W. And Y. Bozorgnia, 2003, "Updated Near-Source Ground- Motion (Attenuation) Relationships for the Horizontal and Vertical Components of Peak Ground Acceleration and Acceleration Response Spectra", *Bulletin of the Seismological Society of America*, Vol. 93, No, 1, pp. 314-331.

Campbell, K. W., and Y. Bozorgnia, 2008, "Campbell-Bozorgnia NGA Horizontal Ground Motion Model for PGA, PGV, PGD and 5% Damped Linear Elastic Response Spectra", *Earthquake Spectra*, Vol. 24, pp.139–171.

Cemen, İ., M. C. Göncüoglu, K. Dirik, 1999, "Structural Evolution of the Tuzgölü Basin in Central Anatolia, Turkey", *Journal of Geology*, Vol. 107/6, pp. 693–706.

Chekunov A. V., B. G. Pustovitenko, and V. E. Kul'chitskiy, 1994, "Seismicity and Deep Tectonic of the Black Sea Depression and its Margins", *Geotectonics*, Vol. 28, No.3, pp. 221- 225.

Chiou, B., and R. R. Youngs, 2008, "An NGA Model for the Average Horizontal Component of Peak Ground Motion and Response Spectra", *Earthquake Spectra*, Vol. 24, pp.173–215.

Coburn A. and R. Spence, 1992B, "Factors Determining Human Casualty Levels in Earthquakes: Mortality Prediction in Building Collapse", *Proc. of the 10th World Conference on Earthquake Engineering*, Madrid, 19 – 24 July 1992, pp. 5989-5994, Spain.

Coburn A. and R. Spence, 1992-A, *Earthquake Protection*, John Wiley & Sons Ltd., Chichester, England.

Coburn, A. and R. Spence R., 2002, *Earthquake Protection" (Second Edition)*, John Wiley and Sons Ltd., Chichester, England.

Cornell, A., 1968, "Engineering Seismic Risk Analysis", *Bulletin of Seismological Society of America*, Vol. 58, No. 5, 1583-1606, October.

DEE-KOERI, 2003, *Earthquake Risk Assessment for the Istanbul Metropolitan Area*, report prepared by Department of Earthquake Engineering-Kandilli Observatory and Earthquake Research Institute, Bogazici University Press, ISBN 975-518-213-6, Istanbul.

Demets, C., R. Gordon, D.F. Argus and S. Stein, 1990, "Current Plate Motions", *Geophysics Journal International*, Vol. 101, pp. 425-478.

Demirbag E., C. Rangin, X. Le Pichon, A.M.C. Sengor, 2003, "Investigation of the Tectonics of the Main Marmara Fault by Means of Deep-towed Seismic Data", *Tectonophysics*,Vol. 361, pp.1-19.

Demircioglu M., K. Sesetyan, E. Durukal, and M. Erdik, 2007, "Assessement of Earthquake Hazard in Turkey", *Proceedings of the Fourth International Conference on Earthquake Geotechnical Engineering*, Thessaloniki, Greece, 25-28 June 2007, Springer Newyork.

Dewey J. F., W. C., Pitman, W. B. F. Ryan, and J. Bonnin, 1973, "Plate Tectonics and the Evolution of the Alpine Sytem", *Geological Society of America Bulletin*, Vol. 84, pp. 3137-3180.

Dewey, J. F., M. R. Hempton, W. S. F. Kidd, F. Saroglu, and A. M. C. Sengör, 1986, "Shortening of Continental Lithosphere; the Neotectonics of Eastern Anatolia, a Young Collision Zone", *Geological Society Special Publications*, Vol. 19, pp. 3 –36.

Dewey, J. F. and A. M. C. Şengör, 1979 "Aegean and Surrounding Regions: Complex Multiplate and Continuum Tectonics in a Convergent Zone", *Geological Society of America Bulletin*, Part I, Vol. 90, pp. 84-92.

Dewey, J. F., 1976, "Seismicity of Northern Anatolia", *Bulletin of the Seismological Society of America*, Vol.66, pp. 843–868.

Dewey, J. F., 2003, *Ophiolites and Lost Oceans: Rifts, Ridges, Arcs, and/or Scrapings? in Ophiolite Concept and the Evolution of Geological Thought,* Vol. 373, pp. 153–158, eds Dilek, Y. Newcomb, S., Boulder , Colorado.

Dewey, J. F., M. L. Helman, E. Turco, D.H.W. Hutton, S.D. Knott, 1989, "Kinematics of the Western Mediterranean, in Alpine Tectonics", pp. 265–283, eds Coward, M.P., Dietrich, D. Park, R.G., *Geol. Soc. Spec. Publ*. 45, London.

DLH, 2007, *Ulaştırma Bakanlığı Demiryolları, Limanlar Ve Havameydanları İnşaatı Genel Müdürlüğü Kıyı Yapıları, Demiryolları Ve Havameydanları İnşaatları Deprem Teknik Yönetmeliği İçin Deprem Tehlikesi Belirlemesi*, Report prepared by Bogazici University, Kandilli Observatory and Earthquake Research Enstitute, Departement of Earthquake Engineering.

Dubois D, Parade H, 1980, *Fuzzy Sets and Systems*, Academic Press, New York

Durukal, E., M. Erdik, K. Sesetyan, Y. Fahjan, 2006, "Building Loss Estimation for Earthquake Insurance Pricing", *Proceedings of the 8th U.S. National Conference on Earthquake Engineering*, San Francisco, California,18 – 22 April, U.S.A.

Ellul F. and D. D'Ayala, 2003, *The Bingol, Turkey Earthquake of the 1st of May 2003, F*ield report prepared by University of Bath, Architecture and Civil Engineering Department, Earthquake Engineering Field Investigation Team.

Erdik M., Y. Biro, T. Onur, K. Sesetyan, and G. Birgoren, 1999, "Assessment of Earthquake Hazard in Turkey and Neighboring Regions - GSHAP", *Annali di Geofisica*, Vol. 42, No.6.

Erdik, M. M. B. Demircioğlu, K. Şeşetyan, E. Durukal ve B.Siyahi, 2004, "Assessment of Probabilistic Earthquake Hazard in the Marmara Region", *Soil Dynamics and Earthquake Engineering*, Vol: 24, pp. 605–631.

Erdik, M., V. Doyuran, N. Akkaş, P. Gülkan, 1985, "A Probabilistic Assessment of the Seismic Hazard in Turkey", *Tectonophysics*, Vol.117, pp. 195-344.

Erdik, M., V. Doyuran, S. Yücemen, P. Gülkan, and N. Akkaş, 1982, "A Probabilistic Assessment of the Seismic Hazard in Turkey for Long Return Periods", *Proceeding of Third Int. Earthquake Microzonation Conf.*, Seattle, Washington, pp. 1261-1272.

Erdik M., E. Durukal, B. Siyahi, Y. Fahjan, K. Şeşetyan, M. B. Demircioğlu, H. Akman, 2003, *Earthquake Risk Mitigation in Istanbul*, Chapter 7, in Earthquake Science and Seismic Risk Reduction, Ed. by F. Mulargia and R.J. Geller, Kluwer.

Erdik, M. and N. Aydınoglu, 2002, *Earthquake Performance and Vulnerability of Buildings in Turkey*, the World Bank Group Disaster Management Facility Report.

Erdik, M. and S. Oner, 1982, *A Rational Approach for the Probabilistic Assessment of the Seismic Risk Associated with the North Anatolian Fault,* A. Işıkara and Vogel (Editors), Multi-disciplinary Approach to Earthquake Prediction, pp. 115-127, Vieweg, Brauschweig-Wiesbaden,.

Erdik, M., 1996, *Natural Hazards and Vulnerabilities in Turkey*, Report prepared for Oxford Center for Disaster Studies, Oxford, England.

Erdik, M., Ö. Mete, P.Gülkan, 1980, *Malatya-Elazig Railway, Karakaya Bridge: Assessment of Design Earthquake Characteristics*, METU/EERI Report No. 8006.

Ergin, K., U. Guclu, and Z. Uz, 1967, *A Catalogue of Earthquakes for Turkey and Surrounding Area (11AD to 1964AD)*, Tech. Univ. Mining Eng. Fac. Publ., 24, 189, 1967.

ESC- SESAME, 2002, *Unified Hazard Model for the European- Mediterranean Region*, http://www.seismo.ethz.ch/gshap/sesame/

Esteva, L. and E. Rosenblueth, 1964, "Spectra of Earthquakes at Moderate and Large Distances", *Sociedad Mexicana de Ingenieria Sismica*, Mexico II, pp.1-18.

Eurocode 8, 2003, *Design of Structures for Earthquake Resistance*, Draft No. 6, European Committee for Standardization, Brussels.

FEMA 433, 2004, *HAZUS –MH Rsik Assessment and User Group Series*, Federal Emergency Management Agency Report.

FEMA 440, 2005, *Improvement of Nonlinear Static Seismic Analysis Procedures,* Federal Emergency Management Agency (FEMA) Report no.440, Applied Technology Council, Washington D.C., USA.

FEMA366, 1999, *HAZUS99 User and Technical Manuals,* Federal Emergency Management Agency Report: HAZUS 1999, Washington D.C., USA.

FEMA366, 2006, *HAZUS-MH MR2 Technical Manual*, Federal Emergency Management Agency.

FEMA366, 2008, *HAZUS-MH Technical Manual*, Federal Emergency Management Agency, Washington, DC, U.S.A.

Finetti, I., G. Bricchi, G., A. Del Ben, M. Pipan, and Z. Xuan, 1988, "Geophysical Study of the Black Sea", *Bulletino di Geofisica Teorica ed Applicata*, Vol. 30, pp.197-324.

Flerit F., R. Armijo, G.C.P. King, B. Meyer A. Barka, 2003, "Slip Partitioning in the Sea of Marmara Pull-apart Determined from GPS Velocity Vectors", *Geophysics Journal International*, Vol.154, pp.1-7.

Frankel, A. 1995, "Mapping Seismic Hazard in the Central and Eastern United States", *Seismological Research Letters*, Vol. 66, pp. 8-21.

Frankel, A., S. Harmsen, C. Mueller, T. Barnhard, E.V. Leyendecker, D. Perkins, S. Hanson, N. Dickman and M. Hopper, 1997b, "USGS National Seismic Hazard Maps: Uniform Hazard Spectra, D-aggregation, and Uncertainty", *Proceedings, FEMA/NCEER Workshop on the National Representation of Seismic Ground Motion for New and Existing Bridges*, NCEER Pub. 97-0010, F1-F30.

Frankel, A., C. Mueller, T. Barnhard, D. Perkins, E.V. Leyendecker, N. Dickman, S. Hanson and M. Hopper, 1996, *National Seismic Hazard Maps*", U.S. Geol. Surv. Open - File Report. 96 – 532.

Frankel, A., C. Mueller, T. Barnhard, D. Perkins, E.V. Leyendecker, N. Dickman, S. Hanson and M. Hopper, 1997a, *Seismic Hazard Maps for California, Nevada, and western Arizona/Utah*, U.S. Geol. Surv. Open-File Rept. 97-130.

Freund, R., I. Zak, M. Goldberg, T. Weissbrod, B. Derin, 1970, "The Shear along the Dead Sea Rift", *Philos Trans R. Society London,* Vol. 267, pp. 107–130.

Galli, P., 1999, "Active Tectonics along the Wadi Araba-Jordan Valley Transform Fault", *Journal Geophysical Research*, Vol.104, pp. 2777–2796.

Garfunkel, Z., I. Zak, R. Freund, 1981, "Active Faulting in the Dead Sea Rift", *Tectonophysics*, Vol. 80, pp. 1-26.

Garfunkel, Z. and B. Derin, 1984, *Permian-early Mesozoic Tectonism and Continental Margin Formation in Israel and its Implication for the History of the Eastern Mediterranean*, in J.E. Dixon and A.H.F. Robertson (Editors), The Geological Evolution of the Eastern Mediterranean, pp. 187-201, Blackwell Publ., Oxford.

Giardini, D. and P. Basham, 1993, "The Global Seismic Hazard Assessment Program (GSHAP)", *Annali di Geofisica*, Vol. 36, pp. 3-14.

Giardini, D., Editor. 1999, "The Global Seismic Hazard Assessment Program (GSHAP) 1992 - 1999", *Annali di Geofisica*, Special Issue, Vol. 42, No. 6.

Giovinazzi S. and S. Lagomarsino, 2003, "Seismic Risk Analysis: a Method for the Vulnerability Assessment of Built-up Areas", *Proceeding of European Safety and Reliability Conference ESREL,* Maastricht, The Netherlands.

Giovinazzi S. and S. Lagomarsino, 2004, "A Macroseismic Model for the Vulnerability Assessment of Buildings", *Proceeding of 13th World Conference on Earthquake Engineering,* Vancouver, Canada.

Giovinazzi S. and S. Lagomarsino, 2005, "Fuzzy - Random Approach for a Seismic Vulnerability Model", *Proceeding of the 9th International Conference on Structural Safety and Reliability (ICOSSAR)*, Rome, Italy, June 19-23 2005, Millpress, Rotterdam.

Giovinazzi S., 2005, *Vulnerability Assessment and the Damage Scenario in Seismic Risk Analysis*", PhD Thesis, University of Florence.

Giunchi C., R. Sabadini, E. Boschi and P. Gasperini, 1996, "Dynamic Models of Subduction Geophysical and Gelological Evidence in the Tyrrhenian Sea", *Geophysics Journal International*, Vol.126, No.2, pp. 555-578.

Glover, C., A. Robertson, 1998, "Neotectonic Intersection of the Aegean and Cyprus Tectonic Arcs: Extensional and Strike Slip Faulting in the Isparta Angle, SW Turkey", *Tectonophysics*, Vol. 298, pp.103-132.

Göncüoğlu, C.M., V. Toprak, I. Kuşçu, A. Erler, and E. Olgun, 1991, *Orta Anadolu Masifinin Batı Bömlümünü Jeolojisi*, Bölüm 1: Güney kesim: Turkish Petroleum Corporation Report no: 2909, p.140.

Görür, N., F. Y. Oktay, İ. Seymen, M. C. Şengör, 1984, "Paleotectonic Evolution of the Tuz Gölü Basin Complex, Central Turkey, Sedimentary Record of a Neo-Tethyan

Closure", in: Dixon, J.E., Robertson, A.H.F. (Eds.), *The Geological Evolution of the Eastern Mediterranean. Geol. Soc. London Spec. Pub*., vol. 17, pp. 467–482.

Grünthal, G. (editor), 1998, *European Macroseismic Scale 1998*, Cahiers du Centre Européen de Géodynamique et de Séismologie. Conseil de l'Europe. Luxembourg.

Gutenberg, B. and C. F. Richter, 1954, *Seismicity of the Earth and Associated Phenomena,* Princeton University Press, 2nd edition.

Gülen, L., A. Barka and N. Toksöz, 1988, "Continental Collision and Related Complex Deformation: Maraş Triple Junction and Surrounding Structures, SE Turkey", *Spec. Publ*. Hacettepe University, Vol. 14, pp. 319 - 336.

Gülkan,P., A. Koçyiğit, M. S.Yücemen, V. Doyuran and N. Başöz, 1993, *A Seismic Zones Map of Turkey Derived from Recent Data (in Turkish)*, Middle East Technical University, Earthquake Engineering Research Center, Report No:93-01, Ankara.

Gürsoy, H., O. Tatar, JDA Piper, A. Heimann, L. Mesci, 2003, "Neotectonic Deformation Linking the East Anatolian and Karatas- Osmaniye Intercontinental Transform Fault Zones in the Gulf of Iskenderun, Southern Turkey, Deduced from Paleomagnetic Study of the Ceyhan-Osmaniye Volcanics", *Tectonics*, Vol.22, No.6, pp. 1067.

Hattori, S., 1979, "Seismic Risk Maps in the World", *Bull. Int Inst. Seismol. Earthquake Engineering.*, Vol. 17, pp.33 - 96.

Herring, T. A., 1999, "Geodetic Applications of GPS", *Proceedings of the IEEE*, Vol. 87, pp. 92–110.

Hubert-Ferrari A, R. Armijo, G. King, B. Meyer and A. Barka, 2002, "Morphology, Displacement, and Slip Rates along the North Anatolian Fault, Turkey", *Journal of Geophysical Research*, Vol. 107, No. B10, pp. 2235.

IBC, 2000, *International Building Code*, International Code Council, U.S.A.

IBC, 2006, *International Building Code*, International Code Council, U.S.A.

IBC,2003, *International Building Code*, International Code Council, U.S.A.

Idriss, I. M., 2008, "A NGA Empirical Model for Estimating the Horizontal Spectral Values Generated by Shallow Crustal Earthquakes", *Earthquake Spectra*, Vol. 24, pp. 217 – 242.

Imren C., X. Le Pichon, C. Rangin, E. Demirbag, B. Ecevitoglu N. Gorur, 2001, "The North Anatolian Fault within the Sea of Marmara: a New Interpretation Based on Multi-channel Seismic and Multibeam Bathymetry Data", *Earth and Planetary ScienceLetters*, Vol.186, pp.143-158.

Jimenez, M., D.Giardini, G.Grünthal, M.Erdik, M.Garcia-Fernandez, J. Lapajne, K. Makropoulos, R. Musson, Ch. Papaioannou, A. Rebez, S. Riad, S. Sellami, A. Shapira, D. Slejko, T. van Eck, A. El Sayed, 2001, "Unified Seismic Hazard Modeling throughout the Mediterranean Region", *Bolletino di Geofisica Teorica ed Applicata*, Vol.42, pp.3-18.

Jordanovski, L. R., and M. I. Todorovska, 1995, "Earthquake Source Parameters for Seismic Hazard Assessment: How to Obtain them from Geoloogic Data, Historic Seismicity and Relative Plate Motions, in G. Duma (Ed.)", *Proc. 10th European Conf. Earthquake Engineering*, Vienna, Austria, 28 August – 2 September 1994, Vol. 4, pp. 2561-2566, Balkema, Rotterdam.

Juteau, T., J. P. Eissen, A. S. Monin, L. P. Zonenshain, O. G. Sorokhtin, V. V. Matveenkov, and A. I. Almukhademov, 1983, "Structure et Pétrologie du Rift Axial de la Mer Rouge vers 18° Nord: Résultats de la Campagne Soviétique de Plongées avec Submersible", *Bulletin du Centre des Recherches Exploration—Production Elf-Aquitaine*, Vol. 7, pp. 217–231.

Ketin, I., 1948, "Uber die Tektonisch-mechanischen Folgerungen aus den Grossen Anatolischen Erdbeben des Letzten Dezenniums", *Geol. Rundsch.*, Vol. 36, pp.77-83.

Ketin I., 1963, *Explanatory Text of the 1/500,000 Scale Geologic Map of Turkey, Kayseri Quadrangle*, Maden ve Teknik Arama (MTA), pp. 83, Ankara.

Ketin, I., 1966, “6 Ekim 1964 Manyas Depremi Esnasıda Zeminde Meydana Gelen Tansiyon Çatlakları”, *Türk. Jeol. Kurumu Bül*., Vol. 10, pp.1-2.

Ketin, I., 1969, “Kuzey Anadolu Fayı Hakkında”, *Bull. Miner. Res. Explor. Inst. Turk*., Vol.76, pp.1-25.

Khair, K., G.F. Karakaisis, and E.E. Papadimitriou, 2000, “Seismic Zonation of the Dead Sea Transform Fault Area”, *Annali di Geofisica*, Vol. 43, pp. 61–79.

Kircher C. A, A. A. Nassar, O. Kustu, W. T. Holmes, 1997, “Development of Building Damage Functions for Earthquake Loss Estimation”, *Earthquake Spectra*, Vol. 13, No.4, pp.663–682.

Kiremidjian, A. S., C. Mortgat and H.Shah, 1992, *Stanford Seismic Hazard Analysis-STASHA*, The John Blume Earthquake Enineering Center, Technical report, Stanford University, Stanford, CA.

KOERI (Department of Earthquake Engineering), 2002, “Earthquake Risk Assessment for Istanbul Metropolitan Area”, Report prepared for American Red Cross and Turkish Red Crescent, Bogazici Univeristy, Istanbul, Turkey.

Kocyigit, A., A. Beyhan, 1997, “A new Intracontinental Transcurrent Structure: the Central Anatolian Fault Zone, Turkey”, *Tectonophysics*, Vol.284, pp.317– 336.

Kocyiğit, A., 1991, “Changing Stress Orientation in Progressive Intracontinental Deformation as Indicated by the Neotectonics of the Ankara Region (NW Central Anatolia): Trk”, *Assoc. Petrol. Geol. Bull.*, Vol. 3, No.1, pp: 48-55.

Koçyiğit, A., 1988, “Tectonic Setting of the Geyve Basin: Age and Total Displacement of Geyve Fault Zone”, *METU Pure Appl. Sci*., Vol. 21, pp. 81-104.

Koçyiğit, A., 1989, “Suşehri Basin: an Active Fault-wedge Basin on the North Anatolian Fault Zone, Turkey”, *Tectonophysics*, Vol.167, pp.13-29.

Koçyiğit, A., 1991, Neotectonic Structures and Related Landforms Expressing the Contractional and Extensional Strains along the North Anatolian Fault at the

Northwestern Margin of the Erzincan Basin, NE Turkey", *Bull. Tech. Univ*ersity, Istanbul 44, 455-473.

Koçyiğit, A., A. Beyhan, 1998, "A new Intracontinental Transcurrent Structure: the Central Anatolian Fault Zone, Turkey", *Tectonophysics*, Vol.284, pp.317– 336.

Kusku, M., H. Okamura, Y. Matsuoka, Y. Awata, 2002, "Active Faults in the Gulf of Izmit on the North Anatolian Fault, NW Turkey: a High-resolution Shallow Seismic Study", *Marine Geology*, Vol. 190, pp.421-443.

Lagomarsino, S., and S. Giovinazzi, 2006, "Macroseismic and Mechanical Models for the Vulnerability and Damage Assessment of Current Buildings", *Bulletin of Earthquake Engineering*, Vol. 4, pp. 415-443.

Le Pichon, *MARMARA SURVEY, 11 Sep - 4 Oct 2000, Cruise Report Web site*, www.cdf.u-3mrs.fr/ lepichon/marmara/

Le Pichon X., A. M. C. Sengor, E. Demirbag, C. Rangin, C. Imren, R. Armijo, N. Gorur, N. Cagatay, B.M. de Lepinay, B. Meyer, R. Saatchilar, B. Tok, 2001, "The Active Main Marmara Fault", *Earth and Planetary Sc.Letters*, Vol.192, pp. 595-616.

Le Pichon X., N. Chamot - Rooke, C. Rangin, A. M. C. Sengor, 2003, "The North Anatolian Fault in the Sea of Marmara", *Journal of Geophysical Research*, Vol. 108, pp. 2170-2179.

Le Pichon, X., T. Taymaz, A.M.C. Sengor, 1999, "The Marmara Fault and the Future Istanbul Earthquake, in: International Conference on the Kocaeli Earthquake, 17 August 1999", *Proceeding of International Conference on the Kocaeeli Earthquake, 17 August 1999*, pp. 41-54.

Matar, A. and G. Mascle, 1993, "Cinematique de la Faille du Levant au nord de la Syrie: analyse microtectonique du Fosse döAlghab", *Geodinamica Acta*, Vol. 6, pp.153-160.

Meredith D. J. and S. S. Egan, 2002, "The Geological and Geodynamic Evolution of the Eastern Black Sea Basin: Insights from 2-D and 3-D Tectonic Modelling", *Tectonophysics*, Vol. 350, pp. 157–179.

Medvedev S. V. (Ed), 1968, *Seismic Zoning of the USSR*, 476 pp., Nauka, Moscow.

McClusky, S., S. Bassalanian, A. Barka, C. Demir, S. Ergintav, I. Georgiev, O. Gurkan, M. Hamburger, K. Hurst, H.-G. Hans-Gert, K. Karstens, G. Kekelidze, R. King, V. Kotzev, O. Lenk, S. Mahmoud, A. Mishin, M. Nadariya, A. Ouzounis, D. Paradissis, Y. Peter, M. Prilepin, R. Relinger, I. Sanli, H. Seeger, A. Tealeb, M.N. Toksaz, G. Veis, 2002, "Global Positioning System Constraints on Plate Kinematics and Dynamics in the Eastern Mediterranean and Caucasus", *Journal of Geophysical Research*, Vol. 105 (B3), pp. 5695-5719.

McGuire R. K., C. A. Cornell, G. R. Toro, 2005, "The Case for Using Mean Seismic Hazard", *Earthquake Spectra*, Vol. 21, No.3, pp. 879–886.

McGuire, K. R, 1976, *FORTRAN Computer Program for Seismic Risk Analysis*, United State Geological Survey open file report, No. 76-67.

McGuire, R. K., 1993, "Computations of Seismic Hazard", *Annali di Geofisica*, Vol.36, pp.181-200.

McGuire, R. K., 1993, "The Practice of Earthquake Hazard Assessment", *Special Volume. IASPEI,* pp. 284.

McGuire, R., 2001, "*FRISK-88M User's Manual* (version 1.80)", Risk Engineering Inc., Boulder, Colorado.

McGuire, R., 2004, *Seismic Hazard and Risk Analysis*, EERI Monograph MNO-10. Earthq. Eng. Res. Inst., Oakland, California.

McGuire, R., W. Silva and C. Costantino, 2002, *Technical Basis for Revision of Regulatory Guidance on Design Ground Motions: Development of Hazard and Risk-Consistent Seismic Spectra for Two Sites*, U.S. Nuclear Reg. Comm., Report NUREG/CR-6769.

McKenzie, D. P., 1970, "Plate Tectonics of the Mediterranean Region", *Nature*, Vol. 226, pp. 239-243.

McKenzie, D. P., 1972, "Active Tectonics of the Mediterranean Region", *Geophysical Journal of Research Astr. Soc.,* Vol. 30, pp. 109-185.

Meghraoui, M., F. Gomez, R. Sbeinati, J.V. derWoerd, M. Mouty, M., A.N. Darkal, Y. Radwan, I. Layyous, H.A. Najjar, R. Darawcheh, F. Hijazi, R. Al-Ghazzi, and M. Barazangi, 2003, "Evidence for 830 Years of Seismic Quiescence from Palaeoseismology, Archaeoseismology and Historical Seismicity along the Dead Sea Fault in Syria", *Earth Planet. Sci. Let*., Vol. 210, pp. 35-52.

Metz, K., 1956, "Aladağ ve Karanfil Dağının Yapısı ve Bunların Kilikaya Torosu Tesmiye Edilen Batı Kenarı Hakkında Malumat Husulu için Yapılan Jeolojik Etud", *MTA Bulletin*, Vol .48, pp. 63-76.

Molina, S. and C. D. Lindholm, 2006, "A Capacity Spectrum Method based Tool Developed to Properly Include the Uncertainties in the Seismic Risk Assessment, under a Logic Tree Scheme", *Proceeding of ECI. Geohazards – Technical, Economical and Social Risk Evaluation, 18–21 June 2006*, Lillehammer, Norway.

Morelli C., 1978, "Eastern Mediterranean: Geophysical Results and Implications" *Tectonophysics*, Vol. 46, Issue 3-4; pp. 333-346.

Muehlberger W. R, M. B. Gordon, 1987, "Observations on the Complexity of the East Anatolian Fault Turkey", *Journal of Structural Geology*, Vol. 9, pp. 899–903.

Multinovic Z., and G. Trendafiloski, 2003, "-*WP4 Vulnerability of Current Buildings*, RISK-UE proje Handbook, September 2003, RISK-UE Project, pp. 111.

Muir-Wood, R., 1993, "From Global Seismotectonics to Global Seismic Hazard", *Annali di Geofisica*, Vol. 36, pp. 153-169.

Murakami H. O., 1992, "A Simulation Model to Estimate Human Loss for Occupants of Collapsed Buildings in an Earthquake," *Proceedings of the 10th WCEE*, Madrid, Spain, 19 – 24 July 1992, pp.5969 -5974,., Balkema, Rotterdam.

Musson R. M. W., 2004, "Objective Validation of Seismic Hazard Source Models", *Proceedings of 13th World Conference on Earthquake Engineering,* Vancouver. 1 – 6 August 2004, Paper 2492, pp. 11.

Musson R. M. W., 2005, "Against Fractiles", *Earthquake Spectra*, Vol. 21, No.3, pp. 887–891.

Musson R.M.W., 2005, "Intensity Attenuation in the UK", *Journal of Seismology*, Vol. 9, No. 1, pp. 73–86.

Nalbant, S., J. McCloskey, and S. Steacy, 2005, "Lessons on the Calculation of Static Stress Loading from the 2003 Bingol, Turkey Earthquake", *Earth and Planetary Science Lette*r, Vol. 235, pp. 632:640.

Nalbant, S., J. McCloskey, S. Steacy and A. Barka, 2002, "Stress Accumulation and Increased Seismic Risk in Eastern Turkey", *Earth and Planetary Science Letters*, Vol. 195, pp. 291-298.

NEHRP2003, 2003, *Recommended Provisions For New Buildings and Other Structures, FEMA-450*, prepared by the Building Seismic Safety Council for the Federal Emergency Management Agency, Washington, DC.

NEHRP97, 1997, *Recommended Provisions for Seismic Regulations for New Buildings and Other Structures, FEMA-303*, Prepared by the Building Seismic Safety Council for the Federal Emergency Management Agency, Washington, DC.

Nikishin A., P. A. Ziegler, D. I. Panov, B. P. Nazarevich, M.-F. Brunet, R. A. Stephenson, S. N. Bolotov, M. V. Korotaev and P. L. Tikhomirov, 2001, "Mesozoic and Cenozoic Evolution of the Scythian Platform–Black Sea–Caucasus Domain", in: P. A. Ziegler, W. Cavazza, A. H. F. Robertson and S. Crasquin-Soleau, Editors, Peri-Tethys Memoir 6: Peri-Tethyan Rift/Wrench Basins and Passive Margins Mémoires du Muséum National d'Histoire naturelle, Paris , Vol. 186, pp. 295–346.

Okay, A.I., A. Kaslilar-Ozcan, C. Imren, A. Boztepe-Guney, E. Demirbag, I. Kuscu, 2000, "Active Faults and Evolving Strike-slip Basins in the Marmara Sea, Northwest

Turkey: a Multichannel Seismic Reflection Study", *Tectonophysics*, Vol. 321, pp. 189-218.

Okay, A. I., O. Tuysuz, S. Kaya, 2004, "From Transpression to Transtension: Changes in Morphology and Structure around a Bend on the North Anatolian Fault in the Marmara Region", *Tectonophysics*, Vol. 391, pp. 259-282.

Oliveira C. S. and Mendes Victor L. A., 1984, "Prediction of Seismic Impact in a Metropolitan Area Based on Hazard Analysis and Microzonation: Methodology for the Town of Lisbon", *Proc. of the 8th World Conference on Earthquake Engineering*, El Cerrito, July 21 -28 1984, Vol. VII, pp. 639-646, El Cerrito, California.

Onur, T., 1997, *Eartquake Hazard in Turkey based on Spectral Acceleration Amplituudes*, M. S. Thesis, Bogazici Univeristy, Department of Earthquake Engineering.

Oral, B., R. E. Reilinger, M. N. Toksoz, R. W. King, A. A. Barka, I. Kinik, and O. Lenk, 1995, "Global Positioning System Offers Evidence of Plate Motions in Eastern Mediterranean", *EOS, Trans. American Geophysical Union.* Vol. 76, pp. 2.

Ordaz, M., 2007, *CRISIS2007 User Manual,* Institute of Engineering, UNAM, Mexico.

Over S., Unlugenc, U. C. and Bellier O., 2002, "Quaternary Stress Regime Change in the Hatay Region (SE Turkey)", *Geophysics Journal International*, Vol. 148, pp. 649–662.

Oztin, F., N. Bayulke, 1990, "Historical Earthquakes of Istanbul and Corrections to the Original Version. Kayseri and Elazig", in: Turkish Atomic Energy Authority (Ed.), *Proceedings of Workshop on Historical Seismicity and Seismotectonics of the Mediterranean Region,* IstanbuI, 10–12 October 1990, pp. 234 – 253, Turkish Atomic Energy Authority Ankara.

Özbey, C., A. Sari, L. Manuel, M. Erdik, Y. Fahjan, 2004, "An Empirical Attenuation Relationship for Northwestern Turkey Ground Motion Using A Random Effects Approach", *Soil Dynamics and Earthquake Engineering*,Vol. 24, No. 2, pp. 115 – 125.

Papazachos, B. C., 1974, "On Certain Aftershock and Foreshock Parameters in the Area of Greece", *Annali di Geofisica*, Vol. 27, pp. 497–515.

Papazachos, C.B., 1999, "An Alternative Method for a Reliable Estimation of Seismicity with an Application in Greece and Surrounding Area", *Bulletin of Seismological Society of America,* Vol. 89, pp. 111 – 119.

Park, S., and S. Elrick, 1998, "Predictions of Shear-wave Velocities in Southern California Using Surface Geology", *Bulletin of Seismological Society of America*, Vol. 88, pp. 677-685.

Parsons, T., S. Toda, R. Stein, A. Barka, A Dieterich, 2000, "Heightened Odds of Large Earthquake near Istanbul: An Interaction-based Probability Calculation", *Science*, Vol.288, pp. 661–665.

Pavoni, N., 1961, "Die Nordanatolische Horizontal Verschieburg", *Geol. Rundsch*, Vol.51, pp. 121-139.

Pinar, N., 1943, "Marmara Denizi Havzasının Sismik Jeolojisi ve Meteorolojisi", *Science Faculty Monographies*, A7, p64.

Ponikarov V. P.(editor-in-chief), 1967, *The Geological Map of Syria Scale 1:500000, Explanatory notes*, Syrian Arab Republic, Ministry of Industry, Damascus, Syria.

Quennell, A. M., 1958, "The Structural and Tectonic Evolution of the Dead Sea Rift Quarterly, *Journal of the Geological Society of London*, Vol. 114, pp. 1–24.

Quennell, A. M., 1959, "Tectonics of the Dead Sea Rift", *Proceedings of the 20th International Geological Congress*, Mexico, pp. 385–403.

Stein R. S., A. Barka, J. H. Dieterich, 1997, "Progressive Failure on the North Anatolian Fault since 1989 by Earthquake Stress Triggering", *Geophysical Journal International*, Vol. 128, pp. 594-604.

RADIUS, 1999, *Risk Assessment Tools for Diagnosis of Urban Areas against Seismic Disasters. Cities Involved: Tijuana-Mexico, Guyaquil-Ecuador, Antofagasta-Chile,*

Skopje-FYROM, Izmir-Turkey, Addis Ababa-Ethiopia, Tachkent-Ouzbekistan, Bandung-Indonesia, Zigong-China Report" United Nations initiative towards Earthquake Safe Cities, http://www.geohaz.org/contents/projects/radius.html

Rangin, C., A. G Bader, G. Pascal, B. Ecevitoglu, N. Görür, 2002, "Deep Structure of the Mid Black Sea High (offshore Turkey) Imaged by Multi-channel Seismic Survey (BLACKSIS cruise)", *Marine Geology*, Vol.182, pp.265–278.

Rangin, C., E. Demirbag, C. Imren, A. Crusson, A. Normand, E. Le Drezen, A. Le Bot, 2001, *Marine Atlas of the Sea of Marmara (Turkey), Special publication by* Ifremer Brest Technology Center, France.

Reilinger, R. E., S. C. McClusky, M. B. Oral, R. W. King, M. N. Toksoz, A. A. Barka, I. Kinik, O. Lenk, and I. Sanli, 1997, "Global Positioning System Measurements of Present-day Crustal Movements in the Arabia-Africa- Eurasia Plate Collision Zone", *Journal of Geophysical Research Solid Earth*, 102(B5), pp. 9983–9999.

Reilinger, R., S. McClusky, P. Vernant, S. Lawrence, S. Ergintav, R. Cakmak, H. Ozener, F. Kadirov, I. Guliev, R. Stepanyan, M. Nadariya, G. Hahubia,.S. Mahmoud, K. Sakr, A. ArRajehi, D. Paradissis, A. Al-Aydrus, M. Prilepin, T. Guseva, E. Evren, A. Dmitrotsa, S. V. Filikov, F. Gomez, R. Al-Ghazzi,17 and G. Karam, 2006, "GPS constraints on continental deformation in the Africa-Arabia-Eurasia continental collision zone and implications for the dynamics of plate interactions", *Journal Of Geophysical Research*, Vol. 111, B05411, Doi:10.1029/2005jb004051.

Reiter, L., 1990, *Earthquake Hazard Analysis*, *Issues and insights*, Colombia University Press.

RGELFE (Research Group for Estimating Losses from Future Earthquakes), 1992, *Estimating Losses form Earthquakes in China in the Forthcoming 50 years,* State Seismological Bureau, Seismological Press, Beijing.

Richter, C.F., 1958, *Elementary Seismology*, W. H. Freeman and Co. Inc., San Francisco.

RISK-UE (2001–2004), *An Advanced Approach to Earthquake Risk Scenarios, with Applications to Different European cities*, http://www.risk-ue.net.

Robinson A.G., Editor, 1997, *Regional and Petroleum Geology of the Black Sea and Surrounding Region American Association of Petroleum Geologists, Memoir*, Vol. 68, pp. 385, Tulsa.

Ross T. J., 1995, Fuzzy *Logic with Engineering Applications*, McGraw Hill, New York.

Sadigh K, C.Y. Chang, J.A. Egan, F. Makdisi, R.R. Youngs, 1997, "Attenuation Relationships for Shallow Crustal Earthquakes Based on California Strong Motion Data*," Seismological Research Letters*, Vol. 68 (1), pp. 180-189.

Sancio R. B., J. D., Bray, J. P. Stewart, T. L. Youd, H. T. Durgunoglu, A. Onalp, R. B. Seed, C. Christensen, M. B. Baturay, T. Karadayilar, 2002, "Correlation Between Ground Failure and Soil Conditions in Adapazari, Turkey", *Soil Dynamics and Earthquake Engineering*, Vol. 22, pp.1093-1102.

Saroglu, F., Emre, O. and Boray, A., 1987, *Active Fault and Seismicity of Turkey (Türkiye'nin Diri Faylari ve Depremsellikleri)*, General Directorate of MTA, Geological Research Department, pp.394, Ankara.

Saroğlu, F., O. Emre and I. Kuscu, 1992, *Active Fault Map of Turkey*, Mineral Res. Explor. Inst., Turkey.

Schwartz, D. P., and K.J. Coppersmith, 1984, "Fault Behavior and Characteristic Earthquakes from the Wasatch and San Andreas Faults," *Journal of Geophysical Research*, Vol 89, pp 5681 - 5698.

Scott B., 1981, "The Eurasian – Arabian and African Continental Margin from Iran to Greece ", *Journal of Geoogical Society of London*, Vol. 138, pp. 7684-7706.

SEAONC, 2007, *Recommended Administrative Bulletin on the Seismic Design and Review of Tall Buildings Using Non-Prescriptive Procedures, Prepared by Structural Engineers Association of Northern California (SEAONC),* AB-083 Tall Buildings Task Group, San Francisco, California.

Segall, P. and J. L. Davis, 1997, "GPS Application for Geodynamics and Earthquake Studies", *Annual Rev. Earth Planet. Sci*., Vol. 25, pp. 301–336.

Şengör , A. M. C. and Y. Yılmaz, 1983, *Türkiye'de Tetis'in Evrimi: Levha Tektonigi Açisindan Bir Yaklaşim*, Türkiye Jeoloji Kurumu Yerbilimleri Özel Dizisi 1, pp. 75, Istanbul.

Sengor A.M.C., N. Gorur, F. Saroglu, 1985, "Strike-slip Faulting and Related Basin Formation in Zones of Tectonic Escape: Turkey as a Case study*"*, Biddle K.D., Christie-Blick N. (eds.) *Strike-slip Deformation, Basin Formation, and Sedimentation. SEPM Spec. Publ.*17, pp. 227-264.

Sengor, A. M. C., 1987, "Cross-faults and Differential Stretching of Hanging Walls in Regions of Low Angle Normal Faulting: Examples from Western Turkey", in: *Continental Extensional Tectonics*, edited by: M. P. Coward, J. F. Dewey and P. L. Hancock, *Geological Society, London, Special Publication*, No: 28, pp: 575-589.

Sengor A.M.C., 1979, "The North Anatolian Transform Fault: its Age, Offset and Tectonic Significance", *Journal of Geological Society of London*, Vol. 136, pp. 269-282.

Sengor A. M. C., O. Tuysuz, C. Imren, M. Sakinc, H. Eyidogan, N. Gorur, X. Le Pichon, C. Claude Rangin, 2004, "The North Anatolian Fault. A new Look," *Ann. Rev. Earth Planet*. Sci. 33, 1-75.

Sesetyan K., E. Durukal, M. B. Demircioglu, and M. Erdik, 2005, "A Revised Intensity Attenuation Relationships for Turkey", *EGU poster presentation.*

Seymen, I. and A. Aydin, 1972, "Bingol Deprem Fayi ve Bunun Kuzey Anadolu Fayi ile Iliskisi", *M.T.A. Bul*., Vol. 79, pp. 33–39.

Shiono, K., Krimgold, F. and Ohta, Y., 1991, "A Method for the Estimation of Earthquake Fatalities and its Applicability to the Global Macro-Zonation of Human Casualty Risk," *Proc. Fourth International Conference on Seismic Zonation*, Standford, August 25 -29 1991, Vol. III, pp. 277 – 284, Stanford, CA.

Spence R., J. Bommer, D. Del Re, J. Bird, N. Aydinoglu and S. Tabuchi, 2003, "Comparison Loss Estimation with Observed Damage: A study of the 1999 Kocaeli Earthquake in Turkey", *Bulletin of Earthquake Engineering*, Vol. 1, pp. 83-113.

Stein, R. S. and A. A. Barka, 1995, "Stress Triggering of Progressive Earthquake Failure on the North Anatolian Fault, Turkey, Since 1939: Implications for the Interaction of Faults and the Forecast of Hazard", *Proc.11th Course: Active Faulting Studies for Seismic Hazard Assessment, Int. School of Solid Earth Geophysics*, Italy.

Strasser F. O., Bommer, J.J., Sesetyan, K., Erdik, M., Cagnan Z., Irizarry J., Goula X., Lucantoni A., Sabetta F., Bal I.E., Crowly H., Lindholm C., 2007, "A Comparative Study of European Earthquake Loss Estimation Tools for A Scenario in Istanbul", *Proceedings of HAZTURK 2007 - International Symposium on Earthquake Loss Estimation for Turkey*, Istanbul.

Strasser F. O., J. J. Bommer, K. Sesetyan, M. Erdik, Z. Çagnan, J. Irizarry, X. Goula, A. Lucantoni, F. Sabetta, I. E. Bal, H. Crowley, C. Lindholm., 2008, "A Comparative Study of European Earthquake Loss Estimation Tools for a Scenario in Istanbul", *Journal of Earthquake Engineering,* Vol. 12, No. 1, pp. 246-256.

Şengör, A. M. C., 1980, *Türkiye'nin Neotektoniğinin Esasları 'Principles of the Neotectonism of Turkey'*, Turkiye Jeoloji Kurumu, Ankara.

Şengör, A. M. C., and Y. Yilmaz, 1981, "Tethyan Evolution of Turkey; a Plate Tectonic Approach", *Tectonophysics*, Vol. 75, No. 3-4, pp. 181-241.

Şengör, A. M. C., Görür, N., Saroglu, F., 1985, "Strike-slip Faulting and Related Basin Formation in Zones of Tectonic Escape: Turkey as a Case Study. In: Biddle, K.T., Christie-Blick, N. (Eds.), Strike-slip Faulting and Basin Formation, *Soc. Econ. Paleontol Mineral. Spec. Publ.*, Vol. 37, pp. 227 - 264.

Şengör, A. M. C., O. Tüysüz, C.İmren, M. Sakınç, H. Eyidoğan, N. Görür, X. Le Pichon, C. Claude Rangin, 2004, "The North Anatolian Fault. A New Look", *Annu. Rev. Earth Planet. Sci,* Vol. 33, pp.1–75.

Spence R., 1999, *Intensity, Damage and Loss in Earthquakes in Seismic Damage to Masonry Buildings*, Balkema, Rotterdam.

Stepp, J. C., 1973, *Analysis of Completeness of the Earthquake Sample in the Puget Sound Area*, In: S.T. Handing (Editor), Contributions to Seismic Zoning. NOAA Tech. Report., ERL 267-ESL 30, U.S. Dep. of Commerce, USA.

Tari E., M. Şahin, A. Barka, R. Reilinger, R.W. King, S. McClusky and M. Prilepin, 2000, "Active Tectonics of the Black Sea with GPS", *Earth Planets Space*, Vol. 52, pp. 747–751.

Tari, E., 1999, "1st and 2nd Progress Reports Submitted to TUBITAK and ITU about the Post Doctoral Research at MIT (unpublished).

Tatar, O., J. D. A Piper, H. Gürsoy, A. Heimann, F. Koçbulut, 2004, "Neotectonic Deformation in the Transition Zone between the Dead Sea Transform and the East Anatolian Fault Zone, Southern Turkey: a Paleomagnetic Study of the Karasu Rift Volcanism", *Tectonophysics*, Vol. 385, pp. 17-43.

Tchalenko J. S., 1997, "A Reconnaissance of the Seismicity and Tectonics at the Northern Border of the Arabian plate (Lake Van region)", *Rev. Géogr. Phys. Géol. Dyn*., Vol.19, pp. 189–208.

Tchalenko, J. S., 1977, "A Reconnaissance of the Seismicity and Tectonics At the Northern Border of the Arabian Plate (Lake Van Region)", *Révue de Géographie Physique et de Géologie Dynamique (2)*, Vol. XIX, Fasc. 2, pp. 189-208, Paris.

TEFER (Turkey Emergency Flood and Earthquake Recovery), 2000, *A Probabilistic Seismic Hazard Assessment For Turkey,* Report prepared in connection with the Improvement Of Natural Hazard Insurance And Disaster Funding Strategy Project, Başbakanlık Hazine ve Dış ticaret Müsteşarlığı - Sigortacılık Genel Müdürlüğü.

Temel Ö. and Çiftçi, 2002, "Gelibolu Yarimadaları, Gökçeada ve Bozcaada Tersiyer Çökellerinin Stratigrafisi ve Ortamsal Özellikleri", *TPJD Bulletin* **,** Vol. 14, No.2**,** pp. 1740 (in Turkish).

Ten Veen, J. H., S. J. Boulton, M. C. Alçiçek, 2009, "From Palaeotectonics to Neotectonics in the Neotethys Rrealm: The Importance of Kinematic Decoupling and

Inherited Structural Grain in SW Anatolia (Turkey)", *Tectonophysics*, No. 473, pp. 261 – 281.

Tsapanos, T. M., Leventakis, G. A., Koravos G. Ch., Tatsiopoulos G. A., and Sertaridou I Ch., 2005, "Seismic Hazard and Seismic Rasik Analysis in Turkey Deduced form Mixed Files", *Journal of Balkan Geophysical Society*, Vol.8, No.3 p:89-98.

Tugolesov, T. A, A. S Gorshkov, L. B. Meisner, V. V. Soloviev, E. M. Khakalev, 1985, "Tectonics of the Black Sea Basin", *Geotectonik*a, Vol.6, pp. 3–20 (in Russian).

TurkStat (Turkiye Istatistik Kurumu, Turkish Statistical Institute), http://www.tuik.gov.tr/Start.do

Uygun, A., 1981, "Tuz Gölü Havzasının Jeolojisi, Evaporit Oluşumları ve Hidrokarbon Olanakları", İç *Anadolu'nun Jeolojisi Sempozyumu, Geological Bulletin of Turkey* pp.66–76 (in Turkish), Turkey.

Vacareanu R., Lungu D., Arion C., Aldea A., 2004, *WP7 Report: Seismic Risk Scenarios. Risk-UE Project - An Advanced Approach to Earthquake Risk Scenarios with Applications,* http://www.risk-ue.net.

Veneziano, D., C. A., Cornell and T. O'Hara, 1984, "Historical Method of Seismic Hazard Analysis*", Elect. Power Res.., Inst*. Rep., NP-3438, Palo, Alto.

Wald, D. J., V. Quitoriano, T. H. Heaton, H. Kanamori, 1999b, "Relationship between Peak Ground Acceleration, Peak Ground Velocity, and Modified Mercalli Intensity for Earthquakes in California", *Earthquake Spectra*, Vol. 15, No. 3, pp. 557-564.

Wald, David J.; Worden, Bruce C.; Quitoriano, Vincent; Pankow, Kris L., 2005, "ShakeMap Manual: Technical Manual, User's Guide, and Software Guide".

Weichert, D. H., 1980, "Estimation of the Earthquake Recurrence Parameters for Unequal Observation Periods for Different Magnitudes", *Bulletin of Seismological Society of America*, Vol. 70, pp. 1337-1346.

Wells and Coppersmith, 1994, "New Emprical Relationships among Magnitude, Rupture Length, Rupture Width, Rupture Area and Surface Displacement", *Bulletin of Seismological Society of America*, Vol. 184, pp 963-1291.

Wenk T., C. Lacave, K. Peter, 1998, *Adana –Ceyhan Earthquake of June 27, 1998*, report on the Reconnaissance Misson from 6-12, 1998 of the Swiss Society of Earthquake Engineering and Structural Dynamics (SGE), http://www.ibk.baum.ethz.ch/publ/Ba/WLP98a.html

Westaway R, J. Arger, 1996, "The Gölbaşı Basin Southern Turkey: a Complex Discontinuity in a Major Strike-Slip Fault Zone", *J Geol Soc (London)*, Vol. 153, pp.729–744.

Westaway, R., 1994, "Present-day Kinematics of the Middle East and Eastern Mediterranean", *Journal of Geophysical Research,* Vol. 99(B6), pp. 12071-12090.

Westaway, R., 2003, "Kinematics of the Middle East and Eastern Mediterranean Updated. Turkish*", Journal of Earth Sciences (Turkish J. Earth Sci.)*, Vol. 12, pp.5- 46.

Wong H. K., T. Ludmann, A. Ulug, N. Gorur, 1995, "The Sea of Marmara: A Plate Boundary Sea in an Escape Tectonic Regime", *Tectonophysics*, Vol. 244, pp. 231-250.

Woodside, J. M., 1976, "Regional Vertical Tectonics in the Eastern Mediterranean", *Geophys. J. R. Astron. Soc.,* Vol. 47, pp. 493-514.

Yaltırak, C., B. Alpar, H. Yuce, 1998, "Tectonic Elements Controlling the Evolution of the Gulf of Saros (Northeastern Aegean Sea)", *Tectonophysics*, Vol. 300, pp. 227-248.

Yang, T., 2005, *ATC-55 Project,* http://peer.berkeley.edu/~yang/ATC55_website

Yarar, R., Ergünay, O., Erdik, M. and Gülkan, P., 1998, "A Preliminary Probabilistic Assessment of the Seismic Hazard in Turkey", *Proc. 7th World Conf. Earthquake Eng.*, Istanbul, pp. 309 – 316.

Yetiş C., 1978, *Camardi (Niğde ili) Yakın ve Uzak Dolayının Jeolojisi İncelenmesi ve Ecemiş Yarılım Kuşağının Maden Boğazı-Kamisli Arasındaki Özellikleri*, Ph.D. Thesis, Istanbul University.

Yetis, C., C. Demirkol, 1986, *Detailed Geologic Investigation of the Western Side of the Adana Basin*, MTA Rep. No: 8037-8037a, Ankara.

Youngs, R. R. ve K. J. Coppersmıth, 1985, "Implications of Fault Slip Rates and Earthquake Recurrence Models to Probabilistic Seismic Hazard Estimates", *Bulletin of Seismological Society of America*, Vol. 75, pp.939-964.

Yurtmen, S., H. Guıllou, R. Westeway, G. Rowbotham, O. Tatar, 2002, "Rate of Strike-slip Motion on the Amanos Fault (Karasu Valley, southern Turkey) Constrained by K-Ar Dating and Geochemical Analysis of Quaternary Basalts", *Tectonophysics*, Vol. 344, pp. 207-246.

Zitter, T. A. C., J.M Woodside and J. Mascle, 2000, "Neotectonic Accommodation between Hellenic and Cyprus Arcs", *Proceeding of EAGE Conference on Geology and Petroleum Geology of the Mediterranean and Circum-Mediterranean Basins*, St. Julians, Malta, 1 – 4 October, pp. 1-4.

APPENDIX A: A BRIEF DESCRIPTION OF THE SOURCE ZONES

A brief description of the source zones is presented in Table A. 1.

Table A. 1. A brief description of the source zones

Seismic Sources	Briefly Definitions
North Anatolian Fault Zone - North Strand (Z10)	This zone locates the western continuation of the northern brunch of North Anatolian Fault System. A zone of mainly strike slip seismic faulting is observed in the region. This zone, which is clearly related to the northern Aegean The January 1, 1982 (M=7) event is known as the maximum earthquake occurred in this zone.
Sisam (Samos)Fault Zone (Z11)	One of the most important in the middle of the Aegean Sea Fault is Samos (Sisam) fault. The Samos and Ikaria Basins form extending of the Menderes Neogene graben system. This asymmetric graben basin is 15 km in length and bounded by a crucial fault zone to its south. Mascle and Martin (1990) obtained the seismic profiles in this area and found its fault mechanism is normal with NE-SW direction.
Cyclades Fault Zone (Z12)	In the southern Aegean, a Tertiary – Quaternary volcanic arc produces a prominent feature. It stretches from Thebes in the northwest across the southern part of the Cylades towards the Bodrum peninsula in south-western Turkey. In the northwest and southeast the Cyclades Arc completed at the stress concentration areas referred to as Corinth and Fethiye, respectively.
Hellenic Arc Fault Zone (Z13)	The south western part of the Hellenic Arc is one of the most seismically active areas in Greece and the entire Mediterranean region (McKenzie, 1972; Makropoulos, 1978; Makropoulos and Burton, 1981; Jackson and McKenzie, 1988). This area has been repeatedly affected by large magnitude earthquakes that have caused severe destruction and human loss (Papazachos and Papazachou, 1997) (*i.e.* 1886 Philiatra M7.3, 1893 Zakynthos-Keri M6.5, 1899 Kyparissia M6.5, 1947 Pylos M7.0, and 1997 Gargaliani M6.6).
Sakiz (Khios)Fault	This zone represents the seismic activity at the western part of the Karaburun Fault. The northern margin of Karaburun is near the

Zone (Z14)	macroseismic epicenter of the Khios Earthquake of 1949 and comprises a north-dipping topographic and bathymetric escarpment. The March 1880 Chios Earthquake of I=IX is associated with this zone.
Midilli (Lesvos)Fault Zone (Z15)	The Edremit Trough is formed by two NE-SW trending asymmetric grabens at the north of Lesvos. The basin between Lesvos and Psara islands has thick sedimentation and structurally complex depression has been developed. It is bounded by N120-oriented normal faults and the basin fill shows seismic evidence of Late Miocene sedimentation (Mascle and Martin, 1994).
North Anatolian Fault Zone - Marmara sea (Z16)	The northern strand of North Anatolian Fault is located between Sapanca Lake and Izmit Bay in the westwards and Tekirdağ and Saros Bay in the east way. From İzmit Bay westwards it lies offshore in the Marmara Sea and its structure has been subject to various interpretations and debate. The segment of the northern branch is associated with the 09.08.1912 (M = 7.4) Sarkoy-Murefte Earthquake. It occurred on the Ganos Fault Zone and was one of the largest earthquakes in the Balkans. The eastern termination of the associated faulting is in the deep West Marmara Trough, westernmost of the successive basins forming the Marmara Sea. Based on the recent multibeam bathymetry and seismic reflection data, estimated total length of the surface rupture is about 56 km and the historical information have presented that the 1912 Earthquake produced a tsunami. Research attention has focused on the offshore segments especially after the devastating İzmit event of August 17, 1999. The last earthquake before this event that had taken place in the eastern part of the Marmara region was the July 22, 1967, Ms = 6.9 Earthquake (Barka and Kandinsky-Cade, 1988). Four segments from the Gulf of İzmit to near Düzce (about 120 km) have been ruptured by the August 17, 1999 event with some discontinuities on surface breaks. All along the fault trace the displacement was right lateral strike-slip. The lateral offsets varied between 5 m (in the west, near the epicenter) to 1.5 m (in the eastern segments) (Toksöz *et al*., 1999). The slip rate in the northern stand is calculated to be around 18-20 mm/yr. The northern half of Marmara Sea is interpreted as a large pull apart basin. The basin is further divided to smaller basins bounded by normal faults in the north and south and separated by northeast-southwest trending right-lateral strike-slip segments.
North Anatolian	The southern strand of the North Anatolian Fault continues into the Northern Aegean and terminates in the Skiros Trough. It consists of sub-

Fault Zone – South Strand (Z17)	parallel strike slip faults, which are active as indicated by seismicity and morphological expressions. Fault plane solutions and surface deformation during earthquakes are consistent with right-lateral motion on this strand (McKenzie, 1972). As this strike-slip fault enters the northern limit of the actively-extending zone in NW Turkey, it splits into three branches forming a number of pull-apart structures which develop a normal slip as well as the predominant right-lateral slip (Barka and Kadinsky-Cade, 1988). The slip rate of the southern stand it is calculated to be around 2-3 mm/yr. There are several basins in the southern strand of the NAF. The Bayramic Basin, the Manyas and Ulubat Basins, the Yenisehir Basin and the Pamuskova Basin (Sengor *et al*., 2005).
Eskisehir Fault Zone (Z18)	The Eskisehir Fault Zone is located between the Inegol Fault in the west and the Tuz Gölü Fault in the east (Kocyigit, 2000; Bozkurt, 2001). The WNW-ESE trending Eskişehir Fault is a right-lateral fault with a significant extensional component, which extends between Uludağ and Afyon (Şaroğlu *et al.*, 1987; 1992; Sengor *et al.*, 1985; Aktunel and Barka, 1998; Barka *et al*, 1995). Many earthquakes with magnitude ≥4 have occurred on the Eskisehir Fault Zone. However, The 1956 Eskişehir Earthquake (Öcal, 1959), M=6.5, occurred along this fault, whose mechanism consists of right-lateral and extensional components is the largest event recorded on this fault zone. Tokay and Altunel (2005) defined the Eskisehir Fault Zone as a 430km long, 15-25 km wide normal fault with significant right-lateral strike slip component having oblique displacement. The annual slip rate is calculated for this zone as 1-2 mm.
Kutahya Fault Zone (Z19)	About 50 km of the Simav Fault, a discontinuous north facing 500m high topographic escarpment west of Kütahya has been interpreted as an active normal fault. The Emet Earthquake of May 2, 1928 (Ms=6.2), occurred near its western end (Ambraseys, 1988).
Bergama – Foca Fault Zone (Z20)	This zone covers the Bergama Foça Fault segments as well as the faults around Izmir City. The NNE-SSW trending and approximately 75 km long left-lateral Bergama-Foça Fault extends between the Bakırçay and İzmir Grabens. This fault zone consists of several parallel faults and splays into more branches towards the Bakırçay Graben (Şaroğlu *et al.*, 1987). In addition, a second set of fault trends SE-NW near Aliağa, displaying normal and right-lateral strike-slip motions. Several more minor faults occur just to the north of İzmir trending NW-SE, the same trend as those bounding the

	Gediz Graben. GPS measurements indicate that velocities increasing along the western coast of Anatolia and further southward could result in the Çandarlı Bay area moving faster than onshore Anatolia along the Bergama-Foça Fault Zone (Barka and Reilinger, 1997). The Dikili or Bakırçay Earthquake of 1939 (Ms = 6.5) occurred beneath the Bakırçay Valley, and may have involved slip along the NNE-SSW normal fault along the valley at the northern end of this fault zone (Westaway, 1990). 215 of 4565 houses in Bergama were damaged and 30 houses were completely devastated. In Dikili, 627 houses were collapsed, 41 people died (Uluç, 1999). Both historical and instrumental catalogs show that seismicity is rather dense between Karaburun–Chios, İzmir Bay-Lesbos and Doğanbey-Samos. The principal faults that were observed from both satellite images and site investigation can be summarized as; Dumanlıdağ, Bornova, İzmir, Cumaovası, Karaburun, Gümüldür and Tuzla Faults. In this century there are several big earthquakes occurred on these fault segments: 1928 Torbali (Ms=6.5), 1939 Dikili (Ms=6.6), 1949 Karaburun (Çeşme) (Ms=6.6), 1953 Karaburun (Ms=5.6), 1955 (Ms=6.7) İzmir (Söke) and 1992 Seferihisar (Ms=6). Throughout the history, 17, 688, 1688, 1739 and 1778 Earthquakes are the biggest events created by the faults around Izmir Bay.
Simav – Sultandag Fault Zone (Z21)	The Sultandag-Aksehir Fault (SAF) is the main border fault on the SW side of the AAG, with a dip slip rate of 0.3 mm/y (Kocyigit and Ozacar, 2003). The major active fault in this system strikes west-northwest along the south border. 1942 Bigadiç, 1969 Demirci and 1970 Gediz Earthquakes are the major events that occurred on this fault. The Simav Fault broke in the 1969 Demirci Earthquake (Ms = 6.0), although no confirmed surface faulting was produced. The Simav Valley floor slopes gently north and the Simav River flows along its north margin, suggesting that this margin may be a major south-dipping normal fault that has tilted the valley north (Westaway, 1990). A high microseismic activity has been observed for last 30 years in this region. A sequence of moderate earthquakes that occurred between 2000 and 2002 provides insight into the incremental growth of the mountain front through individual seismic events. The earthquake sequence consists of three moderate size events: a Mw 5.1 and a Mw 6.0 earthquake (December 15, 2000) and a Mw 6.5 earthquake (February 3, 2002). The Sultandag- Çay Earthquake is related to the Sultandag Fault Zone that is approximately 37 km long and 7 km wide at depth. The average slip over

	the rupture plane during the mainshock is estimated to be 32 cm (Ergin *et al*., 2009).
Gediz Fault Zone (Z22)	Gediz Graben is approximately 200km long normal fault system which extends from Manisa to Pamukkale. Main fault is located at the southern part of the graben system (Karadut Fault). According to the Westaway (1990) Gediz Graben can be considered as at least two sub-parallel normal branches. The faults on the western side of Gediz Graben are defined as normal active faults. NW SE trending Gediz Graben between Turgutlu-Sarıgöl splits into two subgraben (Uluç, 1999). The northen subgraben which is called Manisa Fault extends towards Manisa in the NW SE direction. The southern subgraben which is called Kemalpaşa Fault turns to the west from Turgutlu and ends in Kemalpaşa region. The active Manisa fault is about 25 km long and the Kemalpaşa Fault is about 20 km long. (Emre and Barka, 2000). 1969 Alaşehir Earthquake (Ms = 6.5), which occurred on a segment of the fault branch that separates the uplifted Neogene basin from the actively subsiding basin, resulted in 36km of surface faulting.
Menderes Fault Zone (Z23)	Menderes Massif is comprised of large, coherent blocks that respond as rigid bodies during tectonic deformation, thus it plays a significant role in the regional tectonics. These grabens control the major west-flowing consequent surface drainage of the Western Anatolia. The Zone covers the Büyük Menderes, Küçük Menderes Graben System and Yavansu Fault. Starting form the west of the Gediz Graben, The Büyük Menderes Fault Zone is one of the main active tectonic structures of the Western Anatolia. The fault zone extends for a distance of 150 km between the Denizli Basin in the east and the Aegean Sea in the west. It is divided into two branches around Germencik. The northern branch, which may no longer be active, extends towards to Kuşadası where as the southern branch goes into the Aegean Sea in SW direction. There have been several disastrous earthquakes in this region in the history such as 1645, 1654, 1702 and 1899 events. The 1899 Earthquake (Ms = 6.9) produced 1-2m of normal slip with no documented strike slip. the 1653 and 1899 earthquakes involved surface ruptures along the northern boundary of the Menderes Graben The latest big earthquake with NE-SW trending left-lateral slip motion occurred in the vicinity of Söke-Balat on the west end of the graben in 1955.Yavansu Fault can be considered as the continuation of the Büyük Menderes Fault System.

	It strikes roughly east-west near the south of Kuşadası (Hancock and Barka, 1987; Stewart and Hancock, 1990). Küçük Menderes Valley is accepted as a graben system similar to the Büyük Menderes and the Gediz Grabens. An apparent fault, which trends toward to north, extends along the southwest of the graben system. It is assumed that the Torbalı Earthquake of 1928 (Ms = 6.5) occurred on this fault (Westaway, 1990).
Mugla – Yatagan Fault Zone (Z24)	Mugla-Yatağan Fault system is comprised of normal NW-SE directional faults. Even though high seismicity is not observed in this region, the system has a key role in tectonic regime.
Gokova Fault Zone (Z25)	Gökova Fault Zone, which consists of several parallel, active normal faults, extends 180 km along the Gökova Bay. Even though Sieberg (1932) named this system as "Kos Graben", presently it is mostly known as "Gökova Graben". GF forms is divided into two main segments, the partly submarine Gökova-Kos segment trending E-W to NE-SW and the mainland NE-SW trending main Gökova segment, both dipping to the SE to S. They are predominantly normal with dextral component (Pavlides *et al*., 2009). According to the instrumental earthquake data, a very high seismicity is observed on the fault, which is bounded by Gökova Bay. In this century two prominent earthquakes recorded in this area are 1933 (M=6.5) and 1956 (M=7.2) events (Ergin *et al*., 1967; Ambraseys, 1988). The slip rate calculated for this zone is about 25-30mm/yr.
Hellenic Arc Fault Zone (Z26)	The seismic source referred to as Cretan corresponds to the Hellenic Trench and the Pliny-Strabo Trench complex, which also forms the southern boundary of the Aegean Plate. The Hellenic Trench consists of a series of linear depression of the crust in the northern-most central part of the Eastern Mediterranean sea. Helenic Arc starts from the southern part of the Ionian islands (west of Zante island), and continues along the conez side of the arc (south of Peloponnese-south of Crete-south of Karpathos and Rhodos) up to Rhodos where it changes direction and trends northwest-southeast, that is parallel to the southwestern coast of Anatolia (Turkey). The two earthquakes are known from historical information, the 21 July 365 A.D. Earthquake (Ms=8.0), which occurred in the western part of the trench and the December 1303 Earthquake (Ms=8.0) which occurred in the easternmost part of the trench. Zone 26 is associated with the eastern continuation of the Hellenic Arc into Aegean region.

Fethiye – Burdur Fault Zone (Z27)	The Burdur-Fethiye Fault Zone is located in the southwest of Turkey in a tectonically active area and in the northeast continuation of the Pliny / Strabo complex, which is forming east part of the Hellenic Trench (Dumont *et al*., 1979). This fault zone, extending for 300 km between Burdur and Fethiye, is one of the most important zones and has produced many earthquakes in the recent past. These activities satisfactorily agree with the GPS measurements, which indicate a slip rate of 15-20 mm/yr. The 3 Oct.1914 (M=7) and 12 May 1971(M=6.2) earthquakes are assumed to have occurred on this fault in the vicinity of Burdur. It consists of left lateral strike slip fault with normal components.
Antalya Fault Zone (Z28)	This zone is located between Cyprus Trough, Florence Rise and Fethiye Burdur source zones. Even though there are not specific fault traces in this region, the observed seismic activity with relatively deep events, justifies the region as a seismic source zone. The two areas are connected by a relatively narrow region, north-south-trending, from Afyon to Isparta angle (Kirka-Afyon-Isparta junction-area), in which an alkaline association developed from the Upper Miocene to the Pliocene. The volcanic rocks form a narrow belt, about 200 km long and 50 km wide, and they were erupted mainly along the Antalya Fault Zone (Yagmurlu *et al.*, 1997). Glover and Robertson (1998) have defined as the Kemer linearity.
Cyprean Arc – Florene Rise Fault Zone (Z29)	Cyprus is located on the boundary between Eurasian and African Plates and exhibits a complex tectonic regime. The southern boundary of the Anatolian Plate runs in a large loop from the Gulf of Iskenderun, south of Cyprus and to Rhodes (McKenzie, 1972). The Cyprus Zone ends on the east at the EAF and /or the Bitliz suture zone. The Cyprean Arc forming the three Plate boundaries. In the west the Cyprean Arc is adjacent to the Hellenic Arc. Based on the seismicity data the region was investigated as 3 separate zones as Florence Rise, Trodos Mountains and Hecataus Ridge. In the last century earthquakes are mainly concentrated on the southwest of the island and the maximum event was recorded as M=6.8 in 1996.
Cyprean Arc – trodos Monut Fault Zone (Z30)	
Hecataeus Ridge – Fault Zone (Z31)	
Cyprus Trough Fault Zone (Z32)	To the south of Cyprus the boundary coincides with a deep-sea trench (Robertson *et al*., l995). Though, further east the Plate boundary is illdefined, with several different interpretations of its position: (1) there is no Plate boundary in the area (Ben-Avraham, 1978); (2) two boundary

	segments exist to the north and south of Cyprus (Lort, 1971; Le Pichon & Angelier, 1979); (3) a zone of active convergence extends from Cyprus through the Iskenderun Basin to the Kahramanmaras¸ triple junction where the East Anatolian Fault Zone and Dead Sea Fault Zone meet (McKenzie, 1978; Dewey & Sengor, 1979); (4) the Plate boundary is a wide diffuse zone dominated by sinistral strike-slip (Kempler & Garfunkel, 1994; Robertson, 1998; Vidal, Alvarez- Marron&Klaeschen, 2000; Harrison *et al*., 2004), with the most southerly boundary of this zone of deformation extending onshore in northern Syria (Hardenberg & Robertson, 2007). This zone covers the tectonic structures starting from Beysehir-Egridir Lakes to Iskenderun Bay and covers the Isparta Angle and Aksu suture zone in the west and Adana-Klikya Basin in the east. Along the Cyprean Trough the main sources of earthquakes appear to be the Gulf of Antalya. In the east Maraş triple junction is another area with high seismic activity. The events originating from this part are usually felt throughout the island, as in the case of the recent Adana-Ceyhan Earthquake. The eastern part extending to the İskenderun bay is relatively silent.
Black Sea Fault Zone (Z33)	The zone is related with the Black Sea Fault, extending from Sinop towards east, going parallel with the Black Sea Cost, and then joining the northern part of the Northeast Anatolian Zone. The Black Sea is formed of two deep basins separated by the Mid-Black Sea ridge (Belousov *et al.*, 1988; Finetti *et al*., 1988). The occurrence of strong earthquakes in the Black Sea depression events which would exceed the known Crimea Earthquakes with M=6.8, and the structures they may be related to can be estimated. The occurreence of large blocks in the Black Sea Basin bounded by elongate seismic lineations about 200 km long suggests the possible generation of sources with M ~7-7.5.
North Anatolian Fault Zone (Z34)	The North Anatolian Fault Zone (NAFZ) is a 1000-1500 km long, seismically very active right-lateral strike-slip fault that takes up the relative motion between the Anatolian and Eurasian Plates. The NAFZ extends from the Karlıova triple junction as far as mainland Greece. Its eastern termination beyond the Karliova triple junction is discussed in the tectonics of the East Anatolian region. Offsets of late Miocene sediments and the size of pull-apart basins along the fault zone reveal a total displacement varying from 40 ± 5 km near Erzincan to 25 ± 5 near Bolu (Barka, 1992). The GPS derived slip rate on the North Anaolian Fault is found to be 24 ± 1 mm/yr

	while the geologically derived slip rate amounts to 16/24 ±5 mm/yr (Reilinger *et al*., 2006). Although the classical description of the North Anatolian Fault states its initiation location as the Karlıova triple junction, the alignment of the epicenters of the largest earthquakes after 1939 clearly indicates a seismic zone extending about 75km beyond Karlıova into the Varto region. The point has been confirmed with faulting associated with the Varto Earthquake of August 19, 1966. Trifanov *et al*. (1993), extend the North Anatolian Fault further east of Lake Van, towards Urmiye Lake, and associate the 1648 Van Earthquake and the 1960 Salmas Earthquake with this eastern extension of the North Anatolian Fault. The slip rate is found to be 23 mm/yr for the main strand of the fault.
Alaca – Ezine Pazari Fault Zone (Z35)	The right lateral Alaca-Ezinepazarı Fault consists of two segments. The 90 km long eastern segment is separated from the North Anatolian Fault by a 15 restraining bent southwest of Niksar Basin. This segment is the westernmost of the segments that have been ruptured during the December 26, 1939 Erzincan Earthquake (Ms = 8). The second segment of the Alaca-Ezinepazarı Fault is 150 km long. It is separated from the previous segment by a 24 bent and seismically it is less active (Barka and Kandinsky-Cade, 1988).
Tuz Golu Fault Zone (Z36)	The Tuz Gölü Basin is surrounded by large intraplate faults. The Tuz Gölü Fault (Koçhisar Fault) extends in NW-SE direction at the eastern shore of the basin and is 125 km. long (İlhan, 1976). Tuzla Fault has an important position for the active tectonic structure of West Anatolia. Furthermore, it is also important for the seismic risk of Izmir. As it is indicated in RADIUS (1997) that lots of earthquakes occurred on this fault, for instance, the last one occurred in 1992 with a magnitude of Ms=6.0 (Uluç 1999). This earthquake caused serious damage to 60 buildings in Doğanbey region.
Ecemis Fault Zone (Z37)	The northeast-southwest trending left-lateral Ecemiş Fault is about 100 km long and it extends from the Erciyas Mountain to the Mediterranean Sea. Although the fault initiated in the Eaocene time, its activity within the present-day escape system (Yetiş and Demirkol, 1984) is evidenced by the existence of many macroseismic correlations.
Adana Fault Zone (Z38)	The active faults in the Adana Basin are the Karataş-Osmaniye, Yumurtalık, Misis-Ceyhan and Kozan Faults. Yumurtalık Fault is one of the main structures of Adana Basin (Saroglu *et al.,* 1987). It is a left lateral strike slip

	fault. Yumurtalik Fault is composed of fractures, which can be continuous or parallel to each other with a NE-SW orientation and has a length of 62 km between Yumurtalik-Karagedik. The section with a length of 25 km between Yumurtalik and Imraniye is well observed. The Karataş and Yumurtalık Faults are considered to be a continuation of the East Anatolian Fault. They form an angle of 25° with the Maraş-Osmaniye segment. The annual deformation is calculated to be around 0.8-0.9 cm/year (Barka, personal communication). The region is known to be seismically active, but because of the short length of the faults in the area, large earthquakes (with magnitudes greater than 7) are not historically known or expected. The historical database refers to several damaging earthquakes with magnitudes less than 7.
Goksun Fault Zone (Z39)	Goksun Fault with the length of 60km between Cardak and Geben is a left lateral strike slip fault. Goksun Fault constitutes the far west section of the major fault splay diverging from East Anatolian Fault System. This fault system with a general trend of E-W is composed of Surgu, Elbistan and Goksun Faults (Arpat and Saroglu, 1975; Perincek and Kozlu; Kozlu and Karig; Saroglu *et al*., 1987; 1992). The maximum earthquake magnitude, the estimated maximum and the average displacements are 7.2, 2.75m and 1.32m., respectively.
Dead Sea Rift (Z40)	The part of DSF which extends from the Dead Sea to Palmyra fold belt is the Yammouneh Fault. Along this fault, two major earthquakes were occurred in 1202 and 1759 (Ambraseys and Melville, 1998). The 1202 Earthquake caused a surface rupture of approximately 200 km. On the other hand, the 1759 Earthquake caused a surface 100 long along the Bekaa valley. The two destructive earthquakes indicate that, the recurrence interval of the fault is 557 years.
Hatay Fault Zone (Z41)	The Hatay Graben is an asymmetrical fault-controlled basin trending NE–SW from the Mediterranean Sea, past the city of Antakya/Hatay to the Amik Plain. This type area was previously considered as the extension of another approximately N–S-trending graben to the northeast, variously known as the Hatay Graben (Perincek and Cemen, 1990), the Amanos Fault Zone (Lyberis *et al*., 1992; Over *et al.*, 2002) or the Karasu Rift (Lovelock, 1984; Westaway, 1994; Rojay, Heimann & Toprak, 2001). the NE–SW-trending graben extending from the coast to near Antakya is termed the ‘Hatay

	Graben', which includes the city of Antakya/Hatay, whereas the northern approximately N–S structure is defined as the Karasu Rift. The city of Antakya and a part of the Asi River is located on the NE-SW trending Antakya-Samandag Depression. This depression, covered by marine Miocene, Pliocene and Holocene deposits, is delineated by normal faults on the NW and SE sides. Extensive tectonic deformations can be seen to be associated with these faults (Ilhan, 1976). At Amik Lake, Antakya-Samandag Depression joins with the Hatay-Kahramanmaras Depression and Ghab Depression. Ghab Depression is located at the northern extremity of the Dead Sea Fault System. Earthquake history of this zone extending to two millenia indicates a quite in-homogenous temporal distribution. Fifth, sixth, ninth, twelfth and nineteenth centuries were very active, yet there was no activity in the seventh, thirteenth, sixteenth and seventeenth centuries (Ambraseys and Melville, 1995; Alsinawi, 1988; Demir, 1996; Poirier and Taher, 1980; Ambraseys, 1989).
East Anatolian Fault Zone (Z42)	The EAFZ was first described by Allen (1969) and mapped by Arpat and Saroglu (1972), Seymen and Aydin (1972), Arpat and Saroglu (1975), Saroglu *et al*. (1992), and Imamoglu (1993). It is a belt of active seismicity and tectonics that joins the eastern end of another major Anatolian fault, the right-lateral North Anatolian Fault Zone (NAFZ), at Karliova triple junction where it intersects with the North Anatolian Fault to the Maraş triple junction, extending to the Amik Basin near Antakya (Arpat and Saroglu, 1972; Perincek and Cemen, 1990; Saroglu *et al*., 1992; Over *et al.,* 2004a) or to the Gulf of Iskenderun (McKenzie, 1972; Jackson and McKenzie, 1988). It has a total length of 600 km. (Ovar *et al*., 2004c) The slip rate along this left-lateral fault is calculated to be about 9 cm/yr. (McClusky *et al*., 2000). The Maraş-Osmaniye segment extends from Gölbaşı to Osmaniye and it is the segment of the East Anatolian Fault that, by its intersection with the Karasu segment of the Dead Sea Tranform, forms the Maraş Junction. Based on the strike of the segments, the EAFZ should consist of six segments (Saroglu *et al*., 1992); however, Hempton *et al*. (1981), defined only five segments based on geometry and behavior, while Barka and Kadinsky-Cade (1988), based on fault geometry and seismic activity, suggested that there may be 14 different segments along the EAFZ. The segment between Turkoglu and Celikhan has experienced earthquake events on March 2, 1893 (M = 7.1, 45 km), December 4, 1905 (M = 6.8, 38

	km), and most probably on March 28, 1513 (M = 7.4, 103 km) (Ambraseys and Jackson, 1998; Nalbant *et al*., 2002).
Bitlis – Zagros Fault Zone (Z43)	The Bitlis Thrust Belt is approximately 1000 km along and 150 km wide and constitutes the fore front of the Arabian Plate in the north. It is a late-Quaternary wrench fault and presently active along its northwestern half. The fault is located between Çelikhan – Sincik - Lice up to south of Lake Van and to the southwest of Zagros. The section left between Çüngüş in the east and Kulp in the east has a very obvious thrust component. In the west direction, the tectonic deformation is taken up by the EAF and the E_W trending reverse faults on the Arabian Plate The zone consists of two thrust belts, the southern thrust belt forms the boundary between the Taurids and the border fold zone and it extends between south Hakkari in the east and Amanos mountains in the west (Ketin, 1966; Ilhan, 1971). The same belt extends westward to Cyprus (McKenzie, 1970) and eastward to connect the Zagros Crush Zone (Dewey *et al*., 1973).
North East Anatolian Fault Zone (Z46)	This zone is related with the northern continuation of the East Anatolian Fault *i.e.* the North East Anatolian Fault System. The NEAFZ consists of a NE-SW principal fault zone and several secondary fault sets. The left-lateral Askale Fault Zone (Koçyigit and Rojay, 1984) is one of the important secondary fault sets of the NEAFZ, and is located in the central part of the investigated area. The N040°–070°–trending Askale Fault Zone cuts the formation boundaries and thrust faults northeast of Tercan. The Tercan-Çayirli region is located between the dextral North Anatolian Fault Zone in the south and the sinistral Northeast Anatolian Fault Zone (NEAFZ) (Tatar, 1978) in the north. The NEAFZ follows the Firat River valley in a N045° direction in the southwestern part of the town of Tercan. The strike-slip fault zone broadens toward the southwest around the villages of Mantarli and Sucuali.
Arax Fault Zone (Z45) *Khanasar Fault Zone (Z47)* *Tebriz Fault Zone (Z48)*	The high potential of the Armenia and adjacent countries in terms of seismic activity is well documented by the national historical dataset (*e.g*., earthquakes of 550 BC (M=7.0), 906 (M=7.0), 1139 (M=7.5), 1679 (M=7.0), 1721 (M=7.3), 1780 (M=7.4), 1840 (M=7.4), 1976 (M=7.1), and 1988 (M=7.0) on the Arax, Garni, Zheltorechensk-Sarikamish, Pambak-Sevan, Balik-Göl, Dogoubayazet, North-Tebriz Faults (Ambraseys, Melville, 1982; Berberian, 1995; Karakhanian *et al*., 1997). In Northern Armenia, Eastern Turkey and North-Western Iran, the faults from a

	northward-bending structural arc. The outher part of the arc is defined by wo active faults: Zheltorechensk-Sarighamish Fault (ESF) and Pambak-Sevan-Sunik Fault (PSSF). The ESF Fault is a left lateral strike lip structure, and the PSSF is right lateral strike slip fault. The inner part of the arc is defined by the left lateral strike slip Akhourian Fault (AF), and the right lateral strike slip Garni Fault. The southern part of the arc ends by the active faults that border the Aarat Valley, consisting of Sardarapat Fault (SF), NAkhichevan Fault (NF), Dogubayazet Fault (DF), MAku (MF), GAilatu-Siah Cheshmeh-Khoy Fault (GSKF) and other faults. The Pambak–Sevan–Sunik Fault (PSSF) Zone in Armenia is one of the major active structures of the region. The fault is comprised of four main segments and it displays morphological evidence for dextral movement during the Holocene. However, no large earthquake (M>7) has occurred in the northern or central parts of the fault during the last 2000 years. The December 7, 1988 Ms=6.8 Spitak earthquake is also associated with the PSSF (Balassanian *et al*., 1995; Karakhanian *et al*., 2004). The Tabriz Fault starts in the southeast near Bostanabad, follows a N 300° direction passing along the northern suburbs of the town of Tabriz, and divides near Marand into the Derik Fault and the Northwest Fault system. The town of Tabriz has been devastated by a number of earthquakes during its history, but a critical study is required to establish whether they were actually associated with the Tabriz Fault. No strong earthquakes are known to have occurred near this fault during the late 19th and early 20th centuries. The general direction of the Tabriz Fault is continued after Marand by a system of little known NW-SE faults of probable Quaternary activity, referred as the Northwest Fault system (Tchalenko, 1977).

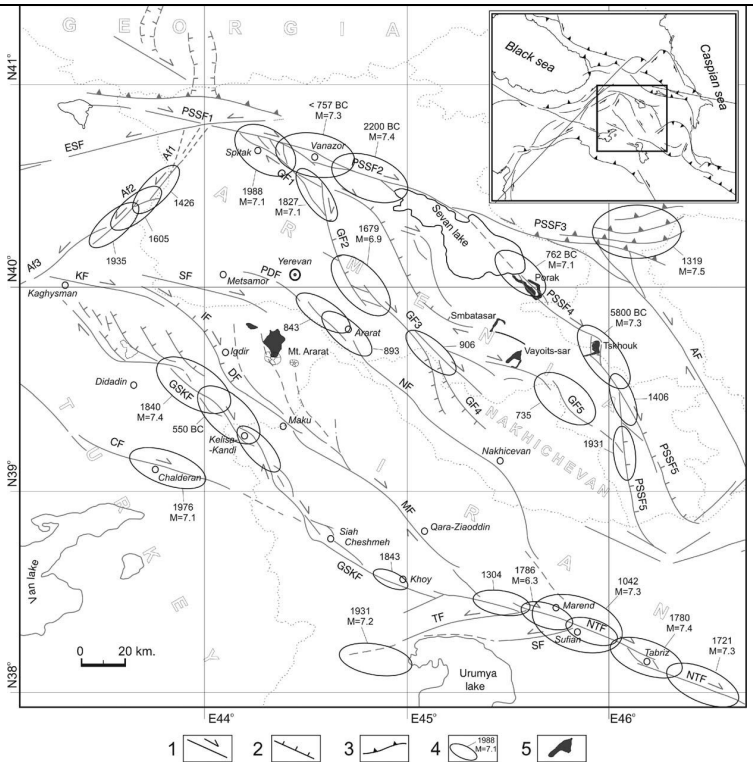

Figure A. 1. Active faults of Armenia, Eastern Turkey and NW Iran 1 – strike –slips; 2 – normal faults; 3 –thrusts; 4– strong earthquake epicenters; 5 – earthquake-triggered volcanic eruptions in the Holocene-historical time (Karakhanian *et al.*, 2004)

APPENDIX B: BUILDING INVENTORY OF TURKEY

Although current methods of inventory development are often not standardized and frequently not available in electronic format, GRM Company has prepared the recent building inventory dataset compiled from Istanbul Metropolitan Municipality (IMM), Turkish Statistical Institute (TurkStat), Department of Housing and Urban Development, Department of Earthquake Risk Management and Urban Development in Turkey.

The following data were utilized to compose the grid based building inventory dataset for Turkey:

1. ***Year 2000 Building Inventory Census of TurkStat***: TurkStat (Turkish Statistical Institute) has conducted an inventory of building study in 2000 and it has been made available for use in this study. The 2000 census of Building within the boundaries of Turkey consists of the 3212 provinces, districts and villages. The building inventory was prepared in four groups based on number of stories, the construction type, construction date and purpose of usage.
2. ***Year 1997 Building Inventory Census at villages:*** Regardless of the population knowledg*e,* the census of building inventory at village level was prepared in two groups based on the number of building and construction type for residential and non-residential and the number of stories for residential buildings. According to the result of 1990 general census of population, the population greater than 2000 has been excluded.
3. ***Administrative boundary of Turkey:*** The GIS based administrative boundary of Turkey at province level has been utilized. These data converted to GIS includes 81 provinces and 923 districts.
4. ***Grid based Landscan population (2005):*** Landscan population database for Turkey is based on Arcview grid format, the datum of WGS84 and the grid size of 1 km by 1 km (30 arc-second).

Previously, the administrative boundary of Turkey has been associated with the point based Landscan population knowledge (2005) and the building census of TurkStat. The ratio of population in each geocell has been determined by dividing the point based

Landscan population to the total TurkStat- population based on district level. Using this point based ratio and point based Landscan population knowledge, the district based building inventory in s GIS format has been improved to comprise a point based building inventory for Turkey. This process has been also repeated for the all building and/or residential building usage type and six different dataset have been prepared as shown in Table B. 1.

Table B. 1. Building inventory for Turkey

Name	Building Inventory of TurkStat used in this study	The Total Number of Building for Turkey
Number of story	Building 2000 (All type) + 1997 Village (Residential)	8387346.0000
Construction type		8387344.2225
Construction Year		8387321.9125
Number of story	Building 2000 (Residential) + 1997 Village (Residential)	7513379.3362
Construction type		7513376.7397
Construction Year		7513370.4777

The building classification taken from the form of structural and Material of Building (2000) are regrouped according to European Building taxonomy as illustrated as in Table B. 2.

Table B. 2. The building classification taken from the form of structural and material of building (2000)

Structural System and Material of Building	
RC1 Moderate	Frame Construction (Concrete block + Hollow Concrete block + Brick + Stone, sun, dried, brick + other + unknown)
M5 – Unreinforced masonry	Bearing Wall Construction (Hollow Concrete + Brick + Stone)
M2 – Adobe	Bearing Wall Construction (Sun, Dried Brick)
M1 – Rubble Stone	Bearing Wall Construction (Other + Unknown) + Other + Unknown
Number of Stories of Building	
Low Rise	Story # 1 + Story # 2 + Story # 3 + Unknown
Mid Rise	Story # 4 + Story # 5 + Story # 6

High Rise	Story # 79 + Story >10
Completed Year of Building	
Pre - 1980	Year (- 1929) + Year (1930 - 1939) + Year (1940 - 1949) + Year (1960 - 1969) +Year (1970 - 1979) + Unknown
Post - 1980	Year (1980 - 1989) + Year (1990 - 2000)